#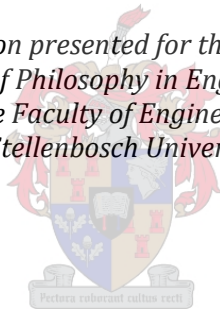 Computational and Experimental Modelling of Masonry Walling towards Performance-Based Standardisation of Alternative Masonry Units for Low-Income Housing

by

Wibke Irmtraut De Villiers

Dissertation presented for the degree of
Doctor of Philosophy in Engineering
in the Faculty of Engineering,
at Stellenbosch University.

Supervisor: Prof G.P.A.G. Van Zijl

Co-Supervisor: Prof W.P. Boshoff

December 2019

Declaration

By submitting this dissertation electronically, I declare that the entirety of the work contained therein is my own, original work, that I am the sole author thereof (save to the extent explicitly otherwise stated), that reproduction and publication thereof by Stellenbosch University will not infringe any third party rights and that I have not previously in its entirety or in part submitted it for obtaining any qualification.

Wibke De Villiers

December 2019

Abstract

South Africa has a housing shortage estimated in excess of 2 million units. This backlog is being addressed predominantly with the construction of 40m^2 low-cost, single storey, detached state subsidised houses built with conventional masonry units (CMU's), namely concrete and burnt clay. The use of these materials has a significant negative impact on the environment and the thermal performance of conventional masonry walls is generally poor. These factors, and others, have led to the development of alternative masonry units (AMU's) in South Africa, and internationally, with a lesser environmental impact and improved thermal performance. However, lack of standards presents a significant barrier to the uptake of AMU's

The regulatory framework governing the use of masonry in South Africa, and possible avenues through which AMU's could gain access to the market, are explored. It is found that AMU's could provide a reasonable and socially acceptable alternative to CMU's in low-income housing (LIH) but the current regulatory framework does not accommodate AMU's in a sufficiently practical manner to enable their widespread, off-the-shelf uptake. The ongoing process of the adoption of Eurocode 6 and the accompanying materials and testing standards by the South African masonry industry, facilitates the transition from prescriptive to performance-based (PB) regulation of masonry design. It is proposed that material non-specific, PB requirements for masonry units for structural application in LIH can be developed to assist the inclusion of AMU's in the open market.

To quantify PB criteria, two critical configurations of single-storey bonded masonry walls are generated, based on the deemed-to-satisfy provisions of the National Building Regulations (NBR). Subsequently, a simplified micro-scale finite element (FE) model is used to analyse these configurations under serviceability and ultimate limit state loading conditions, to serve as a performance prediction model from which PB criteria can be derived.

Four masonry materials are selected for the study; conventional concrete (CON), alkali-activated material or geopolymer (GEO), compressed-stabilised earth (CSE) and adobe (ADB), representing a wide spectrum in terms of strength and stiffness. Characterisation tests of the four materials are used, together with numerical fitting to test data and data taken from literature, to generate the necessary parametric input for the FE model. The results of medium to large-scale in-plane and out-of-plane tests are used for validation of the FE model.

The FE analyses revealed that for most of the load cases, the resistances of the walls failed to achieve the design load, even for the conventional CON blocks. A significant shortfall was found for the out-of-plane resistance against the wind load for all four materials, as well as structural vulnerability under seismic loading due to the geometric layout permitted by the deemed-to-satisfy rules in the NBR. These results preclude the immediate derivation of PB criteria for AMU's but contribute significantly to the body of knowledge surrounding FE modelling of AMU's. They also indicate that the NBR provisions for wall panel geometry require reconsideration, given the recent revision of the South African loading code. However, material non-specific PB regulation is still the recommended avenue for the standardised inclusion of AMU's.

Opsomming

Suid-Afrika het 'n behuisingstekort van meer as 2 miljoen eenhede. Hierdie agterstand word hoofsaaklik aangespreek deur die konstruksie van 40m^2, enkel-verdieping, losstaande, staats-gesubsidieerde behuisingseenhede, wat meestal met konvensionele messelwerkeenhede gebou word, naamlik beton en gebakte klei blokke. Die gebruik van hierdie materiaal het 'n beduidende negatiewe impak op die omgewing en die termiese gedrag van konvensionele messelwerkmure is ook swak. Hierdie faktore, onder andere, het gelei tot die ontwikkeling van alternatiewe messelwerkeenhede (AME's) in Suid-Afrika en internasionaal, met verminderde omgewingsimpak en beter termiese gedrag. 'n Gebrek aan standaarde verhoed egter die aanvaarding en gebruik van AME's.

Die raamwerk van regulasies wat die gebruik van messelwerk in Suid-Afrika beheer, sowel as moontlike maniere om die toelating van AME's te bewerkstellig, word ondersoek. Dit word bevind dat AME's 'n redelike alternatief bied tot konvensionele messelwerk in lae-inkomste behuising, wat ook sosiaal aanvaarbaar is, maar die huidige regulatoriese raamwerk akkommodeer nie AME's op 'n prakties uitvoerbare manier nie. Tans is die aanneming van Eurocode 6 in Suid-Afrika, met gepaardgaande materiaal- en toets standaarde, 'n deurlopende proses en dit fasiliteer die oorgang van voorskriftelike standaarde na 'n stelsel wat op prestasie gebaseer is vir die ontwerp van messelwerk. Dit word voorgestel dat materiaal-onafhanklike, prestasie gebaseerde (PB) vereistes ontwikkel kan word vir messelwerkeenhede vir strukturele toepassings in lae-inkomste behuising, om die gebruik van AME's te vergemaklik.

Om PB kriteria te kwantifiseer word twee kritiese konfigurasies van enkel-verdieping, gebonde messelwerkmure gegenereer, op grond van voorskrifte in die Nasionale Bouregulasies (NBR) wat as bevredigend geag word. Daarna word 'n vereenvoudigde mikro-skaal eindige element (EE) model gebruik om die muur konfigurasies te analiseer onder diensbaarheid en uiterste limietstaat lasaanwending, om as voorspellingsmodel van die gedrag te dien, waarvan PB kriteria afgelei kan word.

Vier messelwerkmateriale is gekies, konvensionele beton (CON), alkali-geaktiveerde materiaal of geopolymer (GEO), saamgeperste, gestabiliseerde grond (CSE) en adobe (ADB), wat 'n wye spektrum aan sterkte en styfheid verteenwoordig. Die nodige parametriese data vir die EE model word verkry vanaf karakteriseringstoetse op die vier blok tipes, so wel as numeriese pas van toetsdata en data van relevante literatuur. Die EE model word gevalideer deur middel van medium- tot grootskaalse in-vlak en uit-vlak toetse.

Die EE analises wys dat die mure se weerstand in die meeste lasgevalle nie die ontwerpslas haal nie, selfs vir die konvensionele CON blokke. 'n Beduidende tekortkoming is gevind vir die uit-vlak weerstand teen die wind lasgeval vir al vier materiale. Die seimiese lasgeval dui ook op strukturele swakhede wat onstaan vanuit die geometriese uitleg wat deur die NBR voorskrifte toegelaat word. Hierdie resultate verhoed die onmiddelik afleiding van PB kriteria vir AME's, maar dit maak 'n beduidende bydrae tot die kennis rakende EE modellering van AME's en dui daarop dat die NBR se voorskrifte vir muurpaneel geometrieë heroorweeg moet word, gegewe die onlangse hersiening van die Suid-Afrikaanse laskode. Materiaal-onafhanklike PB regulasie word egter steeds aanbeveel vir gestandardiseerde insluiting van AME's.

Acknowledgements

My warmest gratitude to

Contents

Abbreviations

AAC	autoclaved aerated concrete
ADB	adobe
AMU	alternative masonry unit
ASA	Agrément South Africa
BS	British Standard
CCSC	combined cracking-shearing-crushing material model
CMA	Concrete Manufacturers Association
CMU	conventional masonry unit
CON	concrete
CS	calcium silicate
CSE	compressed-stabilised earth
CSIR	Council for Scientific and Industrial Research
DHS	Department of Human Settlements
DPC	damp-proof course
EC	Eurocode
EN	European Norm
EXP	experimental results
FE	finite element
FEA	finite element analysis
FEM	finite element model/modelling
GEO	geopolymer (alkali-activated)
GPM	general purpose mortar
HD	high density
IP	in-plane
ISO	International Organization for Standardization
JSD	Joint Structural Division
LD	low density
LIH	low-income housing

MIP	mercury intrusion porosimetry
MOD	model
NA	National Annex
NBR	National Building Regulations
NDP	nationally determined parameters
NHBRC	National Home Builders Registration Council
NPC	National Planning Commission
NUM	numerical results
OP	out-of-plane
PB	performance-based
R	Rand – South African currency
SABS	South African Bureau of Standards
SAICE	South African Institution of Civil Engineers
SANS	South African National Standard
SDOF	single degree of freedom
SEM	scanning electron microscopy
SLS	serviceability limit state
SMM	simplified micro-modelling
UBC	Uniform Building Code
UK	United Kingdom
ULS	ultimate limit state
ULS-S	ultimate limit state – seismic
ULS-W	ultimate limit state – wind
WBCSD	World Business Council for Sustainable Development
WTO	World Trade Organisation

Symbols and Nomenclature

A	area
b	specimen height or width, perpendicular to span direction
$c\ c_c\ c_j$	cohesion, of unit crack interface, joint interface
$C_{ss}\ C_{ss,c}\ C_{ss,j}$	shear traction contribution, of unit crack interface, joint interface
$E\ E_u\ E_m\ E_w\ E_r$	elasticity modulus, of unit, mortar, masonry wallet, reinforcement
f_b	normalised mean compressive strength of masonry unit
$f_c\ f_{c,c}\ f_{c,j}$	compressive strength, of unit crack interface, joint interface
f_k	characteristic masonry compressive strength
f_m	mortar compressive strength
$f_t\ f_{t,c}\ f_{t,j}\ f_{t,r}$	tensile strength, of unit crack interface, joint interface, reinforcement
$f_v\ f_{vk}\ f_{vko}$	masonry shear strength, characteristic, initial
$f_{xk1}\ f_{xk2}$	characteristic flexural strength parallel, perpendicular to bed joints
F	force
g_A	design compressive stress
$G\ G_u\ G_m$	shear modulus, of unit, mortar
$G_c\ G_{c,c}\ G_{c,j}$	compressive fracture energy, of unit crack interface, joint interface
$G_f^I\ G_{f,c}^I\ G_{f,j}^I$	mode I fracture energy, of unit crack interface, joint interface
$G_f^{II}\ G_{f,c}^{II}\ G_{f,j}^{II}$	mode II fracture energy, of unit crack interface, joint interface
$h\ h_s\ h_u\ h_m$	height, of specimen, unit, mortar
K	constant used in calculation of masonry compressive strength
$K_t\ K_s\ K_w$	total stiffness, of testing system, masonry wallet
$k_n\ k_{n,c}\ k_{n,j}\ k_{n,r}$	normal stiffness, of unit crack interface, joint interface, reinforced joint
$k_s\ k_{s,c}\ k_{s,j}\ k_{s,r}$	shear stiffness, of unit crack interface, joint interface, reinforced joint
$l\ l_s\ l_u$	length, of specimen, unit
$t\ t_s\ t_u$	thickness, of specimen, unit
$\Delta_t\ \Delta_s\ \Delta_w$	total displacement, of testing system, masonry wallet
$\kappa_p\ \kappa_{p,c}\ \kappa_{p,j}$	plastic strain, of unit crack interface, joint interface

x

$\kappa_1\ \kappa_2\ \kappa_3$	plastic strain in tension, shear (Coulumb friction), compression
$\rho\ \rho_u$	density, of unit
$\sigma_1\ \sigma_2\ \sigma_3$	yield value in tension, shear (Coulomb friction), compression
σ_d	perpendicular compressive stress
$\sigma_u\ \sigma_{u,j}$	confining stress at which dilatancy is zero, of joint interface
$\tau_u\ \tau_{u,j}$	ultimate shear strength, joint interface
$\upsilon\ \upsilon_u\ \upsilon_m$	Poisson's ratio, of unit, mortar
$\phi\ \phi_c\ \phi_j$	friction angle, of unit crack interface, joint interface
$\psi\ \psi_c\ \psi_j$	dilatancy angle, of unit crack interface, joint interface

List of Figures

List of Tables

1 Introduction

The main objective of this study is to bring alternative masonry units, that are already in existence or yet to be developed, closer to acceptance and implementation on the open market, in so doing providing improved walling solutions to South Africa's housing crisis.

1.1 Problem Statement

South Africa has a housing shortage estimated in excess of 2 million units, affecting over 8 million South Africans. This backlog is being addressed predominantly with the construction of 40 m^2 low-cost, single storey, detached government subsidised housing units (Figure 1.1) built with conventional masonry units (CMU's), namely concrete and burnt clay.

Figure 1.1: Boystown social housing, Cape Town (HDA, 2015)

Building with masonry units is the oldest construction form still in popular use today. However, the use of concrete and burnt clay in these large volumes has a significant negative impact on the environment in the form of carbon dioxide emissions and the use of non-renewable natural resources. The South African government's parliamentary ratification of the Paris Agreement has led to the introduction of a carbon tax, which will penalise cement manufacturers. In addition, the thermal performance of conventional masonry walls is generally poor, contributing to occupant discomfort. These factors, and others, have led to the development of alternative masonry units (AMU's) in South Africa, and internationally, with a lesser environmental impact and improved thermal performance.

In developing AMU's, it is necessary to assure the performance and durability of these over the design life of the housing structure. South African standards for CMU's are well established and in common use in South Africa. However, directly applying these established requirements to AMU's would be inappropriate for several reasons:

1

- **Outdated Mechanical Limits:** Current mechanical limits set in the South African prescriptive standards of CMU's are largely based on yield line theory analysis (JSD, 1995), taken from the withdrawn British Standard BS 5628-1 (1978).
- **Adoption of Eurocode 6:** The South African masonry industry is in the process of updating its suite of masonry standards to the EN approach, Eurocode 6 *Design of Masonry Structures*, marking a transition from prescriptive to performance-based standards.
- **Category 1 Buildings:** The Application of the National Building Regulations (NBR) (SANS 10400-A, 2010) has been revised with significant changes, including the introduction of Category 1 buildings, specifically aimed at drawing more low-cost structures into a regulatory framework. Certain serviceability aspects of these structures are more relaxed compared to non-Category 1 buildings.
- **Loading:** The South African loading code (SANS 10160, 2011) was also recently revised, in the form of an adaption of EN 1990 (2002) and EN 1991 (2002+), with notable changes and additions. The design of single storey masonry structures must take seismic loading into account in certain areas of the country and significant improvements have been made to the South African wind data map. These changes could have implications for the response and performance requirements of masonry structures and of masonry units.
- **Advances in Numerical Analyses:** A significant amount of research has been done to better understand the discontinuous behaviour of masonry structures using finite element modelling and these advances need to be accounted for in the specifications for masonry units. Most research has focused on burnt clay and concrete masonry units which exhibit a specific brittle behaviour. AMU's could consist of various materials, exhibiting a range of strengths and stiffnesses and therefore also a range of structural responses.

1.2   Hypothesis

The current South African specifications for conventional masonry units are not appropriate for direct application to alternative masonry units. **Material non-specific, performance-based requirements of masonry units for structural application in Category 1 residential buildings** can be developed, based on the EN specifications for masonry units and methods of test, to facilitate the inclusion of alternative masonry units in the open market.

1.3   Methodology & Outline

The work undertaken to achieve this, is reported in the following chapters:

- **Chapter 2 - Background:** Context and motivation for the study are provided by considering principal facets, namely the South African housing crisis and the current status of development and use of AMU's.

- **Chapter 3 – Legislative Framework:** The regulatory framework governing the use of masonry in South Africa and possible avenues through which AMU's could gain access to the market are explored, followed by a refinement of the hypothesis provided in Section 1.2.

- **Chapter 4 – Masonry Finite Element Modelling:** The main tool employed in assessing the performance of AMU's in this study is the finite element (FE) method, using DIANA FEA software. It is therefore necessary to give an overview of FE modelling as applied to masonry in general, and AMU's specifically, as well as a description of the constitutive material model chosen for this study.

- **Chapter 5 – Input Parameters:** Four masonry materials are selected for the study: conventional concrete (CON) as benchmark and three alternatives, geopolymer (GEO), compressed-stabilised earth (CSE) and adobe (ADB), representing a wide spectrum in terms of strength and stiffness. The results of characterisation tests of the four masonry materials on a unit and wallet scale are used, together with numerical fitting to test data and data taken from literature, to generate the necessary parametric input for the FE model.

- **Chapter 6 – Model Validation:** The results of medium to large-scale in-plane and out-of-plane tests, conducted on single-leaf masonry walls, constructed of the four selected masonry materials, are used for validation of the FE model.

- **Chapter 7 – Numerical Analyses:** Two critical configurations of single-storey bonded masonry walls are generated, based on the provisions of the National Building Regulations. Subsequently, the simplified micro-scale FE model is used to analyse these configurations under serviceability and ultimate limit state loading conditions, to serve as a performance prediction model.

- **Chapter 8 – Deliberation:** Mitigation strategies to improve the performance of the walls are applied to the FE model and recommendations are made to standardise the regulation of AMU's.

- **Chapter 9 – Conclusions and Future Research:** The main conclusions are distilled and, based on the findings of this study, three avenues of research that can be pursued are highlighted.

1.4   Scope & Limitations

The masonry units, walls and their applications under consideration are limited to:
- solid blocks, 290mm long x 140mm wide x 116mm high
- single leaf, single storey, external, unreinforced walls
- Category 1 buildings (SANS 10400-A, 2010)
- H3 & H4 (residential) occupancy classes (SANS 10400-A, 2010)
- structural performance

Other matters, such as durability and environmental impact, although essential in the assessment and promotion of AMU's, are beyond the scope of this study.

2 Background

Background information on aspects salient to the study are provided, including the low-income housing situation in South Africa and the current status of the development and use of AMU's.

2.1 Low-Income Housing

The 'right to have access to adequate housing' is enshrined in Section 26 of the Bill of Rights of the South African Constitution (Constitutional Assembly, 1996). However, the South African built environment remains distinctly segregated into formal and informal sectors, with the informal sector consisting largely of residential dwellings, concentrated on the poor urban periphery (Muringathuparambil, et al., 2017).

Sea Point, Cape Town (Hilton, 2011)   Khayelitsha, Cape Town (Harrison, 2018)

Figure 2.1: Formal and informal sectors of South Africa's segregated built environment

The South African government has provided nearly 3 million subsidised housing units since 1994 (Department of Human Settlements, 2017), and the households residing in subsidised housing has increased from 5.6 % in 2002 to 13.6 % in 2018 (Statistics South Africa, 2018). However, according to the government, a backlog of over 2 million units persists (Sisulu, 2016). Arguably, the number of informal dwellings should rather be used as an indicator of the actual housing crisis in South Africa, putting the housing need at over 25 million units (Laubscher, 2014).

Government subsidised housing units are typically a stand-alone dwelling of 40m^2 (Laubscher, 2014), containing a kitchen, living area, two bedrooms and a bathroom (Figure 2.2), conforming to the definition of 'adequate housing' in the National Housing Code (NHC, 2009). Only households with a combined income of less than R 3 500 (€ 200) per month qualify for government subsidised housing (Department of Human Settlements, 2015), and ownership is transferred to the beneficiary.

(a)   (b)
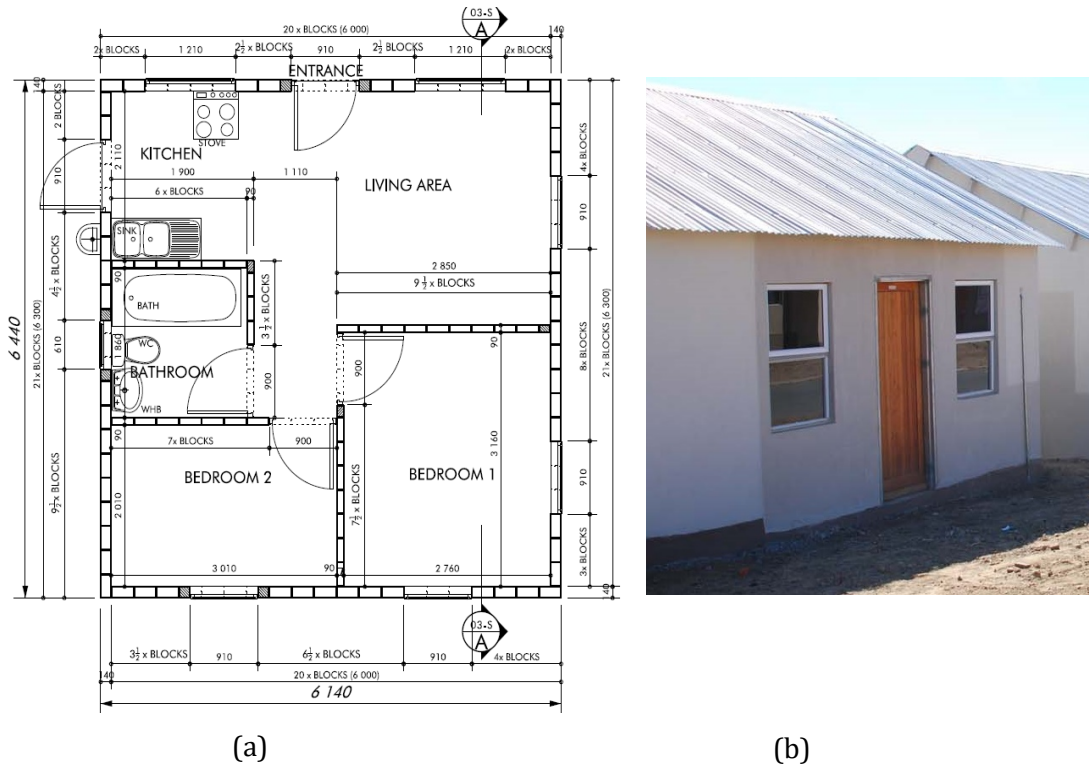
Figure 2.2: Typical 40m² government subsidised concrete masonry house (a) plan (CMA, 2011) and (b) under construction

2.1.1   Category 1 Buildings

In an effort to make buildings that meet regulatory requirements more affordable to low-income communities and to reduce the immense health and safety risk that unregulated informal structures present (Watermeyer, 2004), the Joint Structural Division (JSD) of the South African Institution of Civil Engineers (SAICE) developed a new category of buildings in 2000 (Watermeyer & Milford, 2003). This Category 1 building type was introduced in *The Application of the National Building Regulations: SANS 10400* in 2004.

These buildings are restricted in size and occupancy class. The floor area is limited to 80m², wall lengths to less than 6m between lateral supports and the structure to a single storey with no basement. The wall thickness can be as little as 90mm, compared to 140mm in non-Category 1 buildings (SANS 10400-K, 2011). Occupancy classes are restricted to places of instruction or worship, small shops, offices, dormitories, domestic residences and dwelling houses.

Category 1 buildings also make allowance for lower performance levels with regard to construction accuracy, expected damage, deflections, maintenance, rain penetration and hail resistance, natural lighting and ventilation, in comparison to non-Category 1 buildings (SANS 10400-A, 2010). The differences in performance levels are concentrated around size and serviceability limits and no distinction is made between the categories regarding seismic and wind loading.

It must be noted that, whilst Category 1 buildings were introduced in the NBR to draw a greater proportion of the South African built environment into a regulatory framework, the government, one of the dominant land and building owners in the country (Laubscher, 2014) and the largest role player in housing, is not bound to compliance with the NBR, according to Sections 2(3) and 2(4) of the amended *National Building Regulations and Building Standards Act No 103 of 1977* (2008). However, this does not negate the need for quality low-income housing (LIH).

5

2.1.2 Construction Quality

The LIH sector in South Africa is notorious for its substandard construction quality, despite an abundance of regulation and technical information (Mahachi, et al., 2004). Statistics South Africa found 16% of the government subsidised housing stock to be perceived as defective in their 2013 General Household Survey (Statistics South Africa, 2013). A National Housing Rectification Programme was launched by the Department of Human Settlements (DHS) in 2012, and has spent over R 2 billion (€ 120 million) rectifying substandard constructions. This programme has since been suspended but the then Director General of the DHS, Thabane Zulu, estimated the outstanding rectification bill at R 58 billion (€ 3.5 billion), (Steyn, 2011).

The root causes are wide ranging but can be broadly classified into the following four categories (Sibiya, 2018), (Zuguzane, et al., 2012), (CIDB, 2011):

Lack of Capacity at Government Level

- insufficient grants
- technical staff
- monitoring

Inadequate Quality Control

- management systems
- supervision
- inspections

Non-Compliance by Contractors

- lack of expertise and experience
- unskilled labour
- resource constraints

Corruption

- irregular tender procedures
- theft
- fraud

The majority of structural failures are classified as of the superstructure (42%), followed by foundation settlement (24%), although the former is largely dependent on the latter. In 2002, 73% of the cost of remedial works was spent on the superstructure (Mahachi, et al., 2004). The underlying causes are inadequate soil classification, foundation design and structural detailing. Typical defects in walls (see Figure 2.3) include inadequate connections between internal and external walls, insufficient lintels over large openings and large sections of walls without lateral support (Mahachi, et al., 2004).

Given the economic and social challenges in South Africa, a number of national strategies and policies require that a significant proportion of LIH is constructed by emerging contractors, who often lack the resources and time to develop or attain the requisite skill level (Mahachi, et al., 2004). Perceived or actual reasons for structural defects range from lack of understanding of the NBR, poor workmanship, the use of unsuitable materials and insufficient or inadequate supervision (Zuguzane, et al., 2012).

Since 2002, all state subsidised (and new mortgaged) houses are legally required by the *Housing Consumers Protection Measures Act of 1998* (Act No. 95, 1998) to enrol with the National Home Builders Registration Council (NHBRC), which provides a warranty scheme, insuring the home owner against deficient construction practices. This has resulted in a notable decrease in the frequency of structural deficiencies (Sibiya, 2018). The subsidised housing stock perceived as defective has also reduced from 16% in 2013 to 9% in 2018 (Statistics South Africa, 2018).

However, non-enrolment or late enrolment of subsidised housing projects in the NHBRC warranty scheme, together with a considerable historical backlog of structural defects, ensure that a significant defective housing stock persists (Sibiya, 2018). Apart from the tangible detriment experienced by the housing beneficiaries and tremendous cost of rectification to the government, such deeply entrenched poor construction quality has far reaching, less transparent, effects. For instance, it necessitates the choice of higher material partial factors, compounding the cost of construction across the industry.

Lekwa Municipality, Mpumalanga
(Mkhonto, 2014)

Lekwa Municipality, Mpumalanga
(Mkhonto, 2014)

Victor Kanye Municipality,
Mpumalanga (Mkhonto, 2014)

Victor Kanye Municipality,
Mpumalanga (Mkhonto, 2014)

Nkomazi Municipality, Mpumalanga
(Mkhonto, 2014)

Phoenix, Kwazulu Natal
(Khubisa, 2017)

KwaZulu Natal (KZNDHS, 2010)

KwaZulu Natal (KZNDHS, 2010)

KwaZulu Natal (KZNDHS, 2010)

Figure 2.3: Typical structural defects in LIH due to inadequate construction quality

2.2   Alternative Masonry Units

For the purpose of this study, alternative masonry units (AMU's) are defined as any masonry unit other than what is currently used conventionally in South Africa, in a standardised or regulated manner. The conventionally used masonry units are:

- Autoclaved Aerated Concrete Masonry Units   SANS 50771-4 (2007)
- Burnt Clay Masonry Units   SANS 227 (2007)
- Calcium Silicate Masonry Units   SANS 285 (2010)
- Concrete Masonry Units   SANS 1215 (2008), SANS 50771-3 (2015)

2.2.1 Rationale for AMU's

Concrete, and to a lesser degree burnt clay, are the dominant block materials used in the construction of LIH. The use of concrete and clay in these large volumes has a significant negative impact on the environment. Manufacturing concrete and burnt-clay masonry units consumes vast volumes of limestone, clay and top-soil, all non-renewable resources, the extraction of which alters the natural environment irrevocably (NPC, 2011). Furthermore, the production of both cement and burnt clay bricks are energy intensive processes (Venkatarama Reddy & Jagadish, 2003) and release large amounts of carbon dioxide (CO_2) into the atmosphere (WBCSD, 2009). The production of cement alone accounts for roughly 5-8% of the world's CO_2 emissions (Benhelal, et al., 2013), (Olivier, et al., 2012), in large part due to the decomposition of the limestone in the calcination process (WBCSD, 2009).

In an effort to honour the commitments made in being a signatory to the Paris Agreement, the South African government is in the process of introducing a carbon tax (Department of National Treasury, 2018), which will penalise cement manufacturers for their CO_2 emissions, increasing the cost of concrete masonry units. In addition, the thermal performance of conventional masonry walls is generally poor (Al-Jabri, et al., 2005), contributing to occupant discomfort. These factors, and others, have led to the development of AMU's in South Africa, and internationally, with a lesser environmental impact and improved thermal performance.

Masonry construction is not the only solution to providing affordable, durable, comfortable housing, but the perception that brick-and-mortar represents the pinnacle of quality housing is deeply entrenched in South African society. Most alternative housing or walling systems available in South Africa have not experienced significant uptake and only 0.6% of government subsidised LIH built between 1994 and 2010 made use of a walling system other than masonry (Department of Human Settlements, 2010).

The primary barriers to the implementation of alternative walling systems in South Africa are the perceived inferiority of these systems compared to masonry, a general lack of advanced construction skills to erect these systems and the inability of these systems to accommodate future additions as easily as masonry does (Boshoff, et al., 2013). Since government LIH is intended as a starter house, this inability to accommodate additions economically is a considerable limitation and disadvantage for the beneficiary (Van Wyk, 2010). For these reasons this research is concentrated on advancing the use of AMU's specifically, as opposed to alternative walling systems in general.

2.2.2 Types of AMU's

Research into and development of more sustainable AMU's can be divided into three broad categories:

- unfired soil-based blocks;
- clay bricks or concrete blocks incorporating recycled industrial or post-consumer waste or by-products;
- blocks created predominantly or wholly from recycled industrial or post-consumer waste or by-products.

The soil-based blocks are typically adobe or earth blocks which incorporate mechanical, physical and/or chemical stabilisation of the soil. Mechanical stabilisation is done in the form of compaction, physical stabilisation by correct proportioning of soil types and chemical soil stabilisation ranges from the ancient use of animal dung, plant juices or naturally occurring oils to the relatively modern addition of hydraulic lime or cement (Hossain & Mol, 2011).

The waste materials used in the latter two AMU categories include fly ash, granulated blast furnace slag, welding flux slag, mine tailings, construction and demolition waste, cement kiln dust, volcanic ash, harbour sediments, foundry sand, granite and marble waste and sawdust, limestone dust, wood sawdust, sugarcane bagasse ash, rice husk ash, cotton waste, straw fibres, processed waste tea, glass, perlite, polystyrene foam and fabric, plastic fibre, rubber, sewage treatment residue and sludge, paper processing residues and waste paper pulp, textile effluent treatment sludge, cigarette butts and many others. See Raut et al. (2011), Shakir and Mohammed (2013) and Zhang (2013) for comprehensive reviews.

2.2.3   Barriers to AMU's

In the development of AMU's, the two main considerations by most researchers are the compressive strength and water absorption (Zhang, 2013), since the largest obstacles to the uptake of soil-based AMU's in particular are poor strength and durability in the wet state (Bahar, et al., 2004), (Burroughs, 2006), (Millogo & Morel, 2012), (Maskell, et al., 2014). Despite many AMU's meeting the specifications set for conventional blocks, the production of AMU's on a commercial scale is still limited. Reasons for this include difficulties with new production methods, contamination risks associated with the use of waste materials, slow acceptance of nonconventional products by the public, resistance by established producers in protecting their vested interest and **lack of standards in the form of performance criteria** and production and construction guidelines, (Walker, 1995), (Zhang, 2013). Pursuing alternative material solutions therefore typically results in major approval delays (Greenwood, 2012), and hence impeded construction and project delivery.

The general assumption regarding the structural behaviour of alternative masonry is that it is comparable to conventional masonry behaviour (Tennant, et al., 2013). Especially soil-based blocks with a high cement or binder content can be considered to behave similarly to commercial concrete blocks and can be structurally designed as such (Heath, et al., 2012). However, understanding and knowledge of the structural behaviour of alternative masonry is sparse, especially regarding the out-of-plane response (Tennant, et al., 2013).

Over time, certain structural behavioural aspects have solidified themselves as fact. For example, the seismic response of soil-based masonry structures is considered particularly poor due to the low tensile strengths of the material (Silva, et al., 2012), but these observations do not constitute a thorough understanding of the structural behaviour of alternative masonry. Symptomatic of this lack of understanding is the exclusion of AMU's from the scope definition of internationally accepted masonry design standards, such as Eurocode 6 (Illampas, et al., 2011). In-depth investigation into the structural behaviour of AMU's is necessary for their advancement.

2.3   Summary

Despite extensive provision of government-subsidised LIH over more than two decades, South Africa's residential built environment remains starkly segregated and the quality of construction in the LIH sector is particularly poor, due to a confluence of factors. Category 1 buildings, with lesser serviceability limits, were introduced in the South African NBR to allow a greater proportion of the housing stock to meet regulatory requirements.

Within this context, alternative walling solutions to CMU's are sought to reduce the environmental impact of LIH and improve the thermal comfort of their occupants. Specifically AMU's are considered the most realistic and viable option, given the deep entrenchment of block-and-mortar housing in South African society. Much research has been conducted internationally in the pursuit of AMU development but common obstacles to their uptake are a lack of standards and understanding of their structural behaviour. Further research into these aspects is needed to advance the use of AMU's.

3 Legislative Framework

Background to performance-based regulations and the regulatory context, within which AMU's need to gain entry into the South African market, are outlined in this chapter, together with possible avenues for the inclusion of AMU's within these regulations. This is followed by a review of the current masonry standards applicable in South Africa. Sections 3.1 and 3.2 of this chapter are based on a previous publication by the author (De Villiers, 2012).

3.1 Performance-Based Regulations

Many building material related regulations in South Africa are prescriptive. These regulations enforce consistency and reliability by means of applying a set of rules (May, 2003). They are restrictive and bureaucratic by nature, allowing little scope for innovation, but are straight forward in interpretation and application, thereby also allowing less room for error. By comparison, performance-based regulations, such as the *South African National Building Regulations and Building Standards Act* (Act No. 103, 1977), are focused on what the required level of performance of a building or material is, rather than stipulating how this level is to be achieved. A long history of applying performance-based regulations to housing exists.

3.1.1 Background

The first building code on record, known as the Hammurabi Code, accredited to Babylonian King Hammurabi (1955 – 1913 BC) stipulates the structural safety performance of a house: "Article 229: The builder has built a house for a man and his work is not strong and if the house he has built falls in and kills a householder, that builder shall be slain," (Foliente, 2000). It is clear how the constructed house is expected to perform, but no specifications are given as to how or with what materials this house is to be constructed.

The United States National Bureau of Standards, already recognized the value of performance-based regulations in 1925, in their report 'Recommended Practice for Arrangement of Building Codes', warning that prescriptive requirements hinder progress in the construction industry by excluding new materials or new uses of conventional materials (Foliente, 2000). This was followed up in the 1960's when the US Department of Housing and Urban Development produced a Performance Criteria Resource Document for Innovative Construction (NBS, 1977), to encourage the use of innovative housing systems (Foliente, 2000).

Over the last three decades, a number of countries have or are in the process of transitioning their building regulations, especially with regard to housing, from a prescriptive to a performance basis, generally in response to frustrations with the bureaucracy of a prescriptive system: Australia, Austria, Canada, China, Japan, Netherlands, New Zealand, Norway, Singapore, Spain, Sweden and the United Kingdom (Meacham, 2010).

In more recent years, Technical Sub-Committee TC 59/SC 15 of the International Organization for Standardization (ISO) developed a set of methods to describe the performance of houses, covering structural safety (ISO 15928-1, 2015), serviceability (ISO 15928-2, 2015) and durability (ISO 15928-3, 2015). These standards set out how to qualitatively describe the expected performance of a house, but they do not specify quantified performance levels or criteria.

3.1.2   Developing Performance-Based Standards

The development of performance-based regulations worldwide is generally modelled on the Nordic 5 level system (Foliente, 2000). It was first developed by the Nordic Committee on Regulations in 1963, to harmonize the building regulations of the Nordic countries (Oleszkiewicz, 1994). The Nordic system has gained much recognition and was adopted by the United Nations Economic Commission for Europe as a basis to harmonize building regulation systems. The EU is investing considerably in this process, to facilitate free trade (Burkowski, 2003).

The Nordic model, shown in Table 3.1, describes a 5-tier hierarchy, according to which qualitative performance objectives (Level 1) and functional statements (Level 2) are translated into quantitative performance requirements (Level 3), compliance methods (Level 4) and deemed-to-satisfy-rules or acceptable solutions (Level 5). This table also illustrates how the Nordic model is applied in the South African building regulation context, since the NBR are performance-based in nature (Watermeyer & Milford, 2003) and were also modelled on the Nordic 5 tier system (Reynolds, 2007). Indeed, one of the stated aims of SANS 10400 is to "assist rather than impede the use of innovative building systems and designs".

Table 3.1: Nordic 5-level hierarchy applied to the South African context

Level	Description	South African Building Regulation Context
1	Objective	National Building Regulations and Building Standards Act 103 of 1977
2	Functional Statement	National Building Regulations 1999
3	Performance Requirement	SANS 10400: The Application of the National Building Regulations
4	Performance-Based Compliance Methods	South African Bureau of Standards; Council for Scientific and Industrial Research; Agrément South Africa; rational design
5	Deemed-to-Satisfy or Acceptable Solutions	SANS 10400: The Application of the National Building Regulations

As an example, the Level 2 functional statement for structural strength and stability for walls (K1) in the NBR (SANS 10400-K, 2011) reads as follows:

> "Any wall shall be designed and constructed to safely sustain any actions which can reasonably be expected to occur and in such a manner that any local damage (including cracking) or deformation do not compromise the opening and closing of doors and windows or the weather tightness of the wall and in the case of any structural wall, be capable of safely transferring such actions to the foundations supporting such wall."

The Level 3 performance requirements were considered understated or generally lacking for the South African building regulation context (Watermeyer & Milford, 2003). Since the revision of SANS 10400, in particular Part B (2012), the functional statements concerning structural strength and stability of buildings have been translated to quantified performance parameters to some extent. These are discussed further in Section 3.2.3.

The development of appropriate performance standards creates the essential link between the qualitative performance objectives and quantitative performance criteria. *ISO 6240 Performance Standards in Buildings* (ISO 6240, 1980) requires that each performance requirement be defined in terms of specific properties, typically provided in a performance specification standard (Burkowski, 2003), and have methods specified in which these properties can be assessed, in a so-called performance statement standard (Burkowski, 2003). Identifying commonalities and opportunities for integration in standards and developing product evaluation protocols is essential in removing barriers to implementing innovation (Sanjuán, et al., 2011).

In most countries that are transitioning to performance-based building regulations, allowance has been made for a mixed approach, providing performance objectives, together with deemed-to-satisfy solutions, in the interest of reducing disruption and allowing an evolutionary transition process. Alternative solutions are required to deliver a performance level equal or superior to that of a deemed-to-satisfy solution, as is the case in South Africa.

The deemed-to-satisfy solutions entrenched in most countries' transitioned building regulations implicitly represent society's expectation of a building's performance level. The first step in attaining quantifiable and verifiable performance criteria is to translate this implicit building performance level into quantitative metrics (Meacham, 2010). Furthermore, verification methods and predictive models capable of developing quantitative performance criteria and designing or evaluating the performance of buildings, components or products are essential to the advancement and implementation of performance standards (Foliente, 2000). Currently, these predictive models are largely lacking (Burkowski, 2003).

3.1.3   Strengths and Weaknesses

Performance-based regulations define the functional and performance expectations, as opposed to prescribing specific solutions, making flexibility and responsiveness their greatest strengths. This in turn encourages the diffusion of innovative materials and technologies and allows for faster adaptation to a society's changing needs, such as improved resilience, response to climate change, sustainability and demographic shifts (Meacham, 2010). Buildings can be designed to better satisfy the specific client's operative requirements whilst still satisfying society's expectations in terms of safety. The building regulations of a country also directly impact its industries' ability to operate on an international stage. Adopting a performance-based approach significantly reduces trade barriers and improves transparency in this sphere. The World Trade Organisation's Technical Barriers to Trade Agreement, signed in 1997, of which South Africa is a signatory, commits all Members to "specify technical regulations based on product requirements in terms of performance rather than design or descriptive characteristics" (WTO, 1997).

The Achilles heel of performance-based regulations is the transformation of vague performance objectives into quantifiable performance criteria (May, 2010). Too often professional judgement of the designer is heavily relied upon, to accurately predict the performance of a material or technology, particularly in aspects such as forecasting durability (May, 2010). Additional shortcomings are often the lack of accountability (May, 2010) and insufficient support from regulators and local authorities (Meacham et al, 2005). A general lack of critical assessment of performance-based regulations (May, 2010) compounds the problem.

Not all instances of countries transitioning to performance-based regulations have been entirely successful. The most notable example is the case of the "leaky building crisis" in New Zealand, where a significant number of timber-framed buildings with fixed claddings were not weather-tight, leading to rotting structures. As to be expected, this was due to the confluence of a number of factors, including cost-cutting, substandard workmanship and ineffective supervision. Furthermore, the factors related to the recently introduced performance-based regulations included: qualitative, as opposed to quantitative requirements statements in the code, substantial dependence on expert interpretation and insufficient scrutiny by authorities (Meacham, 2010). Significantly, New Zealand was one of the first countries to adopt a performance-based building code, and suffered the consequences of inexperience. However, their performance-based building code was subsequently revised and there was no call to revert to a prescriptive regulatory system.

Despite the shortcomings, it is still argued that a performance-based regulatory framework will ultimately produce a preferable solution, due to the greater freedom of choice in materials and systems, provided that the regulations are applied correctly (Sexton & Barrett, 2005). This freedom of choice and flexibility has led to the use of performance-based regulations gaining support internationally.

3.2 South African Building Regulations

Upon occupation of the Cape of Good Hope as a refreshment station in 1652, the United East India Company instructed Cape Governor Jan van Riebeeck to construct 3.75m high earth ramparts to mount canons (Laubscher, 2011). This could be considered the first documented prescriptive building specification in South Africa. Since the earth on site was ill-suited and the Company instruction 'did not specify alternative solutions', the structures ultimately collapsed due to heavy rain; the first failure of a prescriptive building specification in South Africa (Laubscher, 2011).

Over three centuries later, a number of acts have been promulgated in support of South Africans' constitutional right to access to adequate housing, that impact on the design and construction of housing:

- *National Building Regulations and Building Standards Act of 1977* (Act No. 103, 1977)
- *Housing Consumers Protection Measures Act of 1998* (Act No. 95, 1998)
- *Occupational Health and Safety Act of 1993* (Act No. 85, 1993)
- *Construction Industry Development Board Act of 2000* (Act No. 38, 2000)
- *Consumer Protection Act of 2008* (Act No. 68, 2008)
- *National Regulator for Compulsory Specifications Act of 2008* (Act No. 5, 2008)
- *Agrément South Africa Act of 2015* (Act No. 11, 2015)

The structural design of housing in South Africa is regulated by the NBR, first published in 1985 by the South African Bureau of Standards (SABS), but since updated a number of times to the current edition SANS 10400 (2010). The NBR are based on the *National Building Regulations and Standards Act of 1977* (Act No. 103, 1977), and are performance-based in nature. However, the NBR contain extensive deemed-to-satisfy solutions, the typical mixed approach taken in transitioning from prescriptive to performance-based regulation.

On a practical level, all housing construction in South Africa, low-income or otherwise, is regulated by the National Home Builders Registration Council (NHBRC), the establishment of which is enshrined in *The Housing Consumers Protection Measures Act* (Act No. 95, 1998), (NHBRC, 2015). The NHBRC is mandated by this act to protect the interests of housing consumers, in particular those in the subsidy housing sector (Act No. 95, 1998, 3j) and stipulates general home building technical requirements and guidelines in the form of the *Home Building Manual and Guide* (*Home Building Manual* for short). This manual is based on Act No. 103 (1977) as well.

The first *Home Building Manual* (1999) was revised in 2015 due to changes in relevant standards (such as the introduction of Category 1 buildings in the NBR) and in response to building technology innovations. It is noteworthy that the *Home Building Manual* Committee, responsible for the revision, contained representatives from every relevant sphere, except masonry. Notable aspects that have been addressed to some extent in the revision are performance descriptions and performance parameters for structural strength and stability. These are largely adopted from the NBR, leading to significant duplication between these documents.

Both the NBR and the *Home Building Manual* rely on normative reference standards for the material-specific design aspects, which are typically prescriptive in nature. In broad terms, the structural building materials and systems provided for are concrete foundations, masonry walling and timber roof constructions. If a non-standardised material or system is to be used in the building of a house, the NBR (SANS 10400-B, 2012) prescribe that the material or system be evaluated against performance-based criteria or a competent (professionally registered) person must submit a rational design or assessment of the system. Use of a non-standardised material or system is permitted, provided that the local authority is satisfied that it is at least as suitable for the intended purpose as a standardised material or system (SANS 10400-A, 2010).

3.2.1 Certification

The primary body performing assessments of non-standardised building materials or systems in South Africa is Agrément South Africa (ASA), established in 1969 under the delegated authority of the Minister of Public Works. However, only in 2008 was Agrément certification introduced in the NBR as a means of demonstrating compliance. ASA became a separate legal entity in 2018 under the *Agrément South Africa Act* (Act No. 11, 2015), is funded by the Department of Public Works (R29 million or €1.8 million in financial year 2017/2018) and is a member of the World Federation of Technical Assessment Organisations (WFTAO), (Agrément, 2018). ASA is mandated to promote innovative building products, protect consumers against unacceptable ones and establish fitness-for-purpose by testing of non-standardised products against performance-based criteria (Agrément, 2019).

The aspects that may be taken into consideration during an Agrément certification process are structural strength and stability, behaviour in fire, water penetration, thermal performance, durability and the maintenance required, the likelihood of condensation forming on the inside of the building, acoustic performance and the applicant's quality system (Agrément, 2019). To have a building product certified by Agrément can cost up to R 300 000 and the assessment process generally takes 6 months (Ndamashe, 2019).

Practically, ASA operates in conjunction with the Council for Scientific and Industrial Research (CSIR), located in Pretoria. A clear distinction is made between the roles of the CSIR and ASA; the CSIR focuses on research and development of new technologies and developing the performance criteria and test methods used during an Agrément certification. Agrément administers the certification process and maintains an up to date register of active certificates. Currently there are 98 active and 48 inactive walling and building systems registered (Agrément, 2019).

In terms of walling products, Agrément certification is currently only available for whole structural or walling systems, and no performance-based criteria have been developed for masonry units. Block-based walling systems that have been certified include BESA, Dri-Block (dry-stack concrete block walls), Hydraform (dry-stacked and mortar bedded soil-cement blocks), Compressed Earth Blocks Building System, Benex Masonry and Everite Hebel AAC. Naturally, the use and application of a certified system is bound to the scope, limitations and conditions as set out in the certificate (SANS 10400-B, 2012). This places stringent limitations on the application scope when an AMU-based system is certified by ASA.

A point of discrepancy between the NBR and the *Home Building Manual* is the matter of certification by bodies other than ASA. In the recent revision, the *Home Building Manual* deems certification by Agrément or by a registered certification body as demonstrating compliance (NHBRC, 2015). The NBR allows local authorities to call for additional test reports by the SABS or CSIR or an Agrément certification (SANS 10400-A, 2010), which are automatically deemed to satisfy the NBR requirements. Test reports from other institutions, such as universities or private laboratories, may also be considered but are not automatically deemed to satisfy or demonstrate compliance.

3.2.2 Competent Person Assessment

The alternative to having a non-standardised building system certified, is for a competent person to carry out a rational design, rational assessment or both. A competent person (SANS 10400-B, 2012), with respect to structures, is a person who

> *"a) is registered in terms of the Engineering Profession Act, 2000 (Act No. 46 of 2000), as either a Professional Engineer or a Professional Engineering Technologist, and*
>
> *b) is generally recognized as having the necessary experience and training to undertake rational assessments or rational designs in the field of structural systems."*

A rational design (SANS 10400-B, 2012) is a design carried out by a competent person involving one or a combination of reasoning and calculation grounded in engineering first principles and research, based on relevant standards or authoritative literature, experience, tests and analyses. The same principles are applied to a rational assessment (SANS 10400-B, 2012) to determine whether the performance of a solution is adequate. In both instances, a similar finding or solution should be arrived at by a peer review of the structural system. The design or assessment process must demonstrate compliance with the NBR, be appropriately documented, kept on record, and made available on demand of the owner or local authority for a period of 10 years.

3.2.3 Current Performance Criteria

One of the main criticisms of performance-based regulations is the lack of or inadequate quantification of performance criteria. The average compressive strengths of masonry units are prescribed, detailed in Table 3.2, but beyond those, no performance criteria exist for masonry units, conventional or alternative. Stellenbosch University has been approached in the past by ASA and the CSIR for consultation on the assessment of alternative masonry units (Van Der Klashorst, 2015), reinforcing that the need exists for performance-based criteria for AMU's.

Table 3.2 Masonry unit compressive strengths (SANS 10400-K, 2011)

Average Compressive Strength [MPa]	Solid Units	Hollow Units
Single storey or upper storey of double-storey buildings	4.0	3.0
Lower storey in double-storey building	10.0	7.0

However, performance parameters have been defined to some extent for housing structures or walling systems in the NBR and been taken up in the *Home Building Manual* and Agrément certification process. The pertinent NBR and *Home Building Manual* structural performance criteria are summarised according to Category 1 and non-Category 1 Buildings in Table 3.3.

Table 3.3 NBR and *Home Building Manual* structural performance criteria (SANS 10400-A, 2010), (SANS 10400-B, 2012), (SANS 10400-K, 2011), (NHBRC, 2015)

Technical Aspect SANS 10400	Non-Category 1 Building	Category 1 Building	SANS 10400	NHBRC
Structural System Design Life	≥ 30 years*	not specified	B – 4.2.1.1	2.1.2.1 a)
Replaceable Components Design Life	≥ 15 years*	≥ 10 years	B – 4.2.1.1	2.1.2.1 b)
Maintenance Cycle	≥ 5 years	more frequent	B – 4.2.1.7	-
Structure Tilt	1:200	1:100 (1:120 in NHBRC)	B – Table 2	Table 4
Structure Settlement	10mm (20mm in NHBRC)	20mm (30mm in NHBRC)	B – Table 2	Table 4
Roof Deflection	1:250	1:175	B – Table 2	Table 4
Wall Deflection	1:250	1:175	B – Table 2	-
Floor Deflection	1:250	1:175	B – Table 2	Table 4
Sharp Body Impacts	4.2J	5.3-7.9J	B – Table 3	Table 3
Soft Body Impacts	130-410J	130-410J	B – Table 3	Table 3

* The Building *Structural System Design Life* and *Replaceable Components Design Life* for Non-Category 1 Buildings do not correspond to the those specified in Table 1 of SANS 10160-1 (2018) of 50 years and 25 years respectively.

15

Masonry walling performance criteria are quantified in the NBR and *Home Building Manual* in Table 3.4 in terms of crack widths, ease and level of repair required and functional and visible impairment. These criteria were originally developed by Watermeyer and Tromp (1992), based on the Australian Standard AS 2870 (1986) and the work of Giles (1985), Burland et al. (1978), and Jennings and Kerrich (1963).

The intention behind formulating these criteria was to provide quantified guidance on serviceability limits for masonry walls and concrete floors (Watermeyer & Tromp, 1992), which were lacking at the time. The authors' focus is on serviceability limits, arguing that excessive deflections, which cause typical serviceability issues such as sticking doors and rupturing pipes, only transpire after cracking has occurred and that it is improbable that they will arise from lateral load applications such as wind. Watermeyer and Tromp recommended that significant damage should not be permitted, hence the exclusion of damage categories 3 and higher from the NBR. Notably, the *Home Building Manual*, perhaps from a practical perspective, includes the significant damage categories.

Table 3.4 NBR and *Home Building Manual* masonry walling performance criteria (SANS 10400-B, 2012), (NHBRC, 2015)

Damage Description	Approximate Max Crack Width in Wall [mm]	Expected Damage Category	SANS 10400-B	NHBRC
Categories 0 to 2: Minor Damage				
Hairline cracks	< 0.25	0 – Negligible		
Fine internal cracks				
External cracks rarely visible	< 1	1 – Very Slight		
Internal cracks easily filled			Table 4	Table 5
Redecoration probably required				
Recurrent cracks masked	< 5	2 – Slight		
External cracks not necessarily visible				
Doors and windows stick slightly				
Categories 3 to 5: Significant Damage				
Cracks can be repaired				
Small amount of masonry replaced	5 – 15	3 – Moderate		
Doors and windows sticking				
Weather tightness impaired				
Extensive repair work				
Replacing wall sections			-	Table 5
Window and door frames distorted	15 – 25	4 – Severe		
Walls leaning and bulging				
Major repair work, partial rebuilding				
Walls tilt badly	> 25	5 – Very Severe		
Danger of instability				

For the Agrément certification of walling systems, full-scale walls are constructed and tested for structural strength and stability according to the following loading procedure (Agrément, 2002):

- Service and ultimate loads are determined based on SABS 0160:1989 (withdrawn loading code)
- Preload: 25% of service load applied, all loads released
- Load Cycle 1: full service load applied, deflections measured, all loads released
- Load Cycle 2: full service load applied, deflections measured, all loads released
- Load Cycle 3: full ultimate load applied, deflections measured, all loads released

The performance criteria for structural strength and stability for this Agrément test are as follows (Agrément, 2002):

- Load Cycle 2 deflection shall not exceed Load Cycle 1 deflection by more than 10%
- Load Cycle 2 deflection shall not be greater than the finished wall thickness
- Structure shall not collapse under Load Cycle 3, i.e. if a piece > 500g breaks away or becomes permanently detached from the structure

Additionally, the Agrément performance criteria include soft body impact on masonry of 176 – 530J and sharp body impact of 5.3-7.9J. In both instances these values are similar, but not identical, to the ones specified in the NBR and the *Home Building Manual* (see Table 3.3)

3.2.4   Summary

Performance-based criteria for structural walling systems have been developed to some extent for the functional statements contained in the *National Building Regulations,* which provide a basis against which to assess a non-standardised walling system. However, whether by Agrément certification or rational design/assessment, both regulatory options available for alternative building systems are expensive and laborious, especially in the context of low-income housing construction and are seldom realised (Department of Human Settlements, 2010).

Additionally, this regulatory framework forces AMU's to be assessed on a structural scale, for specific contexts, including the destructive testing of large scale walls, leading to significant limitations on their scope of application.

3.3   South African Masonry Standards

Following the adaption of the Eurocode into the *South African Loading Code SANS 10160* in 2010, the South African structural materials standards are following suite in the interest of harmonization (Dunaiski, et al., 2010). Development of these standards is undertaken by the engineering profession on a voluntary basis. Thus, the South African masonry industry is in the process of adopting the European suite of masonry standards, overseen by SABS Technical Committee 098/SC 05. At present, two masonry unit standards and the masonry structural design set have been adopted and published in the form of *SANS 50771-3* (2015) – *Aggregate concrete masonry units*, *SANS 50771-4* (2007) – *Autoclaved aerated concrete masonry units* and *SANS 51996* (2018) - *Eurocode 6: Design of masonry structures*. The adoption of the supporting materials, unit, testing and construction standards is probable but undecided (Byron, 2019), resulting in a regulatory environment which is currently in flux, which presents both challenges and opportunities. The following subsections are structured along four facets: units, testing, application and material partial factors, to clarify the status of South African masonry standards.

3.3.1   Unit Regulations

The current South African National Standards (SANS) for masonry units cover burnt clay, calcium silicate, concrete masonry and autoclaved aerated concrete (AAC). The EN suite of specifications for masonry units makes additional provision for manufactured and natural stone materials, as detailed in Table 3.5. Following the adoption of EN 771-3 (2011), the withdrawal of SANS 1215 (2008) was requested in 2015 by the Concrete Manufacturers Association and the Joint Structural Division of the South African Institution of Civil Engineers, (CMA, 2016(a)) (CMA, 2016(b)), but both SANS 1215 and SANS 50771-3 are currently in operation, the former used predominantly.

Table 3.5: Proposed EN and current SANS standards for masonry units

Proposed EN for South Africa		Current SANS Standard	
Standard	***Specification for masonry units***	**Standard**	**-**
EN 771-1	*Clay masonry units*	**SANS 227:2007**	*Burnt clay masonry units*
EN 771-2	*Calcium silicate masonry units*	**SANS 285:2010**	*Calcium silicate units*
EN 771-3	*Aggregate concrete masonry units (dense and lightweight aggregates)*	**SANS 1215:2008**	*Concrete masonry units*
		SANS 50771-3:2015	*Aggregate concrete masonry units (dense and lightweight aggregates)*
EN 771-4	*Autoclaved aerated concrete masonry units*	**SANS 50771-4:2007**	*Autoclaved aerated concrete masonry units*
EN 771-5	*Manufactured stone masonry units*	-	
EN 771-6	*Natural stone masonry units*	-	

The most important distinction between the SANS and EN material standards is the prescriptive nature of the former and the performance-based nature of the latter. Pertinent differences between the two material standards sets are summarised in Table 3.6 and the shift from prescriptive to performance-based is clear. The current SANS standards prescribe the compressive strength and the degree of efflorescence, a simple but limiting system for both the manufacturer and designer. In contrast, the EN standards set no specific limits (except salt content for clay, minimum compressive strengths for calcium silicate and AAC and maximum dimensions for AAC), thereby requiring more onerous testing by the manufacturer and decision-making by the designer but simultaneously creating a distinctly more flexible regulatory framework. It should be noted there is a significant amount of repetition between the subsections of EN 771 for the different masonry unit types, which could be streamlined.

Table 3.6: Differences between SANS and EN standards for masonry units

	EN 771	SANS 227, 285, 1215
Dimensions	Declared by manufacturer to EN 772-16 as work size (length x width x height), max dimensions for AAC $l ≤ 1500mm$, $w ≤ 600mm$, $h ≤ 1000mm$ manufactured stone l & $h ≤ 650mm$ natural stone $w > 80mm$	Stated by manufacturer as work size (length x width x height), nominal dimensions recommended l: 190-390mm w: 90-190mm (clay & concrete) w: 90-100mm (CS) h: 90-190mm
Density	Declared by manufacturer to EN 772-13, EN 1936 when applicable	-
Compressive strength	Declared by manufacturer to EN 772-1: mean or characteristic & normalized compressive strength when applicable, Category I / II, min values specified for: CS ≥ 5.0 N/mm² AAC ≥ 1.5 N/mm² manufactured stone ≥ 13.0 – 20.0 N/mm²	Nominal (& individual) compressive strength specified: clay ≥ 3.5 – 17.0 N/mm² CS ≥ 7.0 – 35.0 N/mm² concrete ≥ 3.5 – 21.0 N/mm²
Flexural strength	Declared by manufacturer to EN 772-6, EN 12372 when applicable (concrete & natural stone only)	-
Shear bond strength	Declared by manufacturer to EN 1052-3 or fixed values	-
Flexural bond strength	Declared by manufacturer to EN 1052-2 (concrete, manufactured stone & natural stone only)	-
Thermal properties	Declared by manufacturer to EN 1745 when applicable or declare density & configuration	-
Freeze/thaw resistance	Declared by manufacturer when applicable (no EN available except for CS to EN 772-18, natural stone to EN 12371)	-
Water absorption	Declared by manufacturer to material specific EN 772-7, -11, -21 manufactured stone < 9.0g/m²s	Limits agreed between supplier & purchaser
Active soluble salts	Declared by manufacturer to EN 772-5, salt content limits specified (clay only)	Limits agreed between supplier & purchaser
Moisture movement	Declared by manufacturer to material specific EN 772-14, -19, EN 680 when applicable	Limits agreed between supplier & purchaser
Water vapour permeability	Declared by manufacturer to EN 1745 or EN ISO 10456, EN ISO 12572 when applicable	-
Open porosity	Declared by manufacturer to EN 1936 (natural stone only)	-
Efflorescence	-	Degree of efflorescence limits set according to visual inspection
Reaction to fire	Declared by manufacturer to EN 13501-1 when applicable	-
Test methods	Separate suite (see Table 3.7)	Various (see Table 3.7)

Note: AAC   autoclaved aerated concrete

           CS   calcium silicate

3.3.2 Testing Regulations

There is no coherent suite of test method standards in the current SANS configuration. Test methods are provided in a fragmented manner (Crofts, 2014) in the various materials and structural design standards, as illustrated in Table 3.7 for masonry units and in Table 3.8 for masonry.

Table 3.7: Proposed EN and current SANS standards for test methods for masonry units

Proposed EN for South Africa		Current SANS Standard Section
Standard	*Methods of test for masonry units*	*-*
EN 772-1	*Determination of compressive strength*	*SANS 227 (6.6); SANS 285 (6.5); SANS 1215 (5.5)*
EN 772-2	*Determination of percentage area of voids in masonry units*	*-*
EN 772-3	*Determination of net volume and percentage voids of clay masonry units by hydrostatic weighing*	*-*
EN 772-4	*Determination of real and bulk density and of total and open porosity for natural stone masonry units*	*-*
EN 772-5	*Determination of the active soluble salts content of clay masonry units*	*SANS 227 (6.10)*
EN 772-6	*Determination of bending tensile strength of aggregate concrete masonry units*	*-*
EN 772-7	*Determination of water absorption of clay masonry damp proof course units by boiling water*	*SANS 227 (6.9) (only of non-damp proof course units)* *SANS 10164-1 (6.5) (Determination of water absorption of clay bricks)*
EN 772-9	*Determination of volume and percentage of voids and net volume of clay and calcium silicate masonry units by sand filling*	*-*
EN 772-10	*Determination of moisture content of calcium silicate and autoclaved aerated concrete units*	*-*
EN 772-11	*Determination of water absorption of aggregate concrete, manufactured stone and natural stone masonry units due to capillary action and the initial rate of water absorption of clay masonry units*	*SANS 10164-1 (6.6) (Determination of initial rate of absorption)*
EN 772-13	*Determination of net and gross dry density of masonry units (except for natural stone)*	*-*
EN 772-14	*Determination of moisture movement of aggregate concrete and manufactured stone masonry units*	*-*
EN 772-15	*Determination of water vapour permeability of autoclaved aerated concrete masonry units*	*-*
EN 772-16	*Determination of dimensions*	*SANS 227 (6.4); SANS 285 (6.4); SANS 1215 (5.3)*
EN 772-18	*Determination of freeze-thaw resistance of calcium silicate masonry units*	*-*
EN 772-19	*Determination of moisture expansion of large horizontally perforated clay masonry units*	*SANS 227 (6.11)*
EN 772-20	*Determination of flatness of faces of masonry units*	*SANS 227 (6.5)*
EN 772-21	*Determination of water absorption of clay and calcium silicate masonry units by cold water absorption*	*SANS 227 (6.9) (burnt clay only)*

Table 3.8: Proposed EN and current SANS standards for test methods for masonry

Proposed EN for South Africa		Current SANS Standard	
Standard	***Methods of test for masonry***	**Standard**	***Structural use of masonry – unreinforced masonry walling***
EN 1052-1	*Determination of compressive strength*	**SANS 10164-1**	*6.3 Determination of characteristic compressive strength of masonry*
EN 1052-2	*Determination of flexural strength*	**SANS 10164-1**	*6.4 Determination of characteristic flexural strength of masonry*
EN 1052-3	*Determination of initial shear strength*	**-**	
EN 1052-4	*Determination of shear strength including damp proof course*	**SANS 10164-1**	*6.9 Determination of short term shear strength at damp-proof courses*
EN 1052-5	*Determination of bond strength by the bond wrench method*	**SANS 10164-1**	*6.7 Determination of bond strength of brickwork*
-		**SANS 10164-1**	*6.8 Determination of flexural bond strength of damp-proof courses*

A detailed comparison of the various test methods is not presented, only the differences highlighted between those where comparison is possible and relevant for masonry units in Table 3.9 and for masonry in Table 3.10. The EN standards are considerably more coherent and comprehensive than the SANS standards. In addition to the aspects that require reporting for the EN standards listed in these tables, the following aspects also need to be reported typically: EN standard used, testing organisation, testing date, type, origin and designation of masonry, number of specimens and date of receipt, conditioning method, surface preparation and specimen dimensions.

Table 3.9: Differences between SANS and EN standards for test methods for masonry units

Aspect Tested		EN	SANS
Unit dimensions	*No of units*	6	32 (clay), 12(CS, concrete)
	Procedure	calliper, 3 position options	steel rule, centreline
	Report	mean values to 0.1 – 1.0mm	average dimensions to 1mm
Unit compressive strength	*No of units*	6	12
	Preparation	grinding or capping, plane to 0.1mm in 100mm	capping
	Conditioning	clay – air dry	immersed 24hrs
		CS – oven dry	
		concrete – air dry or immersed	
		AAC – 6% moisture	
		manufactured stone – air dry or immersed	
		natural stone – air dry	
	Procedure	0.05 – 1.0 N/mm^2, > 1min	5kN preload, 15MPa/min
	Report	individual failure load in N, individual, average & normalised (shape factor) compressive strengths to 0.1N/mm^2, coefficient of variation to 0.1%	individual max failure load in N, individual & average compressive strengths to 0.1MPa

Table 3.10: Differences between SANS and EN standards for test methods for masonry

Aspect Tested		EN	SANS
Masonry compressive strength	*Specimen No*	3	2
	Specimen	$h_s \geq$ 3-5x h_u and $\geq$ 3x t_s and $\leq$ 15x t_s and $\geq l_s$	$h_s \geq$ 6x t_u or 1m, $\leq$ 20x t_u
		$l_s \geq$ 1.5-2x l_u ; $t_s \geq t_u$	$l_s \leq 0.75 h_s$; $A \geq 0.2$m^2
	Preparation	units conditioned, on horizontal surface, faces flat, parallel	-
	Curing	polyethylene sheet 3 days, then uncovered	polyethylene sheet 3 days, then uncovered
	Procedure	failure after 15-30min 0.15-1.25N/(mm^2.min)	28 days, uniform load top & bottom, initial 1MPa/min, increased
	Report	unit & mortar compressive strength, mortar flow value, max load to 1kN, visible cracks load, individual, mean & characteristic compressive strengths to 0.1N/mm^2, coefficients of variation	unit & mortar compressive strength, mean max load
Masonry flexural strength	*Specimen No*	5 each format	8 each format
	Specimen $\perp$	$b \geq$ 240mm and 3x h_u or $\geq$ 1000mm	bricks l = 4-5 units, h = 4 courses
			blocks l = 2.5 units, h = 4 courses
	Specimen =	$b \geq$ 400mm and 1.5x l_u	bricks l = 2 units, h = 10-14 courses
			blocks l = 1.5 units, h = 5 courses
	Preparation	units conditioned, specimen pre-compressed 2.5x10^{-3} – 5.0x10^{-3} N/mm^2	immerse units 5-6min, compress wallet with 3 brick courses
	Curing	polyethylene sheet	polyethylene sheet
	Procedure	28 days, four-point loading, base free from frictional restraint, configuration limits, flexural stress increase 0.03 – 0.3N/mm^2/min	28 days, four-point loading, base free from frictional restraint, configuration limits, load increase 3-4kN/min
	Report	mean unit & mortar compressive strength to 0.01N/mm^2, mortar flow value, inner & outer bearing spacing, time until & max load to 10N, crack patterns, individual, mean & characteristic flexural strengths to 0.01N/mm^2, coefficients of variation	flexural strength
Masonry shear strength (DPC)	*Specimen No*	9	10
	Specimen	l > 400mm, < 700mm	bricks l = 2 units, h = 10 courses
		h/w >2, min 1 vertical joint per course	blocks l = 1.5 units, h = 4 courses
	Preparation	units conditioned, specimen pre-compressed 2.0x10^{-3} – 5.0x10^{-3} N/mm^2	parallel, plane & plumb
	Curing	polyethylene sheet	polyethylene sheet
	Procedure	28 days, 0.2, 0.6 & 1.0MPa compression, double shear under 3-point loading, increase 0.1-0.4MPa/min	28 days, 1MPa compression, horizontal load to middle course, increase 0.3-0.4MPa/min
	Report	unit & mortar compressive strength, mortar flow value, compressive load, max shear load, mean & characteristic initial shear strength to 0.01 N/mm^2, angle of internal friction	failure load to 0.1N, shear strength

Masonry bond strength	*No of specimens*	10 bed joints		upon agreement
	Specimen			l = 1 unit, h = 9 courses
	Preparation	units conditioned, square & level, specimen pre-compressed 2.0×10^{-3} – 5.0×10^{-3} N/mm²		3 piers constructed simultaneously on firm flat surface
	Curing	polyethylene sheet		polyethylene sheet
	Procedure	28 days, stack bonded prism, lever & clamp over top unit, failure in 2-5min		7 days, 3-point bending by brick weights
	Report	mean unit & mortar compressive strength to 1.0 & 0.01N/mm², mortar flow value, weight of top unit, lever and clamp, time until and max force in N, individual, mean & characteristic bond strengths to 0.01N/mm²		pier mass & load mass to 0.1kg, clear span, pier height, bending stress

NOTE   AAC   autoclaved aerated concrete;

         CS   calcium silicate

         ⊥   flexural failure perpendicular to bed joints;

         =   flexural failure parallel to bed joints

3.3.3   Application Regulations

At present, the South African masonry structural design standards are in a harmonisation phase, and both the older SANS 10164 - The Structural Use of Masonry and the new SANS 51996 - Eurocode 6: Design of Masonry Structures (adopted in March 2018, identical implementation of Eurocode 6) are in force (Table 3.11). SANS 10164 was originally published in 1980, based on the withdrawn BS 5628 and is due to be withdrawn in 2020 (Byron, 2019). It is important to note that presently no National Annex (NA) for South Africa exists for Eurocode 6.

Table 3.11: Proposed EN and current SANS standards for masonry structural design

Proposed EN for South Africa		**Current SANS Standard**	
Standard	***Design of masonry structures***	**Standard**	***Eurocode 6 – Design of masonry structures***
EN 1996-1-1	*Rules for reinforced and unreinforced masonry*	**SANS 51996-1-1**	*General rules for reinforced and unreinforced masonry structures*
EN 1996-1-2	*Structural fire design*	**SANS 51996-1-2**	*General rules – Structural fire design*
EN 1996-2	*Selection of materials and execution of masonry*	**SANS 51996-2**	*Design considerations, selection of materials and execution of masonry*
EN 1996-3	*Simplified calculation methods for unreinforced masonry structures*	**SANS 51996-3**	*Simplified calculation methods for unreinforced masonry structures*
		Standard	***The structural use of masonry***
		SANS 10164-1	*Unreinforced masonry walling*
		SANS 10164-2	*Structural design and requirements for reinforced and prestressed masonry*

Since SANS 51996 is an identical implementation of Eurocode 6 and the scope of work of this research is limited to unreinforced masonry, the comparison, given in Table 3.12, is made solely between SANS 51996-1-1 (2018), -3 (2018) and SANS 10164-1 (1989).

Table 3.12: Differences between old and new SANS standards for design of unreinforced masonry

	SANS 51996	SANS 10164-1
Basis	Based on limit state concept, in conjunction with partial factor method	Based on limit state concept, in conjunction with partial factor method
	1.4 Combination of principles (statements for which there are no alternatives) & application rules (comply with principles and satisfy their requirements)	4.1 Combination of adherence to empirical rules of National Building Regulations & deemed-to-satisfy solutions
Scope	1.1.1(2)P Resistance, serviceability & durability of structures	1.1 Recommendations & requirements for design of unreinforced loadbearing masonry walling
	1.1.2(1)P unreinforced (and reinforced) masonry structures	
Characteristic value	Unfactored	2.1 5% exceedance probability
Design load	Factored	Factored
New materials	1.1.2(2) Principles & application rules may be applicable, but may need to be supplemented	3.2 Responsibility rests on designer to provide a level of safety & performance equivalent to that implied by the requirements of the relevant standards & that local authority approval is obtained
Material partial safety factors	2.4.1 Design value is characteristic value / material partial factor (recommended values in NOTE Table)	4.3 Values given based on manufacturing & construction control (Table 5), halved for accidental loads
Loading	Not covered, Eurocode 1 to be used	4.2.1 SABS 0160 to be used (withdrawn), partial safety factors provided
Seismic design	Not covered, Eurocode 8 to be used	Not covered
Masonry compressive strength	3.6.1 Values determined from tests (carried out or database), or based on unit compressive strength, mortar strength & constant K, dependent on masonry unit type & mortar type	4.2.2 Values given based on unit nominal compressive strength & mortar class (Table 3) or by testing (6.3)
Masonry flexural strength	3.6.3 Values determined from tests (carried out or database), or based on masonry unit and mortar type (NOTE Tables)	4.2.3 Values given based on unit material, compressive strength (concrete) & water absorption (clay) & mortar class (Table 4) or by testing (6.4)
Masonry shear strength	3.6.2 Values determined from tests (carried out or database), or based on initial shear strength, design & unit compressive strength. Initial shear strength values given based on masonry unit & mortar type	4.2.4 Values given based on mortar class & design vertical load, coefficient of friction < 0.6
Mortar	3.2.2 Classified & prescribed by compressive strength M	6.1.1 Mortar strength tested 6 weeks prior to construction
Slenderness	5.5.1.4 ratio < 27	5.1.1 ratio < 27
Wall effective height	5.5.1.2 2 or 3 or 4 x clear storey height, depending on edge restraint or stiffening	5.1.2.2 a) 1) 0.75x or 1.0x clear distance between lateral supports, depending on resistance to lateral movement
Wall effective thickness	5.5.1.3 (1) actual thickness for single leaf walls	5.1.2.3 a) 1) actual thickness for single leaf walls

The comparison made in Table 3.12 is by no means comprehensive and only serves to illustrate that, whilst there are a number of similarities, there are significant differences between the two standards for the design of unreinforced masonry. Both standards provide application or empirical rules which, if adhered to, satisfy the requirements of the standard. However, the main difference is the basis of the standards. SANS 51996-1-1 is structured on governing principles which, if interpreted and adhered to, create scope for solutions beyond rote rule application. SANS 10164-1 lacks this flexibility.

3.3.4 Material Partial Factors

In limit states design, partial factors for materials contribute significantly to the design process. The main considerations in both SANS 51996-1-1 (2018) and SANS 10164-1 (1989) in determining partial factors for materials are manufacturing and construction or execution control, and no distinction is made on the basis of material type. Beyond these commonalities, SANS 51996-1-1 also takes into consideration the type of mortar used. The UK National Annex (NA) to Eurocode 6 (2005) makes additional distinctions on whether the masonry is reinforced or not, as well as the loading condition. The greater the certainty regarding the unit and mortar strength and the manner in which they are combined on site, the greater the reward is in terms of the load magnitude that the masonry is allowed to bear.

Table 3.13 summarises the pertinent material partial safety factors for the ultimate limit state in the relevant standards for unreinforced masonry. For the EC-based standards, 'Category' refers to the manufacturing control of the unit, where Category I signifies a 95% probability of achieving the declared compressive strength, whereas Category II implies failure to meet this confidence level. 'Class' refers to the five levels of execution control of the structure. In SANS 10164-1, Category A refers to the manufacturing control, with a 97.5% probability of achieving the declared compressive strength, and Category B implies failure to meet this confidence level. In this case, Category I and II refer to the execution control exercised.

Given the inadequate guidance for the execution control classification in EC6 (Sýkora & Holický, 2010), and the disparity in classifications, a direct comparison of the material partial safety factors is not reasonable, but in broad terms, the SANS 51996-1-1 (least conservative) ranges from 1.5 to 3.0, UK NA to EC6 from 2.3 to 3.0, and SANS 10164-1 (most conservative) from 2.9 to 3.5. Additionally, SANS 10160-4 (2017) recommends using a value two-thirds of the specified material partial safety factor for seismic design verification (B.4.3). Further, to the serviceability limit state, SANS 51996-1-1 (2.4.4) recommends a partial factor of 1.0 for the serviceability limit state, whereas SANS 10164-1 makes no such distinction.

Table 3.13 Material partial factors according to SANS 51996-1-1, UK NA to EC6, SANS 10164-1

			Manufacturing Control			
			Category I	Category II	Category A	Category B
Execution Control	Class 1	SANS 51996-1-1	1.5 – 1.7	2.0	-	-
		UK NA to EC6	2.3 – 2.5	2.3 – 2.6	-	-
	Class 2	SANS 51996-1-1	1.7 – 2.0	2.2	-	-
		UK NA to EC6	2.5 – 2.7	2.5 – 3.0	-	-
	Class 3	SANS 51996-1-1	2.0 – 2.2	2.5	-	-
	Class 4	SANS 51996-1-1	2.2 – 2.5	2.7	-	-
	Class 5	SANS 51996-1-1	2.5 – 2.7	3.0	-	-
	Category I	SANS 10164-1	-	-	2.9	3.2
	Category II	SANS 10164-1	-	-	3.2	3.5

Notably, the factors recommended by EC6 and those implemented in the UK NA differ considerably. In developing these nationally determined parameters (NDP) for the UK, comparative studies were done on unreinforced compression loaded walls using the previous BS 5628-1 (2005) and new EN 1996-1-1 calculation processes (Morton, 2012). The partial safety factors were chosen for the UK NA on the basis of achieving the same level of safety in both calculation sets.

Similarly, the material partial factors prescribed in SANS 10164-1 are based on the British Standard (BS 5628-1, 1978), with some adjustments made to take local conditions into account (Mahachi, et al., 2007). Given the relatively high prevalence of masonry wall structural failures in South Africa (Crofts, 2018) and the increase in untrained construction workers, Mahachi et al. (2007) argue that these design parameters, as well as construction quality control, require review. The development of a stochastic database of material resistance in South Africa is in progress, with the intention of recalibrating the material partial safety factors, presumably leaning even more conservative. Conversely, Sýkora and Holický (2010) contend that the partial factors recommended in EN 1996-1-1 (and by extension in SANS 51996-1-1), the least conservative range of the three standards, are an overestimation.

Needless to say, the determination of partial safety factors is complex, and requires significant data. When considering construction quality control, the uncertainty stems from the builder, and not the material type. When considering manufacturing uncertainty, some variation between materials would be reasonable and the manufacturing processes of future AMU's are unknown. However, none of the standards make a distinction based on material type, and yet these range from concrete to natural stone, representing a wide spectrum of manufacturing methods. In essence, the partial factor corresponds directly to the coefficient of variation and sample size (Holický, et al., 1998). Arguably, provided that a sufficient database exists for conventional masonry materials, penalising AMU's with additional or increased partial safety factors is difficult to justify.

3.4 Conclusion

The South African National Building Regulations are performance-based in nature, and current prescriptive masonry standards are in the process of being replaced by the performance-based Eurocode 6. This follows the global trend of transitioning building regulations from a prescriptive to a performance basis. Similar to most countries, the performance criteria for housing walls and their components, are still under development in South Africa. SANS 10400 sets out what the functional requirements of a wall are but the "technical performance criteria need to be established" (SANS 10400-A, 2010, p. 63).

Deemed-to-satisfy solutions for masonry walls are deeply entrenched and typically considered to be the only viable solution. Practically it is difficult, expensive and time consuming to have alternative masonry units approved in South Africa, and the uptake of these in the LIH market has been slow. There is value in being able to assess the performance of an AMU on a unit or small prism scale, together with the ability to predict its performance in the larger structural context. Ultimately, such an assessment ability would enable off-the-shelf use of AMU's.

Hence, this research proposes to address three shortcomings in the performance-based regulation of housing, specifically with respect to AMU's:

1. Develop a predictive model for the behaviour of AMU's in a Category 1 housing context, by means of FE modelling.
2. Develop performance criteria for AMU's, based on the NBR framework of deemed-to-satisfy solutions, since these represent society's implicit expectation of a building's performance.
3. Propose methods by which the performance levels of AMU's can be verified.

Additionally, given the significant overlap within subsections of EN 771 and within subsections of EN 772, it is proposed that, in the adoption of these standards to the South African context, that:

1. One material non-specific standard *'Specifications for masonry units'* is developed, based on EN 771, with annexes where necessary for specific materials.
2. One material non-specific standard *'Methods of test for masonry units'* is developed, based on EN 772, with annexes where necessary for specific materials.
3. A Product Evaluation Protocol is developed for AMU's, to support the integration of new AMU's into the standards

Going forward, this approach would make the inclusion of future masonry materials simpler from a standards development perspective. Only material specific aspects would need to be addressed in an annex, as opposed to a new standard developed, thereby reducing the barriers to the uptake of innovative masonry materials. The convenience of aligning the regulation of AMU's with CMU's is essential to their success.

The work up to this point (Chapters 1 through 3) lies in identifying the avenue along which AMU's should ideally be regulated in South Africa. The work from this point forwards (Chapters 4 through 8) addresses the shortcomings listed above as a contribution towards implementing such a regulatory approach.

4 Masonry Finite Element Modelling

A brief overview of finite element modelling as it applies to masonry is provided, followed by what approach was used in this study. The extent to which alternative masonry has been modelled using the finite element method is investigated, and the constitutive material model applied in this study is explained.

4.1 Masonry FEM Overview

4.1.1 Masonry Failure Mechanisms

Masonry can be viewed as a composite material, consisting of units and mortar, arranged in a regular pattern forming joints, with the interface between the unit and mortar joint acting as a plane of weakness (Page, 1981), but the failure mechanism activated in masonry is largely dependent on the load application and is generally classified as in-plane or out-of-plane.

For typical in-plane shear loading (Figure 4.1), three types of failure mechanisms are found: sliding, shear and flexural (Salmanpour, 2017). Sliding can take place in a single course (a) or along staircase-shaped cracks through head and bed joints (b) and is marked by large displacement capacity and energy dissipation. This relatively stable failure mode is caused in squat walls by seismic loading but is seldom the dominant failure mode in unreinforced masonry.

(a)	(b)	(c)	(d)
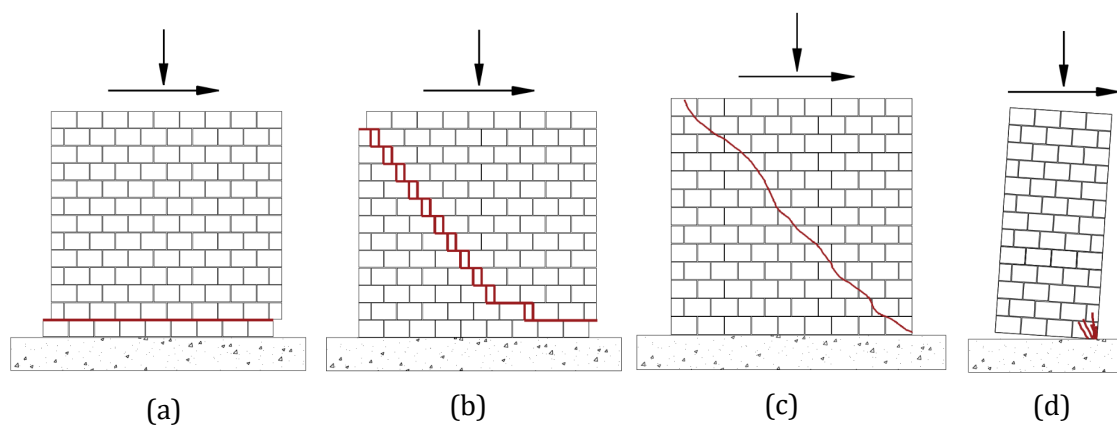
Figure 4.1: Typical in-plane vertical compression loading combined with shear resulting in (a) sliding along a single course, (b) sliding along staircase-shaped cracks, (c) diagonal cracking and (d) rotation, flexural cracking and crushing (Salmanpour, 2017)

Shear failure, marked by diagonal cracking through the units (c), is generally the dominant in-plane failure mode for unreinforced masonry under shear loading and is governed by the tensile capacity of the units (Salmanpour, 2017). Typically, this failure mode exhibits abrupt stiffness and strength reduction, coupled with low displacement capacity and average energy dissipation. In the case of slender walls under shear loading, flexural failure (d) often dominates, identified by cracking of the bed joints and rotation or rocking of the wall about the compressed zone (Salmanpour, 2017). Crushing of the units in the compression zone or overturning of the wall marks the ultimate failure. This failure mode is associated with average energy dissipation and potentially significantly high displacement capacity.

28

Under vertical compression (Figure 4.2), combined with horizontal tension (a), vertical cracking of the units and joints dominates (Massart, et al., 2005). Vertical mid-plane cracking of the units is typically dominant in vertical compression combined with horizontal compression loading (b), especially if the principal stresses are similar in magnitude (Massart, et al., 2005). In the latter case, in-plane loading causes out-of-plane failure. In the overall biaxial compressive state, experiments have shown that the higher unit stiffness leads to a triaxial compressive state in the mortar whereas the units are subject to compression in-plane and tension out-of-plane (c). The inherently weak tensile properties of the units therefore generally cause out-of-plane splitting of the masonry.
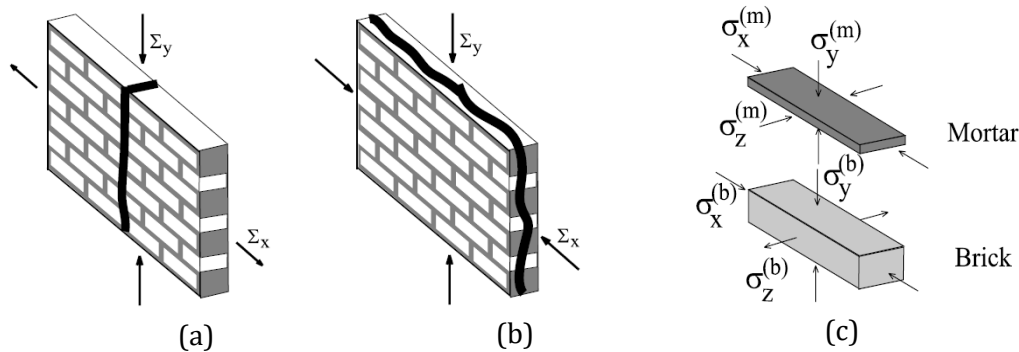
Figure 4.2: Typical in-plane vertical compression loading combined with (a) horizontal tension and (b) horizontal compression and (c) unit and mortar stress states under biaxial compression

For out-of-plane loading, either due to wind or seismic loading, the failure mechanism is largely dependent on the support conditions, one-way or two-way spanning walls, and thus uniaxial or biaxial bending. Uniaxial bending, (Figure 4.3) is classified as either vertical or horizontal bending, the traditional definition of which is based on the direction of the induced internal flexural stresses (Vaculik, 2012). Vertical bending, in (a) and (b), results in flexural stresses perpendicular to the bed joints and, contrary to its name, horizontal cracks. Horizontal bending (c) results in flexural stresses perpendicular to the head joints and vertical cracks.
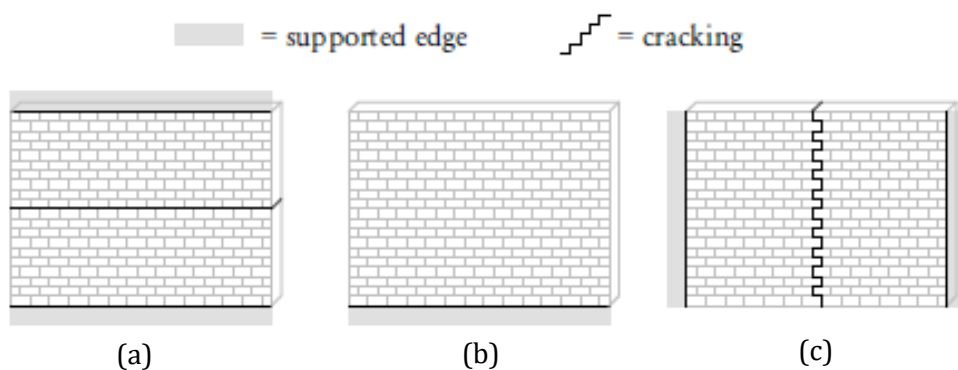
Figure 4.3: Typical out-of-plane flexural cracking patterns for one-way spanning walls with (a) double supported vertical span, (b) single supported vertical span and (c) double supported horizontal span (Vaculik, 2012)

Biaxial bending of two-way spanning walls (Figure 4.4) results in complex structural behaviour due to the anisotropic nature of the material (Vaculik, 2012). A combination of cracking patterns is found, as a result of a combination of stresses, both normal/flexural and shear/torsional, see Figure 4.5.

29
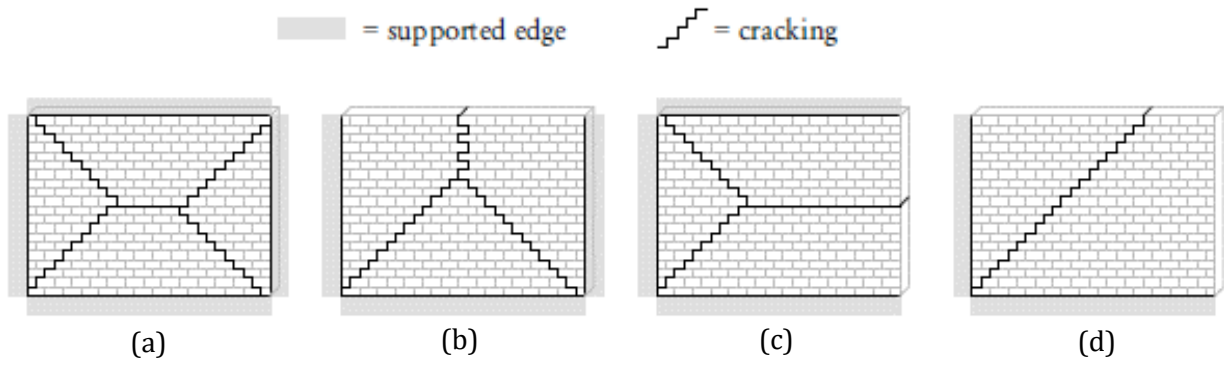
Figure 4.4: Typical out-of-plane flexural cracking patterns for two-way spanning slabs with (a) O-shaped, (b) U-shaped, (c) C-shaped and (d) L-shaped supports (Vaculik, 2012)
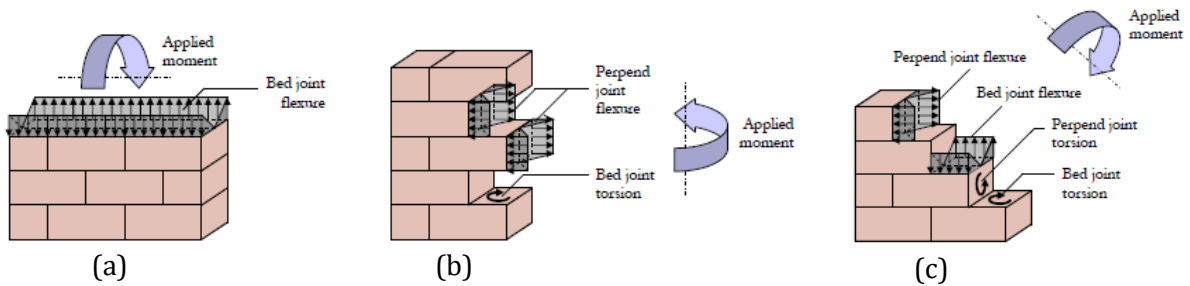
Figure 4.5: Internal joint stress distribution for (a) vertical bending, (b) horizontal bending and (c) diagonal bending (Vaculik, 2012)

Translating this global in- and out-of-plane behaviour to unit, joint and unit/joint behaviour, the failure modes that thus need to be captured by any numerical modelling approach (see Figure 4.6) are joint failure in (a) tension cracking and (b) sliding at low confining stress; unit failure in (c) direct tension cracking; combined failure mechanisms of the unit and joint in (d) diagonal tensile cracking at confining stresses sufficiently high to develop friction in the joint and (e) crushing, (Lourenço, 1996).
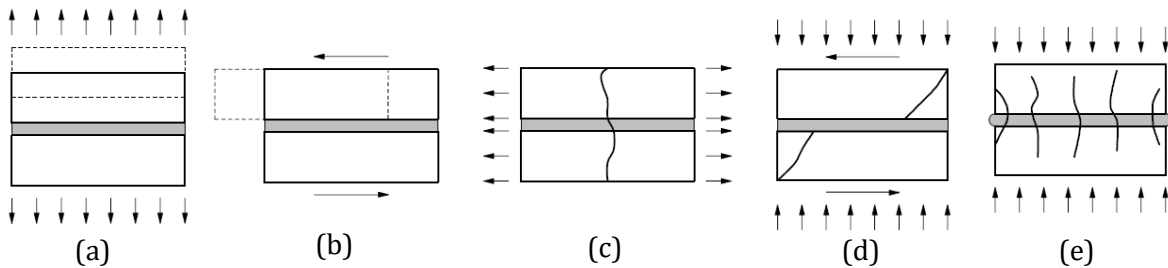
Figure 4.6: Masonry failure mechanisms that require capturing (Lourenço, 1996)

4.1.2 Modelling Approach

Significant advances in numerical methods and computational capabilities in recent decades have altered the way in which masonry is analysed. For masonry finite element modelling, two main approaches have been established, namely macro- and micro-modelling (see Figure 4.7) with the level of abstraction directly related to the complexity and size of the problem to be analysed, Giambanco et al. (2001), Reyes et al. (2008), Roca et al. (2010) and Abdulla et al. (2017).

30
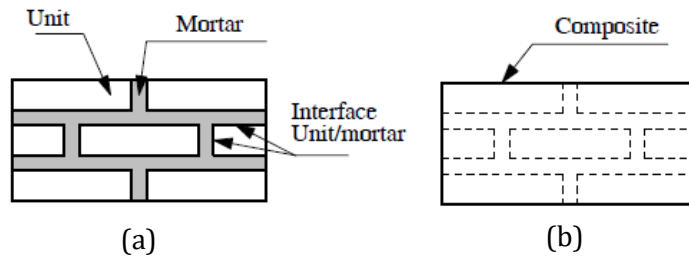
Figure 4.7: Masonry FEM approaches a) micro-modelling, b) macro-modelling (Lourenço, 1996)

Macro-modelling assumes a smeared continuum approach, where the unit, mortar and unit-mortar interface behaviours are combined in a representative continuous material. The computational benefits are clear, and this approach is ideal for the global analysis of masonry structures, however, detailed failure mechanisms are generally not well reproduced. Model input parameters are either determined through expensive large-scale masonry tests or predicted based on the micro-properties of the constituent materials, requiring homogenisation techniques to be applied, such as by Anthoine (1995), Zucchini and Lourenço (2002) or Milani et al. (2006). Both avenues have their challenges. Since the walls analysed in this study are relatively large (up to 6.0m x 3.3m) a macro-modelling approach would be justified but is considered inappropriate for this application due to the omission of individual unit and joint behaviour description.

On the other hand, micro-modelling represents a high degree of detail where the unit, mortar and unit-mortar interface are modelled distinctly. This approach is limited to relatively small scale structural elements and requires significant computational capacity and some material parameters are challenging to measure, but the results are typically accurate in quantity (load magnitude) and quality (failure mechanism type), as shown by Ali and Page (1988) and Lofti and Shing (1994), to name a few. Despite the detailed results obtainable, this approach is considered computationally too expensive for this study, given the size of the walls.

Simplified micro-modelling (SMM), also referred to as meso-modelling, is a subset of micro-modelling as its name implies, wherein the units are modelled as expanded elements, with solely elastic material properties, to encompass the volume of the unit and the mortar in order to maintain the overall geometry. The relatively weak mortar joint and unit-mortar interface are combined into a single zero-thickness interface element in which the nonlinear material behaviour is concentrated. Some accuracy is lost in using zero-thickness elements since the Poisson's effect of the mortar is neglected (Lourenço, 1996). However, this approach reduces the computational effort required compared to micro-modelling but avoids the need for the homogenisation techniques of macro-modelling. This SMM scale is chosen for this study.
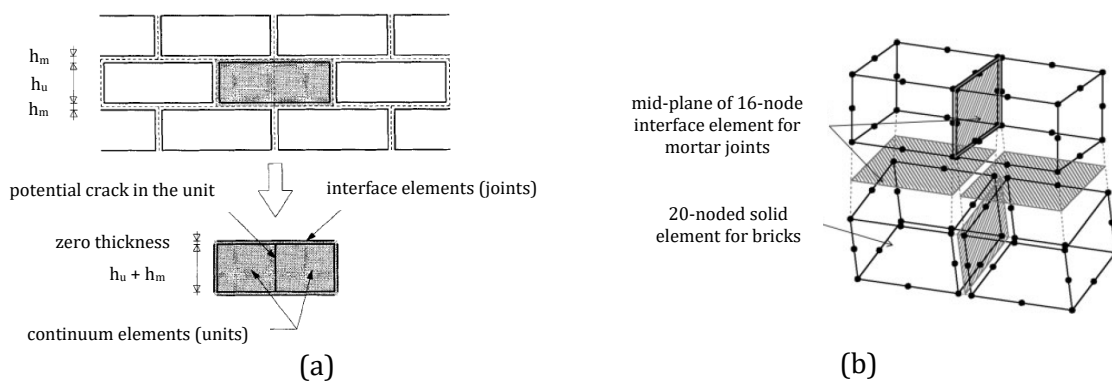
Figure 4.8: Meso-modelling strategy (a) in 2D with expanded unit elements (Lourenço & Rots, 1997) and (b) in 3D solid brick elements and 2D interface elements (Macorini & Izzuddin, 2011)

Early efforts by Page (1978) and Rots (1991) in simplified micro-modelling have been followed up by Lourenço (1996) in 2D and Van Zijl (2000) in 3D, and adapted and applied by many, including Giambanco et al. (2001), Macorini and Izzuddin (2011) and Chisari et al. (2018). In many cases the unit's tensile and shear nonlinear behaviour is concentrated in a single potential vertical zero-thickness crack element in the centre of the unit, as illustrated in Figure 4.8. Lourenço (1996) found principal stresses up to four times the unit's tensile strength if the potential cracks in the units are not included in the model. Some misalignment of cracks is possible, but the effect on the results is considered negligible.

Of the failure mechanisms depicted in Figure 4.6, (a), (b), (d) and (e) are included in the joint interface elements, whereas mechanism (c) is included in the potential crack element in the unit. It is commonly accepted that the mortar joints and their interaction with the units represent the weakest link in a masonry structure and cracks typically run along this joint interface but also can continue through the unit to follow a continuous path (Macorini & Izzuddin, 2011). Since masonry is constructed in an ordered manner, it is possible to know the potential damage location beforehand. It is thus appropriate, generally, to concentrate the post-peak behaviour in the joint interfaces and mid-unit crack.

One exception to this is the crushing of masonry. In reality, compressive failure is a combination of the unit, mortar and their interaction, with the microstructure of the unit playing a significant role. In the model, this failure mechanism is represented by one unit imploding on the other, to maintain the global stress-displacement behaviour (Lourenço & Rots, 1997).

Most SMM of unreinforced masonry focuses on the in-plane nonlinear behaviour for computational efficiency, assuming a plane-stress state, motivated by the relative geometric ratios of a masonry wall (Massart, et al., 2005), wherefore 2D analysis is sufficient. However, under in-plane biaxial compressive loading, out-of-plane splitting of the masonry occurs, as discussed in Section 4.1.1, and 3D analysis is required to capture this failure mode. Moreover, during complex loading conditions, such as seismic loading, simultaneous in-plane and out-of-plane loading takes place and can only be assessed using 3D analysis (Macorini & Izzuddin, 2011). 2D analysis also neglects the governing contribution geometric nonlinearity can make to out-of-plane failure. This study thus employs a 3D analysis strategy and geometric nonlinearity is taken into account using Updated Lagrange description.

4.1.3 Elements

The masonry half-units are each modelled using a single 20-noded 3D solid brick elastic continuum element, named CHX60 in DIANA (Figure 4.9). Quadratic interpolation and 3x3x3 Gauss integration are used.
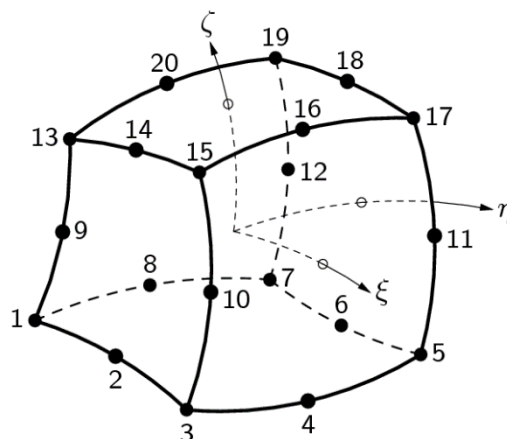
Figure 4.9: Continuum element CHX60 (DIANA, 2017)

The mortar joint and unit-mortar interaction, as well as the unit tensile crack, are modelled using a single 16-noded 2D nonlinear plane quadrilateral isoparametric interface element, named CQ48I in DIANA, which allows for discontinuities (Figure 4.10). Quadratic interpolation and 3x3x3 Newton-Cotes integration are set as the default, whereas Lourenço (1996) recommends a Lobatto integration scheme. In both the Newton-Cotes and Lobatto integration schemes, the integration points correspond to the end points of the interface, whereas with Gauss integration the points lie within the element (Giambanco, et al., 2001). This is an important distinction when discrete cracking is expected, and the element is likely to open at these end points (DIANA, 2017). Giambanco et al. (2001) observed that fictitious oscillating stress responses, reached under Gaussian integration, were eliminated when Lobatto quadrature was used. Given that the integration points in the Newton-Cotes scheme also correspond to the end points of the interface, this default integration scheme setting is used.
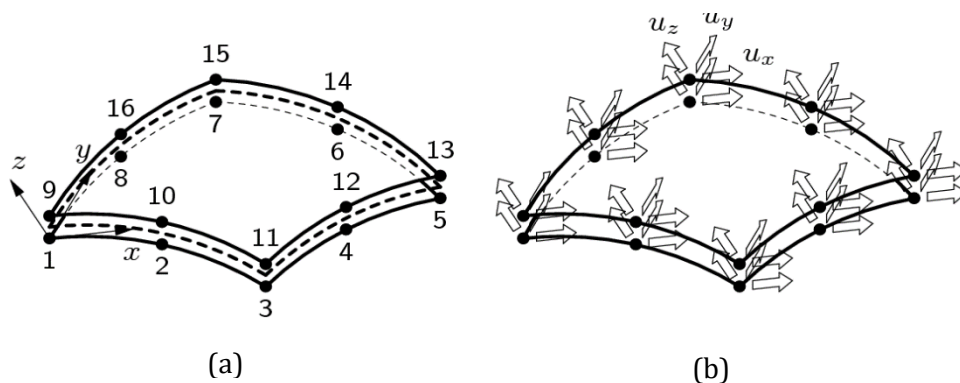
Figure 4.10: Interface element CQ48I a) topology and b) displacements (DIANA, 2017)

Each node has three translational degrees of freedom, and nodes 1 to 8 are on the bottom face of the interface element, corresponding to the face of a solid continuum element below it, and nodes 9 to 16 are on the top face of the interface element, corresponding to the face of a solid continuum element above it. Both faces of the interface element are coincident in the undeformed state.

Lourenço (1996) tested mesh sensitivity executing analyses with each linear continuum unit modelled using 4x2 and 8x4 quadratic plane stress elements (a four-fold increase in the number of elements) and together with the required number of interface elements. The model was found to be mesh insensitive and a 20-noded brick element thus provides sufficient accuracy. The post-peak softening of the interface elements is also not mesh-dependent (Macorini & Izzuddin, 2011) since the model is automatically regularised by using constitutive relations that are defined in terms of relative displacement instead of strains, whereby the fracture energy is dissipated over the crack area as opposed to the crack volume. Aspects regarding mesh dependency are therefore not pursued further.

4.1.4 Solution Method

No attempt is made to compare different solution techniques, the only objective being a stable solution procedure. The incremental procedures used is in this study are displacement controlled in Chapter 6 and force controlled in Chapter 7, with manual adjustment of the increments, as this allows for closer observation of the structural behaviour. A purely incremental procedure is seldom accurate, and several incremental-iterative procedures are available to significantly reduce the error and enable larger increment sizes. The total displacement or force increment is continuously adjusted by iterative increments, until equilibrium is established, according to a predefined tolerance. How these iterative increments are established, is the difference between the iterative procedures.

The Newton-Raphson iterative procedure has two subsets, namely the Regular Newton-Raphson and the Modified Newton Raphson, with the difference between the two being when the stiffness matrix is recalculated (Anand & Shaw, 1980). With the former method the stiffness matrix is evaluated at every iteration within the increment, based on the last known or last predicted state, even if it was not in equilibrium. This method typically only requires a few iterations, but each iteration is time-consuming as the stiffness matrix has to be set up for every iteration, and as the previous state was not necessarily in equilibrium, this easily leads to divergence (Cook, et al., 2001). In the Modified Newton-Raphson method, the stiffness matrix is only evaluated at the start of the increment, which is always based on the previous converged state of equilibrium. This method typically requires more iterations, but each iteration is faster as the stiffness matrix does not need to be computed every time. Since the previous state is in equilibrium, this method may lead to convergence when the Regular Newton-Raphson cannot converge (Cook, et al., 2001).

The Constant Stiffness iterative procedure, a variation of the Linear Stiffness method, makes use of the stiffness matrix used in the previous increment (Cook, et al., 2001). This method is typically more robust, but, at points of bifurcation, can follow unstable equilibrium paths. This method is most time efficient per iteration but is likely the slowest to converge.

For this study, the Regular Newton-Raphson method is employed in most instances, with a line search algorithm improving the method's robustness. This iterative algorithm obtains an increment displacement and scales it in order to minimise the energy potential, which can increase the convergence rate. The maximum number of line searches per increment is set to 5 with an energy convergence tolerance of 0.8. The internal change in strain energy is generally selected as the increment convergence criterion and is set to $\leq 10^{-4}$ times the energy variation at the start of the load increment (Lourenço, 1996). On occasion, the Modified Newton-Raphson or Constant Stiffness methods are employed for improved stability, as well as a force convergence criterion, set to 0.01.

When cracks develop in the modelled structure, elastic energy that is stored in the bulk of the material must be redistributed from the units connected to the damaged interface to the rest of the structure. This can lead to sharp snap backs and jumps in the global solution (Macorini & Izzuddin, 2011). Employing an arc length method can assist in overcoming these numerical difficulties. The Updated Normal Plane arc length method, with regular indirect displacement control, is used, constraining the norm of the displacement increment to a predefined value by adjusting the increment size at the same time. This choice is appropriate for brittle materials in which local failure is typical (Palacio, 2013). The choice between loading and unloading (increments or decrements) is set to the appearance of negative pivots, which can only be used in conjunction with the Regular Newton-Raphson method.

4.2 Constitutive Masonry Material Model

A predefined material model is selected in DIANA, namely combined cracking-shearing-crushing (CCSC). It is plasticity based with the elastic region confined by a composite yield surface (Lourenço & Rots, 1997) defined by three yield functions, tension cut-off $f_1(\sigma, \kappa_1)$, Coulomb friction $f_2(\sigma, \kappa_2)$, and an elliptical compression cap $f_3(\sigma, \kappa_3)$, as described in Figure 4.11 for 2D and 3D.

(a)   (b)
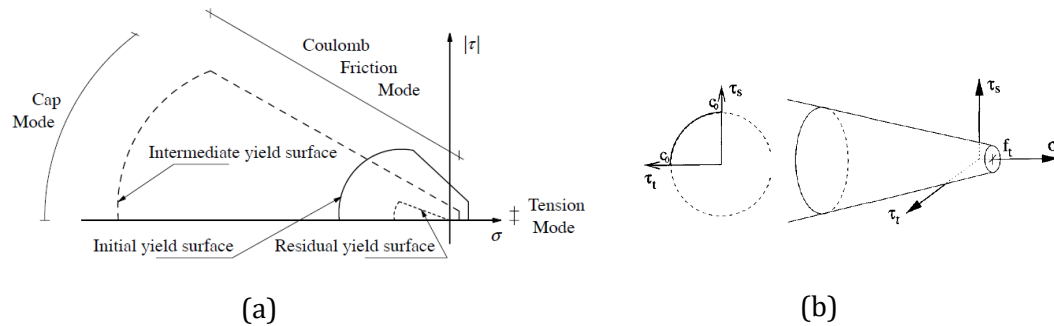
Figure 4.11: Combined cracking-shearing-crushing yield criterion (a) in 2D (Lourenço, 1996) and (b) in 3D (Van Zijl, 2000)

Softening, the moderate reduction in load carrying capacity under an increased enforced deformation of a material, is a principal characteristic of quasi-brittle materials. It is well observed in both tensile and compressive failure and in the loss of cohesion in shear failure (Lourenço, 1996). Softening is thus implemented in all three modes and in compression it is preceded by hardening. It is also assumed in all three modes that the inelastic behaviour can be described by their respective fracture energies, which are taken to be material properties. The three modes are discussed in more detail in subsequent sections.

4.2.1 Tension

The tension cut-off yield function of the CCSC model is described as follows:

$$f_1(\sigma, \kappa_1) = \sigma - \sigma_1(\kappa_1)$$
Equation 4.1

where σ_1 is the unit/joint yield strength (exponential softening is assumed), as in:

$$\sigma_1 = f_t \exp\left(-\frac{f_t}{G_f^I}\kappa_1\right)$$
Equation 4.2

where f_t is the bond strength of the unit/joint interface, G_f^I the mode I or tensile fracture energy and κ_1 the normal plastic strain, which controls the softening behaviour (Lourenço, 1996). The mode I fracture energy (Figure 4.12), describing the inelastic behaviour, is defined as the energy required to form a crack of unit surface area (Lourenço, 1996), and is obtained by integrating the post-peak tensile stress-displacement diagram.
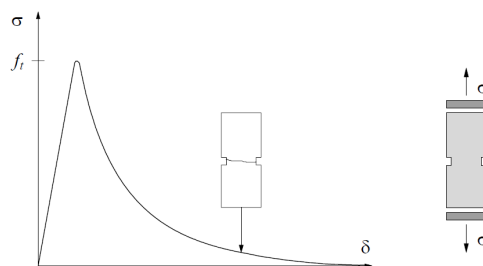
Figure 4.12: Typical uniaxial tensile behaviour of quasi-brittle material (Lourenço, 1998)

4.2.2 Shear

The shear slipping of the Coulomb friction crack initiation criterion in the CCSC model is described by:

$$f_2(\sigma, \kappa_2) = |\tau| + \sigma \, tan\phi(\kappa_2) - \sigma_2(\kappa_2) \qquad \text{Equation 4.3}$$

where $tan\phi$ is the friction coefficient, and the exponential cohesion softening is expressed as in:

$$\sigma_2 = c_0 \exp\left(-\frac{c_o}{G_f^{II}} \kappa_2\right) \qquad \text{Equation 4.4}$$

where c_o is the initial cohesion (or adhesion in the case of the unit-joint interface), G_f^{II} is the mode II (shear) fracture energy and κ_2 the plastic strain, which controls the softening behaviour (Lourenço, 1996). As in the tensile case, the mode II fracture energy describes the inelastic shear behaviour in this model and is obtained by integrating the post-peak shear stress-displacement diagram, with no normal confining pressure (Lourenço, 1996). Typical masonry shear behaviour is illustrated in Figure 4.13.
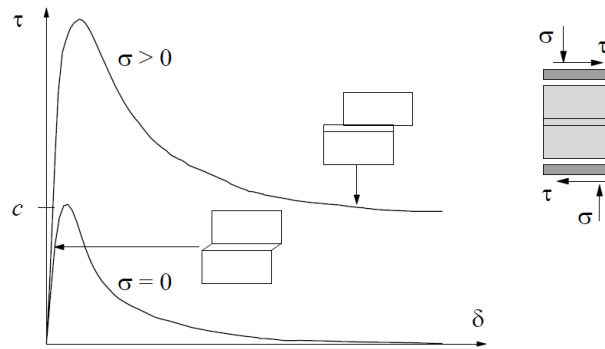
Figure 4.13: Shear behaviour of masonry (Lourenço, 1998)

The friction angle is assumed to be correlated to the exponential cohesion softening, as in:

$$tan\phi = tan\phi_o + (tan\phi_r - tan\phi_o)\frac{c_o - \sigma_2}{c_o} \qquad \text{Equation 4.5}$$

where ϕ_o and ϕ_r are the initial and residual friction angle respectively. This relation implies that the mode II fracture energy increases with an increase in normal stress (Lourenço, 1996), and is expressed as:

$$G_f^{II} = \begin{cases} a\sigma + b & if \ \sigma < 0 \\ b & if \ \sigma \geq 0 \end{cases} \qquad \text{Equation 4.6}$$

where a and b are constants which can be derived from experimental data (Van Zijl, 2000).

Masonry in shear experiences displacement normal to the shear displacement induced, which occurs both at and post-peak (Van Der Pluijm, et al., 2000). This dilatant behaviour is generally defined as a dilatancy angle Ψ, with the tangent being the ratio of the normal displacement u_p to the shear displacement v_p. Experimental evidence, such as in Figure 4.14 (a), shows that the dilatancy is dependent on the confining stress σ and the amount of shear slip and can be expressed as follows,

$$tan\psi = \begin{cases} 0 & if \ \sigma < \sigma_u \\ tan\psi_o \left(1 - \frac{\sigma}{\sigma_u}\right) e^{-\delta v_p} & if \ \sigma_u \leq \sigma < 0 \\ tan\psi_o e^{-\delta v_p} & if \ \sigma \geq 0 \end{cases} \qquad \text{Equation 4.7}$$

where $tan\psi_o$ is the dilatancy angle at no shear slip and confining stress, σ_u is the confining stress at which the dilatancy angle becomes zero and δ is the dilatancy degradation coefficient, which can be derived from experimental data (Van Zijl, 2000).

(a)   (b)
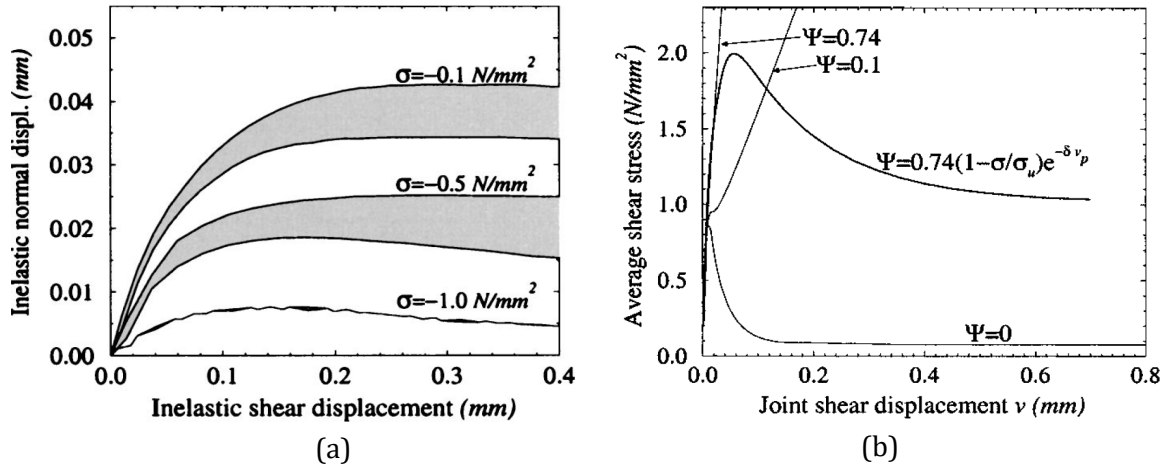
Figure 4.14: (a) dilatancy under pre-compression, normal displacement as a function of shear displacement and (b) reactions to unsuitable dilatancy modelling (Van Zijl, 2004)

The importance of appropriate dilatancy modelling is illustrated in Figure 4.14 (b), since an unsuitable dilatancy coefficient choice can lead to significant errors. A choice of zero dilatancy coefficient ($\Psi = 0$) can be unnecessarily conservative in certain cases (Van Zijl, 2004). Both a small or large constant dilatancy coefficient, such as 0.1 or 0.74, lead to unlimited shear strength. If warranted by the confining pressure ($\sigma_u \leq \sigma < 0$), a variable dilatancy coefficient definition is required, as described Equation 4.7.

4.2.3   Compression

The elliptical compression cap criterion of the CCSC is as follows:

$$f_3(\sigma, \kappa_3) = C_{nn}\sigma^2 + C_{ss}\tau^2 + C_n\sigma - \left(\sigma_3(\kappa_3)\right)^2 \qquad\qquad \text{Equation 4.8}$$

where σ_3 is the compressive yield value, κ_3 the plastic strain and C_{nn}, C_n and C_{ss} are material parameters that control the centre of the cap, the intersection with the tensile (positive) normal stress axis and shear traction contribution to the compression failure, respectively (Lourenço, 1996). Since a tension cut-off is contained in the multi-surface interface model, a centred compression cap is employed with $C_{nn} = 1$ and $C_n = 0$.

As for the previous two modes, the compressive fracture energy is assumed to describe the inelastic compressive behaviour and is obtained from the integral of the post-peak compressive stress-displacement diagram (Lourenço, 1996), with a typical compressive material description shown in Figure 4.15 (a).

(a)   (b)
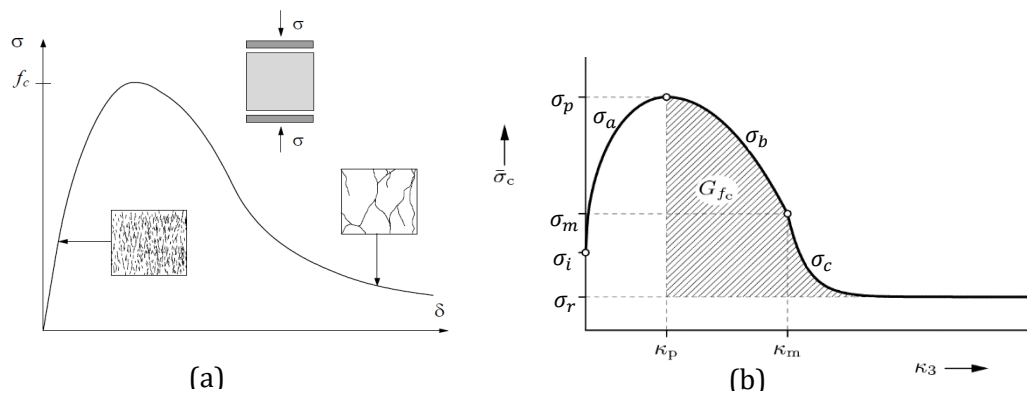
Figure 4.15: (a) typical uniaxial compression behaviour of quasi-brittle material (Lourenço, 1998) and (b) hardening/softening description for compression cap mode (Lourenço, 1996)

The hardening/softening law for the compression cap mode is described in Figure 4.15 (b), with the peak stress σ_p corresponding to the masonry compressive strength. The initial stress σ_i corresponds to $\sigma_p/3$, the medium stress σ_m to $\sigma_p/2$ and the residual stress σ_r to $\sigma_p/7$ (Lourenço, 1996). The different stress and strain values are adjusted to fit experimental data and the three stress regions are described using the following equations (Lourenço, 1996):

$$\sigma_a(\kappa_3) = \sigma_i + \left(\sigma_p - \sigma_i\right)\sqrt{\frac{2\kappa_3}{\kappa_p} - \frac{\kappa_3^2}{\kappa_p^2}} \qquad\qquad \text{Equation 4.9}$$

$$\sigma_b(\kappa_3) = \sigma_p + \left(\sigma_m - \sigma_p\right)\left(\frac{\kappa_3 - \kappa_p}{\kappa_m - \kappa_p}\right)^2 \qquad\qquad \text{Equation 4.10}$$

$$\sigma_c(\kappa_3) = \sigma_r + (\sigma_m - \sigma_r)\exp\left(2\left(\frac{\sigma_m - \sigma_p}{\kappa_m - \kappa_p}\right)\left(\frac{\kappa_3 - \kappa_m}{\sigma_m - \sigma_r}\right)\right) \qquad\qquad \text{Equation 4.11}$$

The post-peak area under the stress/strain curve in Figure 4.15 (b) does not truly represent the finite fracture energy as defined in Figure 4.15 (a) as the stress should reduce to zero, instead of to a residual stress value in an energy-based approach (Lourenço, 1996). However, reducing the stress to zero introduces significant modelling complications, including the need to introduce an additional compression cap/tension cut-off intersection to the multi-surface plasticity limit functions, and the effect of the residual stress value is considered negligible in terms of the results.

4.2.4   Composite

Coupled softening is assumed for tension and shear softening, i.e. the softening is due, by equal amounts, to the tensile strength and cohesion softening (Lourenço, 1996). There is no experimental data to support this due to the highly unstable test conditions required to illustrate this, but physical reasoning resolves that both mechanisms are due to the same linkages being disturbed on a micro-level at the unit-joint interface. Van Zijl (2000) underscores that the tensile cut-off of the Coulomb friction criterion, which implies a distinct separation between the tensile and shear failure, is an estimation of the actual behaviour and the implemented failure envelope can predict an incorrect failure mode in some instances.

In contrast, the compression cap/shear intersection of the composite yield surface is assumed to be unrelated (Lourenço, 1996). Again, by physical reasoning, the compression cap is crushing of the masonry whereas the shear failure is a unit-joint interface mechanism.

4.3 Alternative Masonry FEM

It must be underscored that the content of the previous sections is predominantly based on the experience and knowledge built around clay bricks and concrete blocks. Assumptions and conclusions, typical material behaviour and structural responses are not, by extension, necessarily valid for AMU's. Individual examples of comprehensive finite element modelling (FEM) of AMU's, with validation using experimental data, can be cited, but they are sparse. This section considers the status of FEM as applied to the three AMU's selected for this study, namely geopolymer (GEO), compressed-stabilised earth (CSE) and adobe (ADB).

4.3.1 GEO Masonry Modelling

As a material, GEO (or alkali-activated materials in general) has been extensively modelled based on the FE method in a range of applications. From conventional beam (Nguyen, et al., 2016) or composite beam applications (Bradford & Pi, 2012) to serving as a tunnel lining (Šejnoha, et al., 2013), railway sleepers (Ferdous, et al., 2015) or as a steel fibre reinforced material (Sanjayan, et al., 2015) and investigating the cathodic protection of its reinforcement (Montoya, et al., 2009), are just a few ways in which FEM has been applied to GEO. However, as far as can be reasonably established, there are no examples of the FE method used for GEO in the form of masonry.

Much of what can be gleaned from the FE modelling of GEO in literature could be suitably applied to a homogenized/continuum approach in masonry modelling. However, since a simplified micro-modelling approach is employed in this study, this knowledge is less relevant and therefore not contextualised here.

4.3.2 CSE Masonry Modelling

On a unit-scale, some FE modelling of CSE masonry blocks has been undertaken. In a wider project of investigating the effect of mix design on the strength of CSE blocks, Sitton et al. (2018) modelled single CSE blocks in a 3-point bending test setup to determine the sensitivity of results to the test setup configuration by considering stress concentrations around the block perforations. Geometrically nonlinear analyses were performed, using 8-node brick elements, but no constitutive material model information is provided. The authors were satisfied in their goal to assess the sensitivity to the test configurations, but masonry behaviour as such was not investigated. Similarly, Ayed et al. (2016) tested single, double and triplet dry-stack interlocking CSE prisms in compression, to verify their stress distribution, given the unusual geometry and reduced contact area between the blocks. Linear elastic blocks were used, joined by a friction contact interface, with the E-modulus, compressive and tensile strengths and friction coefficient determined experimentally. Good agreement was found between the experimental crack patterns and numerical stress concentrations; however, no validation was undertaken.

The most notable example of CSE masonry FE modelling is by Tennant (2016). Masonry wallets were tested and modelled in four-point bending with joints both normal and parallel to bending. The FE model employs bulk elements, capable of inelastic behaviour and damage, which are embedded with interface elements, representing the weaker joints. The multi-surface plasticity-based Sandia Geomodel was used, which includes compressive and tensile caps and a shear surface. Parametrization of the material was based on experiments, five-block prisms for compressive and flexural bond strength, as well as stiffness, and fitting of numerical results to the wallet experimental data. Tennant (2016) found the original E-modulus (measured from five-block compression tests) to be an overestimation resulting in a too stiff load-displacement response and subsequently reduced it by 40% to bring it in line with the experimental results. The justification for this reduction was the mortar joints acting as weak planes, as well as the orthotropic behaviour of masonry. Subsequently, overall reasonable agreement between the experimental and numerical results was found.

A multi-year study of the reconstructive work in Nepal, following the destruction of CSE masonry housing by the Gorkha Earthquake in 2015, resulted in the FE modelling of CSE block houses by Mellegård and Steinert (2016), as well as Thudén and Toivonen (2018). Both performed whole building analyses of Nepalese CSE block single-storey houses, including reinforced concrete elements and steel roofs. Mellegård and Steinert (2016) used a homogenous approach for the CSE masonry elements, with the initial input parameters based on E-modulus, compressive and tensile strengths and density tests on individual CSE blocks. The numerical results were calibrated to non-destructive dynamic tests on the actual structure, where after the most credible E-modulus and density were chosen. No separate validation process was applied. Thudén and Toivonen (2018) conducted a linear-elastic analysis of a Nepalese CSE block house, employing a micro-macro approach. Compressive and tensile strengths and Young's modulus, assumed from literature for the unit-scale, were adjusted according to EN 1996-1-1 to the masonry scale, leading to a homogenous model, with the CSE blocks modelled as thin shells. The model also included wall reinforcement and steel roof sections. Verification was done by comparing the deflections of modelled simply supported beams to analytical calculations, giving satisfactory comparative results for the elastic range.

Another, less comprehensive, example of CSE masonry FE modelling is the work of Srisanthi et al. (2014), in which shake table tests on a reduced-scale single-room building built of CSE blocks (and bricks) are analysed elastically. Good comparative results were obtained but little information is provided on the FE approach and constitutive model. Beyond the examples cited, scant data is available on the FE modelling of CSE block masonry.

4.3.3 ADB Masonry Modelling

Of the three alternative materials under consideration, the FE modelling of ADB masonry is, relatively, the most prolific. Several ADB masonry structures have been modelled using the FE method, mainly in the light of assessing historical buildings. In the more comprehensive studies, the most common approach is calibrating numerical results to data from medium- or large-scale experiments, due to the distinct lack of an experimental database for ADB masonry constituent properties. Such calibration analyses are detailed in Table 4.1, together with which modelling approach was used (continuum or discrete), the constitutive material model, as well as the origin of the experimental data used for calibration.

Table 4.1 ADB calibration analyses using FEM

Reference	Model	Material	Calibration
Illampas et al. (2014)	continuum	damaged plasticity	1:2 ADB structure
Miccoli et al. (2014)	continuum	damaged plasticity	uniaxial & diagonal ADB compression wallets
Tarque et al. (2010), (2012)	continuum	damaged plasticity	I-shaped ADB walls
Mahini (2015)	continuum	smeared crack	ADB prisms
Tarque et al. (2010), (2012)	continuum	total strain crack	I-shaped ADB walls
Sarchi et al. (2018)	continuum	total strain crack	I-shaped ADB walls
Ramirez et al. (2015)	continuum	total strain crack	uniaxial ADB compression wallets
Giamundo et al. (2015)	discrete	total strain crack	diagonal ADB compression wallets
Miccoli et al. (2014)	discrete	composite interface	uniaxial & diagonal ADB compression wallets
Tarque et al. (2010), (2012)	discrete	composite interface	I-shaped ADB walls

In most instances, the characterisation tests done were basic to none, assumed parameters were generally used and subsequently calibrated to experimental data. Most analyses were performed following a continuum/homogenized/macro-scale approach. In two instances the authors employed both continuum and discrete modelling approaches. Miccoli et al. (2015) came to the typical conclusion that macro-modelling is adequate for larger structural responses, but micro-modelling is more suited for closer failure mechanism and crack pattern estimation, whereas Tarque et al. (2010) found both models reproduced the general response and crack pattern relatively well. These two discrete/micro-modelling studies employed the composite interface model as described by Lourenço (1996).

Due to the calibrating nature of these approaches, satisfactory general agreement was found between the numerical and experimental results in all the cited ADB FEM cases. Only in one instance did the authors extend their study to a separate validation process. Tarque et al. (2014) went on to analyse a full-scale adobe building that had been previously dynamically tested on a shake table by Blondet et al. (2006), using their previously developed continuum, damage plasticity model. The FE results reproduced the displacements, crack patterns and failure mechanisms satisfactorily. The authors also noted that their use of an explicit solution procedure resolved the divergence issues previously experienced with implicit solution processes.

In the case of all three alternative materials discussed, the most commonly referenced obstacle to FE modelling, apart from the complex behaviour of masonry in general, is the lack of parametric input data for the materials. With the exception of Tarque et al. (2014), none of the cited examples of the three materials followed an independent validation process of the FEM findings.

4.4   Summary

In order to capture the different possible failure mechanisms of masonry, the SMM approach is selected, using linear block elements for the masonry units and concentrating the nonlinear behaviour in zero-thickness interface elements for the joints and central cracks in the units. This approach is appropriate for the scale of walls to be modelled and reasonable in terms of computing requirements. The plasticity-based CCSC model is chosen as the constitutive material model.

In the realm of FE modelling of alternative masonry, scant data is available for both material input parameters and FE results validated experimentally. These aspects are addressed in the following two chapters.

5 Input Parameters

Comprehensive parameterisation is required for the full description of the constitutive material model. The four blocks selected for study are discussed, together with their constituent materials, mix designs and manufacturing processes, followed by the material input parameters. Subsequently, how the input parameters were determined is discussed, structured according to the parameters required for the unit, the potential crack interface in the unit centre and the joint interface. The chapter concludes with a comparison between the values determined experimentally and those based on standardised strength prediction models for certain parameters. This chapter is based on a previous publication by the author (De Villiers, et al., 2018).

5.1 Material Selection

In South Africa the two most commonly used masonry blocks for LIH are the so-called maxi block, a solid 290mm long x 140mm wide x 90mm high concrete block, and a hollow concrete block, 390mm long x 140mm wide x 190mm high (Laing, 2011), depicted in Figure 5.1. Beyond these, the other standardised masonry materials in South Africa are burnt clay, calcium silicate and AAC. For this study AMU's are therefore defined as any masonry unit consisting of materials other than concrete, burnt clay, calcium silicate and AAC.

(a) (b)

Figure 5.1: Commonly used LIH (a) maxi solid and (b) hollow concrete blocks

The selection criteria for the AMU materials for this study were diversity in mechanical properties, reliable and ready access to raw materials and manufacturing equipment and availability of literature regarding mix designs. The need for ready and reliable access to raw materials over several years eliminated most of the waste materials as viable options. The criteria of ready access to the required manufacturing equipment eliminated the possibility of fired blocks. In the interest of simplification, any form of fibre reinforcement, natural or synthetic, was not considered. Additional considerations were that all materials included in the study needed to be formable in the same size mould, to eliminate size effect of the blocks as an additional variable. Secondary considerations were cost effectiveness and materials with an improved environmental or thermal performance.

As the actual AMU's are not the core focus of the study, but rather the regulation of AMU's, just the required effort was spent on optimising the mix designs. Achieving workable mixes with varying strengths and stiffnesses between the four materials was the aim, in order to elicit a wide spectrum of structural responses in the subsequent analyses. The four materials selected for the study are conventional concrete (CON) as benchmark and geopolymer (GEO), compressed-stabilised earth (CSE) and adobe (ADB) as alternatives. The mix designs used for the various experiments are detailed in Table 5.1. For an in-depth discussion on the mix designs see Fourie (2017), Shiso (2019) and Jooste (unpublished).

42

Table 5.1: Mix designs for the four masonry unit types

Material [kg/m³]	CON	GEO			CSE			ADB	
	F, S, J	F	S	J	F	S, J1	J2	F, S, J1	J2
Malmesbury Sand	607	-	700	750	-	-	-	809	1078
Philippi Sand	-	570	-	-	1198	1198	1198	809	540
Crusher Dust	1316	-	-	-	-	-	-	-	-
Clay Soil	-	-	-	-	798	798	798	534	534
13mm stone	-	858	1000	1000	-	-	-	-	-
CEM II 42.5	144	-	-	-	-	-	-	-	-
CEM II 52.5	-	-	-	-	200	200	200	-	-
Fly Ash	48	150	350	400	-	-	-	-	-
Slag	-	500	100	100	-	-	-	-	-
Sodium Silicate	-	90	70	70	-	-	-	-	-
Sodium Hydroxide	-	50	90	90	-	-	-	-	-
Water	212	102	120	76	231	264	224	275	145
Total	**2328**	**2320**	**2428**	**2486**	**2427**	**2460**	**2420**	**2428**	**2297**

NOTE   F: Fourie (2017), S: Shiso (2019), J, J1, J2: Jooste (unpublished)

All blocks manufactured have a length of 290mm, width of 140mm and height of 116mm. These dimensions were chosen to have blocks of similar size to the commonly used maxi block but were subject to the block press moulds available. The CON and CSE blocks were moulded in a Hydraform manual earth block press with an estimated compaction effort of 2.9N/mm², while the GEO blocks were cast into moulds and the ADB blocks were either placed and tamped in a baseless mould or also pressed in the block press. The four block types are depicted in Figure 5.2.
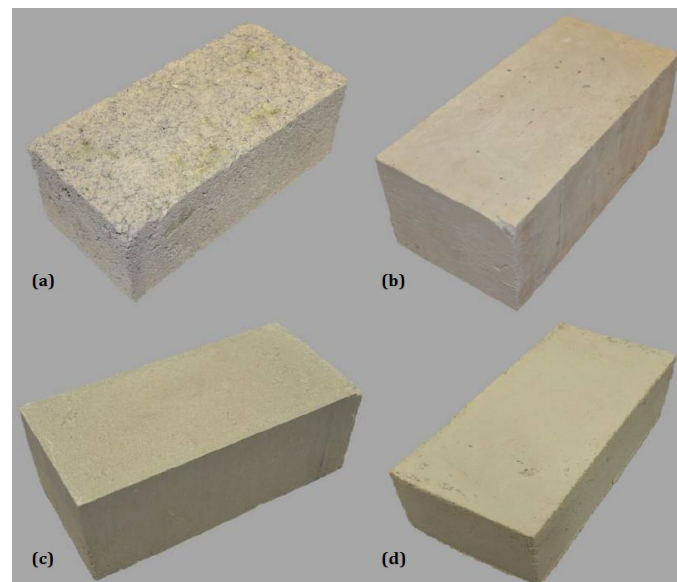
Figure 5.2: Four block types used in study: (a) CON, (b) GEO, (c) CSE and (d) ADB (Fourie, 2017)

The selected DIANA material model, CCSC, requires a comprehensive material description. The input parameters required for the four materials, the method by which they were determined, and their values are detailed in Table 5.2. A combination of literary sources (LIT), experimental data (EXP) and numerical fitting by finite element analysis of the experimental data (FEA) was used. Each parameter is discussed in more detail in the subsequent sections.

43

Table 5.2: Baseline input parameters for Combined Cracking-Shearing-Crushing model

Parameter	DIANA	Method	CON	GEO	CSE	ADB	
Unit							
Density	ρ_u	EXP	2 090	2 080	1 822	2 007	kg/m³
E-modulus	E_u	YOUNG	EXP	17 700	11 020	7 630	2 480	N/mm²
Poisson's Ratio	ν_u	POISON	LIT	0.16	0.17	0.20	0.45	-
Unit Crack Interface							
Tensile Strength	$f_{t,c}$	TENSTR	FEA	0.66	1.56	1.20	0.15	N/mm²
Mode I Fracture Energy	$G_{f,c}^I$	GF	EXP	0.047	0.056	0.016	0.006	N/mm
Cohesion	c_c	COHESI	LIT	1.0	2.3	1.8	0.2	N/mm²
Friction Angle	ϕ_c	PHI	LIT	37	37	37	37	°
Dilatancy Coefficient	ψ_c	PSI	LIT	0	0	0	0	°
Mode II Fracture Energy	$G_{f,c}^{II}$	MO2VAL	LIT	0.47	0.56	0.16	0.06	N/mm
Compressive Strength	$f_{c,c}$	COMSTR	EXP	12.1	17.9	6.6	0.8	N/mm²
Shear Traction Contribution	$C_{ss,c}$	CS	LIT	1.0x10⁻³	1.0x10⁻³	1.0x10⁻³	1.0x10⁻³	-
Compressive Fracture Energy	$G_{c,c}$	GC	LIT	10.0	14.8	5.5	0.7	N/mm
Eq. Plastic Relative Displ.	$\kappa_{p,c}$	DUPEAK	LIT	0.030	0.005	0.010	0.250	mm/mm
Tangential Stiffness	$k_{s,c}$	DSSX/Y	LIT	763 000	471 000	318 000	86 000	N/mm³
Normal Stiffness	$k_{n,c}$	DSNZ	LIT	1 770 000	1 102 000	763 000	248 000	N/mm³
Joint Interface							
Tensile Strength	$f_{t,j}$	TENSTR	LIT	0.12	0.08	0.06	0.04	N/mm²
Mode I Fracture Energy	$G_{f,j}^I$	GF	LIT	0.005	0.006	0.002	0.001	N/mm
Cohesion	c_j	COHESI	EXP	0.17	0.11	0.09	0.05	N/mm²
Friction Angle	ϕ_j	PHI	EXP	49.5	30.0	43.0	45.6	°
Dilatancy Coefficient	ψ_j	PSI	LIT	0	0	0	0	°
Mode II Fracture Energy	$G_{f,j}^{II}$	MO2VAL	LIT	0.05-0.08σ	0.05-0.08σ	0.05-0.08σ	0.05-0.08σ	N/mm
Compressive Strength	$f_{c,j}$	COMSTR	EXP	5.5	6.1	3.1	0.6	N/mm²
Shear Traction Contribution	$C_{ss,j}$	CS	LIT	0.7	2.9	1.1	0.7	-
Compressive Fracture Energy	$G_{c,j}$	GC	FEA	18	19	8	1.2	N/mm
Eq. Plastic Relative Displ.	$\kappa_{p,j}$	DUPEAK	FEA	0.030	0.005	0.010	0.250	mm/mm
Tangential Stiffness	$k_{s,j}$	DSSX/Y	LIT	214	373	131	3.4	N/mm³
Normal Stiffness	$k_{n,j}$	DSNZ	LIT	520	913	314	8.9	N/mm³

5.2 Unit Parameters

5.2.1 Density & E-modulus

The densities ρ_u and E-moduli E_u of the four block types were determined according to standard test methods, EN 772-13 (2000) and EN 12390-13 (2013), respectively. See Fourie (2017) for descriptions of the experimental configurations.

5.2.2 Poisson's Ratio

The Poisson's ratios ν_u could not be determined successfully experimentally, and values are taken from literature for the four materials: CON (Williams, et al., 2007), GEO (Joseph & Mathew, 2012), (Pan, et al., 2011), (Hardjito, et al., 2005), CSE (Venkatarama Reddy, et al., 2007) and ADB (Miccoli, et al., 2014). Due to limited experimental data available (ADB) or large variations in the results (CSE), sensitivity analyses to this parameter are performed for these two materials (see Section 6.3).

5.3   Unit Crack Interface Parameters

5.3.1   Unit Crack Tension Parameters

Tensile failure of masonry units is an important failure mechanism (Chisari, et al., 2018), and emphasis was placed on obtaining these parameters. The mode I fracture energy values $G_{f,c}^I$ for the unit crack interface are taken from the results of wedge splitting tests done by Fourie (2017), based on the experimental setup of Brühwiler and Wittmann (1990).

The tensile strengths $f_{t,c}$ are determined through inverse FEA, using the same wedge splitting test results for calibration. Figure 5.3 depicts the experimental test setup and a graphic of the numerical model used, with the support conditions indicated in red and the load application in green. The blue solid elements are the brick elements with linear material parameters, whereas the nonlinear behaviour is concentrated in the magenta interface elements, located in the position of the anticipated failure plane. In the model, the notch is extended to the depth of the groove for geometrical and mesh simplification.
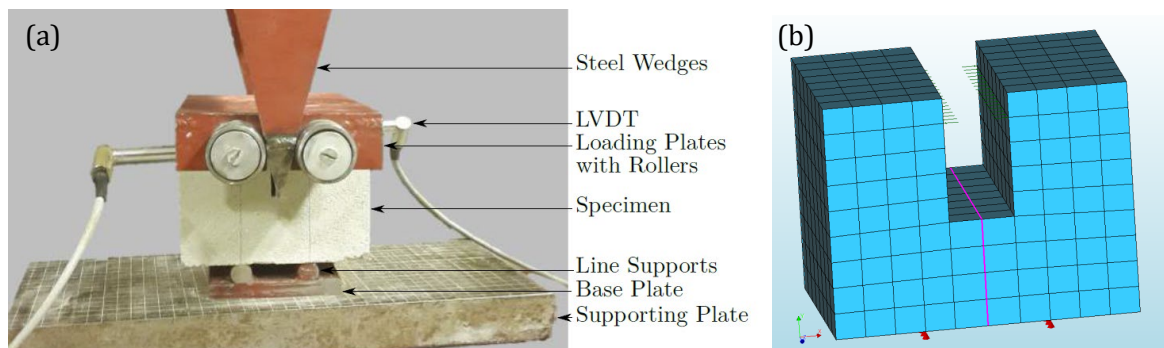
Figure 5.3: Wedge splitting test (a) experimental setup (Fourie, 2017) and (b) numerical model

Figure 5.4 depicts a typical failure crack achieved in the experiments and the modelled failure mechanism. Since the crack interface element is placed at the location of the anticipated failure plane, good correlation is found in the failure mechanism between the two.
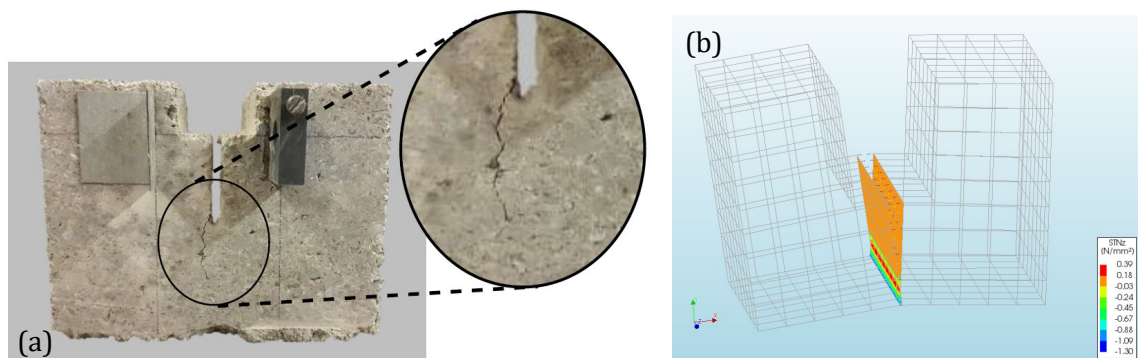
Figure 5.4: Wedge splitting test (a) typical failure crack (Fourie, 2017) and (b) numerical model failure mechanism

Figure 5.5 depicts the splitting force/CMOD curves for the experimental (EXP) envelope and the finite element analyses (NUM) for the four materials investigated. The mode I fracture energy had been determined experimentally, but the tensile fracture energy was determined by fitting the numerical results to each individual specimen's curve.
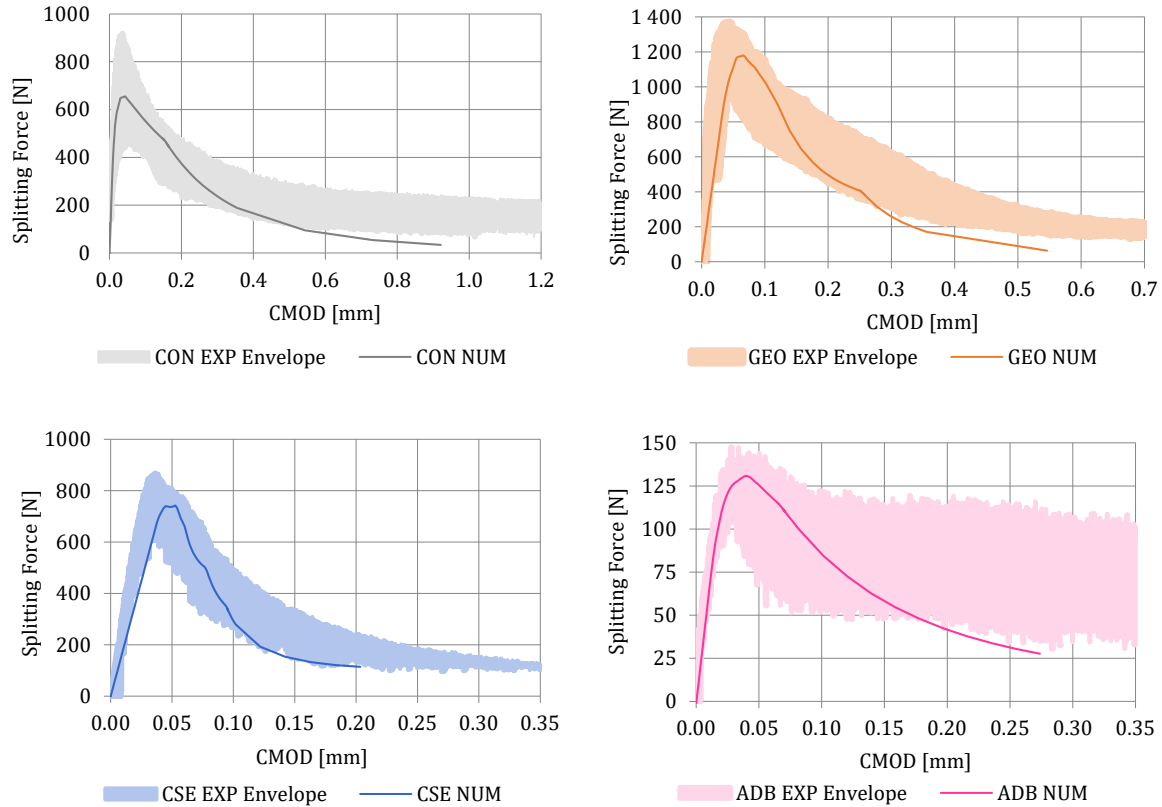
Figure 5.5: Experimental envelope and numerical analyses results for CON, GEO, CSE and ADB wedge splitting tests

The choice of exponential softening leads to slight strength overestimation immediately post-peak, and an underestimation later. A different choice of nonlinear softening function, such as by Hordijk (1991), would perhaps result in an improved fit, but is not available in the combined model used. Nevertheless, satisfactory agreement is established.

For the ratios of $f_{t,c}$ to $f_{c,c}$ (unit crack compressive strength) a range of 0.05–0.19 was found, which compares favourably to the ratios of 0.03-0.10 observed by Schubert (1988) and 0.1 estimated by Silva et al. (2014). For the ratios of $G_{f,c}^{I}$ to $f_{t,c}$, a range of 0.013–0.071 was found, which also compares positively to the ratios of 0.025-0.050 observed by Van Der Pluijm (1992) and 0.029 estimated by Silva et al. (2014). The unit crack interface tensile strength and mode I fracture energy are both included in the sensitivity analysis of Section 6.3.

5.3.2 Crack Shear Parameters

Shear failure in the masonry unit is rare (Chisari, et al., 2018) and the experimental determination of the parameters related to shear is particularly challenging, therefore conventional values are assumed. The cohesion c_c is taken as a function of the unit tensile strength, $1.5f_t$ (Silva, et al., 2014), whereas the friction angle ϕ_c is taken as 37° (Lourenço, 1996), (Silva, et al., 2014), taking into consideration that the material model mathematically limits the tensile strength to $c/tan\phi$ (DIANA, 2017). The dilatancy angle ψ_c of the masonry unit itself is a seldom discussed parameter, due to the low likelihood of shear sliding of the unit taking place, and is therefore assumed to be zero, as done by Chaimoon and Attard (2007).

Lourenço (1996) takes the mode II fracture energy $G_{f,c}^{II}$ to be 0, on the assumption that the shear stress drops to zero in a single load step after crack initiation. This is done for numerical reasons to avoid bifurcation, but numerical robustness is lost, as a large amount of energy is released in a single step. Therefore, this approach is not followed in this study. However, little is reported in literature on what reasonable values for mode II fracture energy would be. Macorini and Izzuddin (2011) as well as Chaimoon and Attard (2007) assume a value of 0.5N/mm. Nazief (2014) assumes the mode II fracture energy to be ten times the mode I fracture energy. This assumption is implemented in this study, resulting in values ranging between 0.06 and 0.56, which compare favourably to the 0.5 found in literature. This parameter is included in the sensitivity analysis in Section 6.3.

5.3.3   Crack Compression Parameters

The compressive strength of the unit crack interface $f_{c,c}$ is taken as the compressive strength of the unit, tested by Fourie (2017) according to EN 772-1 (2011).

For the compressive fracture energy values $G_{c,c}$ a value of 10N/mm was obtained by Mohamad (2007) for concrete blocks, however no data is available for this parameter for the three alternative materials. The compressive fracture energy is therefore estimated using a ductility index of 0.8mm, as in Equation 5.1, based on the relation of the CON compressive strength of the units, to the concrete compressive fracture energy obtained in literature. This parameter is included in the sensitivity analysis in Section 6.3.

$$G_{c,c} = 0.8mm \times f_{c,c} \qquad\qquad\qquad\qquad \text{Equation 5.1}$$

For lack of data, the equivalent plastic relative displacement $\kappa_{p,c}$, or strain at maximum compressive strength, for the crack interface is taken as the same value obtained for the joint interface for each of the four materials.

Considering that the post-peak shear behaviour is assumed to be negligible for the crack interface (Lourenço, 1996), the shear traction contribution $C_{ss,c}$ is taken as negligibly small (1×10^{-3}) for this study.

5.3.4   Crack Stiffness Parameters

The normal stiffness of the unit crack interface $k_{n,c}$ is assumed to be high, to prevent focusing the elastic deformation in the interface elements, and is taken as 100 times E_u and tangential stiffness $k_{s,c}$ is determined as done by Silva et al. (2014):

$$k_{s,c} = \frac{k_{n,c}}{2(1+v_u)} \qquad\qquad\qquad\qquad \text{Equation 5.2}$$

Lourenço and Rots (1997) recommend a normal stiffness of the same order of magnitude, namely 1×10^6N/mm³.

5.4   Joint Interface Parameters

Although bed joints and head joints will differ in their properties, no distinction is made between the bed and head joint interface parameters and the same values are assigned to the two joint types for each parameter. This is done mainly due to lack of data on the head joint behaviour. The determined joint interface parameter values are more representative of the bed joint behaviour due to the bed joint orientation of the shear triplet test, which is used as a basis to determine a number of the joint interface parameters. The parameter values are likely an overestimation for the head joint interface, and the effect of this on the structural masonry behaviour thus unconservative.

47

5.4.1 Joint Tension Parameters

The tensile strength $f_{t,j}$ of the joint interface was not determined experimentally. Instead the relationship between the joint tensile strength and cohesion c_j is used, $f_{t,j} = c_j/1.4$, as done by Lourenço and Rots (1997). Similar tensile strength/cohesion ratios can be obtained from experimental data reported in Haach et al. (2011), Chaimoon and Attard (2007) and Shieh-Beygi and Pietruszczak (2008). Employing this tensile strength/cohesion ratio also ensures that the tensile strength is limited to $f_{t,j} \leq c_j/tan\varphi_j$. This is necessary to satisfy the limitations placed on the dilatancy coefficient by the second law of thermodynamics (Van Zijl, 2004).

Similar to the mode I fracture energy for the crack interface, wedge splitting tests according to Brühwiler and Wittman (1990) were attempted to establish the joint interface mode I fracture energy $G_{f,j}^I$ but were unsuccessful. From the definition of tensile fracture energy, some correlation between it and the bond strength is expected but cannot be established for concrete (Van Der Pluijm, 1999), whereas a stronger correlation is found between the fracture energy and the type of concrete. This cannot be extended to the non-homogenous nature of masonry.

The most oft implemented mode I fracture energy value is 0.018N/mm for solid clay masonry, used by Lourenço (1996), Van Zijl (2004) and Macorini and Izzuddin (2011), to name a few, originating from CUR (1997). On the lower end of the scale, Van Zijl used 0.005 for calcium silicate masonry, originating from Van Der Pluijm (1992). Following tests performed on clay and calcium silicate masonry, Van Der Pluijm (1992) noted that the mode I fracture energy of the joint was approximately 1/10th of that of the units. Although this observation is anecdotal, this ratio is used in this study to provide an estimation of the order of magnitude of the mode I fracture energy for the joint interfaces.

In a parametric sensitivity study, Lourenço (1998) also found the results to be almost insensitive to variation in the joint tensile strength (1.1% difference to original) and the mode I fracture energy (0.9%). However, Lourenço's study (1998) was limited to the application of shear walls and Macorini and Izzuddin (2011) argue that these two parameters are key in the meso-modelling of unreinforced masonry walls when analysing their out-of-plane capacity. The joint tensile strength and mode I fracture energy are therefore included in the parameter sensitivity analysis (see Section 6.3).

5.4.2 Joint Shear Parameters

The constituent material model makes provision for the definition of fracture properties in one shear mode. Therefore, the mode II (shear), as opposed mode III (torsional), properties are defined for this model. Given the relatively low normal stresses anticipated in the application of the analyses, namely single-storey residential walls, the effect of neglecting the torsional resistance of the bed joints is minimal.

The cohesion c_j and friction ϕ_j for the joint interface are assumed to be constant (Chisari, et al., 2018) and the values are taken from the triplet tests performed by Fourie (2017), according to EN 1052-3 (2002).

The dilatancy angle ψ_j, measuring the amount of uplift of one unit over another under shear action, and dependent on the level of confining stress, can be significant to the analysis (Lourenço, 1996). Various values can be found, mostly for clay bricks: 7.1° (Burnett, et al., 2007), 27.5° (Haach, et al., 2011) and 31.0°, 33.8° and 36.5° (Van Zijl, 2004). According to Lourenço (1996) the confining stress sufficient to reduce the normal displacement under shearing, and hence the dilatancy angle, to zero, $\sigma_{u,j}$, is in the order of magnitude of 1.0 – 2.0N/mm2. This level of confining stress is based on shear tests (Figure 5.6) performed by Van Der Pluijm (1993) on two types of clay bricks, namely Joosten, a yellow wire cut brick denoted JG, and Vijf Eiken, a red soft mud brick, denoted VE.
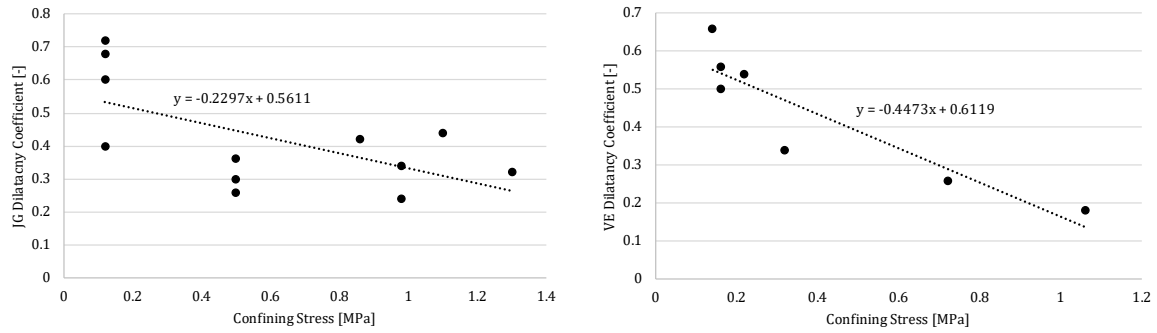
Figure 5.6: Dilatancy coefficient as a function of confining stress for JG and VE bricks (Van Der Pluijm, 1993)

On extrapolation of the linear trend line, the confining stress level at which the dilatancy coefficient reduces to zero is found to be 2.44N/mm² for the JG bricks and the 1.37N/mm² for VE bricks. The cohesion for these bricks was reported as 2.76N/mm² for the JG bricks and 1.33N/mm² for the VE bricks (Van Der Pluijm, 1993). Whilst similar in values, no direct relation can be drawn between the cohesion, a chemical bond, and the confining stress at which the dilatancy angle, a physical characteristic related to surface roughness, reduces to zero. However, the cohesion is an important characteristic of the joint/unit interface and, for lack of experimental data, is used as an indicator for this limiting confining stress, $\sigma_{u.j}$. Based on this assumption, the confining stress at which the dilatancy would reduce to zero for the four selected materials would be in the range of 0.05 – 0.17N/mm². Given this significantly low threshold below which the dilatancy could have an effect, the dilatancy angle is set to 0°. This assumption also prevents unconservative overestimation of the shear resistance (Van Zijl, 2004).

Post-peak experimental data for the four materials is not available to determine the mode II fracture energy $G_{f,j}^{II}$ for the joint interface. It was found to be between 0.01 and 0.25N/mm by Van Der Pluijm (1993) for clay bricks and calcium silicate blocks, for a range of cohesion and confining pressure values between 0.1 and 1.0N/mm². The following confining pressure σ dependent formulations for joint interface mode II fracture energy are found in literature:

clay:	$G_{f,j}^{II} = 0.058 - 0.13\sigma$	(Lourenço, 1996)	Equation 5.3
	$G_{f,j}^{II} = 0.006 - 0.09\sigma$	(Van Zijl, 2004)	Equation 5.4
calcium silicate:	$G_{f,j}^{II} = 0.005 - 0.02\sigma$	(Van Der Pluijm, et al., 2000)	Equation 5.5
	$G_{f,j}^{II} = 0.020 - 0.14\sigma$	(Van Der Pluijm, et al., 2000)	Equation 5.6
	$G_{f,j}^{II} = 0.020 - 0.03\sigma$	(Van Zijl, 2004)	Equation 5.7

Others use a constant mode II fracture energy value, independent of confining stress, ranging from 0.05 (Macorini & Izzuddin, 2011) to 2.0 (Haach, et al., 2011), with several in between: 0.059 (Burnett, et al., 2007), 0.08 (Berto, et al., 2005), 0.125 (Lourenço & Rots, 1997) and 0.167 (Chaimoon & Attard, 2007). Based on these ranges, the following formulation is used for this study:

$$G_{f,j}^{II} = 0.05 - 0.08\sigma \qquad\qquad\qquad \text{Equation 5.8}$$

Lourenço's (1998) parametric sensitivity study found the results to be almost insensitive to variation in the cohesion (0.6% difference to original) and mode II fracture energy (1.4%) but moderately sensitive (9.6%) to variations in the friction angle. However, all three parameters are included in the sensitivity analysis (Section 6.3).

49

5.4.3   Joint Compression Parameters

The compressive strength for the joint interface $f_{c,j}$ is taken as the compressive strength of the wallets (Macorini & Izzuddin, 2011), as tested by Fourie (2017), according to EN 1052-1 (1999). The compressive fracture energy $G_{c,j}$ and the equivalent plastic relative displacement, $\kappa_{p,j}$ values are determined through inverse FEA, using the same wallet compression test results for calibration. Figure 5.7 depicts the experimental test and numerical model used, with the support conditions indicated in red and the load application in green. The blue elements are the linear brick elements with the nonlinear behaviour concentrated in the magenta for the joints and black for the crack interface elements.
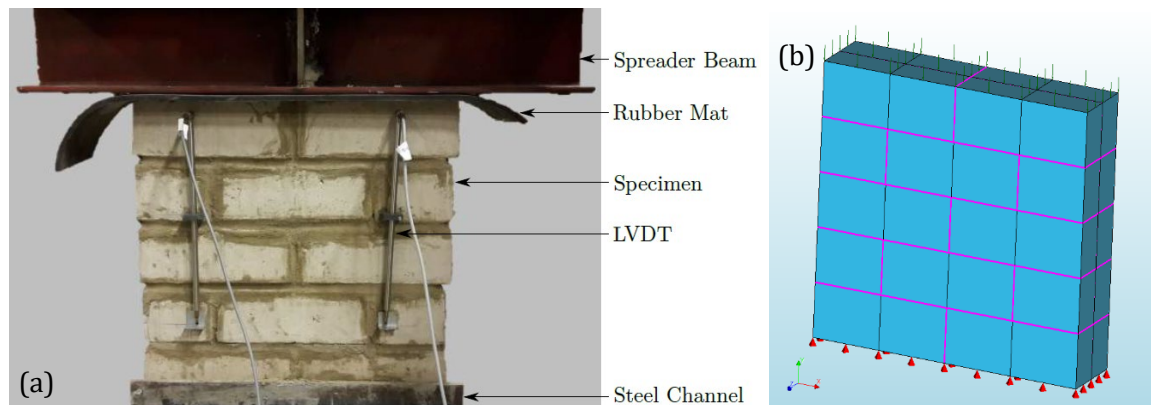
Figure 5.7: Wallet compression test (a) experimental setup (Fourie, 2017) and (b) numerical model

Figure 5.8 depicts the typical failure mechanism of the experiments and the numerical model. All specimens experienced crushing of the top course, but this was accompanied by tensile cracks through the mortar and units on the head face and a vertical splitting crack in the head face. The latter is a common failure type coupled to masonry crushing due to the mortar joint dilatancy under high confining stress (Lourenço, 1996). The high compressive forces, and the greater unit stiffness compared to the joint stiffness, prevents the mortar from expanding laterally. This in turn creates a tri-axial compressive state in the mortar and a compressive/biaxial tensile state in the unit (Macorini & Izzuddin, 2011). This failure mechanism is relevant to CON, GEO and CSE. However, in the case of ADB, the inverse relationship exists, in that the joint is stiffer than the unit. This changes the failure mechanism from tensile cracking of the unit to crushing of the unit, due to lack of confinement of the joints (Sousa, et al., 2015).
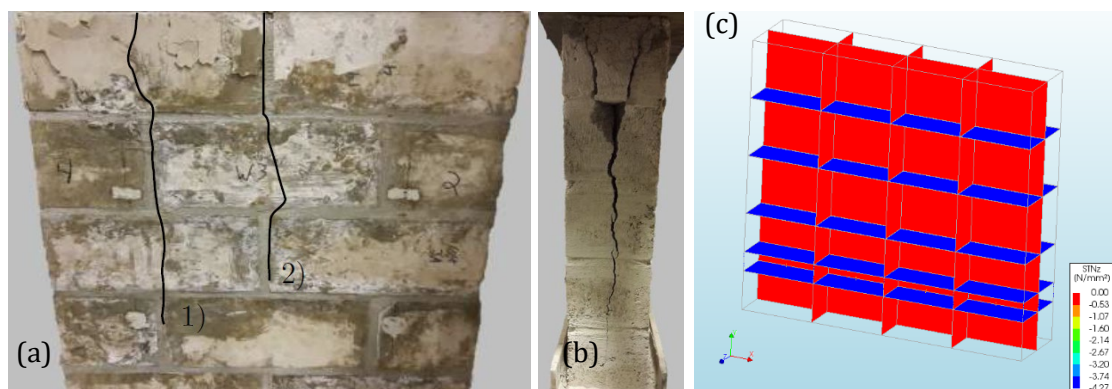
Figure 5.8: Wallet compression test (a) front face cracks and crushing of top course, (b) head face vertical splitting crack (Fourie, 2017) and (c) numerical model failure mechanism

The vertical cracks were a significant contributor to failure in the CON, GEO and CSE wallets. Only in the ADB wallets was crushing of the top course the dominant failure mode. In the numerical model, the failure mechanism was crushing of the lowest bed joint in all instances. The nonlinear behaviour is concentrated in the joints and therefore crushing failure will occur in the joints and not in the unit elements, and manifests as the lowest joint interface penetrating the adjacent units in Figure 5.8(c). Since the own weight of the specimens was included in the analyses, there is sufficient load differentiation numerically to cause crushing at the bottom of the specimen.

Figure 5.9 depicts the load/displacement curves for the experimental envelope and the finite element analyses for each of the four materials investigated. The linear portion of the experimental data was obtained directly from LVDT readings on the specimen. The nonlinear displacements (Δ_w) were derived from the testing machine's total displacement (Δ_t) and load cell (F), taking into account the stiffness of the testing system as a whole (K_s) by determining the wallet stiffness (K_w) and the total stiffness (K_t) at a specific elastic point, and isolating the displacement of the testing system (Δ_s), according to the following three equations:

$$K_w = \frac{F}{\Delta_w} \qquad \text{and} \qquad K_t = \frac{F}{\Delta_t} \qquad\qquad\qquad \text{Equation 5.9}$$

$$K_s = \frac{K_t K_w}{K_w - K_t} \qquad\qquad\qquad \text{Equation 5.10}$$

$$\Delta_s = \frac{F}{K_s} \qquad\qquad\qquad \text{Equation 5.11}$$

For these analyses, the compressive strength and elastic stiffness had been determined experimentally, but the compressive fracture energy and equivalent relative plastic displacement were estimated by fitting the numerical results (NUM) to each specimen set's general trend (EXP).
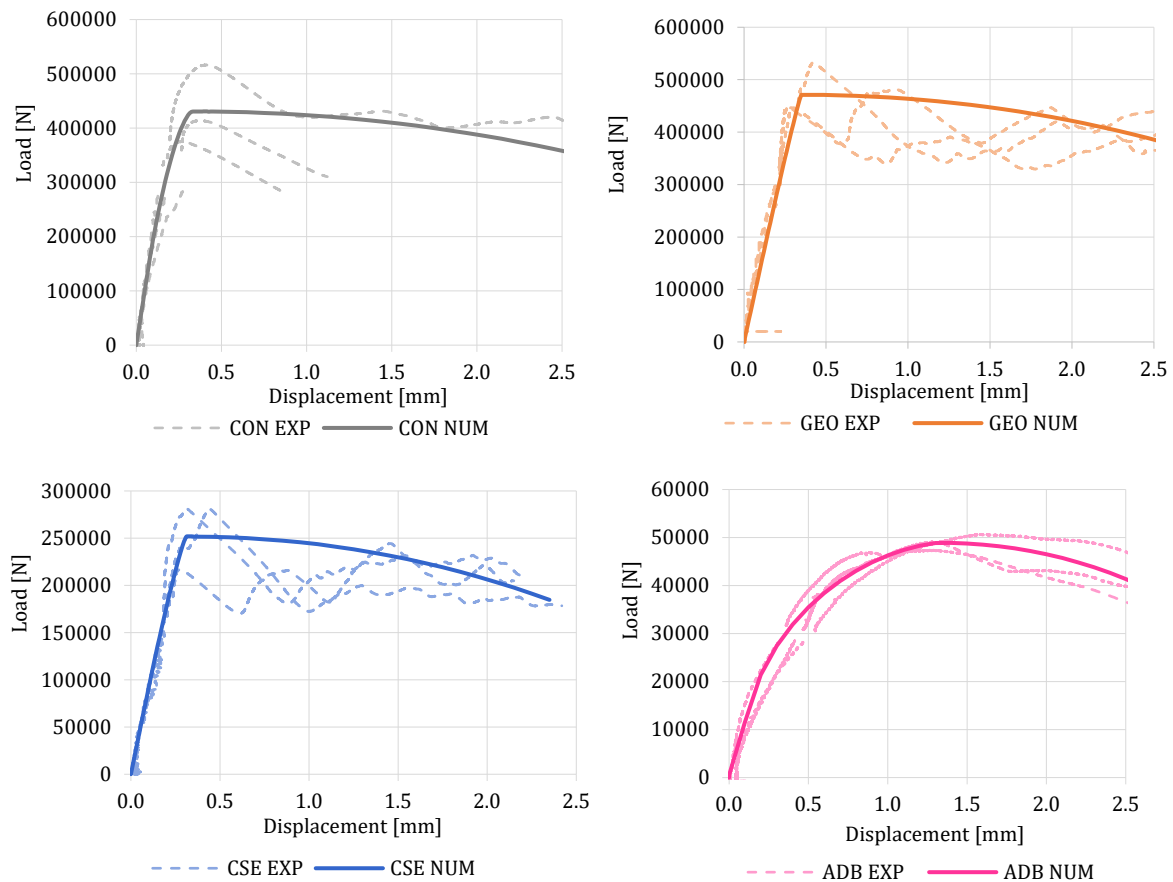
Figure 5.9: Experimental data and numerical analyses results for CON, GEO, CSE and ADB wallet compression tests

The wallet compression test setup is not ideal for the determination of the compressive fracture energy, as it is intended for the determination of the compressive strength and stiffness, and the subsequent fracture zones are localized and varied. Of the four wallet types, the ADB compressive fracture energy estimated is the most appropriate since the primary failure mechanism was top course crushing. The failure mechanisms of the other three materials were a combination of crushing and vertical cracking and the compressive fracture energies estimated are most likely an underestimation, however, as more appropriate experimental data is currently not available for these materials, these fracture energies are used as an indication. Therefore, and since Lourenço (1998) found the analyses to be sensitive to this parameter (18.6% difference to original), it is included in the sensitivity analysis in Section 6.3.

From the definition of the compression cap, $C_{ss,j}$ controls the shear stress contribution to compressive failure of the joint interface (Lourenço, 1996) but was found to have an insignificant influence. Nevertheless, this parameter was determined from the masonry compressive strength $f_{c,j}$ and the ultimate shear strength $\tau_{u,j}$, as follows (Lourenço, 1996):

$$\tau_{u,j} = \frac{f_{c,j}}{\sqrt{C_{ss,j}}}$$
Equation 5.12

The ultimate shear strengths, given in Table 5.3, are extrapolated based on the shear/compressive stress relationship obtained from the shear triplet tests performed by Fourie (2017), to the point of the masonry compressive strength.

Table 5.3: Ultimate joint interface shear strengths

	CON	GEO	CSE	ADB
τ_u $[N/mm^2]$	6.6	3.6	3.0	0.7

5.4.4 Joint Stiffness Parameters

A number of models have been proposed to determine both the normal stiffness $k_{n,j}$ and the tangential stiffness $k_{s,j}$ of the joint interface. One option is to employ a high artificial stiffness in the interface elements and a reduced stiffness of the unit elements (Lourenço, 1996). This is typically done to prevent interpenetration of the unit and interface elements. However, this phenomenon is an intrinsic component of the zero-thickness interface element formulation and this approach is not followed for this study.

In its simplest form, Spada et al. (2009) use a ratio of the mortar elastic modulus E_m, to the mortar joint thickness h_m, for the normal stiffness, as described in the following equation, and similarly for the tangential stiffness:

$$k_{n,j} = \frac{E_m}{h_m}$$
Equation 5.13

$$k_{t,j} = \frac{G_m}{h_m}$$
Equation 5.14

This approach only incorporates the mortar characteristics and is inappropriate for the current study, given that the mortar and mortar/unit interface are lumped in a single zero-thickness element.

Rots (1997) and Lourenço (1996) recommend using a combination of the unit and mortar moduli of elasticity, E_u and E_m respectively, and the mortar joint thickness h_m, for the normal stiffness, as described in Equation 5.15. A similar approach is followed for the tangential stiffness using the respective shear moduli, as in Equation 5.16. This is done to account for the reduction of the mortar joint to a zero-thickness interface, assuming that the unit elastic properties remain constant and a uniform stress state in the mortar and unit, depicted in Figure 5.10. This stiffness model is an indication of the relationship between the unit and mortar elastic moduli, and not a mortar characteristic as such.

$$k_{n,j} = \frac{E_u E_m}{h_m(E_u - E_m)}$$
<div align="right">Equation 5.15</div>

$$k_{s,j} = \frac{G_u G_m}{h_m(G_u - G_m)}$$
<div align="right">Equation 5.16</div>
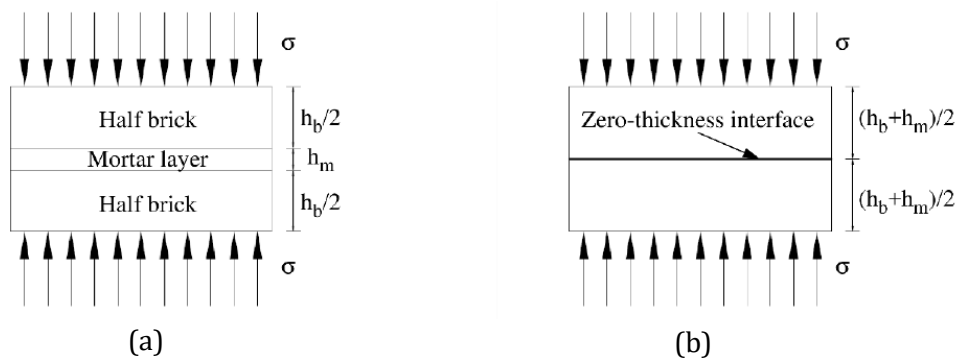
Figure 5.10: (a) unit-mortar element in compression, and (b) zero-thickness interface meso-scale representation (Chisari, et al., 2018)

As can be deduced from Equation 5.15, a high normal stiffness is not an indication of a stiff mortar joint, but rather of similar unit and mortar moduli of elasticity. It is also apparent that for a unit/mortar combination where $E_m = E_u$, an invalid normal stiffness is obtained, and when $E_m > E_u$, a negative normal stiffness results. For most conventional masonry, it can safely be assumed that $E_u > E_m$, however, for alternative masonry, this is not necessarily the case, and this must be considered with care. Despite this, the method is considered the most appropriate.

In order to use this approach, the mortar elastic modulus must be known. Establishing this experimentally insitu in a direct manner is challenging, therefore Van Der Pluijm's (1999) approach is used to extract the mortar elastic moduli from masonry wallet compression tests, as in Equation 5.17, where E_u and E_w are the unit and masonry wallet elasticity moduli respectively, and $h_{u,g} (= 1.5 \times h_u)$ and $h_{m,g} (= 2 \times h_m)$ are the height of the units and the thickness of mortar joints within the gauge length on the specimen respectively. The mortar shear moduli G_m, are determined based on an assumed mortar Poisson's ratio v_m of 0.2, Equation 5.18. Similarly, the unit shear moduli G_u, are determined based on the assumed unit Poisson's ratios, discussed in Section 5.2.2.

$$E_m = \frac{h_{m,g} E_w E_u}{E_u(h_{u,g} + h_{m,g}) - E_w h_{u,g}}$$
<div align="right">Equation 5.17</div>

$$G_m = \frac{E_m}{2(1+v_m)}$$
<div align="right">Equation 5.18</div>

The masonry modulus of elasticity E_w was determined for each material according to EN 1052-1 (1999) by Fourie (2017) and the values obtained are presented in Table 5.4, together with the mortar elastic moduli and mortar and unit shear moduli obtained.

Table 5.4: Elastic and shear moduli for wallet and mortar

	CON	GEO	CSE	ADB
$E_w\ [N/mm^2]$	13 100	9800	6100	600
$E_m\ [N/mm^2]$	4017	4992	2223	79
$G_m\ [N/mm^2]$	1674	2080	926	33
$G_u\ [N/mm^2]$	7629	4709	3179	855

This approach does assume that the Poisson's ratios for the mortar and the unit are the same. Although this is not the case in all instances, the effect is deemed negligible. The parametric sensitivity study conducted by Lourenço (1998) found the results to be noticeably sensitive (6.2% difference to original) to the stiffness of the joints and this parameter is included in the sensitivity analysis indirectly, by varying the unit E-modulus (see Section 6.3).

54

5.5 Parameter Relationships

None of the masonry parameters discussed and quantified in the previous sections act in isolation and some are used as predictors or indicators of others. These relationships, although presented in the previous sections, are summarised in Table 5.5 for convenience. Even though they are presented as dependent relationships, these dependencies have no physical basis in most instances, and are derived for lack of accurate testing capabilities or used for benchmarking purposes. For those relationships where a range was presented previously, a reasonable average is presented in Table 5.5. The term 'unit crack' refers to the 'unit crack interface' and 'joint' to 'joint interface' in all instances.

Table 5.5: Summary of parameter relationships used

Parameter	Origin	Relationship
unit crack tensile strength*	unit crack compressive strength	$f_{t,c} = 0.1 f_{c,c}$
unit crack mode I fracture energy*	unit crack tensile strength	$G_{f,c}^I = 0.035 f_{t,c}$
unit crack cohesion	unit crack tensile strength	$c_c = 1.5 f_{t,c}$
unit crack mode II fracture energy	unit crack mode I fracture energy	$G_{f,c}^{II} = 10 G_{f,c}^I$
unit crack compressive fracture energy	unit crack compressive strength	$G_{c,c} = 0.8 f_{c,c}$
unit crack normal stiffness	unit E-modulus	$k_{n,c} = 100 E_u$
unit crack tangential stiffness	unit crack normal stiffness \ unit Poisson	$k_{s,c} = \dfrac{k_{n,c}}{2(1 + v_u)}$
joint tensile strength	joint cohesion	$f_{t,j} = c_j / 1.4$
joint mode I fracture energy	unit crack mode I fracture energy	$G_{f,j}^I = G_{f,c}^I / 10$
joint mode II fracture energy	confining stress	$G_{f,j}^{II} = 0.05 - 0.08\sigma$
joint shear traction contribution	joint compressive strength \ joint ultimate shear strength	$c_{ss,j} = \left(\dfrac{f_{c,j}}{\tau_{u,j}}\right)^2$
joint normal stiffness	unit E-modulus \ mortar E-modulus \ mortar height	$k_{n,j} = \dfrac{E_u E_m}{h_m(E_u - E_m)}$
joint tangential stiffness	unit shear modulus \ mortar shear modulus \ mortar height	$k_{s,j} = \dfrac{G_u G_m}{h_m(G_u - G_m)}$

* relationship is used for benchmarking purposes only, not for the determination of the parameter

After finalisation of the material parameter input for the FE analyses, Ghiassi, Vermeltfoort and Lourenço (2019) published a compilation of conventional masonry mechanical properties for numerical modelling of the unit, mortar, interface and masonry, as well as suggestions for mechanical properties when experimental data is not readily available. The properties or relationships between properties relevant to this work are summarised in Table 5.6, and compared to the values used in this work for CON and the three AMU's.

Table 5.6: Summary and comparison of parameters to Ghiassi et al. (2019)

Parameter	Relationship		Ghiassi et al. (2019)	CON	GEO	CSE	ADB	
Unit E-modulus	E_u	$E_u/f_{c,c}$	160 - 380	1463	616	1156	3100	-
Unit Tensile Strength	$f_{t,c}$	$f_{t,c}/f_{c,c}$	0.07 - 0.10	0.05	0.09	0.18	0.19	-
Unit Mode I Fracture Energy	$G^I_{f,c}$	$G^I_{f,c}/f_{t,c}$	0.029	0.071	0.036	0.013	0.040	N/mm
Unit Compression Ductility Index	$d_{c,u}$	$G_{c,c}/f_{c,c}$	1.6	0.8	0.8	0.8	0.8	mm
Joint Tensile Strength	$f_{t,j}$	-	0.1 - 0.2	0.12	0.08	0.06	0.04	N/mm^2
Joint Mode I Fracture Energy	$G^I_{f,j}$	$G^I_{f,j}/c_j$	0.1	0.03	0.05	0.02	0.01	N/mm^2
Joint Cohesion	c_j	$c_j/f_{c,j}$	0.055	0.031	0.018	0.029	0.083	N/mm^2
Joint Tangent Friction Angle	tan φ	-	0.4 - 0.75	1.17	0.58	0.93	1.02	-
Joint Mode II Fracture Energy	$G^{II}_{f,j}$	$G^{II}_{f,j}/c_j$	0.1	0.29	0.45	0.56	1.00	N/mm^2

Of the parameters in Table 5.6, the unit tensile strength and mode I fracture energy relationships, as well as the joint tensile strength values and joint cohesion and mode II fracture energy relationships for the four materials (CON, GEO, CSE, ADB) compare reasonably well to the values or ranges proposed by Ghiassi et al. (2019) for conventional materials. Based on the limited AMU experimental data of this study, the recommendations made for conventional materials could also be valid for AMU's.

The four shaded parameters in Table 5.6 compare less well. The recommended range for determining the unit E-modulus based on the unit compressive strength (160 – 380) is well below the values obtained for the four block types in this study (616 – 3100). The joint tangent friction angle recommended range (0.4 – 0.75) is also lower than the range obtained for the four block types (0.58 – 1.17). Given that these parameters were all determined experimentally for each specific block type, the obtained values are used with confidence and the discrepancies are indicative of the high variability of masonry properties and the inherent differences in material types.

The recommended unit compression ductility index, based on the unit compressive fracture energy and compressive strength (1.6) is considerably different to the index used in this study (0.8), which was derived from literature for concrete blocks (see Section 5.3.3). The recommended ratio of joint mode I fracture energy to joint cohesion (0.1) is higher than the ratio range in this study (0.01 – 0.05). Whilst the joint cohesion was determined experimentally, the joint mode I fracture energy was taken as 0.1x the unit mode I fracture energy, as recommended by Van Der Pluijm (1999), (see Section 5.4.1). The unit compressive fracture energy and the joint mode I fracture energy cannot readily be confirmed experimentally, but since reasonable findings in literature were used to determine them, these values are used with confidence. However, careful consideration is necessary before recommendations for these parameters can be made for AMU's.

5.6   Strength Prediction Models

The material parameters discussed in the previous sections fully describe the selected material model, Combined Cracking-Shearing-Crushing. Before validation of the FE model is laid out in the following chapter, a brief digression into standardised strength prediction models is pursued. Whilst these predictive models in masonry standards were developed based on the experience and data of conventional masonry materials, it is compelling to consider their validity for alternative masonry, given the material data and test results at hand in the previous sections.

The empirical models for nominal masonry compressive, flexural and shear strength, provided in SANS 51996-1-1 (2018) and SANS 10164-1 (1989) are compared to the compressive, flexural and shear strength test results for the four materials used in this study, tested according to EN 1052-1 (1999), EN 1052-2 (1999) and EN 1052-3 (2002) respectively.

5.6.1   Compressive Strength of Masonry

In the EC6-based standard, SANS 51996-1-1, the characteristic compressive strength f_k, is determined by the following equation:

$$f_k = K f_b^{0.7} f_m^{0.3}$$ Equation 5.19

based on f_b, the unit normalised mean compressive strength and f_m, the mortar compressive strength, as well as a probabilistic model constant K, for which values are provided, depending on masonry unit material type and group. This constant is intended to include model uncertainties such as insufficient experimental data, simplifications and unknown execution quality (Sýkora & Holický, 2010).

A K-value of 0.55 is assumed for this comparative exercise, the recommended value for all Group 1 units, except stone. Additionally, a fitted K-value is determined for each material which delivers a masonry compressive strength matched to the experimental results.

In SANS 10164-1, based on the withdrawn BS 5628-1 (1978), characteristic compressive strengths for masonry are provided in table format, depending on masonry unit material type (clay brick and concrete block) and unit compressive strength as well as mortar class. Linear interpolation between the unit compressive strengths is permitted, but not between mortar classes.

The mean masonry compressive strengths obtained experimentally (EXP) by Fourie (2017), according to EN 1052-1 (1999) and the characteristic values determined by means of the two standardised models (MOD), are detailed in Table 5.7 and Figure 5.11. As presumed, the results are scattered, but some points of interest are highlighted. It appears as though the higher the unit compression strength, the larger the discrepancy between the EXP and MOD results. However, when considering the average percentage difference between the EXP and MOD results per material, CON exhibits the lowest discrepancy (11%), followed by CSE (17%), ADB (31%) and GEO (33%).

Regarding the three strength prediction models, the SANS 10164 model for clay bricks revealed the lowest discrepancy averaged over the four materials, at 17%, followed by the SANS 10164 model for concrete blocks at 20% and SANS 51996 at 32%. Both SANS 51996 and SANS 10164 for concrete blocks overestimate the masonry compressive strength (except in the case of ADB), which should not occur.

Table 5.7: Compressive strength of masonry to SANS 51996-1-1 (2018) and SANS 10164-1 (1989) and experimental values

		Reference			CON	GEO	CSE	ADB
EXP	Unit compressive strength	EN 772-1	f_b	N/mm²	12.1	17.9	6.6	0.8
	Mortar compressive strength	EN 1015-11	f_m	N/mm²	10.3	15.3	9.9	0.8
	Masonry compressive strength	EN 1052-1	f_k	N/mm²	5.5	6.1	3.1	0.6
MOD	**Masonry compressive strength**	SANS 51996-1-1, Eq. 3.2, Table 3.3	f_k	N/mm²	6.3	9.4	4.1	0.4
	Masonry compressive strength	SANS 10164-1, Table 3a (clay)	f_k	N/mm²	4.6	6.7	3.0	0.4
	Masonry compressive strength	SANS 10164-1, Table 3b (concrete)	f_k	N/mm²	5.5	8.1	3.6	0.4
	Constant K: Best Fit	SANS 51996-1-1, Eq. 3.2	K	-	0.48	0.36	0.42	0.75
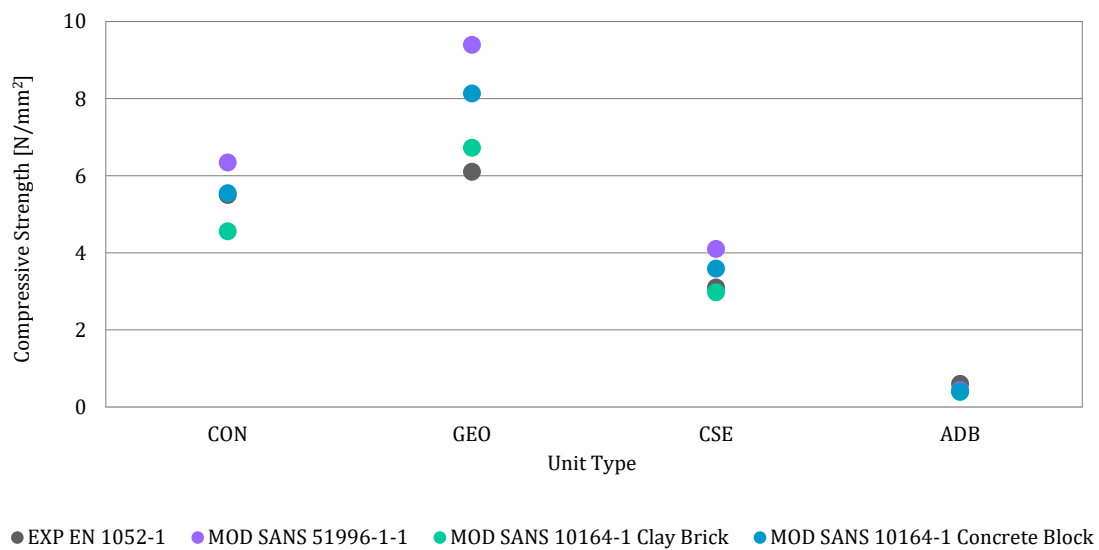
Figure 5.11: Compressive strength of masonry to SANS 51996-1-1 (2018) and SANS 10164-1 (1989) and experimental values

Some of the discrepancy in masonry strengths between the EXP and MOD results can be ascribed to the difference in Poisson ratios for the different unit materials. Incompatible lateral deformation between the units and mortar leads to tension in the units and compression in the mortar, perpendicular to the compressive load (Vermeltfoort, et al., 2007), except for the case of ADB, where the reverse would occur. The tensile stress in the units causes splitting cracks parallel to the compressive load. The larger the Poisson difference, and hence lateral deformation incompatibility, the more pronounced this effect may be. As an aside, the CON masonry compressive strength of 5.5N/mm² is predicted precisely by the SANS 10164 model for concrete blocks. The model is developed for this exact material and compressive strength range, but given that the EXP results consist of relatively small test sets, the correlation is remarkable.

58

5.6.2 Flexural Strength of Masonry

For the characteristic flexural strength, SANS 51996-1-1 provides empirical values within Note 2 of Clause 3.6.3(3), differing only on the basis of the failure plane and mortar strength, not unit type. However, these values are only a recommendation, and the characteristic flexural strengths, in lieu of testing, are classified as nationally determined parameters (NDP's).

The values prescribed for masonry flexural strength in both the UK NA to EN 1996-1-1 and SANS 10164-1 are taken from BS 5628-1, and are identical. Flexural strength is differentiated based on failure plane, mortar class, unit type, unit compressive strength and wall thickness. Linear interpolation for the latter two parameters is permitted.

The mean masonry flexural strengths, with failure parallel to the bed joints, obtained experimentally (EXP) by Jooste (unpublished), according to EN 1052-2 (1999), and the characteristic strengths determined by means of the two standardised models (MOD), are detailed in Table 5.8 and Figure 5.12.

Table 5.8: Flexural strength of masonry parallel to bed joints to SANS 51996-1-1 (2018), UK NA to BS EN 1996-1-1 (2005) and SANS 10164-1 (1989) and experimental values

		Reference			CON	GEO	CSE	ADB
EXP	**Masonry Flexural Strength**	EN 1052-2	f_{xk1}	N/mm²	0.35	0.26	0.13	0.05
MOD	**Masonry Flexural Strength**	SANS 51996-1-1, 3.6.3 (3) NOTE 2	f_{xk1}	N/mm²	0.10	0.10	0.10	0.10
	Masonry Flexural Strength	NA to BS EN 1996-1-1, Table NA.6 & SANS 10164-1, Table 4	f_{xk1}	N/mm²	0.25	0.25	0.22	0.22
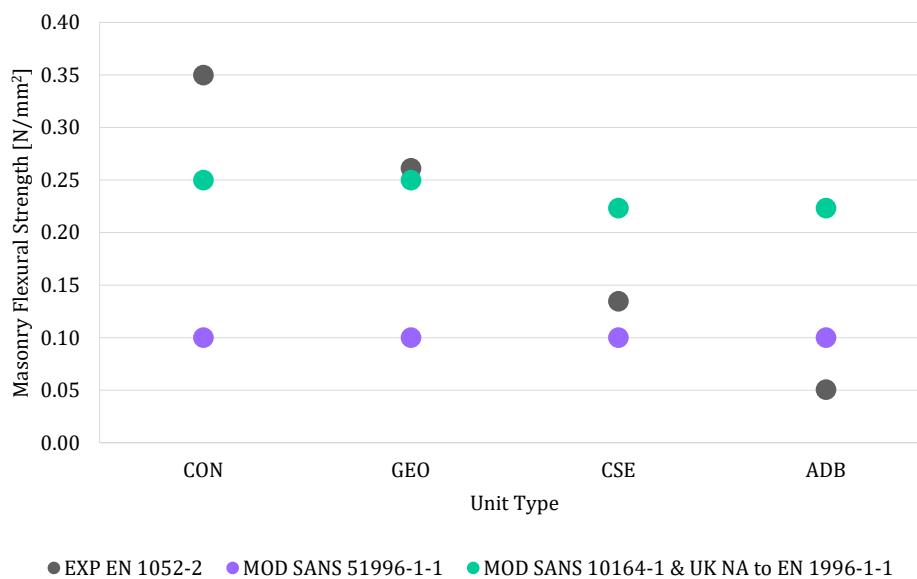
Figure 5.12: Flexural strength of masonry parallel to bed joints to SANS 51996-1-1 (2018), UK NA to BS EN 1996-1-1 (2005) and SANS 10164-1 (1989) and experimental values

59

The significant difference between the EXP and MOD flexural strength results for failure parallel to the bed joints is not unexpected, especially for SANS 51996, given the empirical (conventional) basis of the MOD flexural strength values. For both CON and GEO, the SANS 51996 values recommended for flexural strength parallel to bed joints are markedly more conservative (29% and 38% of the EXP values respectively) compared to the values from SANS 10164 and the UK NA to EN1996 (71% and 96% of the EXP values respectively). However, for CSE the EXP value falls between the two model values and for ADB both models overestimate the flexural strength, by 50% and 77% respectively.

The mean masonry flexural strengths, with failure perpendicular to the bed joints, obtained experimentally (EXP) by Jooste (unpublished), according to EN 1052-2 (1999) and the characteristic values determined by means of the two standardised models (MOD), are detailed in Table 5.9 and Figure 5.13.

Table 5.9: Flexural strength of masonry perpendicular to bed joints to SANS 51996-1-1 (2018), UK NA to BS EN 1996-1-1 (2005) and SANS 10164-1 (1989) and experimental values

		Reference			CON	GEO	CSE	ADB
EXP	**Masonry Flexural Strength**	EN 1052-2	f_{xk2}	N/mm²	0.66	0.73	0.24	0.12
MOD	**Masonry Flexural Strength**	SANS 51996-1-1, 3.6.3 (3) NOTE 2	f_{xk2}	N/mm²	0.40	0.40	0.40	0.40
	Masonry Flexural Strength	NA to BS EN 1996-1-1, Table NA.6 & SANS 10164-1, Table 4	f_{xk2}	N/mm²	0.89	0.90	0.59	0.07

● EXP EN 1052-2   ● MOD SANS 51996-1-1   ● MOD SANS 10164-1 & UK NA to EN 1996-1-1
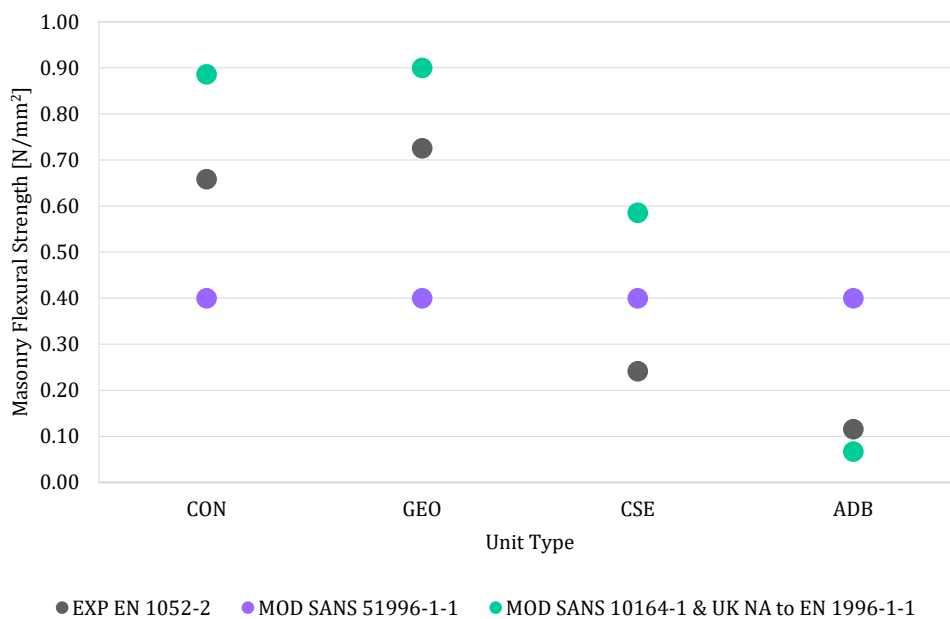
Figure 5.13: Flexural strength of masonry perpendicular to bed joints to SANS 51996-1-1 (2018), UK NA to BS EN 1996-1-1 (2005) and SANS 10164-1 (1989) and experimental values

Again, the SANS 51996 values recommended for flexural strength perpendicular to bed joints are consistent for all four materials, since the model makes no distinction on the basis of unit type. This model underestimates the flexural strengths of CON and GEO (by 40% and 45% respectively) and overestimates them for CSE and ADB (by 40% and 70% respectively). Notably, the flexural strength values according to SANS 10164 and UK NA to EN1996, whilst generally an overestimation, do follow the relative trend of the different unit types.

5.6.3 Shear Strength of Masonry

In SANS 51996-1-1 the characteristic shear strength f_{vk}, is determined by the following equation:

$$f_{vk} = f_{vko} + 0.4\sigma_d \hspace{4cm} \text{Equation 5.20}$$

based on f_{vko}, the characteristic shear strength, determined under no compressive stress, and σ_d, the design compressive stress perpendicular to the shear plane.

In SANS 10164-1 a constant adhesive shear strength is assumed, which differs depending on the mortar class. The only variable is the design compressive stress, g_A, which governs the frictional contribution to shear resistance:

Mortar Class I $\hspace{2cm} f_v = 0.35 + 0.6g_A \hspace{3cm}$ Equation 5.21

Mortar Class II $\hspace{2cm} f_v = 0.15 + 0.6g_A \hspace{3cm}$ Equation 5.22

However, only models for mortar classes I and II exist, therefore ADB (Class III mortar) was also calculated based on Class II mortar. The mean masonry shear strengths obtained experimentally (EXP) by Fourie (2017), according to EN 1052-3 (2002), and the characteristic values determined by means of the two standardised models (MOD), are detailed in Table 5.10 and Figure 5.14. Two levels of design compressive stress are included, 0.3N/mm² and 0.5N/mm² for CON, GEO and CSE, and 0.05N/mm² and 0.1N/mm² for ADB, based on the precompression levels employed in the experiments by Fourie (2017).

Table 5.10: Shear strength of masonry to SANS 51996-1-1 (2018) and SANS 10164-1 (1989) and experimental values

				CON		GEO		CSE		ADB	
	Reference			0.3	0.5	0.3	0.5	0.3	0.5	0.05	0.1
EXP	Initial shear strength	EN 1052-3	f_{vko}	N/mm²	0.17		0.09		0.09		0.05	
	Compressive stress	EN 1052-3	σ_d	N/mm²	0.29	0.50	0.30	0.50	0.31	0.50	0.06	0.11
	Masonry shear strength	EN 1053-2	f_{vk}	N/mm²	0.52	0.76	0.34	0.35	0.43	0.56	0.11	0.16
MOD	**Masonry shear strength**	SANS 51996-1-1, Eq. 3.5	f_{vk}	N/mm²	0.29	0.37	0.21	0.29	0.21	0.29	0.07	0.09
	Masonry shear strength	SANS 10164-1, 4.2.4	f_{vk}	N/mm²	0.53	0.65	0.33	0.45	0.53	0.65	0.39	0.42
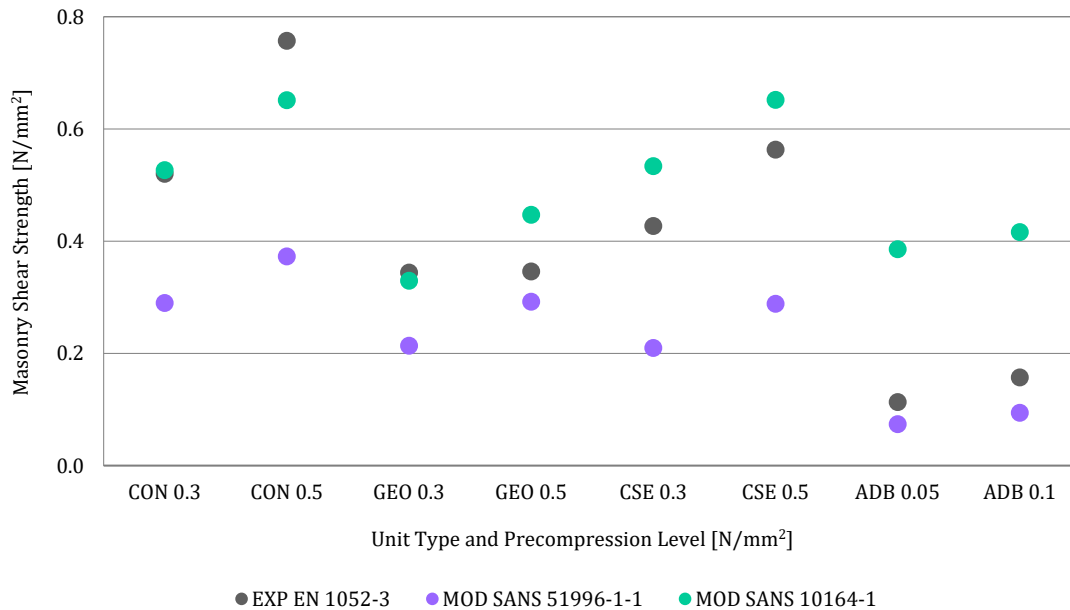
Figure 5.14: Shear strength of masonry to SANS 51996-1-1 (2018) and SANS 10164-1 (1989) and experimental values

Again the results are scattered, but points of interest can be distinguished. Since the SANS 10164 model does not make provision for the mortar class used with ADB (and the results subsequently deviate significantly) the ADB results are not included in the discussion that follows. Of the remaining three materials the average percentage difference between the EXP and MOD results are lowest for GEO (21%), followed by 28% for CON and 35% for CSE. The discrepancies found for the two design compression levels are similar, 27% for 0.3N/mm² and 29% for 0.5N/mm².

Regarding the two strength prediction models, the SANS 10164 model revealed a significantly lower average discrepancy of 15%, compared to 41% of SANS 51996. SANS 51996 consistently underestimates the masonry shear strength, whereas SANS 10164 is mostly an overestimation. Similar to the SANS 10164 predictions for the compressive strength, the CON shear strength prediction, with 0.3N/mm² precompressive load, of 0.53N/mm² is remarkably close to the EXP result of 0.52N/mm².

5.6.4   Conclusion

Notably, SANS 51996 does not distinguish between masonry unit material types (only perforation level) for any of the three strength prediction models, which is conducive of a material non-specific standard. Strength underestimation by the predictive model, as SANS 51996 generally does for shear (and flexure to a lesser degree), is also a consistent approach for such a development. A reasonable strategy would be to recommend a conservative nominal strength, with the allowance in the form of a qualifying statement that a more accurate strength prediction for particular masonry types could be included in NA's, if sufficient data is available, or determined through testing. Further investigation into improved prediction of masonry composite strength falls beyond the scope of this study.

5.7   Summary

Four block types, CON, GEO, CSE and ADB, were selected for the study, and subsequently parametrised using a combination of literary sources, small and medium scale testing and fitting of FE results to experimental data. This results in a near-comprehensive material model description of three alternative materials, otherwise not well described in literature.

Nonetheless, a number of assumptions, approximations and extrapolations were necessary, given the scarcity of reliable data for the alternative materials and difficulty level and lack of refinement in testing procedures. The validity and significance of these assumptions are assessed, quantified and discussed in the following chapter.

6 Model Validation

Critical to the quality assurance of a predictive FE model is the validation process. The proposed model is validated for both in-plane and out-of-plane behaviour by comparing the results of large scale single leaf wall experiments and their respective numerical analyses for the materials under consideration in the study. Subsequently a sensitivity analysis is performed on the most critical parameters.

6.1 In-Plane Model Validation

Large scale single leaf walls were constructed and tested in-plane by Shiso (2019) using the three AMU types, GEO, CSE and ADB. The specimen configurations were subsequently modelled, using the FE approach detailed in Section 4.1.2, and the horizontal force-displacement responses are compared, together with the failure mechanism, crack pattern, peak horizontal loads and horizontal displacements at peak load.

6.1.1 In-Plane FE Model

The wall specimens, 1790mm in height and 1790mm in length with 10mm mortar joints, were tested with two different sets of boundary conditions, described in Figure 6.1. Test Setup 1 represented a fixed/free configuration (without the indicated high tensile bars) whereas Test Setup 2 represented fixed/fixed boundary conditions (with the indicated high tensile bars). In both cases, a precompression load was applied and distributed by means of a steel spreader beam, equivalent in magnitude to 15% of the compression capacity of the masonry assemblage. This compressive strength was determined according to EN 1052-1 (1999).

For Test Setup 1, the precompression load was maintained for the duration of the test. For the second test setup, the displacement of the Instron actuator was fixed once the precompression load had been applied, and the high tensile bars were applied to prevent rotation of the wall. Subsequently, a horizontal load was applied by means of a hydraulic jack to the top north corner of the wall for both test setups.

For the FE models of these walls, depicted in Figure 6.2, the support conditions are indicated in red and the load application in green and yellow. The light blue elements are the linear brick elements with the nonlinear behaviour concentrated in the magenta for the joints and black for the crack interface elements. The dark blue elements represent the spreader beam.
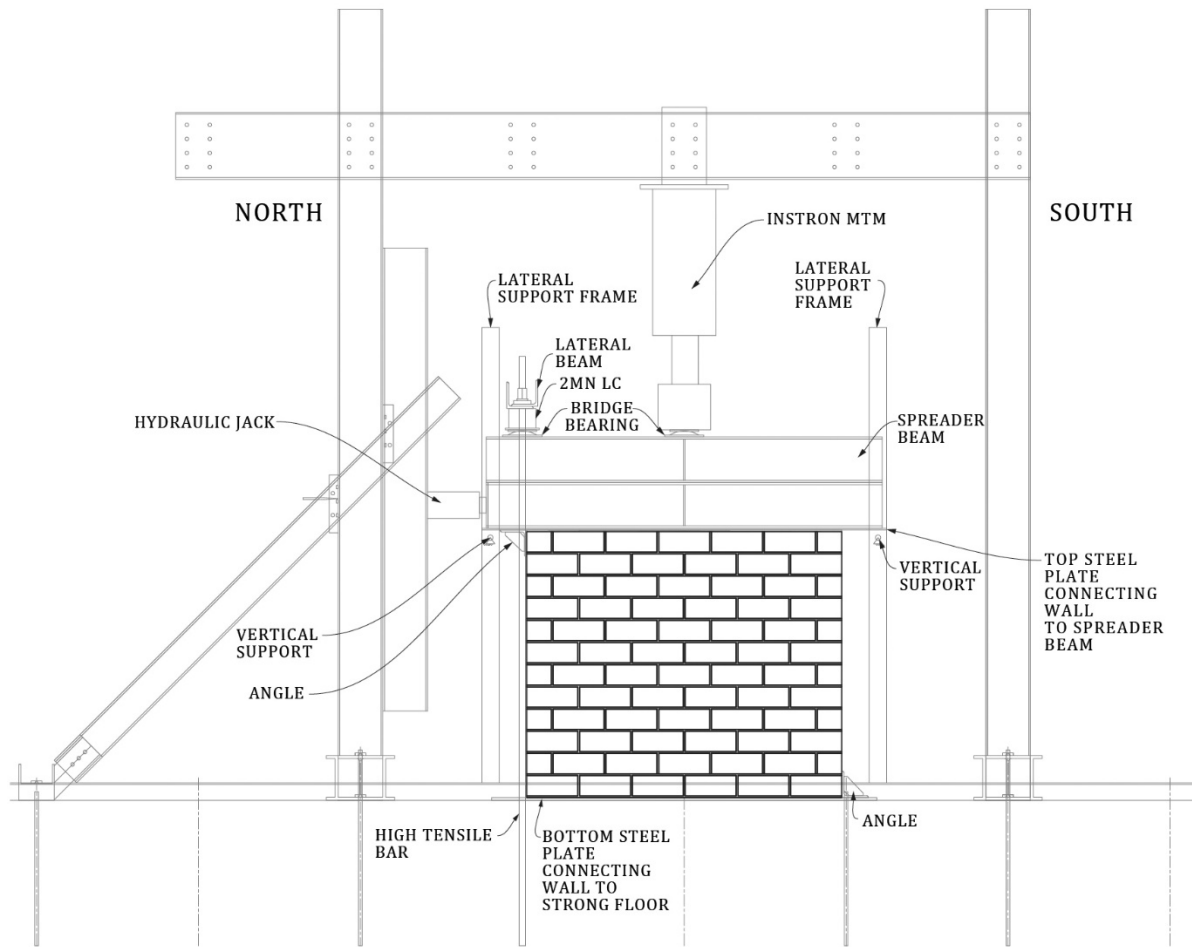
Figure 6.1: Test setup for in-plane loading of AMU walls (Shiso, 2019)
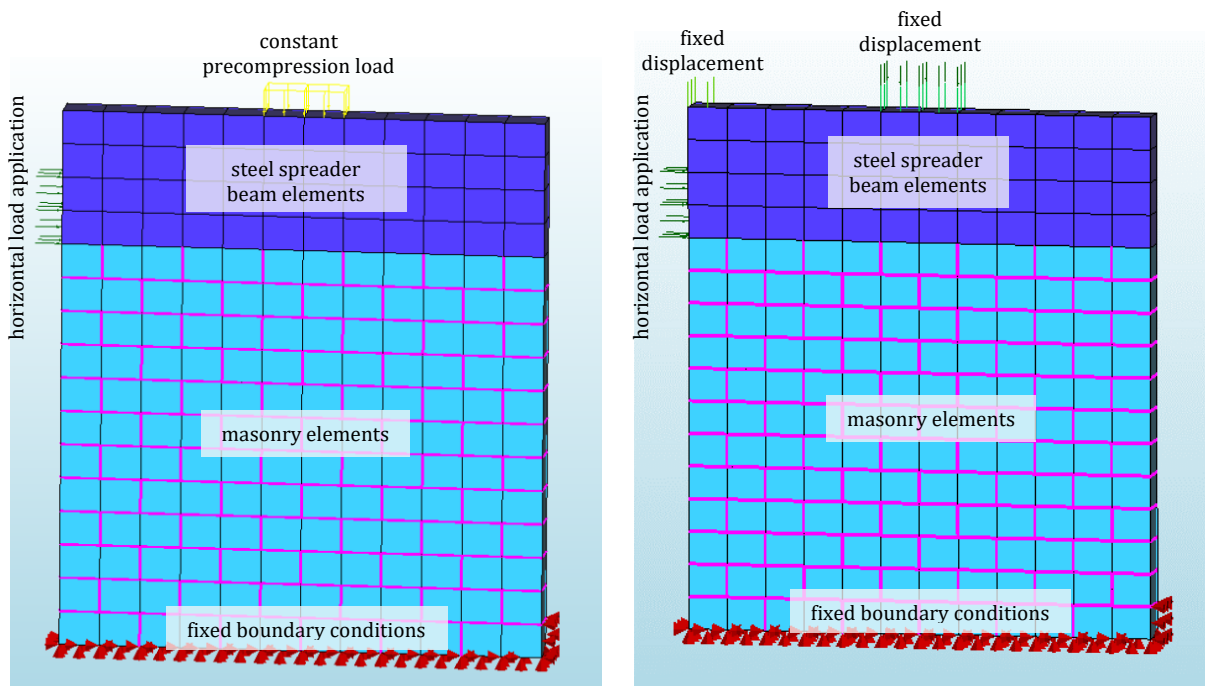
Figure 6.2: FE wall model for a) Test Setup 1 and b) Test Setup 2 of in-plane loading

The input parameters used for the material model are provided in Table 6.1, with the numerals 1 and 2 after the material type (e.g. GEO1) indicating the wall specimen tested under Test Setup 1 and Test Setup 2, respectively. The majority of the parameters are the baseline values as presented in Table 5.2, exceptions to this are as indicated by shading in Table 6.1 and were tested by Shiso (2019) in the same manner as described in Chapter 5 at a masonry unit age of 28 days: the unit density and E-modulus, unit crack interface compressive strength and joint interface compressive strength and E-modulus. As a result of this, a number of dependent factors are also affected: unit crack interface normal and tangential stiffness and joint interface normal and tangential stiffness. The masonry units in the large scale wall specimens were not at 28 day age at the time of testing the walls, therefore the unit compressive strength and E-modulus were again determined at the time of wall specimen testing. Most parameters are thus identical for both walls of each material, except as indicated.

Table 6.1: Input parameters for in-plane model validation

Parameter		GEO1	GEO2	CSE1	CSE2	ADB1	ADB2	
Unit								
Density	ρ_u		2 117		1 810		1 915	kg/m³
E-modulus	E_u	12 140	11 410	6 340	6 550	2 190	2 120	N/mm²
Poisson's Ratio	ν_u		0.17		0.20		0.45	-
Unit Crack Interface								
Tensile Strength	$f_{t,c}$		1.56		1.20		0.15	N/mm²
Mode I Fracture Energy	$G_{f,c}^{I}$		0.056		0.016		0.006	N/mm
Cohesion	c_c		2.3		1.8		0.2	N/mm²
Friction Angle	ϕ_c		37		37		37	°
Dilatancy Coefficient	ψ_c		0		0		0	°
Mode II Fracture Energy	$G_{f,c}^{II}$		0.56		0.16		0.06	N/mm
Compressive Strength	$f_{c,c}$	22.4	20.9	8.3	8.8	1.1	1.2	N/mm²
Shear Traction Contribution	$C_{ss,c}$		1.0×10^{-3}		1.0×10^{-3}		1.0×10^{-3}	-
Compressive Fracture Energy	$G_{c,c}$	17.9	16.7	6.6	7.0	0.9	1.0	N/mm
Eq. Plastic Relative Displ.	$\kappa_{p,c}$		0.005		0.01		0.25	mm/mm
Tangential Stiffness	$k_{s,c}$	519 000	488 000	264 000	273 000	75 000	73 000	N/mm³
Normal Stiffness	$k_{n,c}$	1 214 000	1 141 000	634 000	655 000	219 000	212 000	N/mm³
Joint Interface								
Tensile Strength	$f_{t,j}$		0.08		0.06		0.04	N/mm²
Mode I Fracture Energy	$G_{f,j}^{I}$		0.006		0.002		0.001	N/mm
Cohesion	c_j		0.11		0.09		0.05	N/mm²
Friction Angle	ϕ_j		30.0		43.0		45.6	°
Dilatancy Coefficient	ψ_j		0		0		0	°
Mode II Fracture Energy	$G_{f,j}^{II}$		0.05-0.08σ		0.05-0.08σ		0.05-0.08σ	N/mm
Compressive Strength	$f_{c,j}$		6.5		2.9		0.5	N/mm²
Shear Traction Contribution	$C_{ss,j}$		3.3		1.0		0.5	-
Compressive Fracture Energy	$G_{c,j}$		19		8		1.2	N/mm
Eq. Plastic Relative Displ.	$\kappa_{p,j}$		0.005		0.010		0.250	mm/mm
Tangential Stiffness	$k_{s,j}$	29	30	12	12	2	2	N/mm³
Normal Stiffness	$k_{n,j}$	71	73	29	28	6	6	N/mm³

6.1.2 Test Setup 1 Validation Results

The comparison of the experimental (EXP) and numerical (NUM) results of Test Setup 1 is provided based on the horizontal load-displacement progression (Figure 6.3) and the type of failure mechanism encountered (Figure 6.4). The peak horizontal loads, horizontal displacements at peak load and failure mechanism types are summarised in Table 6.2.

The experimental results are reproduced satisfactorily by the numerical model (Figure 6.3), with all the numerical peak loads within 11% of the experimental values (see Table 6.2), considering loads within the first 5mm of displacement. Notable differences are the initial stiffness of the GEO1 NUM results, sustained for longer than in the numerical case, and the strength gain seen in the CSE1 NUM results. However, given that the comparison is made to a single experimental result in each instance, the agreement between the experimental and numerical results is considered to fall within the inherent variability of masonry.
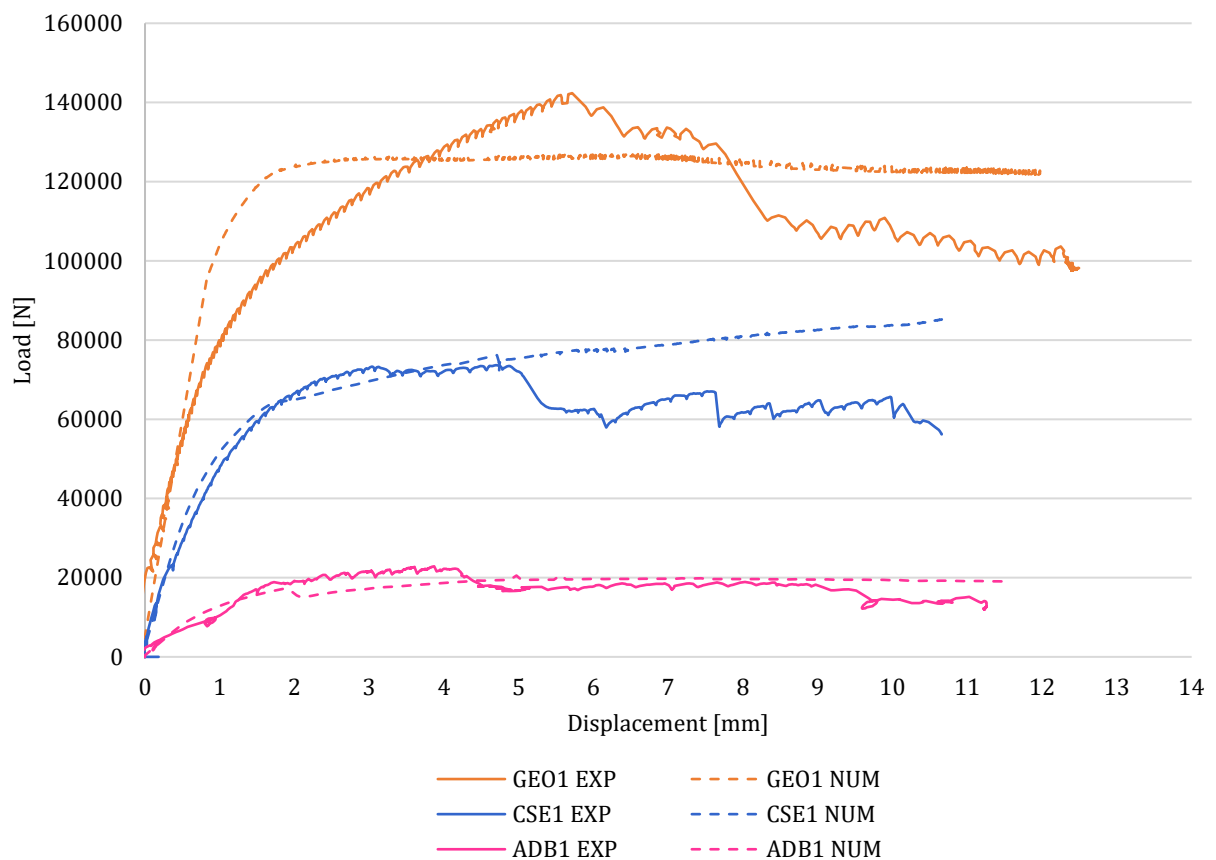
Figure 6.3: Test Setup 1 experimental and numerical horizontal force-displacement

Remarkable also is the evidenced relatively ductile behaviour, both experimentally and numerically for all three materials. Traditionally, in confined masonry shear walls, high precompression loads are associated with increased peak/failure loads, but also accompanying increased brittleness. The increased ductility observed in these results is ascribed to the internal force redistribution taking place, as found by Lourenço (1996) for solid clay bricks. Following initial diagonal cracking and the subsequent rotation of the adjacent compressive struts, the stress transmission over the diagonal crack occurs through bed joint shearing, leading to more ductile behaviour.

67

GEO1

CSE1

ADB1

a) EXP   b) EXP   c) NUM

Figure 6.4: Test Setup 1 experiment a) photo and b) crack diagram and c) crack representations of numerical analyses for GEO, CSE and ADB

Experimentally, all three walls experienced initial uplift at the northern toe, followed by thorough diagonal cracking through the joints and units and crushing of the southern toe (see Figure 6.4 a and b). These failure mechanisms are successfully captured in the numerical results. For the CSE1 EXP wall, partial shear sliding also occurred two courses from the top, which was reproduced in the numerical outcome. Two discrepancies in crack patterns are observed (shaded in Table 6.2), to be anticipated in masonry analysis, and are as follows: the GEO1 NUM results indicated shear sliding two courses from the bottom, which was not observed in the EXP case and the ADB1 EXP wall exhibited shear diagonal cracks, whereas ADB1 NUM presented stepped shear cracks.

Table 6.2: Test Setup 1 experimental and numerical peak loads, displacements and failure mechanisms

	GEO1		CSE1		ADB1	
	EXP	NUM	EXP	NUM	EXP	NUM
Peak Load [N]	142 400	127 300	73 700	76 200	22 8900	20 600
Displacement at Peak Load [mm]	5.71	6.63	4.69	4.71	3.87	5.57
Initial Uplift	X	X	X	X	X	X
Shear Diagonal Cracks	X	X	X	X	X	-
Shear Stepped Cracks	X	X	-	X	-	X
Shear Sliding	-	X	X	X	-	-
Toe Crushing	X	X	X	X	X	X

The difference between the experimental and numerical displacement measured at peak load varies for the three materials from 16% for GEO1 to 44% for ADB1 (Table 6.2). Given the relatively ductile behaviour observed for both the experimental and numerical cases, this variation is not as peculiar as typical brittle masonry shear wall behaviour would suggest.

6.1.3   Test Setup 2 Validation Results

In Test Setup 2 the vertical displacement, attained once the precompression load had been applied, was maintained at the centre of the spreader beam for the duration of the experiment. This, together with the application of the high tensile bars on the northern edge of the specimen, significantly reduced the rotation and uplift of the specimen. The comparison of the experimental and numerical results of Test Setup 2 are provided based on the horizontal load-displacement progression (Figure 6.5) and the type of failure mechanism encountered (Figure 6.6). The peak horizontal loads, horizontal displacements at peak load and failure mechanism types are summarised in Table 6.3.

.
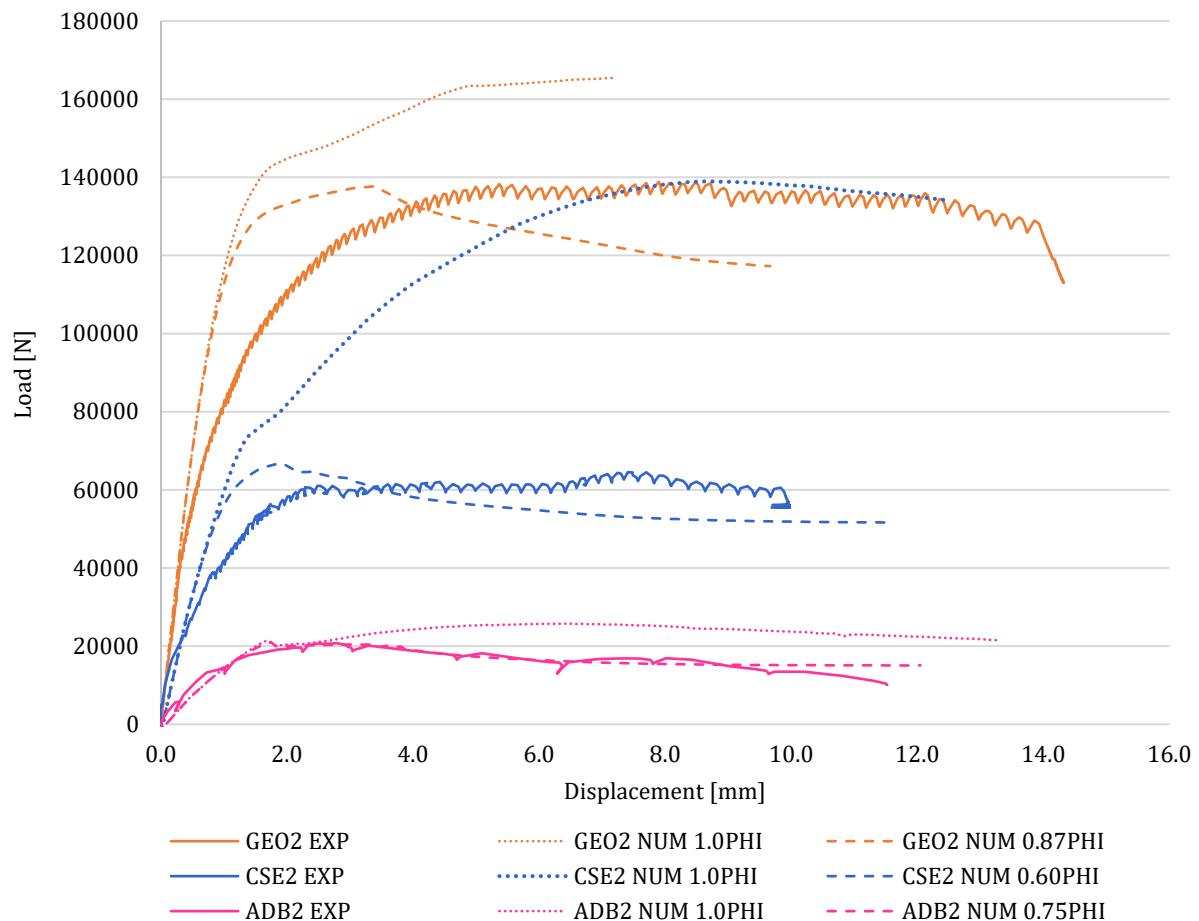
Figure 6.5: Test Setup 2 experimental and numerical horizontal force-displacement

69

For Test Setup 2, the experimental results are not reproduced satisfactorily by the numerical model (Figure 6.5), with the numerical peak loads varying between 19% (GEO) and 115% (CSE) of the experimental values (see Table 6.3). This is illustrated by the horizontal load-displacement progression designated by '1.0PHI' for each material in Figure 6.5, obtained using the input data as presented in Table 6.1. Given the significant discrepancy between the experimental and numerical results thus elicited, the joint friction angle, φ_j, PHI, was reduced for each material, until a peak load match between the experimental and numerical results was attained, within 4%. These adjusted friction angles are designated by their respective reductions in Figure 6.5, relative to the original value: 0.87 times the original PHI for GEO (or 26.1°), 0.60xPHI for CSE (or 25.8°) and 0.75xPHI for ADB (or 34.2°). The joint friction angle was the only input parameter adjusted, for a number of reasons, discussed further in Section 6.1.4.
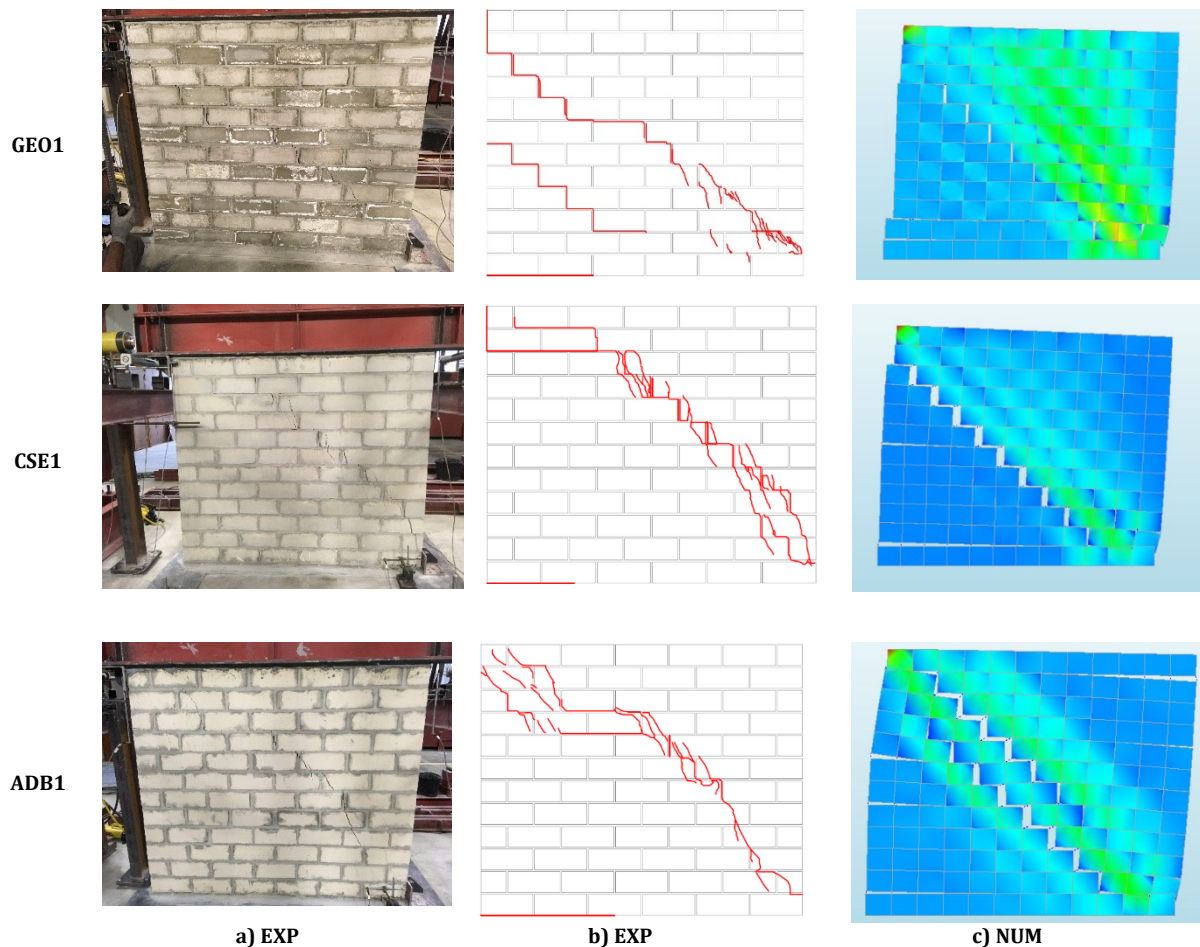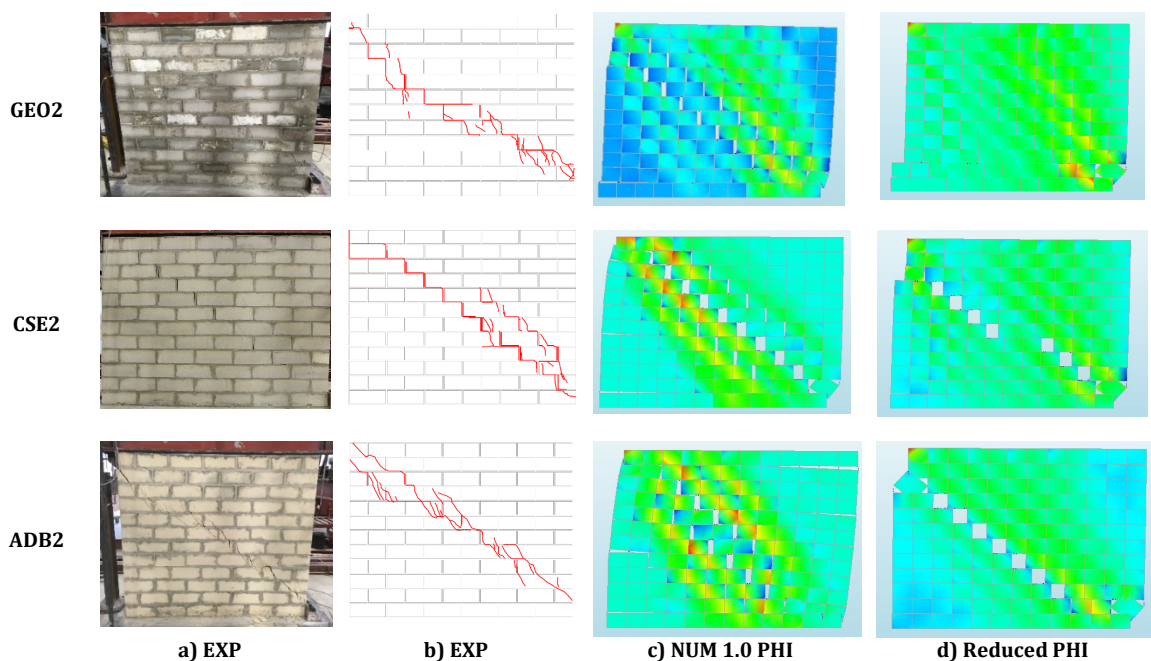

Figure 6.6: Test Setup 2 experiment a) photo and b) crack diagram and crack representations of numerical analyses c) the original friction angle and d) the reduced friction angle for GEO, CSE and ADB

Experimentally, in none of the three walls was initial uplift observed, due to the additional vertical restraint offered by the high tensile bars. All three walls experienced crushing of the southern toe together with a combination of shear diagonal or stepped cracks (see Figure 6.6 a and b). These failure mechanisms are reproduced relatively well for the cases of CSE2 and ADB2, when considering the numerical model employing the reduced friction angle (see Figure 6.6d).

The opposite is observed for GEO2. The failure mechanism observed experimentally is better reproduced by the numerical model employing the original friction angle value, but differs significantly in the peak load attained (Figure 6.6c). When considering the numerical model with the reduced friction angle, the dominant failure mechanism is shear sliding, along the joint two courses from the bottom (Figure 6.6d).

Table 6.3: Test Setup 2 experimental and numerical peak loads, displacements and failure mechanisms

	GEO2			CSE2			ADB2		
	EXP	NUM		EXP	NUM		EXP	NUM	
		1.0 PHI	0.87PHI		1.0PHI	0.6PHI		1.0PHI	0.75PHI
Peak Load [N]	138 900	165 400	137 700	64 500	138 9300	66 800	20 700	25 700	21 100
Displacement at Peak Load [mm]	7.90	7.16	3.34	7.41	8.72	1.92	2.79	6.51	1.74
Initial Uplift	-	X	X	-	X	X	-	X	X
Shear Diagonal Cracks	X	-	-	-	-	-	X	X	-
Shear Stepped Cracks	X	X	-	X	X	X	-	X	X
Shear Sliding	-	-	X	-	-	-	-	-	-
Toe Crushing	X	X	X	X	X	X	X	X	X

Again inconsistencies arise for the difference between the experimental and numerical displacements measured at peak load, see Table 6.3. For GEO2 and CSE2, the difference is relatively small (9% and 18% respectively) when considering the numerical model with the original friction angle, but becomes significant for the numerical model with the reduced friction angle (57% and 74% respectively). Conversely, the difference between the experimental and numerical displacements measured at peak load is significant for the numerical model with 1.0PHI (133%), whilst it is less conspicuous (38%) for the reduced friction angle. Although inconsistent, these results highlight the variability of masonry behaviour, and the sensitivity to the joint friction angle.

6.1.4   Discussion

The experimental results of Test Setup 1 were reproduced satisfactorily numerically, whereas the contrary was found for Test Setup 2. The latter ensured a more uniform confining stress over the length of the specimen, which underscored the dominance of the joint friction angle under these conditions. Cognisance of the following factors is necessary.

Firstly, the original friction angles used as input parameters for the numerical analyses of both Test Setups 1 and 2, were those determined by Fourie (2017), as described in Section 5.4.2. Shear triplet tests were not conducted on the specific unit and mortar combination used by Shiso (2019) in the large-scale in-plane wall tests.

Secondly, considering the inherent variability of experimental data, the reduced friction angle determined to be the best-fit for GEO2 in Section 6.1.3, namely 87% of the original PHI, falls within the variability (72% - 114%) of the shear triplet test results obtained by Fourie (2017).

Table 6.4 depicts this variability for all three materials under consideration, normalised to the original friction angle, obtained by linear regression. The reduced best-fit friction angles determined for CSE2 and ADB2, namely 60% and 75% of the original friction angle, respectively, fall outside their band of experimental variability. Yet, given that the lower bands are merely 74% and 81% for CSE and ADB respectively, together with the sizeable number of influencing factors, from mortar water retention to unit conditioning and surface roughness, these reduced friction angles are still well within reason.

Table 6.4: Variation in friction angle expressed as ratio of shear triplet test linear regression result

	Variation in Triplet Test PHI Results			Reduced PHI to Test Setup 2 Results
	Minimum	Linear Regression	Maximum	
GEO	0.72	1.00	1.14	0.87
CSE	0.74	1.00	1.21	0.60
ADB	0.81	1.00	1.14	0.75

Finally, the friction angles determined by Fourie (2017) were established at precompression levels as low as 50% of those used in the in-plane wall tests of Shiso (2019). Evidence of the effect on the friction angle at elevated confining pressure is sparse, however, the work of Drysdale et al. (1994) indicates that the linear relationship assumed at lower normal stress is no longer valid due to a levelling of the friction angle at higher normal stress. This substantiates the reduced friction angles deemed necessary to elicit a satisfactory numerical response in Section 6.1.3. This overall sensitivity to the joint friction angle is corroborated by the sensitivity analysis presented in upcoming Section 6.3.

The joint friction angle sensitivity was brought to the fore by the numerical modelling of Test Setup 2, as opposed to Test Setup 1, due to the rotation and uplift, and hence reduced confining stress, experienced in the latter. However, the confining stresses of Test Setup 1 are more comparable to the precompression levels present in the shear triplet tests used to determine the original joint friction angles and are also more representative of the normal stresses in the structures of the intended application of the analyses, namely single-storey residential walls. Therefore, the joint friction angles used in the numerical model of Test Setup 1 are not reduced. This choice is reinforced by the good correlation between failure mechanisms, as well as peak loads, reproduced numerically for Test Setup 1. Considering the inherent variability of both the constituent masonry materials and masonry behaviour, the satisfactory numerical reproduction of the experimental results of Test Setup 1 is considered sufficient validation of the FE approach for the in-plane behaviour of a wide spectrum of AMU's.

6.2 Out-of-Plane Model Validation

Single leaf flexural wallets were constructed and tested out-of-plane by Jooste (unpublished) according to EN 1052-2 (1999) using the four unit types, CON, GEO, CSE and ADB. Both failure plane orientations were tested, namely plane of failure parallel (PAR) and perpendicular (PER) to the bed joints. The tests were conducted with mortar of a 5N/mm² target strength. The two specimen configurations were subsequently modelled, using the FE approach detailed in Section 4.1.2, and the failure patterns, flexural strengths and horizontal load-displacement progressions are compared.

6.2.1 Parallel Failure Plane FE Model

The PAR wall specimens, 630mm in height and 450mm in length with 10mm mortar joints, were tested with the boundary conditions, described in Figure 6.7. In the PAR test setup the wallet is free to rotate at the bottom support, due to the inclusion of a rod beneath the steel support plate. Two specimens were tested per material type.
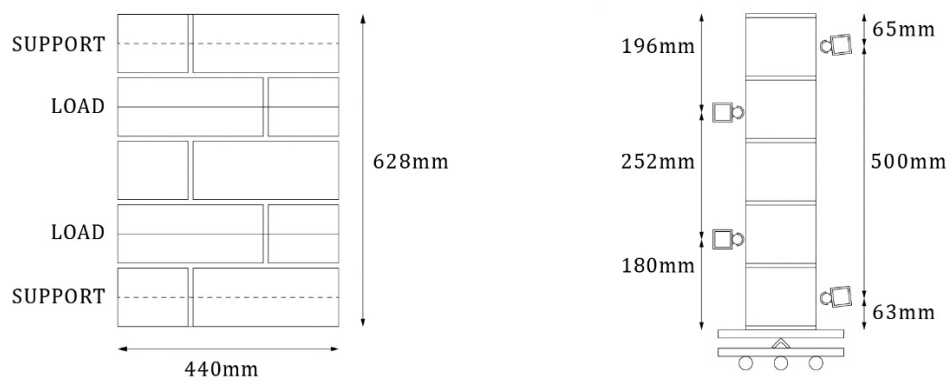
Figure 6.7: Front (left) and side view (right) of PAR test setup for AMU wallets (Jooste, unpublished)

For the FE model of these wallets, depicted in Figure 6.8, the support conditions are indicated in red and the load application in green. The light blue elements are the linear brick elements with the nonlinear behaviour concentrated in the magenta for the joints and black for the crack interface elements.
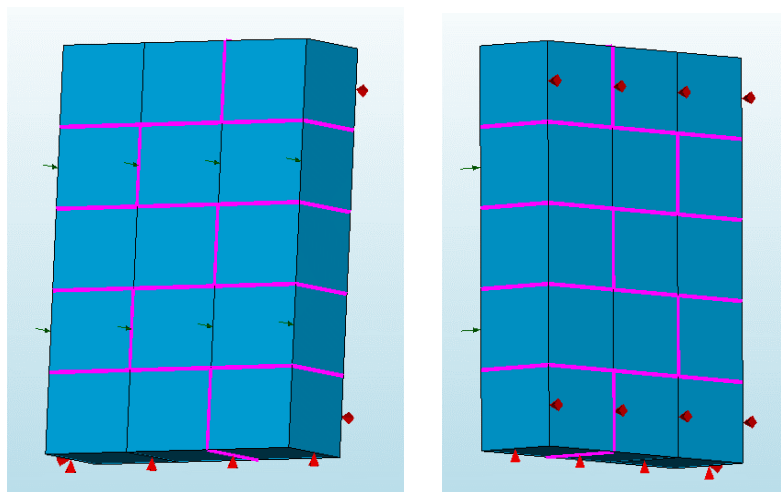
Figure 6.8: Front (left) and rear view (right) of FE wallet model of PAR test setup

73

The input parameters used for the material model are provided in Table 6.5. The majority of the parameters are the baseline values as presented in Table 5.2. Exceptions to this are as indicated by shading in Table 6.5 and were tested by Jooste (unpublished) in the same manner as described in Chapter 5, at the time of conducting the flexural wallet tests: the unit E-modulus, unit crack interface compressive strength and joint interface compressive strength and E-modulus. As a result of this, a number of dependent factors are also affected: unit crack interface normal and tangential stiffness, unit compressive fracture energy, joint shear traction contribution and interface normal and tangential stiffness.

Table 6.5: Input parameters for PAR model validation

Parameter		CON	GEO	CSE	ADB	
Unit						
Density	ρ_u	2 090	2 080	1 822	2 007	kg/m³
E-modulus	E_u	18 256	23 630	6 280	800	N/mm²
Poisson's Ratio	ν_u	0.16	0.17	0.20	0.45	-
Unit Crack Interface						
Tensile Strength	$f_{t,c}$	0.66	1.56	1.20	0.15	N/mm²
Mode I Fracture Energy	$G^I_{f,c}$	0.047	0.056	0.016	0.006	N/mm
Cohesion	c_c	1.0	2.3	1.8	0.2	N/mm²
Friction Angle	ϕ_c	37	37	37	37	°
Dilatancy Coefficient	ψ_c	0	0	0	0	°
Mode II Fracture Energy	$G^{II}_{f,c}$	0.47	0.56	0.16	0.06	N/mm
Compressive Strength	$f_{c,c}$	22.9	48.4	9.6	0.5	N/mm²
Shear Traction Contribution	$C_{ss,c}$	1.0x10⁻³	1.0x10⁻³	1.0x10⁻³	1.0x10⁻³	-
Compressive Fracture Energy	$G_{c,c}$	18.3	38.7	7.7	0.4	N/mm
Eq. Plastic Relative Displ.	$\kappa_{p,c}$	0.030	0.005	0.010	0.250	mm/mm
Tangential Stiffness	$k_{s,c}$	787 000	1 010 000	262 000	28 000	N/mm³
Normal Stiffness	$k_{n,c}$	1 826 000	2 363 000	628 000	80 000	N/mm³
Joint Interface						
Tensile Strength	$f_{t,j}$	0.12	0.08	0.06	0.04	N/mm²
Mode I Fracture Energy	$G^I_{f,j}$	0.005	0.006	0.002	0.001	N/mm
Cohesion	c_j	0.17	0.11	0.09	0.05	N/mm²
Friction Angle	ϕ_j	49.5	30.0	43.0	45.6	°
Dilatancy Coefficient	ψ_j	0	0	0	0	°
Mode II Fracture Energy	$G^{II}_{f,j}$	0.05-0.08σ	0.05-0.08σ	0.05-0.08σ	0.05-0.08σ	N/mm
Compressive Strength	$f_{c,j}$	10.6	14.8	2.8	0.3	N/mm²
Shear Traction Contribution	$C_{ss,j}$	2.6	16.9	0.9	0.1	-
Compressive Fracture Energy	$G_{c,j}$	18	19	8	1.2	N/mm
Eq. Plastic Relative Displ.	$\kappa_{p,j}$	0.030	0.005	0.010	0.250	mm/mm
Tangential Stiffness	$k_{s,j}$	3 438	63	12	1	N/mm³
Normal Stiffness	$k_{n,j}$	9 714	292	56	3	N/mm³

6.2.2　Parallel Failure Plane Validation Results

The typical failure pattern encountered is cracking of one of the joints between lines of load application for the experimental (EXP) results and cracking of both of these joints in the numerical (NUM) results, shown in Figure 6.9, thereby dissipating double the energy in the numerical analyses compared to the experiments. This may have been avoided with the use of adjusted material parameters in one of the anticipated failure planes. Exceptions to this typical failure pattern are CSE EXP I, where failure occurred in the lowest joint of the specimen, prior to failure in one of the central joints, as well as ADB EXP I, where failure occurred across the central units instead of through the joint.
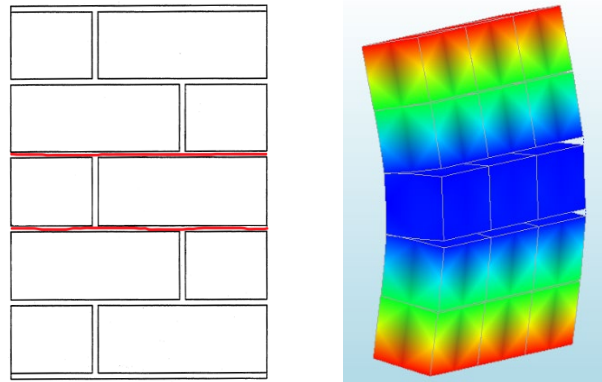
Figure 6.9: PAR experimental (left) and numerical (right) typical failure pattern

The experimental and numerical flexural strengths obtained are summarised in Figure 6.10, which are all obtained according to EN 1052-2 (1999).

Figure 6.10: PAR experimental and numerical flexural strengths

The results are further compared based on the horizontal load-displacement progression for each unit type (Figure 6.11). The plotted values are the total horizontal load applied and the average horizontal displacement measured at the centre line of the specimen. Due to experimental complications, only one specimen's experimental results are available for CON and CSE.

75

The brittle tensile failure of this test setup impedes the complete capturing of the post-peak behaviour under experimental conditions. Typically, the post-peak experimental behaviour is captured by a single data point, thereby nullifying a sensible comparison beyond that point. However, the peak loads, and hence flexural strengths, compare relatively well. The CON experimental and numerical flexural strengths match whereas the GEO, CSE and ADB differ as little as 7%, 15% and 16% respectively. Failure in the lowest joint of the CSE EXP I specimen also leads to a more uncharacteristic load-displacement path.
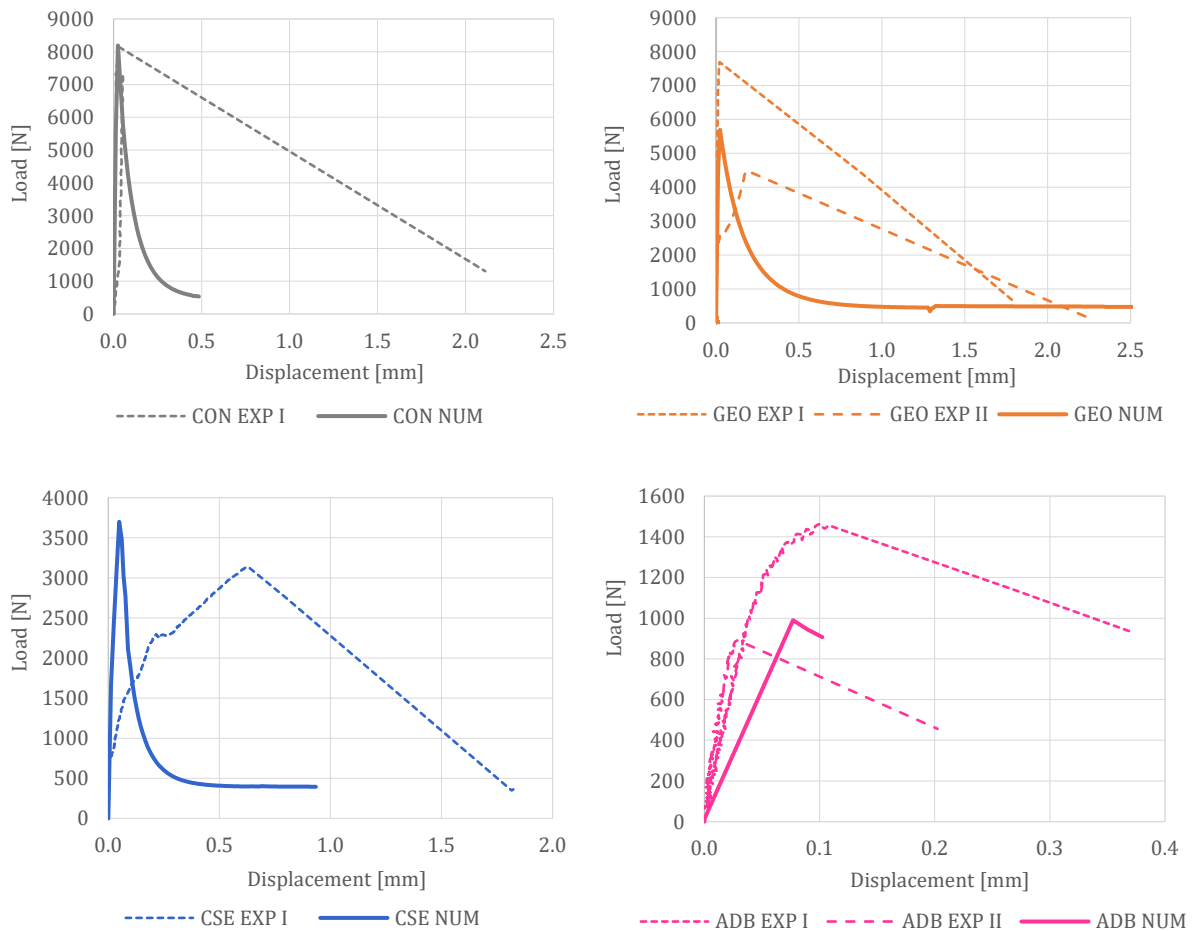
Figure 6.11: PAR experimental and numerical horizontal load-displacement for CON, GEO, CSE and ADB

The two ADB experimental results illustrate the high variability of the tests, with the peak loads measuring 1 462N and 894N. Given that two of the four materials only have one experimental set available for comparative purposes, as well as the brittle failure nature, the agreement between the experimental and numerical results is considered reasonable.

6.2.3 Perpendicular Failure Plane FE Model

The PER wall specimens, 504mm in height and 1200mm in length with 10mm mortar joints, were tested with the boundary conditions, described in Figure 6.12. In the PER test setup the wallet is relatively free to slide at the bottom support, due to the inclusion of two greased damp-proof course (DPC) layers beneath the specimen. Two specimens were tested per material type.
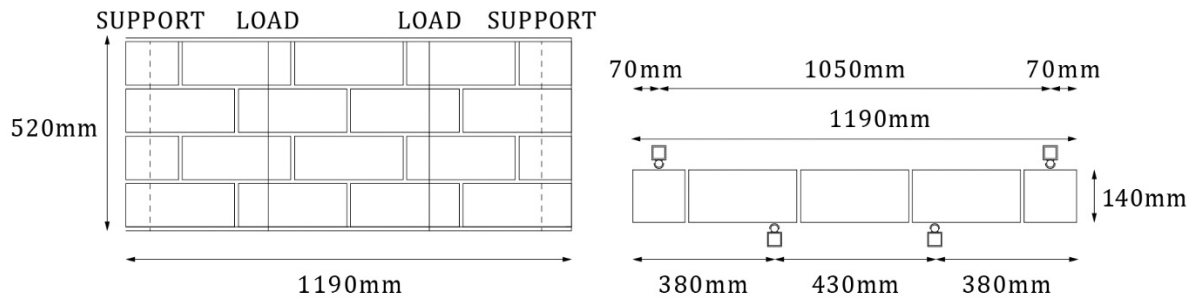
Figure 6.12: Front (left) and top view (right) of PER test setup for AMU wallets (Jooste, unpublished)

For the FE model of these wallets, depicted in Figure 6.13, the support conditions are indicated in red and the load application in green and yellow. The light blue elements are the linear brick elements with the nonlinear behaviour concentrated in the magenta for the joints and black for the crack interface elements.
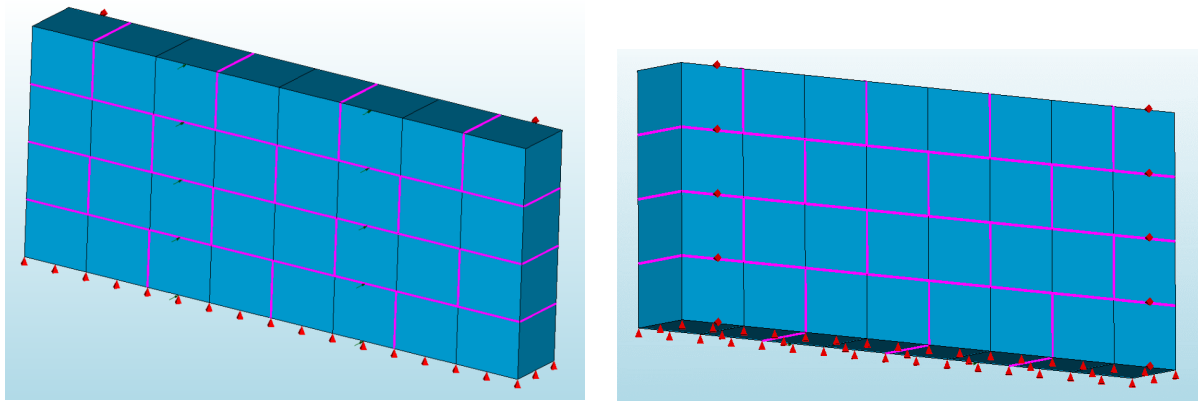
Figure 6.13: Front (left) and rear view (right) of FE wallet model of PER test setup

The input parameters used for the material model are provided in Table 6.6. The majority of the parameters are the baseline values as presented in Table 5.2, with the same exceptions (shaded) as discussed for the PAR configuration.

Table 6.6: Input parameters for PER model validation

Parameter		CON	GEO	CSE	ADB	
Unit						
Density	ρ_u	2 090	2 080	1 822	2 007	kg/m³
E-modulus	E_u	17 565	12 500	6 440	1 220	N/mm²
Poisson's Ratio	ν_u	0.16	0.17	0.20	0.45	-
Unit Crack Interface						
Tensile Strength	$f_{t,c}$	0.66	1.56	1.20	0.15	N/mm²
Mode I Fracture Energy	$^I_{f,c}$	0.047	0.056	0.016	0.006	N/mm
Cohesion	c_c	1.0	2.3	1.8	0.2	N/mm²
Friction Angle	ϕ_c	37	37	37	37	°
Dilatancy Coefficient	ψ_c	0	0	0	0	°
Mode II Fracture Energy	$G^{II}_{f,c}$	0.47	0.56	0.16	0.06	N/mm
Compressive Strength	$f_{c,c}$	16.8	25.4	8.7	0.5	N/mm²
Shear Traction Contribution	$C_{ss,c}$	1.0x10⁻³	1.0x10⁻³	1.0x10⁻³	1.0x10⁻³	-
Compressive Fracture Energy	$G_{c,c}$	13.5	20.3	7.0	0.4	N/mm
Eq. Plastic Relative Displ.	$\kappa_{p,c}$	0.03	0.005	0.01	0.25	mm/mm
Tangential Stiffness	$k_{s,c}$	757 000	534 000	268 000	42 000	N/mm³
Normal Stiffness	$k_{n,c}$	1757 000	1 250 000	644 000	122 000	N/mm³
Joint Interface						
Tensile Strength	$f_{t,j}$	0.12	0.08	0.06	0.04	N/mm²
Mode I Fracture Energy	$G^I_{f,j}$	0.005	0.006	0.002	0.001	N/mm
Cohesion	c_j	0.17	0.11	0.09	0.05	N/mm²
Friction Angle	ϕ_j	49.5	30.0	43.0	45.6	°
Dilatancy Coefficient	ψ_j	0	0	0	0	°
Mode II Fracture Energy	$G^{II}_{f,j}$	0.05-0.08σ	0.05-0.08σ	0.05-0.08σ	0.05-0.08σ	N/mm
Compressive Strength	$f_{c,j}$	7.1	7.0	2.5	0.2	N/mm²
Shear Traction Contribution	$C_{ss,j}$	1.1	3.8	0.7	0.1	-
Compressive Fracture Energy	$G_{c,j}$	18	19	8	1.2	N/mm
Eq. Plastic Relative Displ.	$\kappa_{p,j}$	0.03	0.005	0.01	0.25	mm/mm
Tangential Stiffness	$k_{s,j}$	164	12	37	1	N/mm³
Normal Stiffness	$k_{n,j}$	396	83	309	3	N/mm³

6.2.4   Perpendicular Failure Plane Validation Results

The typical failure pattern encountered experimentally (EXP) for the PER test setup is cracking through the joints and units in all instances except CSE EXP I (where cracking occurred through the joints), shown in Figure 6.14. The failure pattern encountered numerically is cracking through the joints only for all unit types, shown in Figure 6.15. This relatively consistent difference in failure modes between the experimental and numerical results may indicate an overestimation of the numerical unit tensile strength.
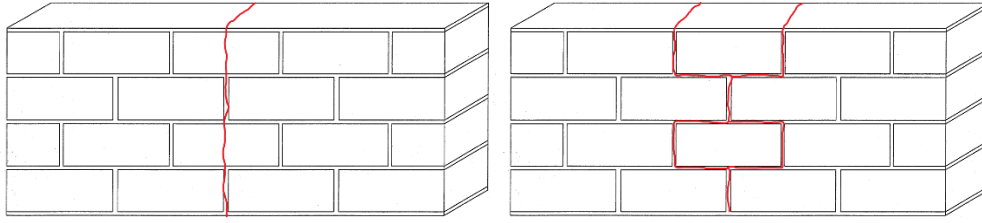
Figure 6.14: PER experimental failure through joints and units (left) and joints only (right)
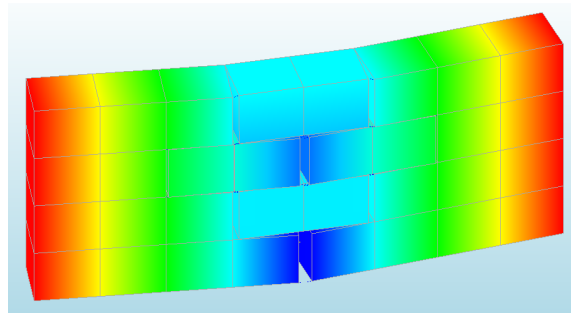
Figure 6.15: PER numerical failure through joints only

The experimental and numerical flexural strengths obtained are summarised in Figure 6.16, which are all obtained according to EN 1052-2 (1999).
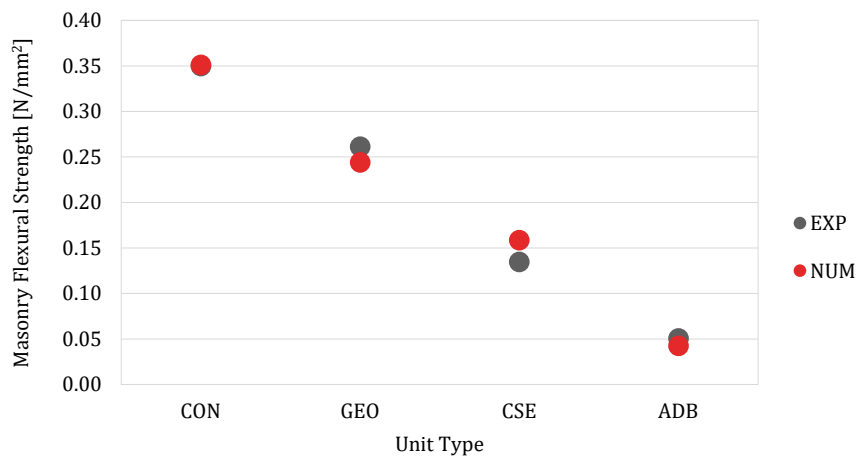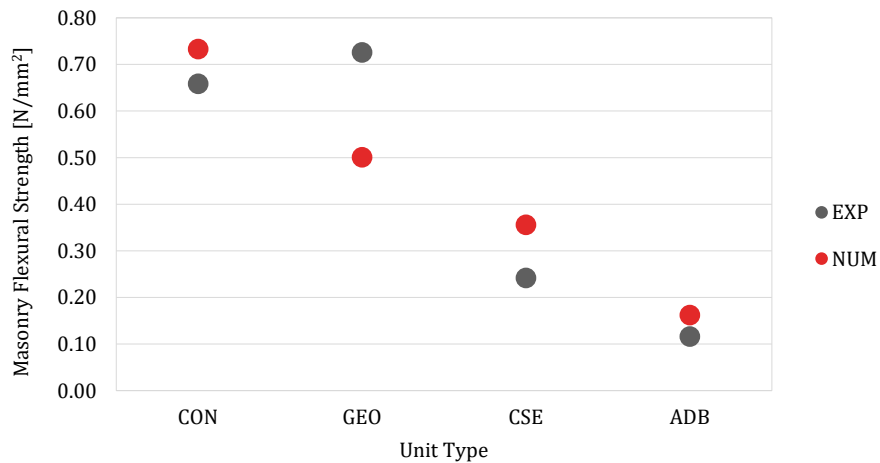

Figure 6.16: PER experimental and numerical flexural strengths

The results are discussed further based on the horizontal load-displacement progression for each unit type (Figure 6.17). The plotted values are the total horizontal load applied and the average horizontal displacement measured at the centre line of the specimen. All the numerical results are compared to two experimental results per unit type. With reference to Figure 6.17, the CON experimental and numerical load-displacement paths compare well, as do the flexural strengths, differing by 10%. The GEO results compare relatively well with regards to the post-peak behaviour, but a larger difference is found between the experimental and numerical flexural strengths of 31%. The GEO experimental results again highlight the variability of the tensile test setup, with peak loads measuring 10 732N and 5 198N for the two experiments.
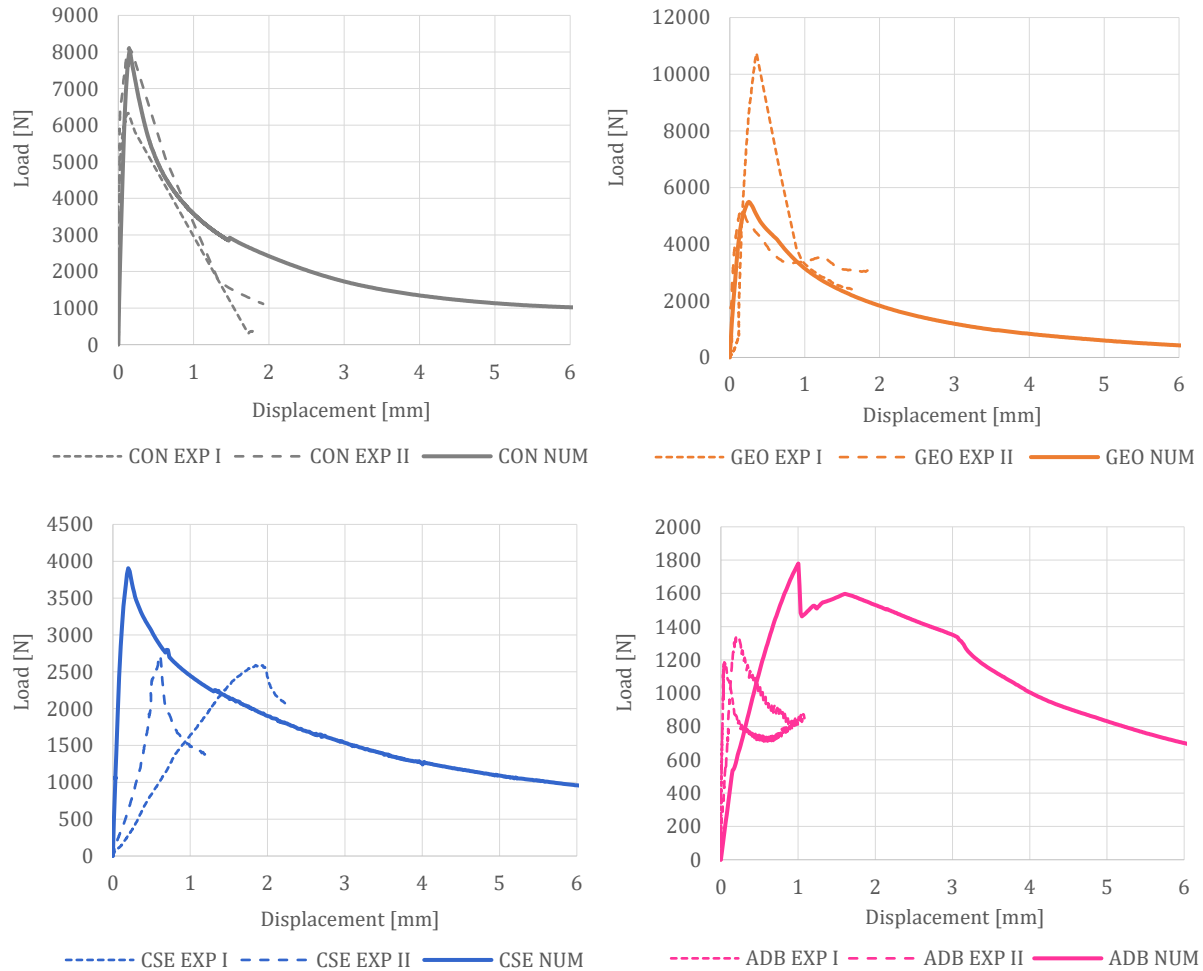
Figure 6.17: PER experimental and numerical horizontal load-displacement for CON, GEO, CSE and ADB

In the case of the CSE comparison, the lower stiffness of the experimental results is notable and, whilst the peak loads of these results are relatively consistent, they are exceeded by the numerical peak load, resulting in a flexural strength difference of 32%. Additionally, poor bond was observed upon demolition of the CSE test specimens (Jooste, unpublished), which may contribute to this difference. In the ADB case, the two experimental results are also relatively consistent, whereas the numerical flexural strength exceeds it by 29%. Again, given the variability of the test results, the agreement between the numerical and experimental results is considered fair.

6.2.5 Discussion

The numerical flexural results are dependent on the joint tensile strength specified, which is based on the joint cohesion ($f_{t,j} = c_j/1.4$). As discussed in Section 5.4.1, the joint cohesion was determined experimentally using shear triplet tests by Fourie (2017), on the same four unit types and similar, but not identical, mortar to the one used in the PAR and PER tests. This mortar inconsistency thus influences the joint tensile strength and, together with the brittle nature of the test and intrinsic masonry material variability, could account for a large proportion of the differences in flexural strength and failure mechanisms determined. Nevertheless, the experimental and numerical results are considered to agree adequately to serve as validation of the FE approach for the out-of-plane behaviour of a wide spectrum of AMU's.

80

6.3 Sensitivity Analyses

A sensitivity analysis is performed on certain parameters to ascertain their influence on the response of a structure, and to aid in establishing which parameters are sufficiently influential to warrant costly testing. In Chapter 5, 11 of the 27 masonry parameters were earmarked for the sensitivity analysis and are listed in Table 6.7. In addition to these parameters, three more core parameters were identified and included in the sensitivity analyses, namely the unit E-modulus, the unit or crack interface compressive strength and the joint interface compressive strength, also detailed in Table 6.7.

The sensitivity analyses of the three core parameters are applied to all four materials under consideration, whereas the sensitivity analyses of the 11 earmarked parameters are only applied to CSE, to keep the analyses to an executable number. The CSE material is chosen as representative as it falls in the middle of the chosen material spectrum in terms of strength and stiffness. One exception to this is the unit Poisson's value. The sensitivity of this parameter is also investigated for the ADB material, as explained in Section 5.2.2.

The sensitivity analyses are applied to a small-scale shear wall application, in which all three failure modes of the material model could be triggered. Shear and tensile failure modes are more likely to occur in this specimen and loading configuration than crushing failure, but since the former two are generally considered critical in unreinforced masonry, this configuration is deemed sufficient. Accuracy of the in-plane shear wall model was demonstrated in Section 6.1 and a smaller version of this setup is used for the sensitivity wall analysis, in order to maintain a realistic analysis timeframe. The shear wall consists of 5 courses (620mm) in height and 3 blocks per course (890mm long), giving an aspect ratio of 1:1.4, as illustrated in Figure 6.18. As before, the support conditions are indicated in red and the load application in green. The blue elements are the linear brick elements with the joints in magenta and the crack interface elements in black.
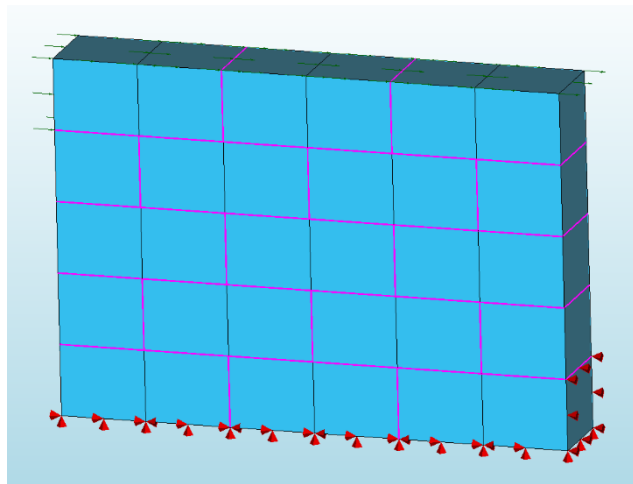
Figure 6.18: Shear wall configuration used in sensitivity analysis

The baseline values, as defined in Table 5.2, of the unit's E-modulus, the unit crack interface's compressive strength, tensile strength and mode I fracture energy and the joint's compressive strength, cohesion and friction angle are considered relatively accurate, and are therefore divided and multiplied by a factor 1.25, providing a variation of 0.8 to 1.25 of the baseline values. The baseline values of the remaining parameters in the sensitivity analyses are an estimate and are therefore divided and multiplied by a factor 2.0, providing a variation of 0.5 to 2.0 of the baseline values. The only exceptions to this are the ADB unit Poisson's value and the joint tensile strength and mode II fracture energy.

For the ADB Poisson's value, the baseline value is divided by both 1.25 and 2.0, since multiplying the baseline value of 0.45 by any factor would result in a nonsensical Poisson's value. In the case of the joint tensile strength, multiplied by 2.0 for CSE, the analysis would not converge, and the joint tensile strength was multiplied by a factor of 1.5 instead of 2.0 to achieve convergence for this specific case. The joint mode II fracture energy baseline was taken as confining stress-dependent ($G_{f,j}^{II} = 0.05 - 0.08\sigma$) and for the variations of this parameter only the confining stress-independent component is considered.

The percentage difference achieved between the maximum load in the baseline analysis for each material and the maximum load in the varied parameter analysis is provided in Table 6.7, together with the average difference over all four materials (for the core parameters), as well as a classification of the influence of each parameter on the model. The model is considered insensitive if the percentage difference is 0%, almost insensitive between 0.1 and 0.9%, slightly sensitive between 1.0 and 5.9%, moderately sensitive between 6.0 and 9.9 % and sensitive over 10.0%, as done similarly by Lourenço (1998), in a study on the sensitivity of conventional masonry structures using the FE micro-modelling approach.

Table 6.7: Percentage difference in maximum load obtained in parametric sensitivity analysis

Parameter		Factor	Difference in Max Load [%]				Average Difference [%]	Influence
			CON	GEO	CSE	ADB		
Unit E-modulus	E_u	1.25	0.5	0.5	0.4	0.5	0.5	Almost Insensitive
Unit Crack Interface Compressive Strength	$f_{c,c}$	1.25	0.3	0.0	0.0	0.6	0.2	Almost Insensitive
Joint Interface Compressive Strength	$f_{c,j}$	1.25	2.3	1.7	0.8	1.3	1.5	Slightly Sensitive
Unit Poisson's Ratio	ν_u	1.25	-	-	0.1	0.2	0.2	Almost Insensitive
Unit Crack Tensile Strength	$f_{t,c}$	1.25	-	-	0.1	-	-	Almost Insensitive
Unit Crack Mode I Fracture Energy	$G_{f,c}^{I}$	1.25	-	-	0.1	-	-	Almost Insensitive
Joint Cohesion	c_j	1.25	-	-	2.3	-	-	Slightly Sensitive
Joint Friction Angle	ϕ_j	1.25	-	-	8.2	-	-	Moderately Sensitive
Unit Crack Mode II Fracture Energy	$G_{f,c}^{II}$	2.0	-	-	0.1	-	-	Almost Insensitive
Unit Crack Compressive Fracture Energy	$G_{c,c}$	2.0	-	-	0.1	-	-	Almost Insensitive
Joint Tensile Strength	$f_{t,j}$	2.0*	-	-	2.1	-	-	Slightly Sensitive
Joint Mode I Fracture Energy	$G_{f,j}^{I}$	2.0	-	-	0.9	-	-	Almost Insensitive
Joint Mode II Fracture Energy	$G_{f,j}^{II}$	2.0	-	-	0.8	-	-	Almost Insensitive
Joint Compressive Fracture Energy	$G_{c,j}$	2.0	-	-	0.1	-	-	Almost Insensitive

*CSE Joint Tensile Strength x1.5

The shear wall peak resistance was found to be almost insensitive (<0.9%) to all parameters, bar four. The shear wall's response was classified as slightly sensitive to the joint interface's compressive strength (Figure 6.19), cohesion and tensile strength (Figure 6.20), whereas it was classified as moderately sensitive to the joint friction angle (Figure 6.21). The figures below show the sensitivity to these four parameters by means of horizontal force-displacement diagrams of the shear wall.
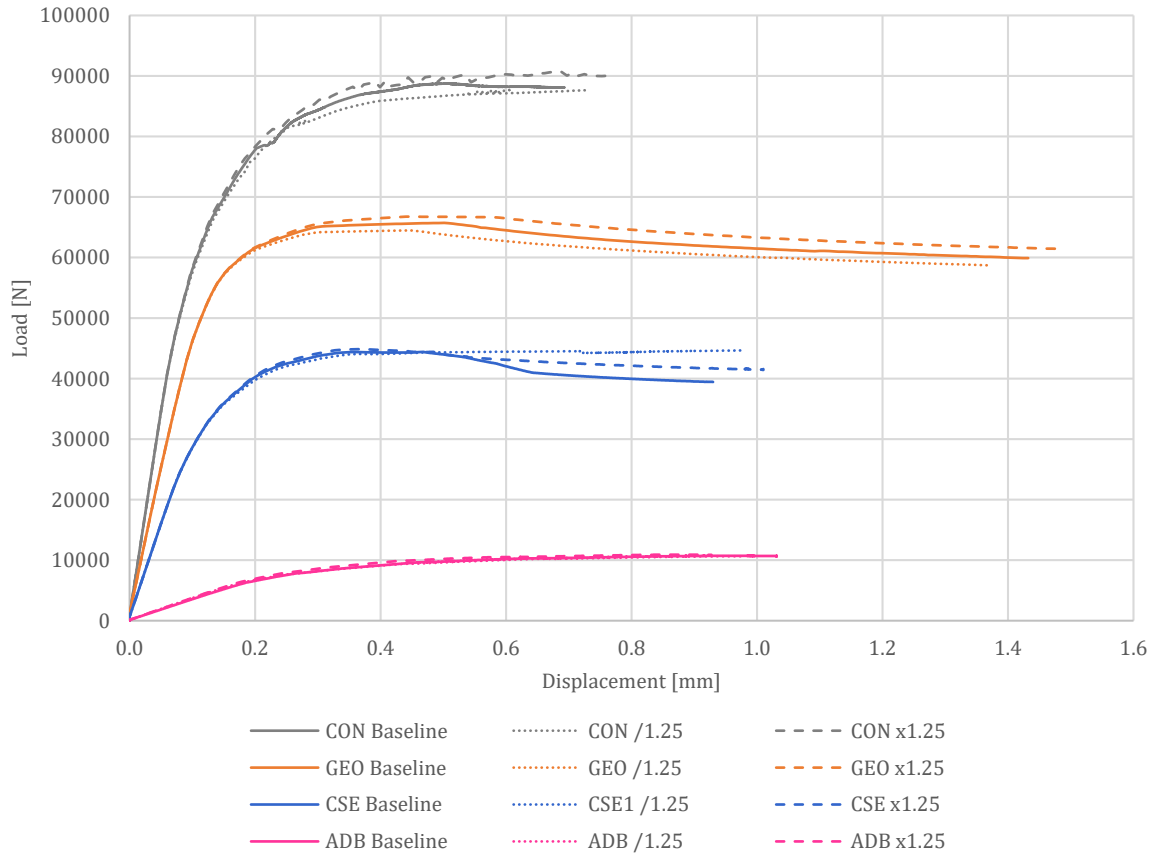
Figure 6.19: Response of shear wall slightly sensitive to joint interface compressive strength for CON, GEO, CSE and ADB
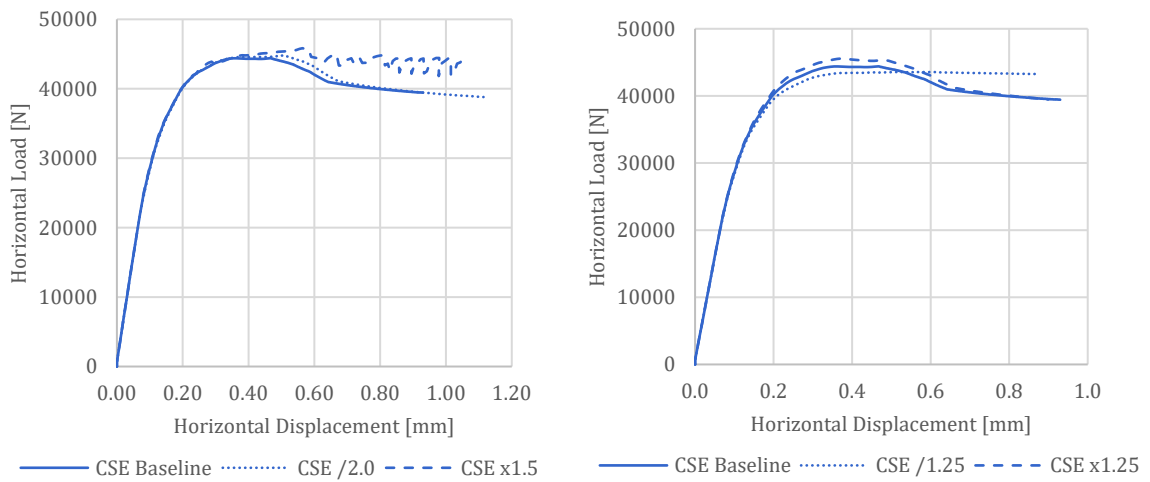
Figure 6.20: Response of shear wall slightly sensitive to joint interface a) tensile strength and b) cohesion for CSE
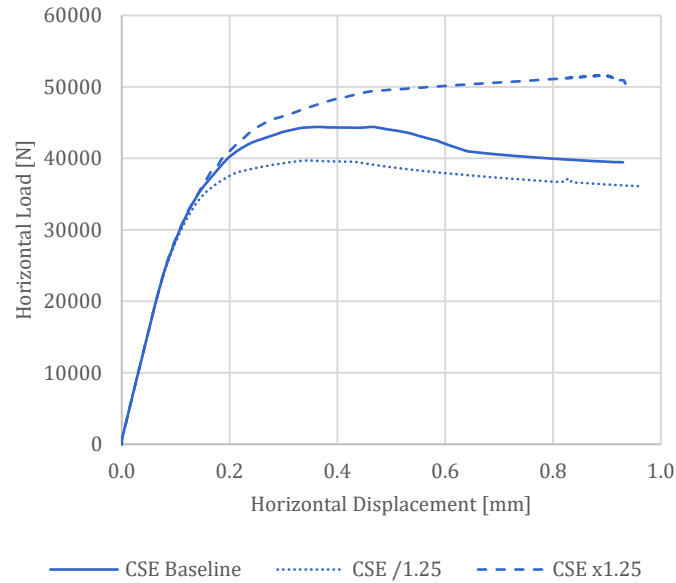
Figure 6.21: Response of shear wall sensitive to joint interface friction angle for CSE
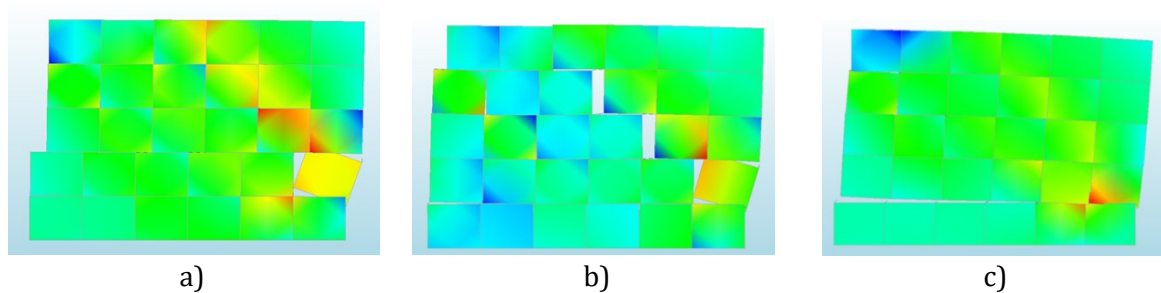
Figure 6.22: Examples of encountered failure mechanisms: a) shear sliding, b) diagonal cracks and c) uplift

The presented sensitivity analyses are not comprehensive. Not all parameters were included in the study and the failure mechanisms encountered by the specimen configuration are limited to shear sliding, diagonal cracks and uplift, examples of which are shown in Figure 6.22. The variation in parameters is also not always restricted to the single parameter under investigation, since a number of parameters are defined as dependent on others, as discussed in Chapter 5. In some instances the relation is apparent, such as the joint tensile strength is affected if the joint cohesion is altered. In others, such as between the unit mode I fracture energy and the joint mode I fracture energy, the relation is more tenuous. Therefore not every parameter is investigated in complete isolation. Certain observations can be made nonetheless:

- All four parameters to which the shear wall specimen displayed any form of sensitivity were of the joint interface, which is commensurate with the general view that the joint is masonry's weak link.
- Regarding the tensile properties, the only parameter that elicited a sensitivity was the joint tensile strength (2.1%). Bearing in mind that the joint tensile strength was multiplied by a factor of 1.5 instead of 2.0, the sensitivity to this parameter may be higher than determined. Lourenço (1998) found the sensitivity to the joint tensile strength to be 1.1%, whilst the other tensile properties' influences were also negligible. Tensile tests on

84

the joint interface are challenging and the effort required to explicitly determine this parameter is deemed too onerous given the relatively low sensitivity to this parameter.

- For the compression properties, the shear wall specimen only showed sensitivity to the joint compressive strength, which was classified as slight (1.5%). Failure in compression was not a dominant mode for this specimen configuration. Contrastingly, Lourenço (1998) found both the joint compressive strength and joint compressive fracture energy to be considerably more influential, 14.6% and 18.6% respectively. This can be ascribed, in part, to the difference in specimen configurations used. Lourenço made use of a specimen with a central opening. This resulted in weak piers alongside the opening and the formation of a compressive strut on either side. The dominant mechanism was failure of the compression toes, and hence significant sensitivity to the joint compression parameters. The joint compressive strength is determined experimentally with relative ease to prescribed standards, whereas the joint compressive fracture energy is challenging to obtain. Determining the joint compressive strength experimentally is recommended, together with the development of a predictive model for joint compressive fracture energy, based on the compressive strength.

- Similarly, Lourenço (1998) found much greater sensitivity to a change in the elastic stiffness (6.2%), compared to a 0.5% sensitivity in the present study to the unit E-modulus. Since the unit E-modulus is used in part to determine the joint linear stiffness (see Section 5.4.4), this comparison is appropriate. Again, the discrepancy is attributed to the differences in specimen configuration used. Lourenço made use of a more slender specimen with a width to height ratio of 1.0, compared to 1.4 of this study, which strongly affects the influence of the stiffness on the response of the structure. Both the unit E-modulus and wallet E-modulus, used to determine the joint linear stiffness, can be obtained reliably through standardised tests and, given the possible sensitivity to this parameter, are thus recommended.

- Shear failure modes dominated the specimen's response and the joint friction angle (8.2%) and, to a lesser degree, the cohesion (2.3%) influenced the peak resistance most. Lourenço (1998) attained a similar sensitivity level for the joint friction angle of 9.6%, but found the cohesion to be almost insensitive (0.6%). These parameters are dependent on the masonry unit's surface roughness and conditioning and can be determined with some effort by means of a standardised shear triplet test, or similar. However, these parameters are also largely dependent on the mortar used, specifically it's cement content, sand quality, water retention, etc. (Crosswell, 2009). The wider applicability of such test results is therefore limited, yet still recommended. It is telling that, despite the difference in specimen configurations, both sensitivity analyses (Lourenço (1998) and present study) found a significant sensitivity to the friction angle.

A more comprehensive sensitivity analysis is warranted. Of the 27 masonry parameters, 13 were not included. The analysis could be extended to these parameters, but their influences' are anticipated to be negligible. More importantly, the spectrum of specimen configuration used to perform the sensitivity analysis must be widened, including aspects such as the slenderness ratio, openings and out-of-plane loading. Nevertheless, the present sensitivity analysis is considered sufficient for the immediate purpose of the study of identifying which parameters are influential enough to require testing for adequate material model description.

6.4 Summary

The numerical results obtained correlate well with the in-plane (Test Setup 1) experimental data, especially the failure mechanisms, and sufficiently with the out-of-plane experimental results. Considering the variable and nonlinear nature of masonry, this satisfactory correlation between numerical and experimental data is regarded as fair validation of the FE model for both in-plane and out-of-plane loading conditions. This substantiates the choice of SMM approach, as well as the determined material parameter values.

The sensitivity analysis, whilst limited in scope, does highlight the significance of the joint friction angle, and to a lesser degree the joint cohesion. The insensitivity of parameters such as the joint tensile strength and mode I fracture energy is perhaps more indicative of the limitations of the sensitivity analysis, imposed by the boundary conditions and load application, than of the parameters themselves.

7 Numerical Analyses

The wall configurations used in the numerical analyses are detailed, including layout, dimensions and support conditions. The material input parameters and critical load cases for each configuration are presented for these analyses. Subsequently, the results of the in-plane and out-of-plane numerical analyses are presented and discussed.

The large-scale FE analyses are performed to gain insight into the structural behaviour of the three selected AMU materials, especially relative to the conventional concrete masonry unit and relative to the expected loading. A total of 24 analyses are performed, summarised in Table 7.1, for four materials (CON, GEO, CSE, ADB), two wall layouts (W1 and W2), and three load cases: serviceability limit state (SLS) and ultimate limit state for wind (ULS-W) and for seismic (ULS-S).

Table 7.1: Summary of large scale FE analyses performed

Wall Layouts	2	W1, W2
Materials	4	CON, GEO, CSE, ADB
Load Cases	3	SLS, ULS-W, ULS-S

7.1 Wall Configurations

As discussed in Section 3.1.2, the deemed-to-satisfy solutions entrenched in the NBR for masonry walls (SANS 10400-K, 2011), implicitly represent society's expectation regarding the wall's performance. These solutions are therefore used as the basis to identify suitable low-income housing wall configurations, applied as representative masonry walls in the numerical analyses. Additional limitations and recommendations set in SANS 10400-A (2010), SANS 10400-L (2011), SANS 10160-4 (2017) and SANS 10400-XA (2011) for geometry, seismic loading and energy use are also taken into consideration. The most critical and extreme combinations of wall height, distance between lateral supports and openings are selected to arrive at two different wall configurations: a panel wall, W1, and a gable wall, W2, detailed in Figure 7.1 and Figure 7.2, respectively. Hatched areas indicate lines of lateral support in the form of return walls.
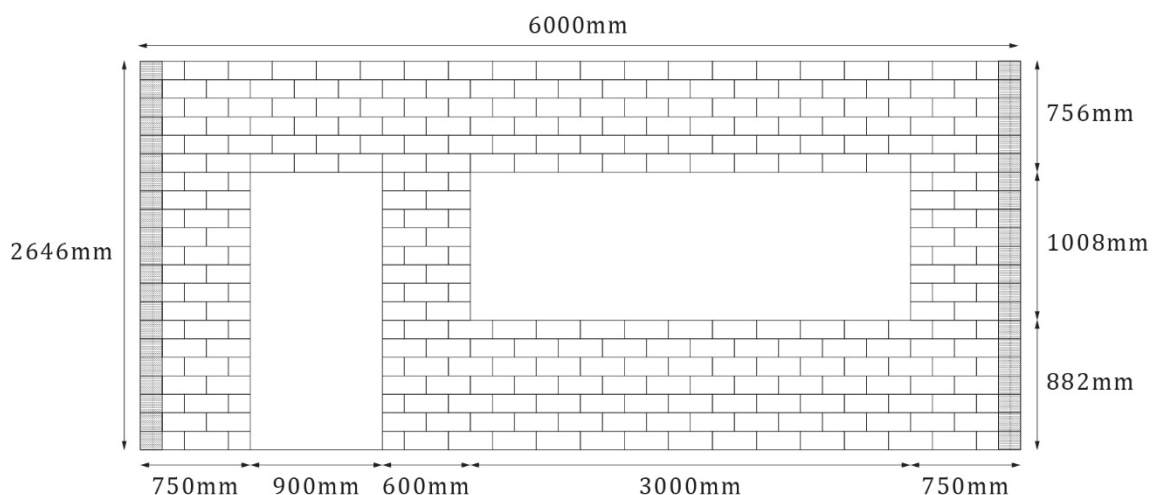
Figure 7.1: Wall W1 layout and dimensions
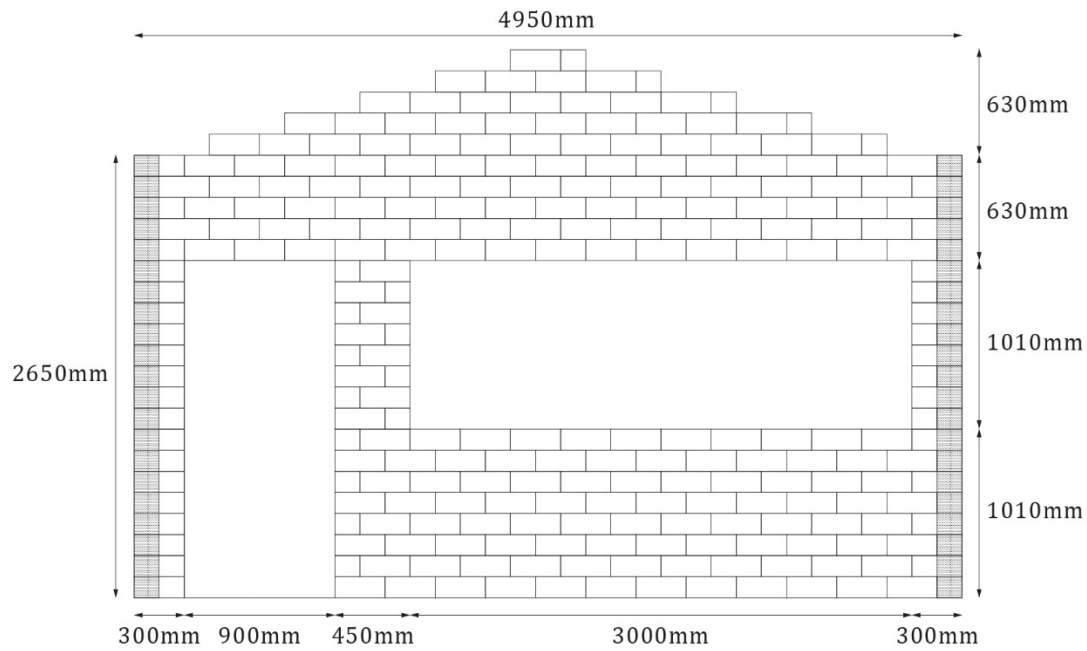
Figure 7.2: Wall W2 layout and dimensions

The selection criteria for these two representative single-leaf wall layouts are detailed in Table 7.2. Although only the walls are modelled, the walls are set within the context of representative 40m² Category 1 houses to derive loading and support conditions. The roof construction is assumed to be timber, with metal sheet covering.

Table 7.2: Selection criteria for representative houses and wall layouts

		Selection	Clause	Standard
Wall Effective Thickness		140mm*	B.3.3 a)	SANS 10160-4 (2017)
Wall Length	W1	6.0m	3.6 c)	SANS 10400-A (2010)
			Table 1, Panel C	SANS 10400-K (2011)
	W2	5.0m	3.6 c)	SANS 10400-A (2010)
			Tables 5 & 6	SANS 10400-K (2011)
Wall Height	W1	2.7m**	Table 1, Panel C	SANS 10400-K (2011)
			B.3.3 b)	SANS 10160-4 (2017)
	W2	2.6m**	Figure 4	SANS 10400-K (2011)
			B.3.3 b)	SANS 10160-4 (2017)
Roof Slope		15°	4.2.2.1	SANS 10400-L (2011)
Truss Spacing		1.2m	Table 4	SANS 10400-L (2011)
Openings		Various	Figure 6a, Table 7	SANS 10400-K (2011)
			6.2.2	SANS 10160-4 (2017)
			4.4.4	SANS 10400-XA (2011)
Reinforcement		5.6mm rods	Tables 20, 21& 23, Figure 27	SANS 10400-K (2011)
		2.8mm brickforce	B.3.3 d), f)	SANS 10160-4 (2017)
Vertical Control Joint		none	Table 19	(SANS 10400-K, 2011)

* shear wall t_{eff} requirement of 190mm is not met (SANS 10160-4 (2017) B.3.3 a)

** shear wall $h_{eff}/t_{eff} < 17$ requirement is not met (SANS 10160-4 (2017) B.3.3 b)

88

The following assumptions are made regarding the support conditions for the wall models. The foundations are fully supported and fixed, with no differential settlement potential, see Figure 7.3. For the lateral supports, short return walls are modelled with pin supports in the lateral direction to allow for some rotation at these joints. The top support along the roof line is modelled as free for both walls, on the assumption that the roof truss system provides negligible lateral load transfer. This assumption is based on the type of, and typically poor quality, connection provided between the roof and walling systems in LIH.
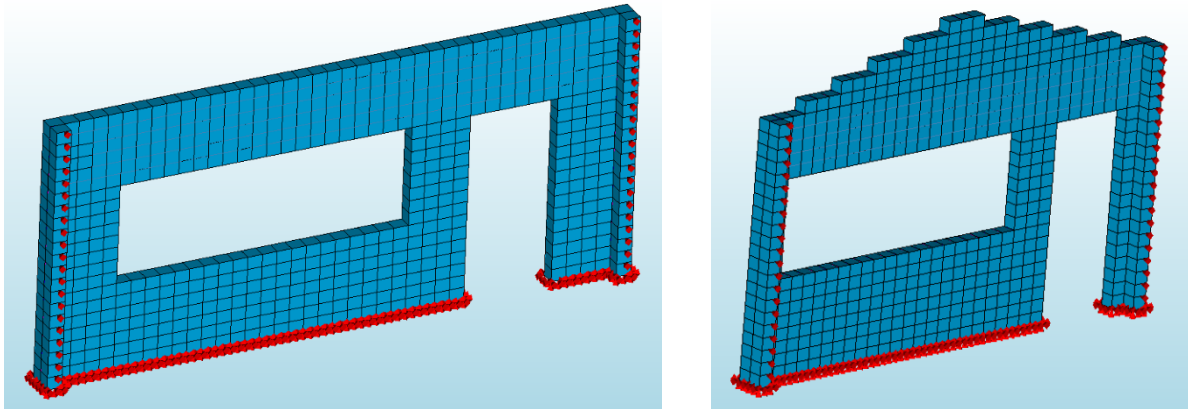
Figure 7.3: Boundary conditions for wall W1 (left) and W2 (right), inner perspective

7.2 Input Parameters

The material input parameters used in the analyses of this chapter are identical to those discussed in Chapter 5, but presented again for clarity in Table 7.3, and are mean, not design values, obtained experimentally, by inverse FEA or from literature. The current input data is statistically insufficient to establish characteristic values. SANS 10160-1 (2018) makes allowance for the use of nominal values in such instances (Clause 5.6.5) and requires the use of mean values for the structural stiffness parameters (Clause 5.6.8.)

Admittedly, the omission of material partial factors renders an evaluation of the AMU walls against design loads, adjusted with partial factors, less conclusive. However, the application of material partial factors obfuscates the FE output, impacting especially the fracture behaviour and the investigation of the relative importance of parameters.

In lieu of modelling concrete lintels above the openings, typical reinforcement (SANS 10400-K, 2011) in the form of 5.6mm diameter steel rods and 2.8mm brickforce is included in the bed joints above the openings, as detailed in Figure 7.4. The rod reinforcement yield strength is taken as the required proof stress of rod reinforcement by the NBR (SANS 10400-K, 2011), namely 485N/mm² . Whilst brickforce proof stress is not specified in the NBR, tensile tests conducted by Talocchino (2005) on typical South African brickforce found a proof yield stress of 500N/mm². Therefore the brickforce yield strength is taken as 485N/mm² as well. The elastic modulus of both reinforcement types is taken as 200 000N/mm².

Table 7.3: Input parameters for wall numerical analyses

Parameter		DIANA	Method	CON	GEO	CSE	ADB	Unit
Unit								
Density	ρ_u		EXP	2090	2080	1822	2007	kg/m³
E-modulus	E_u	YOUNG	EXP	17 700	11 020	7630	2480	N/mm²
Poisson's Ratio	ν_u	POISON	LIT	0.16	0.17	0.20	0.45	-
Crack Interface								
Tensile Strength	$f_{t,c}$	TENSTR	FEA	0.66	1.56	1.20	0.15	N/mm²
Mode I Fracture Energy	$G_{f,c}^{I}$	GF	EXP	0.047	0.056	0.016	0.006	N/mm
Cohesion	c_c	COHESI	LIT	1.0	2.3	1.8	0.2	N/mm²
Friction Angle	ϕ_c	PHI	LIT	37	37	37	37	°
Dilatancy Coefficient	ψ_c	PSI	LIT	0	0	0	0	°
Mode II Fracture Energy	$G_{f,c}^{II}$	MO2VAL	LIT	0.47	0.56	0.16	0.06	N/mm
Compressive Strength	$f_{c,c}$	COMSTR	EXP	12.1	17.9	6.6	0.8	N/mm²
Shear Traction Contribution	$C_{ss,c}$	CS	LIT	1.0x10⁻³	1.0x10⁻³	1.0x10⁻³	1.0x10⁻³	-
Compressive Fracture Energy	$G_{c,c}$	GC	LIT	10.0	14.8	5.5	0.7	N/mm
Eq. Plastic Relative Displ.	$\kappa_{p,c}$	DUPEAK	LIT	0.030	0.005	0.010	0.250	mm/mm
Tangential Stiffness	$k_{s,c}$	DSSX/Y	LIT	763 000	471 000	318 000	86 000	N/mm³
Normal Stiffness	$k_{n,c}$	DSNZ	LIT	1 770 000	1 102 000	763 000	248 000	N/mm³
Joint Interface								
Tensile Strength	$f_{t,j}$	TENSTR	LIT	0.12	0.08	0.06	0.04	N/mm²
Mode I Fracture Energy	$G_{f,j}^{I}$	GF	LIT	0.005	0.006	0.002	0.001	N/mm
Cohesion	c_j	COHESI	EXP	0.17	0.11	0.09	0.05	N/mm²
Friction Angle	ϕ_j	PHI	EXP	49.5	30.0	43.0	45.6	°
Dilatancy Coefficient	ψ_j	PSI	LIT	0	0	0	0	°
Mode II Fracture Energy	$G_{f,j}^{II}$	MO2VAL	LIT	0.05-0.08σ	0.05-0.08σ	0.05-0.08σ	0.05-0.08σ	N/mm
Compressive Strength	$f_{c,j}$	COMSTR	EXP	5.5	6.1	3.1	0.6	N/mm²
Shear Traction Contribution	$C_{ss,j}$	CS	LIT	0.7	2.9	1.1	0.7	-
Compressive Fracture Energy	$G_{c,j}$	GC	FEA	18.0	19.0	8.0	1.2	N/mm
Eq. Plastic Relative Displ.	$\kappa_{p,j}$	DUPEAK	FEA	0.030	0.005	0.010	0.250	mm/mm
Tangential Stiffness	$k_{s,j}$	DSSX/Y	LIT	214	373	131	3	N/mm³
Normal Stiffness	$k_{n,j}$	DSNZ	LIT	520	913	314	8	N/mm³
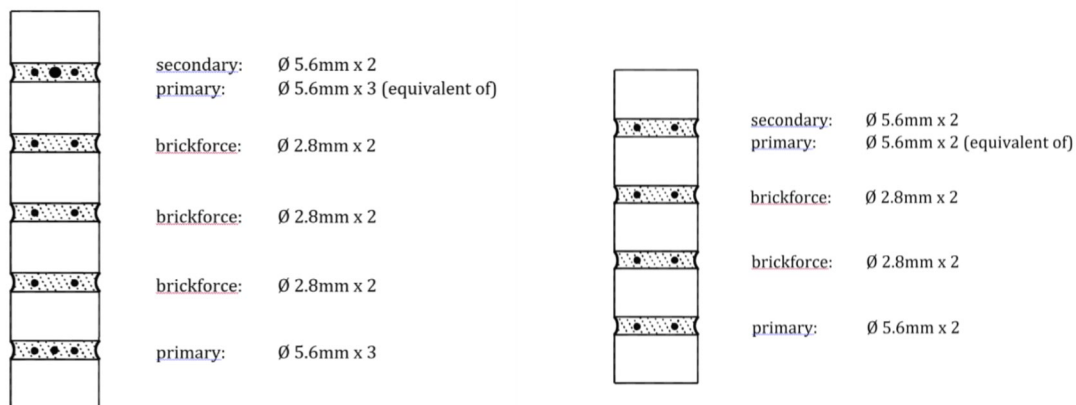
Figure 7.4: Bed joint reinforcement above openings for wall W1 (left) and W2 (right)

7.3 Design Loads

To assess structural strength and stability, the NBR (SANS 10400-B, 2012) requires the loading on the structure and structural elements to be determined according to the relevant part of the South African loading code (SANS 10160, 2011), including permanent, imposed and seismic action. All relevant design situations are considered and the most critical situations identified. The load cases considered are for the SLS, regarding the functioning of the structure under normal use, and the two ULS, regarding the safety of persons and the structure. The equivalent lateral static force method is employed for the seismic actions. The factored loads applied in the FE analyses are summarised in Table 7.4, Figure 7.5 (W1) and Figure 7.6 (W2) for the SLS and ULS-W and in Table 7.5, Figure 7.7 (W1) and Figure 7.8 (W2) for the ULS-S.

Table 7.4: Critical design loads for SLS and ULS-W to SANS 10160 (2011)

	W1		W2		
	SLS	ULS-W	SLS	ULS-W	
Roof Selfweight	-10.05×10^{-3}	-9.00×10^{-3}	-	-	N/mm²
Roof Wind	43.92×10^{-3}	117.14×10^{-3}	-	-	N/mm²
OP Zone A	1.39×10^{-3}	3.71×10^{-3}	2.26×10^{-3}	6.02×10^{-3}	N/mm²
OP Zone B	1.05×10^{-3}	2.79×10^{-3}	1.00×10^{-3}	2.66×10^{-3}	N/mm²
IP	24.41×10^{-3}	65.09×10^{-3}	17.58×10^{-3}	46.86×10^{-3}	N/mm²

Table 7.5: Critical design loads for ULS-S to SANS 10160 (2011)

	W1	W2	
OP	0.79×10^{-3}	0.96×10^{-3}	N/mm²
IP	53.88×10^{-3}	56.43×10^{-3}	N/mm²

The out-of-plane (OP) load is a uniform distributed load, applied over the entire wall. This load includes the wind or seismic load, as applicable. The load is segmented into A and B for the wind loads according to Figure 8 of SANS 10160-3 (2018), since the wall under consideration being situated as the side wall is found to be the most critical load case in all wind loading configurations. The total OP force (N) determined, is distributed uniformly over the masonry portions of the wall, to compensate for the lack of surface area over the model openings to which OP load cannot be applied.

The in-plane (IP) load is a horizontal load over the full height of the wall, distributed over the thickness of the wall. This load includes the wind or seismic load, as applicable, and originates from the lateral loads on the adjacent walls. For the wind load cases, the load varies linearly with the maximum value, applied at the top of the wall, presented in Table 7.4. For the seismic load case, the load is distributed uniformly over the height of the wall, following the principle that lateral loads are applied at the location of the mass (EN 1998-1 (2004) 4.3.3.4.2.2 (2)P).

The roof load is the load applied by the roof at each truss support point, distributed over one masonry block to avoid stress concentration. This load includes the roof self-weight and wind load, if applicable. A positive value indicates uplift, whereas a negative value indicates a compressive force. A roof load is only applied to wall configuration W1, since W2 is a gable wall and does not support trusses.

Roof Wind
SLS: 43.92×10^{-3}
ULS-W: 117.14×10^{-3}

IP
SLS: 24.41×10^{-3}
ULS-W: 65.09×10^{-3}

OP A
SLS: 1.39×10^{-3}
ULS-W: $3.71 \times 10^{-}$

OP B
SLS: 1.05×10^{-3}
ULS-W: 2.79×10^{-3}
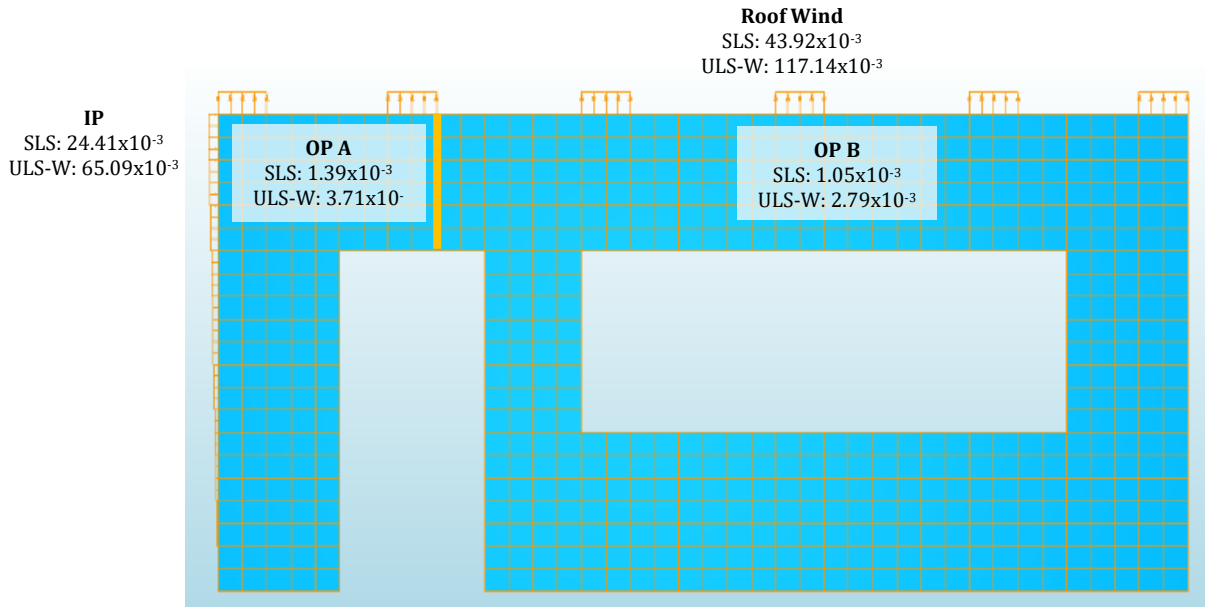
Figure 7.5: Critical design load pressures [N/mm^2] for wall W1 SLS and ULS-W

IP
SLS: 17.58×10^{-3}
ULS-W: 46.86×10^{-3}

OP A
SLS: 2.26×10^{-3}
ULS-W: 6.02×10^{-3}

OP B
SLS: 1.00×10^{-3}
ULS-W: 2.66×10^{-3}
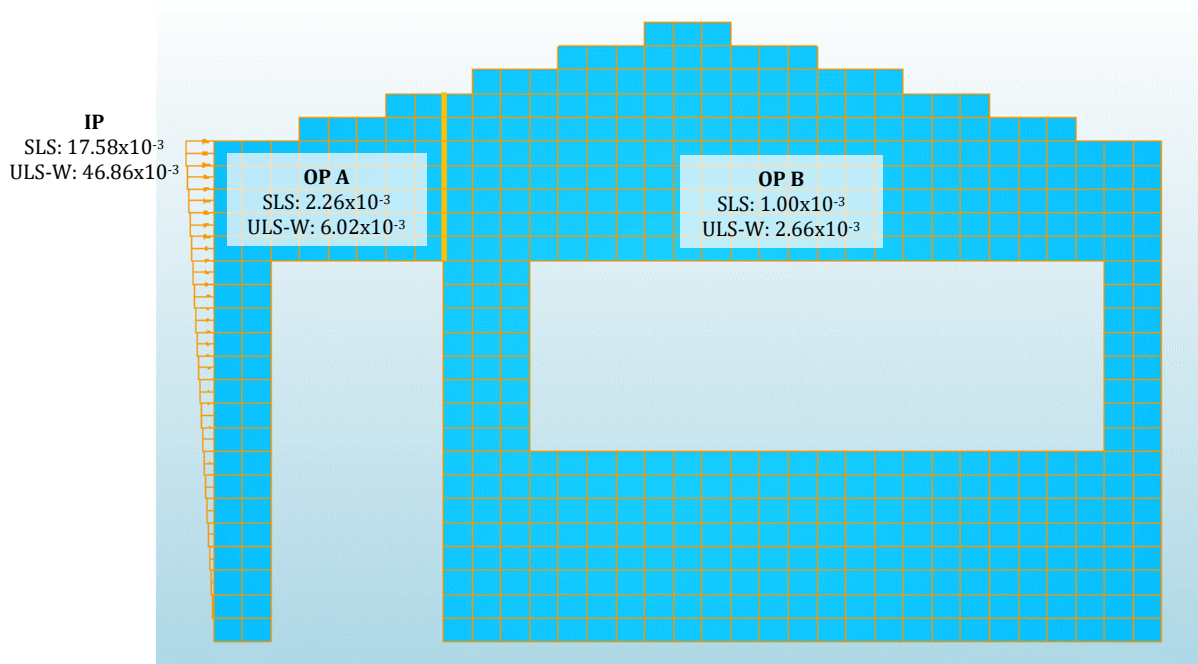
Figure 7.6: Critical design load pressures [N/mm^2] for wall W2 SLS and ULS-W

92
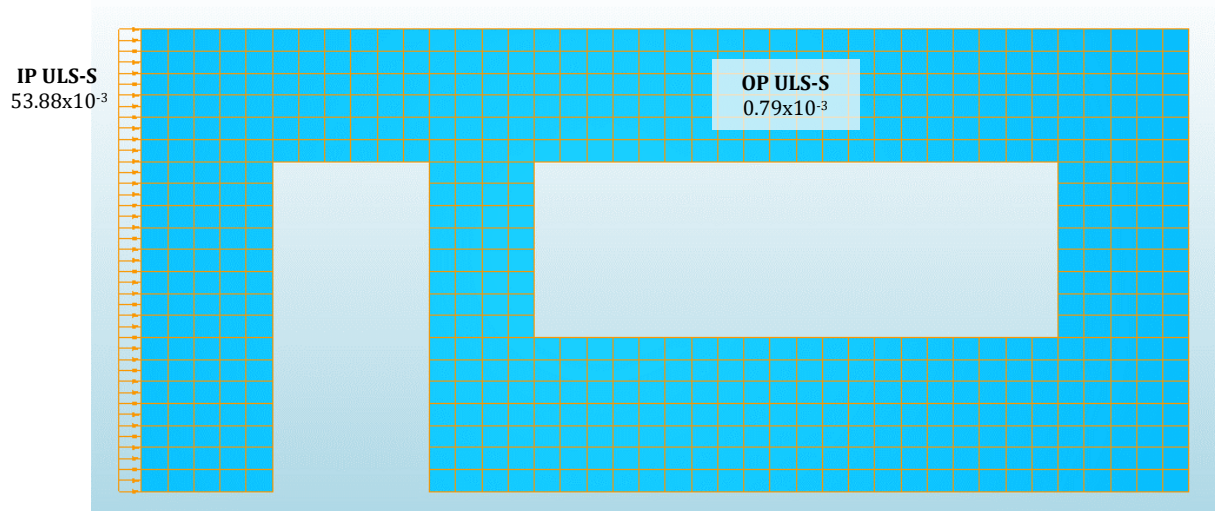
Figure 7.7: Critical design load pressures [N/mm²] for wall W1 ULS-S
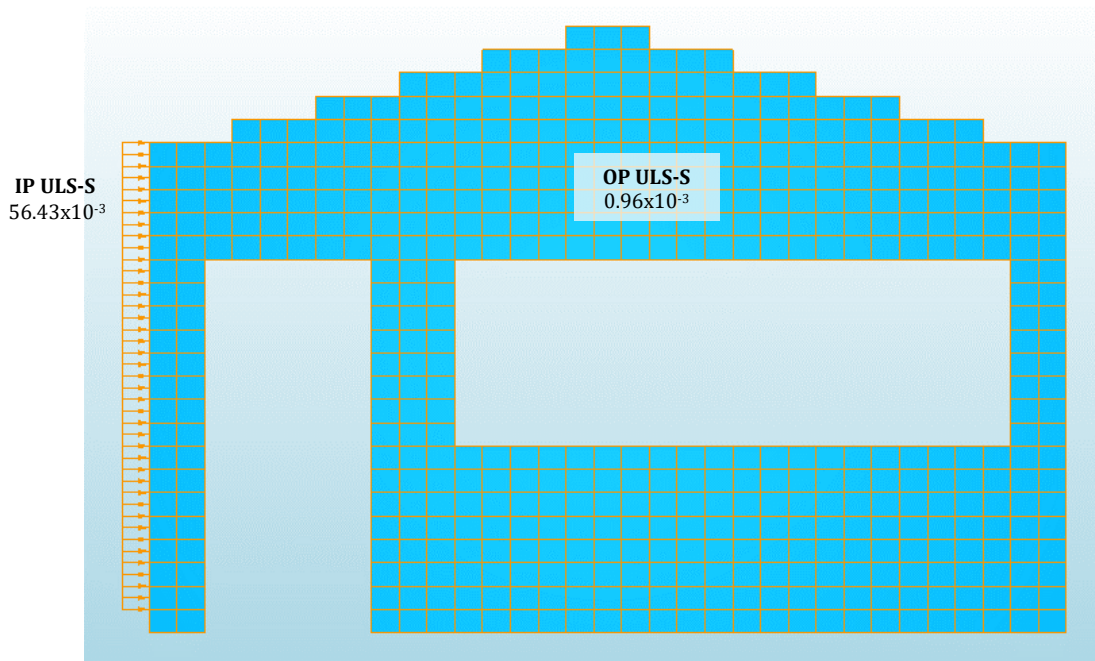
Figure 7.8: Critical design load pressures [N/mm²] for wall W2 ULS-S

Previously, experimental and numerical studies have concentrated on the effect of either IP or OP loading. More recently, the importance of the interaction of these loading conditions has come to the fore, but with a focus on infill masonry walls. Only a few numerical studies have considered the combined effects on load-bearing URM and even less experimental campaigns, (Milani, 2008), (Agnihotri, et al., 2013), (Najafgholipour, et al., 2013), (Dolatshahi, et al., 2015). Typical findings include that the IP load may significantly affect the OP capacity and the interaction level is dependent on the wall aspect ratio and slenderness ratio. Hence, the relevant IP and OP loads are applied simultaneously in this study.

The design values of the load cases are determined using the partial factors summarised in Table 7.6, according to SANS 10160-1 (2018).

Table 7.6: Load combination partial factors according to SANS 10160-1 (2018)

Load Case	Self-Weight	Roof Imposed	Wind	Seismic
SLS	1.0	0.0	0.6	-
ULS-W	0.9	0.0	1.6	-
ULS-S	1.0	0.0	-	1.0

The assumptions made in determining these critical load cases are detailed in the following three sub-sections according to self-weight and imposed load, wind load and seismic load.

7.3.1 Self-Weight & Imposed Load

The self-weight of the walls is based on the densities determined experimentally of each material block type, detailed in Table 7.3 and discussed in Section 5.2.1. The roof assembly consists of six bay Howe type trusses, assuming a timber density of $5000 N/m^3$ according to Table A.4 of SANS 10160-2 (2011) for the structural pine, and 0.5mm metal sheeting with a self-weight of $39.5 N/m^2$ according to Table A.5 of SANS 10160-2 (2011). The roof is classified as an inaccessible roof according to Table 5 of SANS 10160-2 (2011) and loads for normal maintenance and repair of $400 N/m^2$ would be included. However, since an additional compressive load on the walls is favourable, the load combination nullifies the roof imposed load.

7.3.2 Wind Load

The loads due to wind actions are determined according to SANS 10160-3 (2018). The pertinent parameters are summarised in Table 7.7 and assumptions discussed thereafter. For further details, refer to Appendix A.

Table 7.7: Wind load parameters to SANS 10160-3 (2018)

Parameter	Symbol	Value	Clause
Fundamental Value of Basic Wind Speed	v_b	44 m/s	7.2.2
Terrain Category	-	C	Table 2
Terrain Roughness Factor	$c_r(z)$	0.73	7.3.2, Table 3
Topography Factor	$c_0(z)$	1	7.3.3
Air Density	ρ	1.2 kg/m³	Table 4
Peak Wind Pressure	$q_p(z)$	1213 N/m²	7.4, Eq 6

In most instances, the parameter resulting in the most critical load is selected. The basic fundamental wind speed is taken as the highest value for any area in South Africa. The terrain category is chosen as the most likely scenario for single-storey residential structures in a suburban or peri-urban setting. The default topography factor is chosen, on the assumption that it is unlikely that low-income housing is developed on extreme terrain, which is costly to construct on. The highest air density value is chosen, to result in the highest critical load.

94

Additionally, the NBR (SANS 10400-B, 2012) specify minimum wind pressures to be applied to housing structural systems of $370N/m^2$ and to housing structural elements of $450N/m^2$. The peak wind pressures determined according to SANS 10160-3 exceed these minimum load requirements.

7.3.3 Seismic Load

The loads due to seismic actions are determined according to SANS 10160-4 (2017). The pertinent parameters are summarised in Table 7.8 and assumptions discussed thereafter. For further details, refer to Appendix B.

Table 7.8: Seismic load parameters to SANS 10160-4 (2017)

Parameter	Symbol	Value	Clause
Peak Ground Acceleration	a_g	0.15g	5.2, Figure 1
Ground Type	-	4	5.1.2 Figure 2, Table 2
Building Importance Factor	γ_1	1.0	7.3, Table 3
Reliability Redundancy Factor	ρ	1.2	7.3, Eq 6
Behaviour Factor	q	1.5	8.2, Table4
Fundamental Period of Vibration Factor	C_T	0.05	8.5.2.1

The highest peak ground acceleration for natural seismicity in South Africa is selected. The most unfavourable of ground types is chosen and the selected building importance factor is commensurate with a typical residential structure. The behaviour factor for unreinforced masonry is used, given that minimum detailing and reinforcement requirements are adhered to. The fundamental period of vibration is chosen based on structural system type.

The reliability redundancy factor is not present in the parent standard, Eurocode 8 (EN 1998-1, 2004), but was taken from the Uniform Building Code (UBC, 1997) and introduced in the South African loading code to compensate for a lower nominal peak ground acceleration of 0.1g (Wium, 2010). However, the UBC permits a reliability redundancy factor range of 1.0 to 1.5, compared to a range of 1.2 to 1.5 in SANS 10160-4 (2017). The lower limit of 1.2 was set to compensate for the higher behaviour factors for reinforced concrete shear walls used in the UBC (1997) compared to Eurocode 8 (2004), (Wium, 2010).

For determining the seismic design load, the reliability redundancy factor is chosen as the lower limit of the allowable range (1.2 to 1.5), hence less conservative, for two reasons. First, a higher peak ground acceleration of 0.15g was selected for the analyses, not 0.1g. Second, the lower limit of 1.2 in SANS 10160-4 was introduced to compensate for the higher behaviour factors of reinforced concrete shear walls. This discrepancy in behaviour factors is less relevant for this study, given that a consistent behaviour factor for unreinforced masonry of 1.5 is used. It would hence be justifiable to use a reliability redundancy factor of 1.0. However, compliance with SANS 10160-4 (2017) is considered salient and a factor of 1.2 is used.

7.4 Results

The results are presented in the following subsections, starting with a key to facilitate the interpretation of the results, typical failure mechanisms and crack patterns found, followed by the IP load-displacement and OP load-deflection responses and crack damage classification.

7.4.1 Interpretation Key

The results are presented predominantly according to the IP load and displacement and the OP load and deflection. The IP displacement is measured at the top left corner of each wall, shown in Figure 7.9, and the OP deflection is measured at the top midspan position. The typical crack positions are also indicated and named in this figure, as reference for the discussion on crack width and damage classification in later subsections.
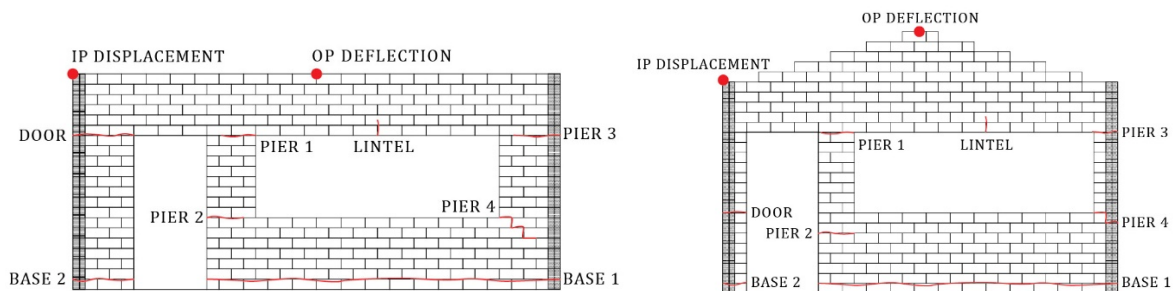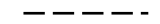
Figure 7.9: Crack position and deflection/displacement measurement legend (W1 left, W2 right)

All block material type (CON, GEO, CSE, ADB) and load case (SLS, ULS-W, ULS-S) specific results in Section 7.4 are communicated according to the legend in Table 7.9.

Table 7.9: Results Interpretation Key

Line Colour	Block Material		Line Type	Load Case
————	CON		– – – – – – – –	SLS
————	GEO		— — — — –	ULS-W
————	CSE		————	ULS-S
————	ADB			

The following two graphs are shown merely to serve as illustrative examples, containing only one material type, for ease of interpretation. Thereafter, the results are presented simultaneously for all four material types to facilitate comparison.

In Figure 7.10, the OP numerical response for Wall W1 for CSE is shown (i.e. load carrying capacity), for each of the three load cases. The OP design load, determined according to the South African loading code (SANS 10160, 2011) is also included for each of the three load cases to provide context for the results. The design loads were provided in the form of pressures (N/mm²) in Tables 7.4 and 7.5 but to enable effective comparison, these design loads and the walls' resistance capacities are converted to forces (N), according to the relevant surface area. Additionally, the maximum allowable OP deflection, determined according to the NBR (SANS 10400, 2010) for Category 1 buildings, is included for deflection contextualisation.

The crack damage classification, as exampled in Figure 7.11, is presented along the same principles. For clarity, only the dominant crack for each material type/load case combination is included. The crack width frame of reference is provided by the maximum crack width and damage categories specified in the NBR (SANS 10400-B, 2012) and Home Building Manual (NHBRC, 2015), detailed in Table 3.4. The damage categories range from <0.25mm (negligible) to >25mm (very severe).
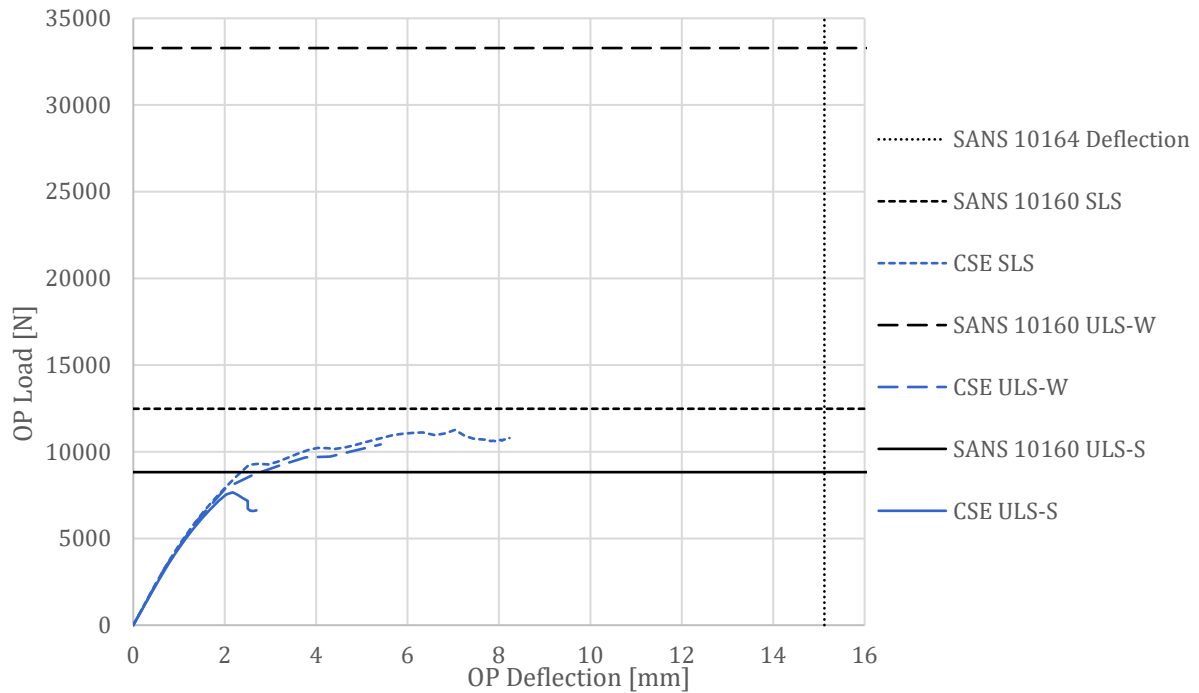
Figure 7.10: Interpretation key example – Wall W1 CSE out-of-plane response
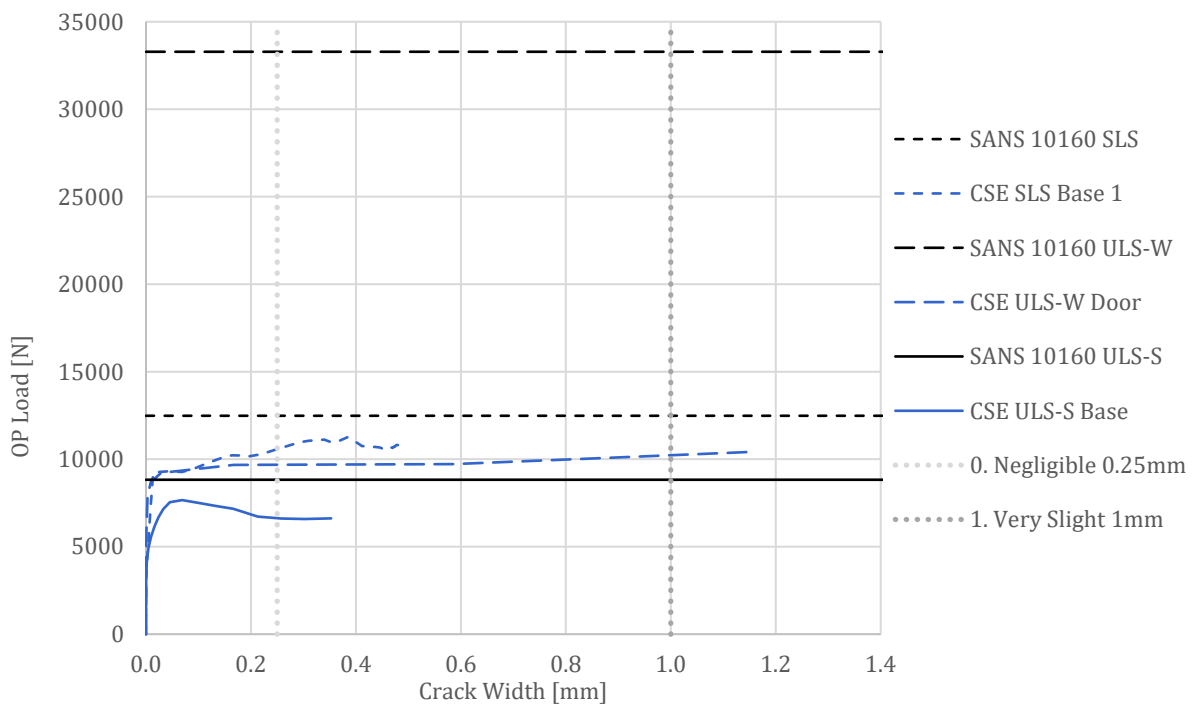
Figure 7.11: Interpretation key example – Wall W1 CSE crack damage classification

7.4.2 Results Overview

The following three figures illustrate the typical failure modes for the three load cases. In neither the OP nor the IP failures is crushing or compressive failure noted in either of the wall configurations. Given the small structure size and relatively low vertical imposed loads, this is not extraordinary.

For the SLS (Figure 7.12) and the ULS-W (Figure 7.13), OP failure dominates, since the larger proportion of the total load applied is lateral. The contours in these two figures are thus of the OP deflection. However, no scale is provided since the deflections vary for each material type and the figures are only intended to illustrate typical failure patterns. OP deflection magnitudes are provided in Figure 7.17 for W1 and Figure 7.18 for W2.
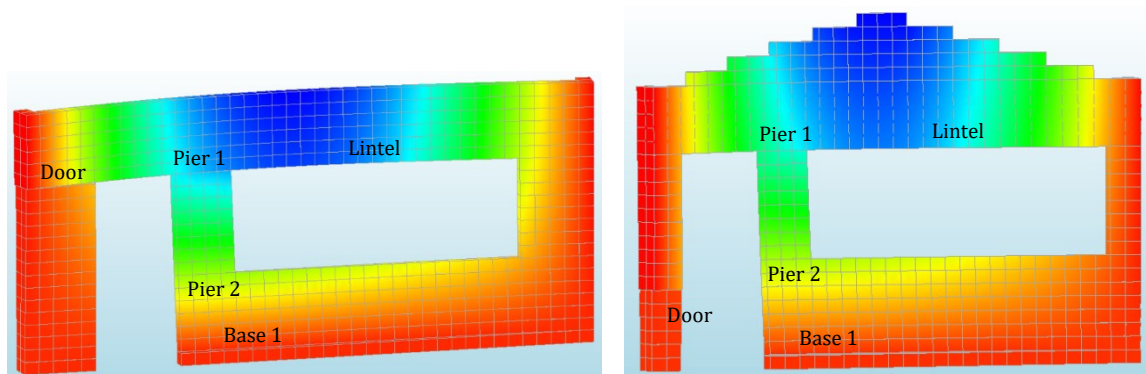
Figure 7.12: Typical failure for SLS for walls W1 (left) and W2 (right)
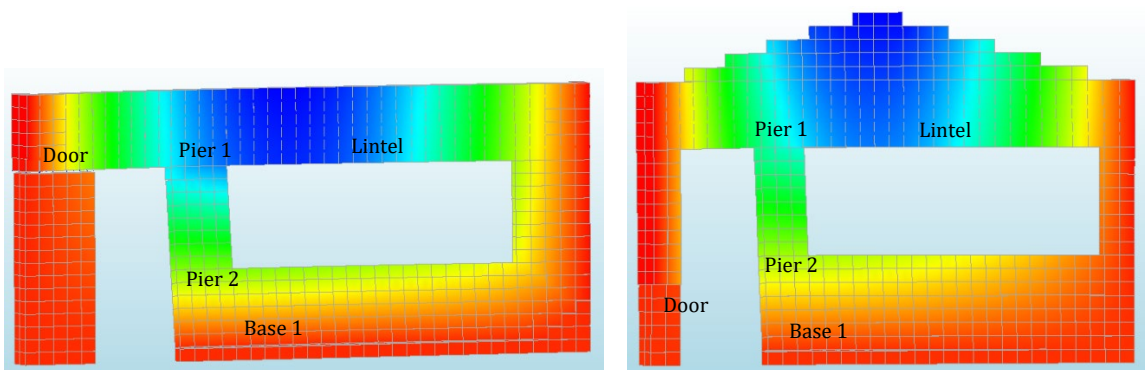
Figure 7.13: Typical failure for ULS-W for walls W1 (left) and W2 (right)

Crack onset is the tensile failure in the lowest joint in the longest wall section ('Base 1') and shear failure in the column to the left of the door ('Door') for both wall configurations W1 and W2 for the SLS and ULS-W load cases. Tensile cracks also form at the top ('Pier 1') and bottom ('Pier 2') of the pier to the left of the window. For the ADB case, considerable cracks also occur in the 'Lintel' above the window due to the own weight of the wall above and negligible tensile capacity of ADB.

For the ULS-S (Figure 7.14), IP failure dominates, since the majority of the seismic load is expected to be carried as shear action in the walls. Thus the contours in this figure are the IP displacement, the magnitudes of which are provided in Figure 7.15 for W1 and Figure 7.16 for W2.
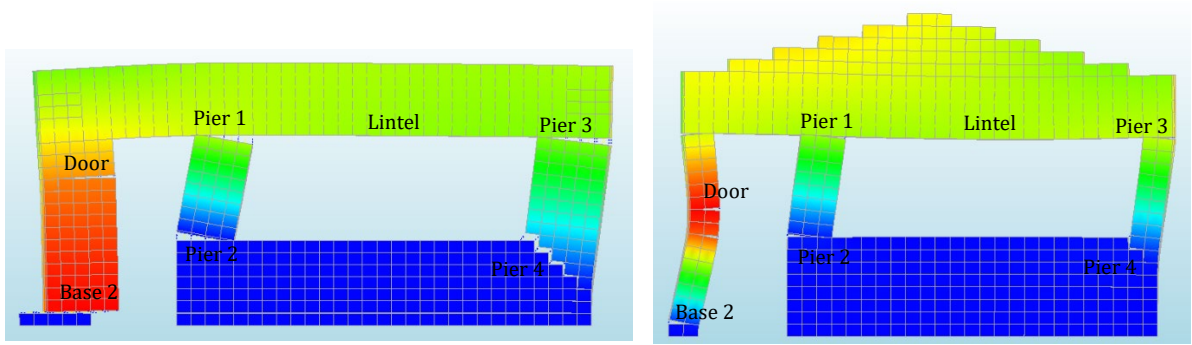
Figure 7.14: Typical failure for ULS-S for walls W1 (left) and W2 (right)

The majority of the cracks in the ULS-S are tensile/flexural, at the base of the column to the left of the door ('Base 2'), at the top and bottom of the pier to the left of the window ('Pier 1' and 'Pier 2' respectively) and likewise to the right of the window ('Pier 3' and 'Pier 4'). 'Pier 4' is a combined tensile/shear failure of stepped cracks and 'Base 2' starts as a tensile failure in most cases and progresses to sliding shear for some of the material types. Again, considerable tensile cracks occur in the 'Lintel' above the window in the ADB case. In the case of W2, the slender column to the left of the door, as well as the significant own weight of the wall above the large window opening due to the gable, make this wall configuration particularly vulnerable.

The IP design loads, resistance and displacements determined through the numerical analyses, for the different load cases and material types are summarised in Table 7.10 as an overview. Likewise, the summary is presented in Table 7.11 for the OP case. The ratio of the design load to the numerical wall resistance for the critical load direction for each instance is included. A ratio of > 1.0 therefore indicates a failure to resist the design load and, for more convenient visual interpretation, these ratios are graded further by colour. The W2 ADB results for the ULS-W and ULS-S are omitted, since failure occurred prior to the application of any horizontal loading. The selfweight above the window opening caused excessive tensile cracking in the lintel. The results are discussed in more detail in the following sub-sections.

Table 7.10: Summary of IP loads and displacements

		SANS 10160 IP Design Load		IP NUM Resistance		IP Design Load / IP NUM Resistance		IP NUM Displacement	
		[N]		[N]		[-]		[mm]	
		W1	W2	W1	W2	W1	W2	W1	W2
SLS	CON	4 613	3 199	5 751	6 050	0.8	0.5	0.02	0.09
	GEO			5 650	5 967	0.8	0.5	0.08	0.10
	CSE			4027	3 788	1.1	0.8	0.13	0.11
	ADB			1 723	2 757	2.7	1.2	0.11	0.92
ULS-W	CON	12 302	8 530	5 656	4 669	2.2	1.9	0.02	0.06
	GEO			5 479	5 807	2.2	1.5	0.05	0.10
	CSE			3 779	3 714	3.3	2.3	0.04	0.12
	ADB			2 308	-	5.3	-	0.16	-
ULS-S	CON	19 613	20 539	25 964	11 295	0.8	1.8	0.18	0.71
	GEO			24 670	10 383	0.8	2.0	1.25	0.53
	CSE			14 969	7 253	1.3	2.8	0.74	1.59
	ADB			8 851	-	2.2	-	0.50	-

	KEY	≤ 1.0	1.1-2.0	2.1-3.0	> 3.0

99

Table 7.11: Summary of OP loads and deflections

		SANS 10160 OP Design Load		OP NUM Resistance		OP Design Load / OP NUM Resistance		OP NUM Deflection	
		[N]		[N]		[-]		[mm]	
		W1	W2	W1	W2	W1	W2	W1	W2
SLS	CON	12 482	11 530	16 086	21 430	0.8	0.5	2.76	5.96
	GEO			15 803	21 136	0.8	0.5	7.13	11.17
	CSE			11 264	13 424	1.1	0.9	8.23	6.10
	ADB			4 818	10 956	2.6	1.1	6.44	17.45
ULS-W	CON	33 285	30 746	15 597	16 543	2.1	1.9	2.44	2.70
	GEO			15 109	20 576	2.2	1.5	6.16	10.52
	CSE			10 423	13 160	3.2	2.3	5.41	6.13
	ADB			3 783	-	8.8	-	9.33	-
ULS-S	CON	8 826	9 243	11 486	4 997	0.8	1.8	1.49	0.65
	GEO			10 913	4 591	0.8	2.0	2.70	0.87
	CSE			7 663	3 206	1.2	2.9	2.69	0.99
	ADB			1 593	-	5.5	-	5.32	-

KEY	≤ 1.0	1.1-2.0	2.1-3.0	> 3.0

7.4.3 In-Plane Response

The following two figures depict the IP load/displacement response for W1 (Figure 7.15) and W2 (Figure 7.16), for the four material types and three load cases. To address the most conspicuous inference first: of the 24 analyses, in only seven instances does the IP load carrying capacity exceed the IP design load, namely for CON SLS (W1 and W2), CON ULS-S (W1), GEO SLS (W1 and W2), GEO ULS-S (W1) and CSE SLS (W2). In all other instances, the IP design load exceeds the IP load carrying capacity of the walls and significantly so for W2. The reasons for and implications of this are discussed further in Chapter 8.

For both walls, the responses of the different material types achieve an intentionally wide spectrum and the responses in relation to each are as anticipated, the CON walls exhibiting the largest load capacity and stiffness, followed by GEO, CSE and ADB performing particularly poorly. The similarity in responses under SLS and ULS-W loading is also to be expected. The same loading condition is applied, only with slightly different proportions between the selfweight and wind load, due to the partial load factors.

The IP displacement is not significant (<1mm) for either of the walls, and arguably would be larger if the load path is continued, but this is not pursued due to the laborious nature of overcoming post-peak divergence. No limiting specifications exist for IP displacements as they do for OP deflections in the South African NBR. Marked reduction in load-carrying capacity, coupled with negligible IP displacement, attest to the severely brittle nature of masonry for both the conventional and alternative material types.

The ADB IP load/displacement paths for both wall configurations distinctly lack any post-peak response. The difficulty in attaining convergence in these cases is symptomatic of the exceptionally weak material parameters. The geometry selected for W2 makes it particularly vulnerable to high IP, i.e. seismic, loading, which rationalises in part the significant difference in peak IP loads between W1 and W2. W1 maximum seismic IP capacities are on average 2.2 times higher than for W2. This is discussed further in Chapter 8.
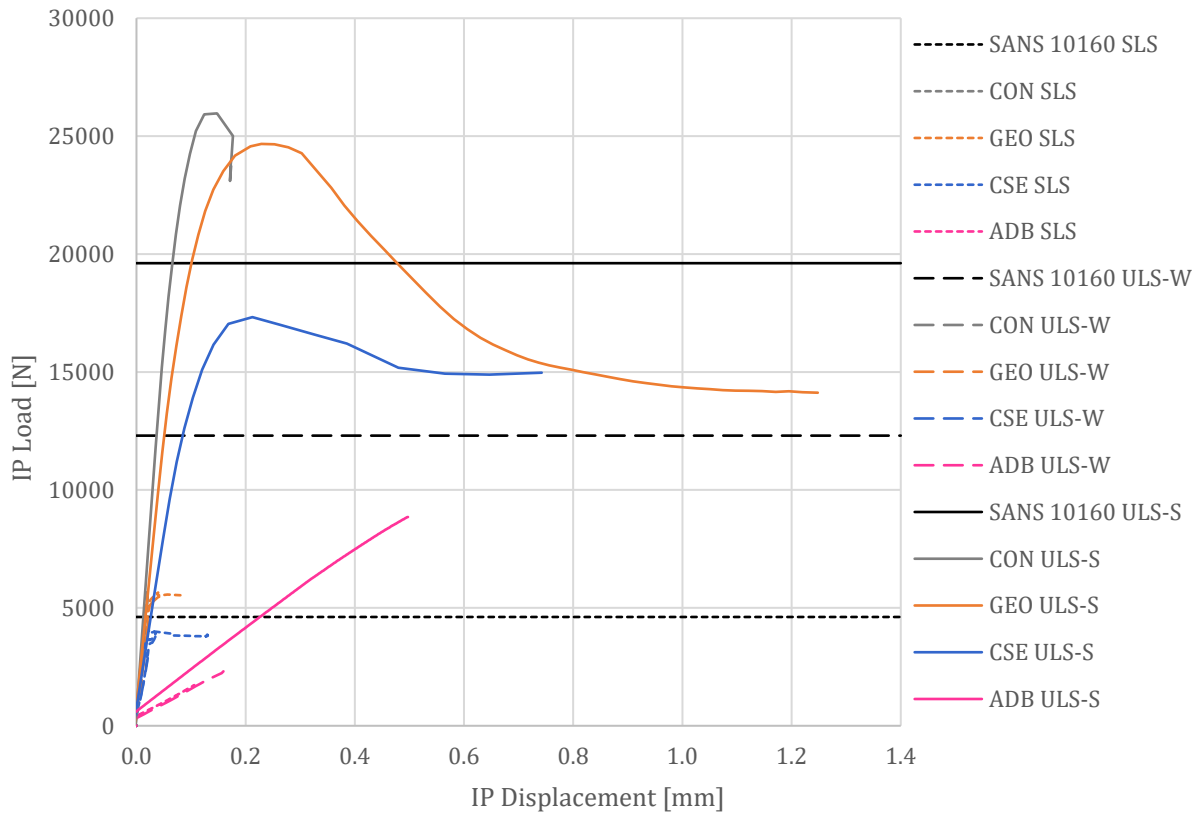
Figure 7.15: Wall W1 CON, GEO, CSE and ADB in-plane response
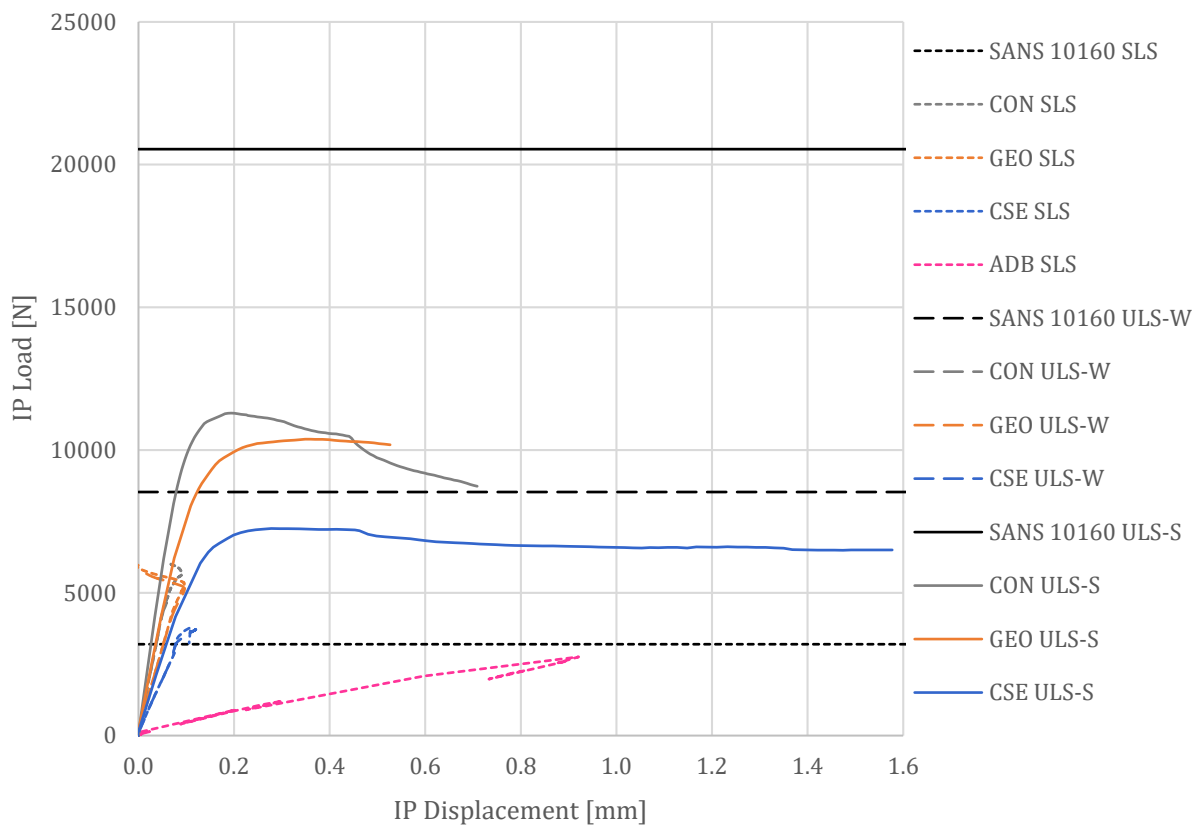
Figure 7.16: Wall W2 CON, GEO, CSE and ADB in-plane response

7.4.4 Out-of-Plane Response

The following two figures depict the OP load/deflection for W1 (Figure 7.17) and W2 (Figure 7.18) for the four block types and three load cases. Again, the W2 ADB results in Figure 7.18 for the ULS-W and ULS-S are omitted due to tensile failure in the window lintel under the selfweight of the gable wall.

As was found for the IP response, only in seven of the analyses did the OP load carrying capacity exceed the OP design load, namely CON SLS (W1 and W2), CON ULS-S (W1), GEO SLS (W1 and W2), CON ULS-S (W1) and CSE SLS (W2). In all other cases the OP design load far exceeds the load carrying capacity. This is discussed further in Chapter 8. Again, the similarity in responses to the SLS and ULS-W loading for both walls is expected. Contrary to the IP peak loads, the maximum (SLS) OP loads attained in W2 are on average 1.5 times higher than those in W1. This may be ascribed to the fact that W2 possesses a shorter span (4.95m compared to 6.0m) and has no vertical uplift imposed on it from the roof wind load, making it less vulnerable to tensile failure.

The OP deflection is naturally of a greater magnitude than the IP displacement measured in the previous two figures. Most OP deflections range between 2.5mm and 10mm, still well below the 1:175 deflection limit imposed in the NBR (SANS 10400-B, 2012) for Category 1 buildings. The only exception being the W2 ADB SLS response (Figure 7.18), an unexpected outcome, given the relatively more brittle response of ADB for the W1 configuration.

The gable of the W2 configuration was presumed to be an issue, since it is not buttressed, contrary to the specifications of SANS 10160-4 (2017), Clause 6.2.5. However this element proved to be noncritical in all of the OP loading conditions considered. In all likelihood this is due to the more vulnerable, slender elements elsewhere in the wall. A better proportioned wall opening geometry may well render the gable critical, requiring buttressing.

Regardless that the IP load carrying capacity of both walls for the ULS-S case is insufficient (excepting CON and GEO of W1), it is notable that the OP response for this load case is also inadequate, in accordance with more recent assertions in literature (Vaculik, 2012), (Derakhshan, et al., 2018) that OP unreinforced masonry behaviour cannot be overlooked in seismic loading.

7.4.5 Crack Damage Classification

Cracks occurred in a number of typical positions for the IP and OP dominant loading conditions, as illustrated in Figure 7.9, as well as in Figure 7.13 for the ULS-W and in Figure 7.14 for the ULS-S. For each analysis performed, the most dominant crack is identified and plotted against the OP load for W1 in Figure 7.19 and for W2 in Figure 7.20. For the cases where the OP load is critical (SLS and ULS-W), the most prolific maximum crack width is the tensile 'Base 1' crack, followed by the shear 'Door' crack, and in one instance of ADB W1 a tensile crack in the 'Lintel' dominates. In the IP load dominant cases, the widest cracks are located in 'Base 2', 'Pier 2', 'Pier 4' or one instance of the 'Door'.

The crack damage classification used to provide context to the crack width results in these figures was developed by Watermeyer and Tromp (1992) as serviceability performance criteria for masonry walls, which were then incorporated in the NBR. Details of the damage categories are provided in Table 3.4 in Section 3.2.3, but in brief, the damage is broadly classified as either minor (crack widths up to 5mm), or significant (over 5mm, requiring significant repair). All cracks measured in the FE analyses fall below the 5mm threshold, with the majority falling in the 'negligible' (< 0.25mm) and 'very slight' (< 1.0mm) damage bands.

With further post-peak tracing of the walls' responses, these crack widths would most certainly increase, however in most instances these initial cracks are sufficient to result in a marked reduction in load carrying capacity, typical of brittle masonry behaviour, and demonstrating crack development.
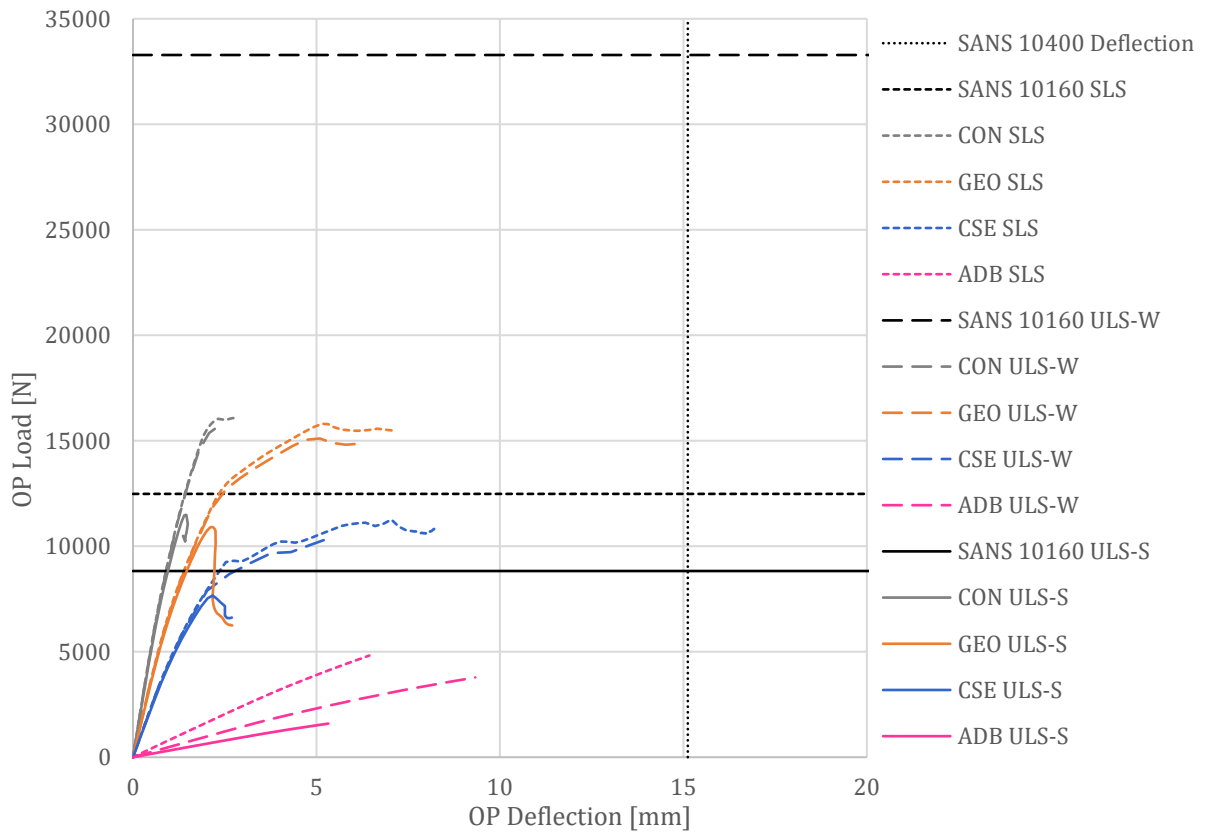
Figure 7.17: Wall W1 CON, GEO, CSE and ADB out-of-plane response
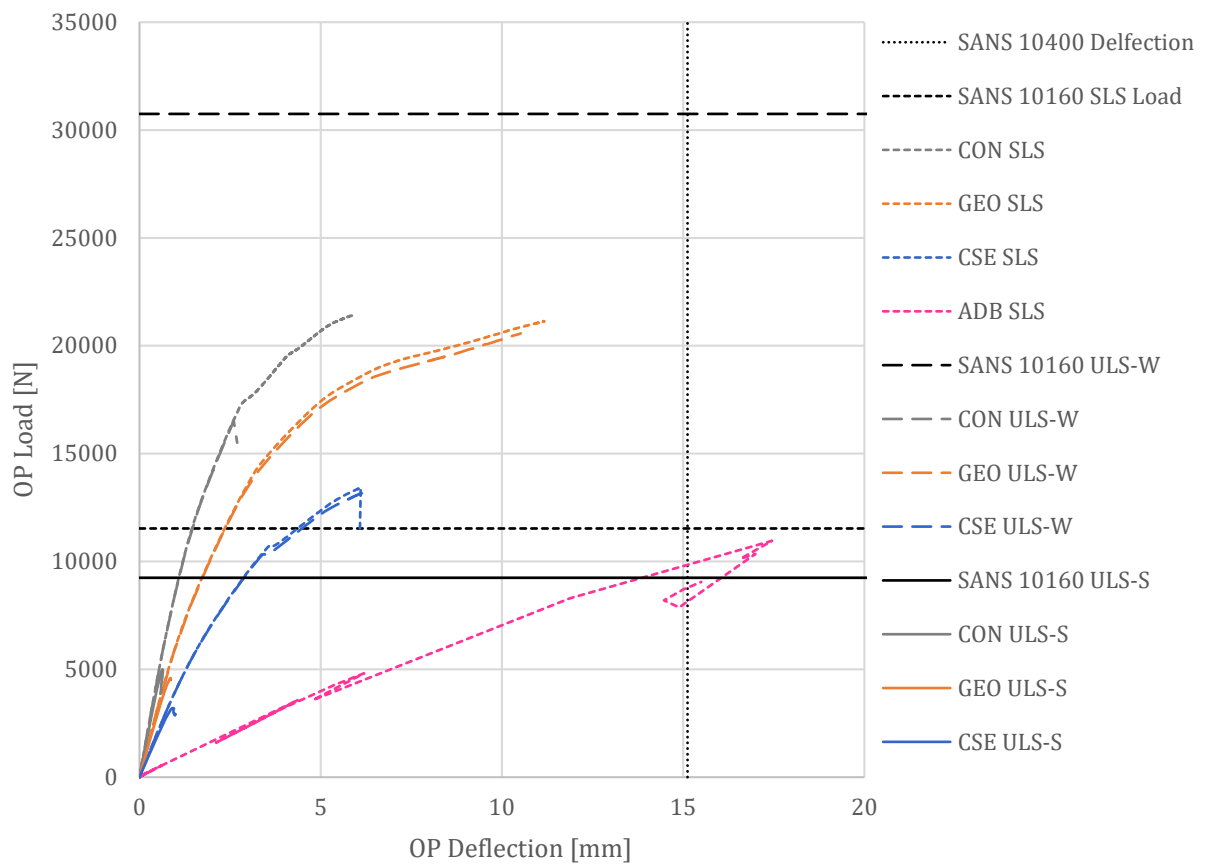
Figure 7.18: Wall W2 CON, GEO, CSE and ADB out-of-plane response
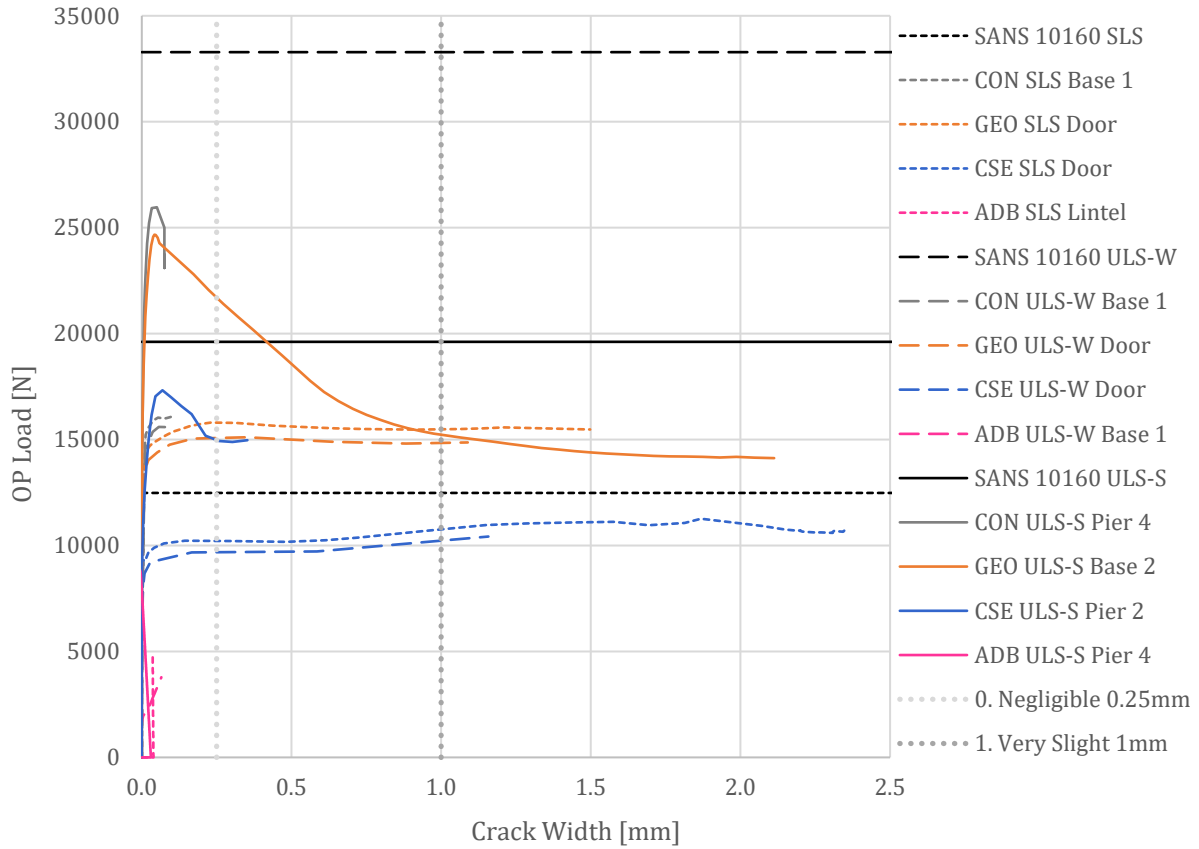
Figure 7.19: Wall W1 CON, GEO, CSE and ADB crack damage classification
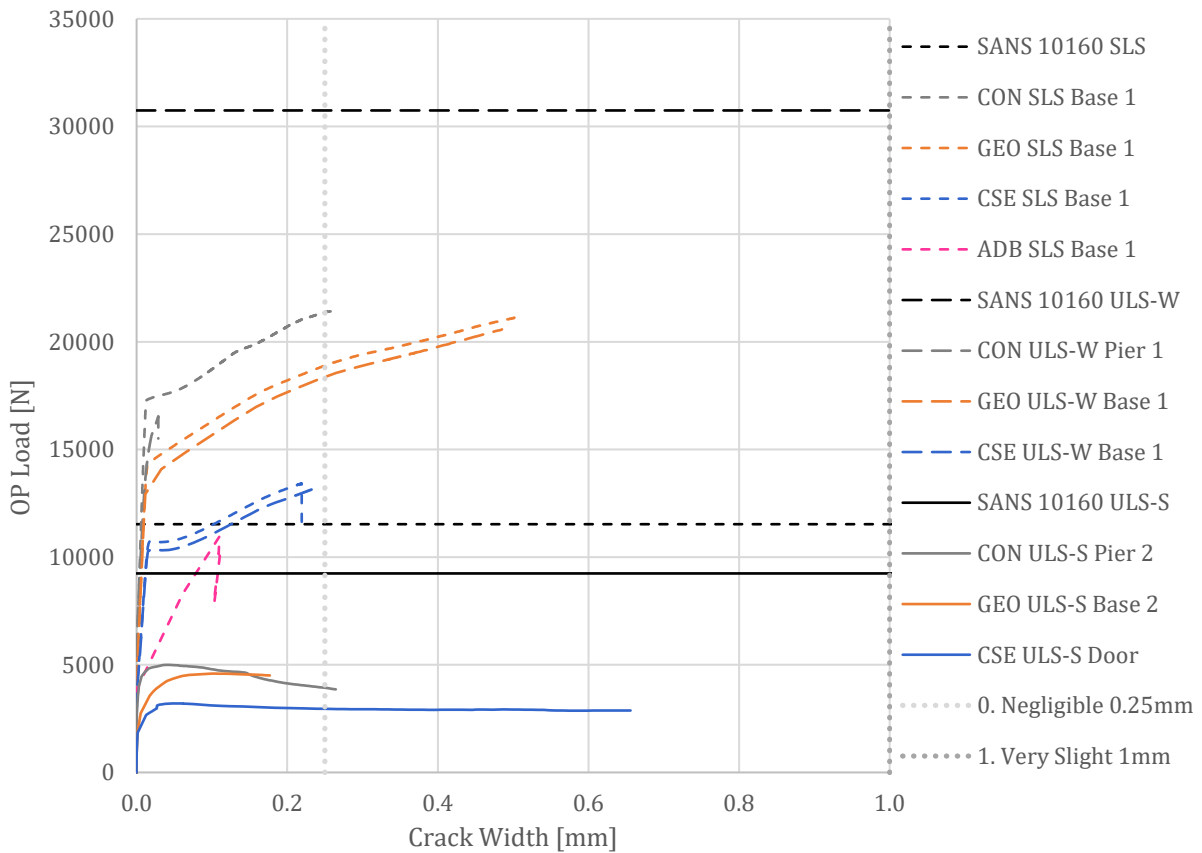
Figure 7.20: Wall W2 CON, GEO, CSE and ADB crack damage classification

104

7.5   Conclusion

In most instances, divergence was the limiting factor in the analyses. A number of measures were taken to overcome these points of divergence, including step size adjustment, more tolerant convergence criteria, alternate iterative procedures, etc., and the arc length method was consistently employed, but convergence could seldom be achieved. In most analyses it is clear from the load-displacement progression that the post linear-elastic region has been reached and that any stiffening of the global response beyond that point is unlikely. One exception is the results of the ADB analyses in which it is not always clear whether the linear-elastic region has been passed. However, considering the combination of deflection limits and required load resistance levels, it is clear that although failure as such is not achieved in most analyses, the required resistance level cannot be achieved within the deflection limits.

Prior to the analyses of this chapter, the expectation was that the resistance of the CON, and most likely the GEO, walls would exceed the design loads in all three load cases, given the conventional range of strength and stiffness of these materials, and the deemed-to-satisfy wall configurations. However, in most cases, the walls failed to resist the design loads, and by a large margin in the out-of-plane loading case due to wind (ULS-W). This outcome precludes the derivation of performance-based criteria for AMU's on this basis. Possible sources for this failure can be categorized as the applied design load, the material parameters, the geometry of the walls and the boundary conditions. These four categories are investigated and discussed further in the following chapter.

8 Deliberation

The applied design load, material parameters, wall geometry and boundary conditions are considered as sources of potential improvement to the walls' performance. This is followed by a summary of the findings and recommendations for the standardised regulation of AMU's.

8.1 Performance Improvement

8.1.1 Load

Studies on the resistance and capacity of unreinforced masonry in South Africa have concentrated on the behaviour under seismic loading (Van Der Kolf, 2014), (De La Harpe, 2015), (Maybery, 2017) but the FE results of the previous section illustrate that the OP wind loading cannot be discounted.

Most of the assumptions or selections detailed in Section 7.3.2 for determining the wind load, were made to achieve the most critical wind loading, not the most likely. However, it is noteworthy that the wind pressure determined in this study (1213N/m^2, Table 7.7) is over three times the minimum wind pressure specified in the NBR (370N/m^2), (SANS 10400-B, 2012). The substantially higher design load for the ULS-W case is in part due to the recent revision of the wind loading code (SANS 10160-3, 2018).

The wind load partial factor has increased from 1.3 to 1.6 and the highest fundamental basic wind speed has increased from 36m/s to 44m/s. These two changes combined result in a 1.5 times higher load than would have been the case before these revisions. However, the ratios of design load to resistance are 2.1 and 1.9 for original configurations of CON W1 and CON W2, respectively. These revisions alone do not account for the discrepancy, and they were implemented for good reason. The reliability performance of the original wind load partial factor of 1.3 was found to be inadequate (Botha, et al., 2018) and the South African wind map has improved due to, in part, a seven-fold increase in the historical extreme wind data available in South Africa (Kruger, et al., 2017).

8.1.2 Material

To investigate the potential increase in OP load carrying capacity due to improved material properties, reasonable maximum values for the three most influential OP parameters (joint tensile strength, joint cohesion and joint mode I fracture energy) were sought in literature. Thereafter, ULS-W load analyses were performed on W1 and W2 with these three adjusted joint parameters.

As discussed in Section 5.4, experimental data on the joint tensile properties is scarce, even more so for the AMU's. Therefore this investigation is limited to CON. Reasonable maximum values for mode I fracture energy and cohesion were found in literature for normal density concrete blocks (MBI) with general purpose mortar (GPM) joints, conducted by Van Der Pluijm (1999), and are detailed in Table 8.1. All other parameters, as provided in Table 7.3, are kept constant. Van der Pluijm did obtain a joint tensile strength of 0.73N/mm^2 for this block/mortar configuration, however, the relationship selected in Section 5.4.1 for the definition of the joint tensile strength ($f_{t,j} = c_j/1.4$) is maintained here for the analyses, and a joint tensile strength of 0.84N/mm^2 is selected. Merely for information, the MBI blocks are 207mm x 100mm x 50mm in size and have a reported normalised compressive strength of 53N/mm^2, whereas the GPM has a compressive strength of 11.6N/mm^2.

Table 8.1: CON adjusted joint parameters

Joint Interface Parameter			CON Baseline	CON Adjusted	
Tensile Strength	$f_{t,j}$	TENSTR	0.12	0.84	N/mm²
Mode I Fracture Energy	$G_{f,j}^I$	GF	0.005	0.011	N/mm
Cohesion	c_j	COHESI	0.17	1.17	N/mm²

The outcome of these analyses (Table 8.2 and Figure 8.1) shows an increase in the load carrying capacity of 53% for W1 and 11% for W2, due to the improved material properties. This reduces the discrepancy to the design load by 47% and 13% for W1 and W2 respectively.

Table 8.2: Peak OP loads for CON adjusted joint parameters to ULS-W

CON OP Load	W1	W2	
SANS 10160 Design Load	33 285	30 746	N
Baseline Peak Load	15 597	16 543	N
Adjusted Joint Parameters Peak Load	23 835	18 373	N
Adjusted Joint Parameters / Baseline Ratio	1.53	1.11	-
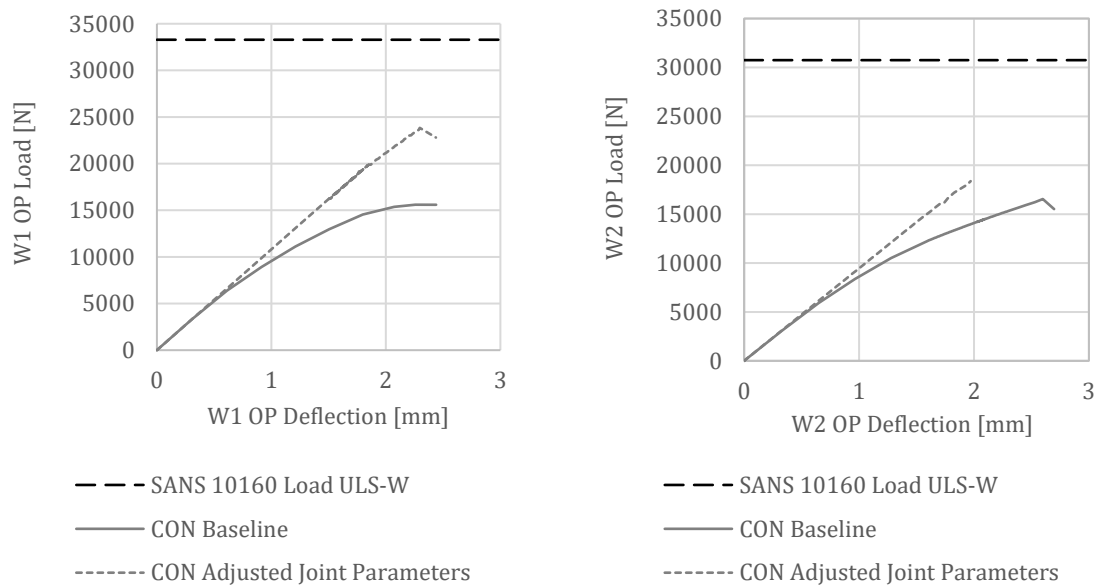
Figure 8.1: OP ULS-W response for CON adjusted joint parameters for W1 (left) and W2 (right)

Increasing the critical joint parameters to reasonable maximum values does not increase the walls' resistances sufficiently to withstand the full design load. It is important to recall that in all the analyses of W1 and W2, mean material parameter values are used, and the material resistance has not been reduced by means of material partial safety factors. Applying this necessary reduction for ULS-based design would further widen this discrepancy.

8.1.3 Geometry

The limitations on wall panel sizes and openings set out in the NBR deemed-to-satisfy solutions are taken from the JSD *Code of Practice: Foundations and Superstructures for Single Storey Residential Buildings of Masonry Construction* (1995). Different wall panel configurations were analysed using the yield line approach to derive the panel sizes and the then current South African masonry structural design code *SABS 0164-1* (1980) was applied to the respective elements to derive the opening limitations (Watermeyer, 1996).

The total area of openings for both W1 and W2 falls within the specifications of seismic design principles set out in the loading code (SANS 10160-4, 2017), Clause 6.2.2, of being less than one-third of the overall wall area. The openings are positioned "as uniform as possible", but given the large opening length of 3m permitted in the deemed-to-satisfy solutions of the NBR (SANS 10400-K, 2011), it does result in large openings at both wall ends, which is undesirable according to the seismic design principles of the loading code.

To investigate the potential improvement in OP resistance of both walls under ULS-W loading and IP resistance for W2 under ULS-S loading due to more robust geometry, the original window opening length is halved to 1500mm, and the door and window openings are positioned in less extreme positions in the wall, illustrated in Figure 8.2 for W1 and Figure 8.3 for W2. All other original dimensions of the walls are maintained. These analyses are done for CON only, to serve as an indicator of potential improvement.
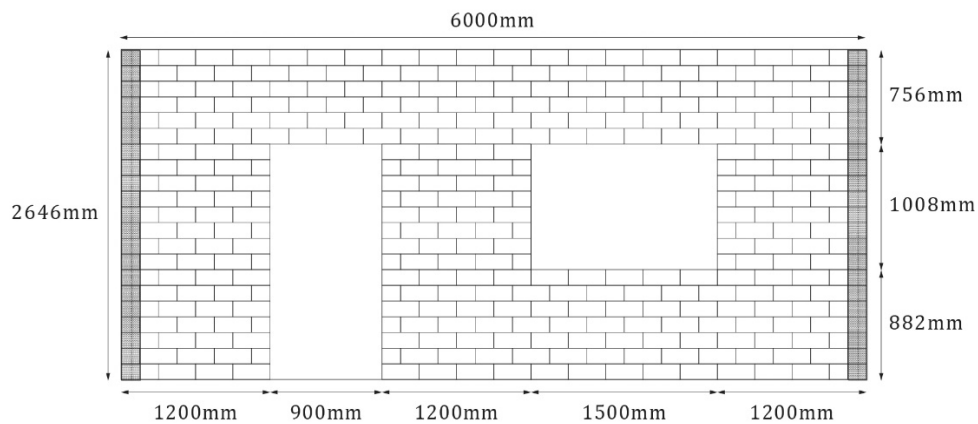
Figure 8.2: Wall W1 layout and dimensions for reduced window opening
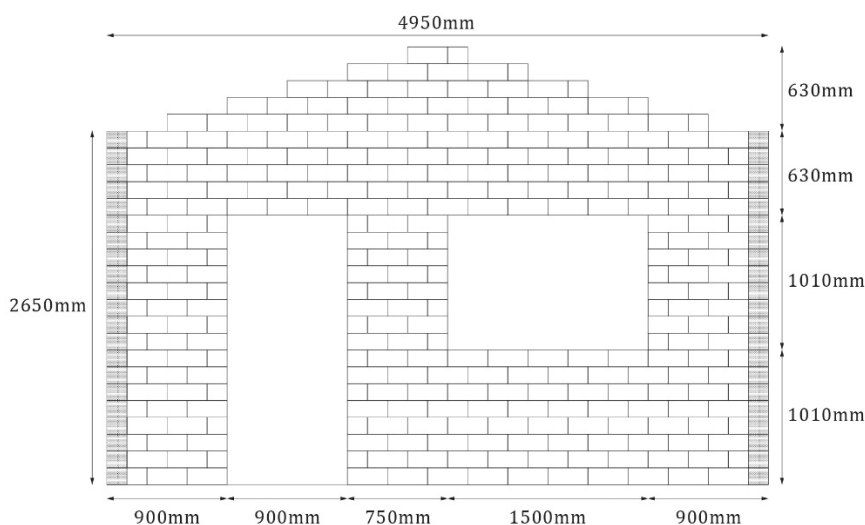
Figure 8.3: Wall W2 layout and dimensions for reduced window opening

The outcome of the OP ULS-W analyses (Table 8.3 and Figure 8.4) shows an increase in the load carrying capacity of 20% for W1 and 15% for W2, due to the reduced window opening and the less extreme positions of the openings. This reduces the discrepancy to the design load by 17% for both W1 and W2.

Table 8.3: Peak OP load for CON reduced window opening to ULS-W

CON OP Load	W1	W2	
SANS 10160	33 285	30 746	N
Baseline Peak	15 597	16 543	N
Reduced Window Opening Peak	18 687	18 946	N
Reduced Window Opening / Baseline Ratio	1.20	1.15	-
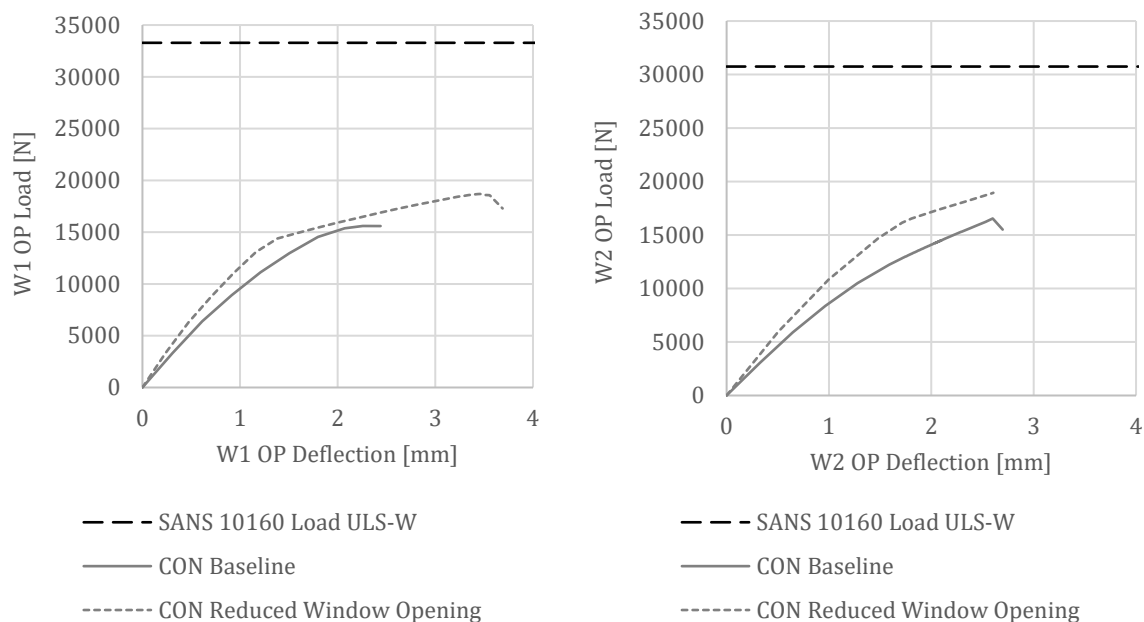
Figure 8.4: OP ULS-W response for CON reduced window opening for W1 (left) and W2 (right)

The outcome of the IP ULS-S analyses on W2 (Table 8.4 and Figure 8.5) shows an increase in the load carrying capacity of 160% for W2, due to the reduced window opening and the less extreme positions of the openings. The IP resistance of W2 now exceeds the seismic design load by 40%.

Table 8.4: Peak IP load for CON reduced window opening to ULS-S

CON IP Load	W2	
SANS 10160 Design Load	20 539	N
Baseline Peak Load	11 295	N
Reduced Window Opening Peak Load	29 534	N
Reduced Window Opening / Baseline Ratio	2.6	-
Reduced Window Opening / SANS 10160	1.4	-
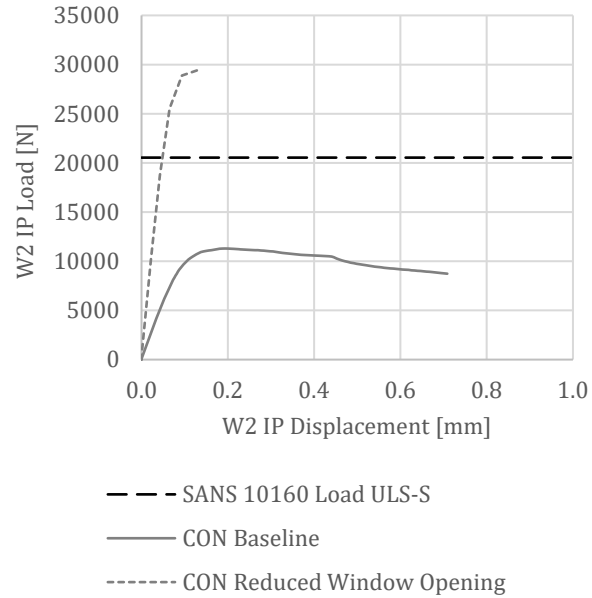
Figure 8.5: IP ULS-S response for CON reduced window opening for W2

Reducing the window opening by half does not increase the walls' OP resistances sufficiently to withstand the full wind design load. However, this mitigation strategy significantly increases W2's IP load carrying capacity to successfully resist the full seismic design load.

8.1.4 Boundary Conditions

The conservative assumption was made that the timber truss system provides negligible lateral support to the top of the walls. The effect of this assumption could be meaningful but its validity is sustained given the similarly weak OP resistance of the opposite wall, which is meant to provide the additional lateral resistance, as well as the typically poor quality of connection between truss and wall in LIH.

A potential source of error could be excessive rotation of the short return walls, which provide lateral restraint to the walls. The pinned modelling of the walls could underestimate the rotational restraint that a full length return wall would offer, thereby allowing greater OP deflection. To investigate the effect of this, the translational restraint on the return walls is applied to all nodes in the boundary plane, as opposed to just the central row of nodes, as shown in Figure 8.6.
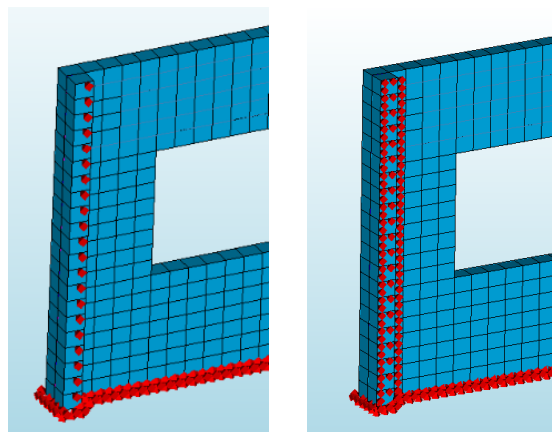
Figure 8.6: Baseline (left) and adjusted (right) boundary conditions for return walls

110

The outcome of the OP ULS-W analyses (Table 8.5 and Figure 8.7) shows an increase in the load carrying capacity of 15% for W1 and 10% for W2, due to the adjusted boundary conditions and increased rotational restraint. This reduces the discrepancy to the design load by 14% for W1 and 12% for W2.

Table 8.5: Peak OP load for CON adjusted boundary conditions to ULS-W

CON OP Load	W1	W2	
SANS 10160	33 285	30 746	N
Baseline Peak	15 597	16 543	N
Adjusted Boundary Conditions Peak	18 011	18 197	N
Adjusted Boundary Conditions / Baseline Ratio	1.15	1.10	-
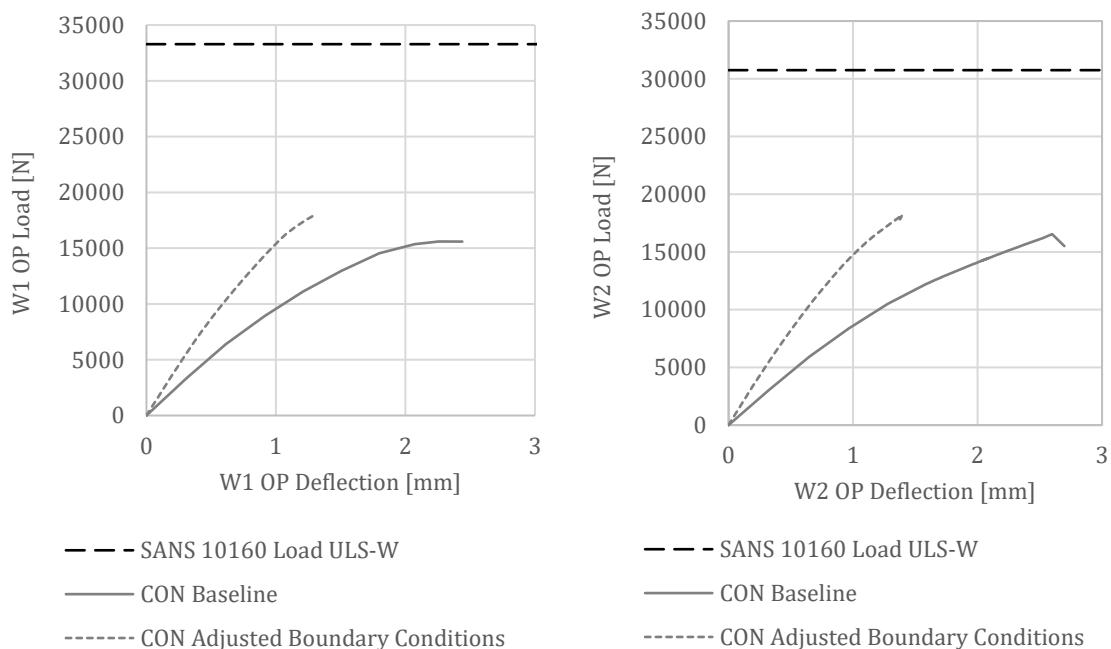
Figure 8.7: OP ULS-W response for CON adjusted boundary conditions for W1 (left) and W2 (right)

Increasing the rotational restraint provided by the return walls does not increase the walls' resistances sufficiently to withstand the full design load.

8.1.5   Conclusion

The FE analyses were executed successfully for the two wall configurations and four block types, under three load cases. The failure modes can be broadly classified as tensile for the OP dominant cases and a combination of tensile/shear failure for the IP dominant cases. The analyses revealed the wall configurations' failure to resist the design load in most instances, and significantly so in the OP response to the ULS-W load case. This is in part, but not exclusively, due to recent increases to two important parameters in the wind loading code. Possible errors in the pre-processing, modelling and post-processing stages of the research are not discounted, but every reasonable effort is made to avoid these.

Three mitigation strategies were employed, namely improving the tensile performance by increasing three critical joint material parameters, improving the distribution of openings by halving the length of the window openings and increasing the rotational restraint of the return by adding lateral translational restraints over the full boundary plane. None of these strategies improved the resistance of the walls to the point of successfully resisting the design wind load. However, reducing the length and improving the distribution of openings significantly increased the IP resistance of W2 to seismic loading.

Additionally, it is important to recall that these analyses were performed without the use of material partial safety factors. Current standardised partial factors for conventional masonry materials range between 1.5 and 3.5 (see Table 3.13). Reducing the material strength by these factors, as is required by limit states design, would further significantly increase the discrepancy between the wall's resistances and the design loads.

This outcome does not allow for the immediate derivation of performance-based criteria for AMU's, since none of the four masonry materials consistently attain the required level of performance. This also raises the issue of possible inconsistencies between the deemed-to-satisfy provisions in the NBR for wall panel and opening sizes (which were derived by yield line analysis, presumably using the then current 1989 loading code) and the current EC-based loading code, both for wind (SANS 10160-3, 2018) and seismic (SANS 10160-4, 2017) loads.

Based on a case study of extreme wind loads on an inland housing development in South Africa, Mahachi et al. (2018) came to the conclusion that a review of the technical standards in housing development require review, specifically the NHBRC *Home Building Manual*. Griffith (2000) reports on a similar case of discrepancies between the capacity of the 'deemed-to-comply' wall provisions of the South Australian Housing Code and the Australian masonry standard's design load. It has long been found that, within the field of masonry buildings, low-rise, unreinforced ones with light roofs (such as LIH), experience the most wind damage (Sparks, et al., 1989), especially non-engineered ones, relying on empirical design procedures. This, coupled with the significant changes in the required wind and seismic design loads with the revision of the loading code, warrant a reconsideration of the NBR deemed-to-satisfy wall provisions, prior to the derivation of PB criteria of AMU's.

8.2   Summary

In a review of the South African low income housing situation and its regulatory framework, as well as that of masonry design, it was shown that:

- There is room for improvement in the quality, thermal performance and environmental impact of the conventional block and mortar walling solutions currently implemented to address the South African housing crisis (Section 2.1)
- AMU's are best suited to provide a reasonable and socially acceptable alternative to conventional masonry units in low income housing (Section 2.2) but the current regulatory framework, whilst making provision for alternative building materials and systems, does not accommodate AMU's in a sufficiently practical manner to enable their widespread, off-the-shelf uptake (Section 3.2)
- The ongoing process of the adoption of EC6 by the South African masonry industry facilitates the transition from prescriptive-based to performance-based regulation of masonry design (Section 3.3)
- Performance-based criteria for housing and house walling in South Africa have been developed to some extent, but not for masonry units (Section 3.2.3)
- Identifying commonalities and opportunities for integration in standards is essential in removing barriers to implementing innovative building materials (Section 3.1.2)
- And material partial safety factors used for conventional masonry materials could arguably be extended to AMU's (Section 3.3.4)

The intention was to establish, by means of FEM, what typical performance levels of masonry units would need to be, for walls meeting the deemed-to-satisfy solutions of the NBR, constructed of a range of AMU types, and exposed to simultaneous IP and OP loads according to the South African loading code. In this process it was shown that:

- Little to no validated FE modelling results can be found for most AMU's (Section 4.3)
- The simplified micro-modelling approach is suitable for the intended application of single-storey masonry wall analysis (Section 4.1.2) and sufficient constitutive material models exist for the description of the AMU materials (Section 4.2)
- The input for the material parameters for the four selected materials (CON, GEO, CSE, ADB) can be determined reasonably well for the unit (Section 5.2), unit crack interface (Section 5.3) and joint interface (Section 5.4), by way of experimental data, literature and best-fit to FEA results
- Ranges for the joint tensile strength and relationships between unit tensile strength/unit compressive strength, unit mode I fracture energy/unit tensile strength, joint cohesion/joint compressive strength and joint mode II fracture energy/joint cohesion established in literature for conventional materials could be extended to AMU's, whereas values for the unit compression ductility index and joint friction angle and relationships between unit E-modulus/unit compressive strength and joint mode I fracture energy/joint cohesion require more careful consideration (Section 5.5)
- The standardised strength prediction models are sometimes unconservative in their estimation of the masonry strength for both CMU and AMU materials, particularly for the compressive strength (EC6 and SANS 10164), flexural strength (SANS 10164) and shear strength (SANS 10164), (Section 5.6)
- The modelling process and input parameters are validated satisfactorily for both the IP (Section 6.1) and OP (Section 6.2) loading condition, when compared to medium- to large-scale experimental results
- The choice of SMM approach is justified both in terms of accuracy and computational efficiency (Sections 6.1 and 6.2)
- Under shear loading conditions, the model results are moderately sensitive to the friction angle and slightly sensitive to the joint cohesion (Section 6.3)

The outcome of the FEA of the two selected wall configurations (W1 and W2) revealed:

- That the walls' resistances do not meet the design load for most of the load cases, for both IP and OP considerations, even for the conventional masonry material CON (Section 7.4)
- An exceptional discrepancy between the design load and the walls' OP resistance for the ULS-W, highlighting the importance of considering the OP failure of masonry walls not only under seismic loading, but under wind loading as well (Section 7.4.4)
- That structural vulnerability is created by the geometric layout permitted by the deemed-to-satisfy rules in the NBR, especially the length of window opening (3000mm) relative to the wall length (4950mm) in the case of W2 (Section 7.4.3)
- And that the recent increases to the partial load factor for the ULS-W and the fundamental basic wind speed in the South African loading code are significant (Section 8.1.1)

Measures taken to mitigate the load/resistance discrepancies indicate that:

- Increasing the critical joint material parameters to reasonable maximum values for the CON W1 and W2 configurations under ULS-W loading does not improve the resistance of the two walls consistently, reducing the discrepancy by 47% for W1 and 13% for W2 (Section 8.1.2)

- Reducing the length of the window openings by half for the CON W1 and W2 configurations under ULS-W loading increases their resistance but only reduces the discrepancy by 17% (Section 8.1.3)
- Reducing the length of the window opening by half for the CON W2 configuration under ULS-S loading increases the resistance by 160%, which then exceeds the seismic design load by 40% (Section 8.1.3)
- Increasing the rotational restraint of the lateral return walls under ULS-W loading does not affect the resistance of the two walls significantly (Section 8.1.4)

8.3   Recommended AMU Regulation

Given the disparate built environment in South Africa, which is underscored by the definition of Category 1 buildings in the NBR, essentially slackening serviceability requirements for low-income housing, a two-pronged approach is recommended for the regulation and thus advancement of AMU's. The first, more ideal approach, is the development of material non-specific standards for masonry. The second, more easily implemented approach, is the definition of minimum performance criteria.

8.3.1   Material Non-Specific Standards

The essence of, motivation for and obstacles to material non-specific standards are outlined.

What:

- One material non-specific standard *'Specifications for masonry units'*, based on EN 771, with annexes where necessary for specific materials
- One material non-specific standard *'Methods of test for masonry units'*, based on EN 772, with annexes where necessary for specific materials
- Subsequently, the standardised design procedures set out in EN 1996/SANS 51996 are applied

Properties that require declaration, based on the requirements of the EN 771 suite, include the:

- type of unit
- gross and net dry density
- dimensions, configuration, appearance and tolerances
- compressive, bond and shear strength
- water absorption and moisture movement
- durability and abrasion resistance
- thermal properties
- reaction to fire

Why: The ongoing adoption of EC6, and accompanying material and testing standards, by the South African masonry industry provides the necessary performance-based framework. Moving towards a material non-specific masonry standard from that platform is both convenient and imminently more attainable than it would have been from the prescriptive SANS 10164 basis. Convenience is essential for innovative materials to overcome regulatory barriers. Since EC6 was developed to make provision for a wide range of bricks and blocks used traditionally across Europe, the code also naturally lends itself to accommodating a wide range of materials.

114

Barriers: This approach requires a complete shift to a fully engineered, performance-based masonry building design as well as a statistically sufficient database of test results for the properties that require declaration, for the uptake of a new AMU. This is not a cost-effective option for the LIH sector where design fees are under extreme pressure. However, the scope and inclination to bear the developmental cost for such an approach to AMU's could be found in the high-end of the building market.

8.3.2 Minimum Performance Criteria

The essence of, motivation for and obstacles to minimum performance criteria are outlined.

What: Establishment of material non-specific minimum performance levels for

-	masonry compressive strength	(tested to EN 1052-1)
-	masonry flexural strength	(tested to EN 1052-2)
-	masonry shear strength	(tested to EN 1052-3)

Alternatively, provided sufficient masonry compressive strength tests are performed on a specific AMU and mortar type, the unit and mortar compressive strength could be specified, tested to EN 772-1 and EN 1015-11 respectively.

These minimum performance criteria are limited to and used in conjunction with deemed-to-satisfy provisions for wall panel sizes and opening limitations, for application in non-engineered low-rise, unreinforced masonry buildings, such as Category 1 buildings.

Why: The South African masonry industry is comfortable with the prescriptive nature of minimum block compressive strength currently specified in the masonry design standards and the deemed-to-satisfy solutions of the NBR. Even if only considering conventional masonry materials, the transition to the EC performance-based design approach will be sluggish and met with resistance. Establishing material non-specific minimum performance levels for these three masonry parameters, to be used in conjunction with deemed-to satisfy wall provisions, is a palatable method to facilitate the uptake of AMU's in low-income housing. However, there are inherent dangers in mixing prescriptive and performance-based approaches (Sparks, et al., 1989) and a clear distinction and scopes of application are necessary between this second approach and the first approach of comprehensive material non-specific standards used in conjunction with fully engineered designs.

Barriers: This approach of establishing performance-based criteria for alternative masonry, hinges on deemed-to-satisfy wall layout provisions that meet the desired performance level. The findings of this study indicate that the current NBR wall layout provisions are not necessarily compatible with the extreme load cases of the revised South African loading code. Reconsideration of these deemed-to-satisfy wall layout provisions is needed in order for reasonable minimum performance-based criteria to be specified for low-income housing.

9   Conclusions and Future Research

The main conclusions are distilled and, based on the findings of this study, three avenues of research that can be pursued are highlighted.

9.1   Conclusions

From the scrutiny of the South African masonry regulatory framework and international trends in Chapters 1 to 3, the subsequent physical and computational modelling of alternative masonry wall parts and walls in Chapters 4 to 7, and deliberation in Chapter 8, the following conclusions are drawn.

– Valuable detailed strength, stiffness and fracture model parameter input data has been generated for three alternative masonry unit (AMU) types, namely geopolymer (GEO), compressed-stabilised earth (CSE) and adobe (ADB).

– The detailed parameter testing for AMU's and their interfaces conducted in this study is too laborious for standardisation and practical regulation purposes.

– Certain AMU model parameter relationships have been established or confirmed as sensible for AMU's. Thereby, significantly reduced characterisation testing effort is facilitated for future computational studies of AMU masonry.

– The medium to large-scale in-plane (IP) and out-of-plane (OP) experimental validation processes for GEO, CSE and ADB masonry contribute significantly to the AMU FE modelling body of knowledge.

– Masonry walls consisting of AMU's, representing a wide spectrum of strengths and stiffnesses, can be modelled using the FE simplified micro-modelling approach with reasonable accuracy and the major failure mechanisms are well captured.

– The computational cost experienced during the FE analyses justifies the chosen modelling simplification of isolated walls instead of entire houses.

– The low-income housing (LIH) walls modelled in this study, including the walls modelled with conventionally used concrete blocks, failed to resist the loads required by the South African loading code. These failures were observed without the inclusion of material partial safety factors.

– The investigated mitigation strategies of higher unit-mortar bond, shear strength and fracture energy, smaller window openings more favourably placed in the walls, as well as higher connecting wall rotational restraint, made no consequential improvement to the OP resistance of the walls to the wind load. However, geometric changes to the wall layout significantly improved the IP resistance to seismic loading.

– Bearing in mind the limited scope of wall configurations studied, these failures may point to underlying issues regarding the compatibility of the South African National Building Regulation (NBR) deemed-to-satisfy wall layout provisions and the revised loading code.

– Performance-based regulation of AMU's is recommended for the high-end sector of the market in the form of material non-specific masonry unit standards and testing standards based on EN 771 and EN 772, respectively.

– Performance-based regulation of AMU's is recommended for the LIH sector in the form of material non-specific minimum performance levels for masonry compressive, flexural and shear strength in conjunction with revised NBR deemed-to-satisfy wall layout provisions.

9.2   Future Research

A number of research avenues can be pursued following on the findings of this study. Three are highlighted here, namely reviewing the NBR deemed-to-satisfy wall provisions to enable quantification of minimum performance criteria for AMU's for LIH, FE macro-modelling of AMU LIH to improve global structural behaviour understanding and developing durability performance criteria for AMU's.

9.2.1   Minimum Performance Criteria

Establishing minimum performance criteria for alternative masonry low-income housing, requires a review of the NBR deemed-to-satisfy wall panel sizes and opening limitations, in light of the revision to the South African loading code and the design load/resistance discrepancies found in this study. The FE simplified micro-model used in this study can be extended for this purpose, if applied systematically to an extensive array of single-storey wall configurations.

One of two methodologies could be followed. The first is determining conventional material parameters for the concrete and burnt clay masonry typically used in South Africa, and applying the loading conditions as required by SANS 10160 to this array of wall configurations, to develop deemed-to-satisfy limitations for the wall geometry. This would essentially limit the minimum performance criteria (masonry compressive, flexural and shear strength) to the level of the conventional materials selected. The second methodology would be to first specify desired wall configurations, based on constructability, typical South African building practice and skill level, fenestration requirements for building energy usage, natural lighting and ventilation and fire safety. Numerous such specifications are well documented in the relevant sections of the NBR and could be used as a basis. This second methodology is recommended in establishing an ultimately preferential housing solution.

9.2.2   Macro-Modelling

Developing the simplified micro-model of this study further into the macro-modelling realm, ideal for the global analysis of masonry structures, would be valuable in improving the understanding of the structural behaviour of alternative masonry buildings. In assuming a smeared continuum approach, the unit, mortar and unit/mortar interface behaviours are combined in an analogous continuous material. The computational benefits are clear but the model input parameters are either determined through expensive large-scale masonry tests or predicted based on the micro-properties of the constituent materials, requiring homogenisation techniques to be applied. Both avenues, macro-tests and homogenisation techniques, have their challenges, but the most significant difference is the predictive capability of homogenisation techniques. Data obtained from large-scale masonry tests for a macro-model, limits the applicability of the data to the same conditions as those of the tests (Milani, et al., 2006). In the event of new materials requiring modelling, or conventional materials used under new loading conditions, another set of large-scale experiments may be needed. Contrastingly, with homogenisation techniques, the anisotropic macro-constitutive laws are developed from the micro-constitutive laws, as well as the masonry assemblage geometry (Lourenço, 1996). Thereby, large-scale testing is avoided in the event of changes to the constituent materials, geometry or loading conditions, which is preferable in the development of AMU's.

9.2.3 Durability

The durability of masonry depends on its capability to withstand freeze/thaw and wet/dry cycles, as well as the absorption of environmental contaminants (Jordan, 2010). In the development of AMU's, the two main durability considerations by most researchers are the compressive strength and water absorption (Zhang, 2013), since the largest obstacles to the uptake of soil-based AMU's in particular are poor strength and durability in the wet state (Maskell, et al., 2014). Porosity, the distribution of the pore sizes and the interconnectedness of the pores are therefore important aspects in establishing masonry durability (Abu Bakar, et al., 2009). A number of standardised methods exist to establish the freeze/thaw resistance, water absorption, water vapour permeability, porosity and moisture movement for certain conventional masonry materials. These hydric test results can be verified by additional means, such as mercury intrusion porosimetry (MIP) or scanning electron microscopy (SEM), especially for establishing porosity in the unit/mortar contact zone (Cultrone, et al., 2007). An additional concern in soil-based AMU's specifically is resistance to abrasion. Several test methods have been put forward, however, as yet, none has been standardised. Which contaminants are detrimental to the masonry depends on its constituent materials, as is the case with soluble salts in clay bricks. This aspect requires careful consideration in establishing the durability of new masonry materials.

References

Abdulla, K., Cunningham, L. & Gillie, M., 2017. Simulating masonry wall behaviour using a simplified micro-model approach. *Engineering Structures,* Volume 151, pp. 349-365.

Abu Bakar, B., Ibrahim, M. & Megat Johari, M., 2009. A review: Durability of fired clay brick masonry wall due to salt attack. *International Journal of Integrated Engineering,* Volume 2, pp. 111-127.

Act No. 103, 1977. National Building Regulations and Building Standards Act. *Government Gazette of the Republic of South Africa,* 6 July.145(5640).

Act No. 103, 2008. National Building Regulations and Building Standards Act. *Government Gazette of the Republic of South Africa,* 1 September.

Act No. 11, 2015. Agrément South Africa Act of 2015. *Government Gazette of the Republic of South Africa,* 15 December.606(39511).

Act No. 38, 2000. Construction Industry Development Board Act of 2000. *Government Gazette of the Republic of South Africa,* 17 November.425(21755).

Act No. 5, 2008. National Regulator for Compulsory Specifications Act of 2008. *Government Gazette of the Republic of South Africa,* 4 July.517(31216).

Act No. 68, 2008. Consumer Protection Act of 2008. *Government Gazette of the Republic of South Africa,* 29 April.467(32186).

Act No. 85, 1993. Occupational Health and Safety Act. *Government Gazette of the Republic of South Africa,* 337(14918).

Act No. 95, 1998. Housing Consumers Protection Measures Act. *Government Gazette of the Republic of South Africa,* 2 November.401(19418).

Agnihotri, P., Singhal, V. & Rai, D., 2013. Effect of in-plane damage on out-of-plane strength of unreinforced masonry walls. *Engineering Structures,* Volume 57, pp. 1-11.

Agrément, 2002. *Performance Criteria: Building and Walling Systems,* Pretoria: Agrément South Africa.

Agrément, 2018. *Agrément South Africa Annual Report 2017/18,* Pretoria: Agrément South Africa.

Agrément, 2019. *Agrément South Africa.* [Online] Available at: www.agrement.co.za

Ali, S. & Page, A., 1988. Finite element model for masonry subjected to concentrated loads. *Journal of Structural Engineering,* 114(8), pp. 1761-1784.

Al-Jabri, K., Hago, A., Al-Nuaimi, A. & Al-Saidy, A., 2005. Concrete Blocks for Thermal Insulation in Hot Climate. *Cement and Concrete Research,* pp. 1472 - 1479.

Anand, S. & Shaw, R., 1980. Mesh-refinement and substructuring technique in elastic-plastic finite element analysis. *Computers and Structures,* Volume 11, pp. 13-21.

Anthoine, A., 1995. Derivation of the in-plane elastic characteristics of masonry through homogenization theory. *International Journal of Solids and Structures,* 32(2), pp. 137-163.

AS 2870, 1986. *Australian Standard: Residential Slabs and Footings.* s.l.:Standards Association of Australia.

Ayed, H., Limam, O., Aidi, M. & Jelidi, A., 2016. Experimental and numerical study of interlocking stabilized earth blocks mechanical behaviour. *Journal of Building Engineering,* Volume 7, pp. 207-216.

Bahar, R., Benazzoug, M. & Kenia, S., 2004. Performance of compacted cement-stabilised soil. *Cement and Concrete Composites,* Volume 26, pp. 811-820.

Benhelal, E., Zahedi, G., Shamsaei, E. & Bahadori, A., 2013. Global strategies and potentials to curb CO_2 emissions in cement industry. *Journal of Cleaner Production,* Volume 51, pp. 142-161.

Berto, L., Saetta, A., Scotta, R. & Vitaliani, R., 2005. Failure mechanism of masonry prism loaded in axial compression: computational aspects. *Materials and Structures,* Volume 38, pp. 249-256.

Blondet, M., Vargas, J., Velasquez, J. & Tarque, N., 2006. *Experimental study of synthetic mesh reinforcement of historical adobe buildings.* New Delhi, India, s.n.

Boshoff, W. et al., 2013. *Alternative materials for masonry units.* Cape Town, The South African Housing Foundation.

Botha, J., Retief, J. & Viljoen, C., 2018. Reliability assessment of the South African wind load design formulation. *Journal of the South African Institution of Civil Engineering,* 60(3), pp. 30-40.

Bradford, M. & Pi, Y., 2012. Nonlinear plastic analysis of composite members of high-strength steel and geopolymer concrete. *Computer Modeling in Engineering and Sciences,* 89(5), pp. 387-414.

Bruhwiler, E. & Wittmann, F., 1990. The wedge splitting tests, a new method of performing stable fracture energy mechanics tests. *Engineering Fracture Mechanics,* Volume 35, pp. 117-125.

BS 5628-1, 1978. *Code of practice for the use of masonry, Structural use of unreinforced masonry.* London: BSI.

BS 5628-1, 2005. *Code of practice for the use masonry, Structural use of unreinforced masonry.* London: BSI.

Burkowski, R., 2003. *The role of standards in a performance-based regulatory system.* Malaysia, s.n.

Burland, J., Broms, B. & De Mello, V., 1978. *Behaviour of foundations and structures.* Tokyo, s.n., pp. 495-546.

Burnett, S. et al., 2007. The performance of unreinforced masonry walls subjected to low-velocity impacts: Finite element analysis. *International Journal of Impact Engineering,* 34(8), pp. 1433-1450.

Burroughs, S., 2006. Strength of compacted earth: Linking soil properties to stabilizers. *Building Research and Information,* 34(1), pp. 55-65.

Byron, P., 2019. *Mr* [Interview] (8 January 2019).

Chaimoon, K. & Attard, M., 2007. Modeling of unreinforced masonry walls under shear and compression. *Engineering Structures,* Volume 29, pp. 2056-2068.

Chisari, C., Macorini, L., Amadio, C. & Izzuddin, B., 2018. Identification of mesoscale model parameters for brick-masonry. *International Journal of Solids and Structures,* Volume 146, pp. 224-240.

CIDB, 2011. *Construction Quality in South Africa: A Client Perspective,* Pretoria: Construction Industry Development Board.

CMA, 2011. *Concrete Manufacturers Association.* [Online] Available at: http://www.cma.org.za/Initiatives/The-CMA-House

CMA, 2016(a). CMA enters a new era. *Precast*, Issue 1, pp. 9 - 13.

CMA, 2016(b). The CMA is on track. *Precast*, Issue 2, pp. 5 - 9.

Constitutional Assembly, 1996. *The Constitution of the Republic of South Africa.* s.l.:ISBN 978-0-621-39063-6.

Cook, R., Malkus, D., Plesha, M. & Witt, R., 2001. *Concepts and Applications of Finite Element Analysis.* Fourth ed. s.l.:John Wiley & Sons, Inc..

Crofts, F., 2014. The Case for the Adoption of Eurocode 6 in South Africa. *Civil Engineering,* pp. 46 - 50.

Crofts, F., 2018. Notable masonry facade failures - who is ultimately responsible?. *Civil Engineering*, March, pp. 11-16.

Crosswell, S., 2009. *Fulton's Concrete Technology.* 9th ed. Midrand: Cement & Conrete Institute.

Cultrone, G., Sebastian, E. & Ortega Huertas, M., 2007. Durability of masonry systems: A laboratory study. *Construction and Building Materials,* Volume 21, pp. 40-51.

CUR, 1997. *Structural masonry: An experimental/numerical basis for practical design rules,* Rotterdam: A.A. Balkema.

De La Harpe, C., 2015. *The development of a seismic risk reduction procedure for the prioritization of low cost, load bearing masonry buildings,* s.l.: Stellenbosch University.

De Villiers, W., 2012. *Regulation of alternative building materials and systems in South Africa.* Cape Town, South African Housing Foundation.

De Villiers, W., Fourie, J. & Boshoff, W., 2018. *Numerical modelling of alternative masonry units.* Delft, RILEM.

Department of Human Settlements, 2010. The use of alternative technologies in LCH construction: Why the slow pace of delivery?. *Human Settlements Review,* 1(1), pp. 266-270.

Department of Human Settlements, 2015. *Human Settlements Subsidy Pocket Guide,* Cape Town: Department of Human Settlements.

Department of Human Settlements, 2017. *Delivery Serviced Sites and Houses/Units from HSDG,* s.l.: Department of Human Settlements.

Department of National Treasury, 2018. *Media Statement - Tabling of Carbon Tax Bill.* [Online] Available at: http://www.treasury.gov.za/comm_media/press/2018/2018112101%20Media%20Statement %20-%20Carbon%20Tax%20Bill%20Tabling.pdf

Derakhshan, H., Lucas, W., Visintin, P. & Griffith, M., 2018. Out-of-plane strength of existing two-way spanning solid and cavity unreinforced masonry walls. *Structures,* Volume 13, pp. 88-101.

DIANA, 2017. *DIANA Finite Element Analysis User's Manual 10.2,* Delft: DIANA FEA BV.

Dolatshahi, K., Aref, A. & Whittaker, A., 2015. Interaction curves for in-plane and out-of-plane behaviours of unreinforced masonry walls. *Journal of Earthquake Engineering,* Volume 19, pp. 60-84.

Drysdale, R., Hamid, A. & Baker, L., 1994. *Masonry Structures: Behaviour and Design.* s.l.:s.n.

Dunaiski, P., Retief, J. & Barnardo, C., 2010. Harmonization of South African Standards for Structural Design to International Practice.

EN 1052-1, 1999. *Methods of test for masonry - Part 1: Determination of compressive strength.* Brussels: European Committee for Standardization.

EN 1052-2, 1999. *Methods of test for masonry - Part 2: Determination of flexural strength.* Brussels: European Committee for Standardization.

EN 1052-3, 2002. *Methods of test for masonry - Part 3: Determination of initial shear strength.* Brussels: European Committee for Standardization.

EN 12390-13, 2013. *Testing hardened concrete - Part 13: Determination of secant modulus of elasticity in compression,* Brussels: European Committee for Standardization.

EN 1990, 2002. *Eurocode - Basis of Structural Design.* Brussels: European Committee for Standardization.

EN 1991, 2002+. *Eurocode 1 - Actions on Structures.* Brussels: European Committee for Standardization.

EN 1998-1, 2004. *Eurocode 8: Design of structures for earthquake resistance - Part 1: General rules, seismic actions and rules for buildings.* Brussels: European Committee for Standardization.

EN 771-1, 2011. *Specification for masonry units, Part 1: Clay masonry units,* Brussels: European Committee for Standardization.

EN 771-3, 2011. *Specifications for masonry units, Part 3: Aggregate concrete masonry units (Dense and lightweight aggregates),* Brussels: European Committee for Standardization.

EN 772-13, 2000. *Methods of test for masonry units - Part 13: Determination of net and gross dry density of masonry units (except for natural stone).* Brussels: European Committee for Standardization.

Ferdous, W., Manalo, A., Khennane, A. & Kayali, O., 2015. Geopolymer concrete-filled pultruded composite beams - Concrete mix design and application. *Cement and Concrete Composites,* Volume 58, pp. 1-13.

Foliente, G., 2000. Developments in performace-based building codes and standards. *Forest Products Journal,* 50(7/8), pp. 12-21.

Fourie, J., 2017. *Characterisation and evaluation of the mechanical properties of alternative masonry units,* s.l.: Stellenbosch University.

Ghiassi, B., Vermeltfoort, A. & Lourenço, P., 2019. Masonry Mechanical Properties. In: B. Ghiassi & G. Milani, eds. *Numerical Modelling of Masonry and Historical Structures - from Theory to Application.* s.l.:Woodhead Publishing, Elsevier, pp. 239-261.

Giambanco, G., Rizzo, S. & Spallino, R., 2001. Numerical analysis of masonry structures via interface models. *Computer Methods in Applied Mechanics and Engineering,* Volume 190, pp. 6493-6511.

Giamundo, V., Lignola, G., Prota, A. & Manfredi, G., 2015. Nonlinear analyses of adobe masonry walls reinforced with fiberglass mesh. *Polymers,* Volume 6, pp. 464-478.

Giles, E., 1985. *Remedial measures for cracked houses built on heaving clays.* s.l., SAICE Geotechnical Division.

Greenwood, J., 2012. An Examination of Performance Based Building Code on the Design of a Commercial Building. *The Australian Journal of Construction Economics and Building,* 7(1), pp. 37 - 44.

Griffith, M., 2000. *Experimental study of the flexural strength of URM (brick) walls,* Adelaide: University of Adelaide.

Haach, V., Vasconcelos, G. & Lourenço, P., 2011. Parametrical study of masonry walls subjected to in-plane loading through numerical modling. *Engineering Structures,* Volume 33, pp. 1377-1389.

Hardjito, D., Wallah, S., Sumajouw, D. & Rangan, B., 2005. Fly ash-based geopolymer concrete. *Australian Journal of Structural Engineering,* 6(1), pp. 77-86.

Harrison, D., 2018. *Informal settlement, Indlovu, Khayelitsha, Cape Town.* [Art].

HDA, 2015. *N2 Gateway Community Newsletter*, July, Issue 44.

Heath, A. et al., 2012. Modern earth masonry: Structural properties and structural design. *The Structural Engineer,* 90(4), pp. 38-44.

Hilton, 2011. *Aerial view of Sea Point, Cape Town, South Africa.* [Art].

Holický, M., Middleton, J. & Vorlíček, M., 1998. *Statistical analysis of partial safety factors for structural masonry.* London, Taylor & Francis, pp. 325-338.

Hordijk, D., 1991. *Local approach to fatigue of concrete, Doctor dissertation,* Deflt: Delft University of Technology.

Hossain, K. & Mol, L., 2011. Some engineering properties of stabilized clayey soils incorporating natural pozzolans and industrial wastes. *Construction and Building Materials,* Volume 25, pp. 3495-3501.

Illampas, R., Charmpis, D. & Ioannou, I., 2014. Laboratory testing and finite element simulation of the structural response of an adobe masonry building under horizontal loading. *Engineering Structures,* Volume 80, pp. 362-376.

Illampas, R., Ioannou, I. & Charmpis, D., 2011. A study of the mechanical behaviour of adobe masonry. *WIT Transactions on the Built Environment,* Volume 118, pp. 485-496.

ISO 15928-1, 2015. *Houses - Description of performance - Part 1: Structural safety.* Geneva, Switzerland: International Organisation for Standardization.

ISO 15928-2, 2015. *Houses - Description of performance - Part 2: Structural Serviceability.* Geneva, Switzerland: International Organization for Standardization.

ISO 15928-3, 2015. *Houses - Description of performance - Part 3: Structural durability.* Geneva, Switzerland: International Organization for Standardization.

ISO 6240, 1980. *Performance Standards in Buildings - Contents and Presentations.* s.l.:International Organisation for Standardization.

Jennings, J. & Kerrich, J., 1963. The heaving of buildings and the associated economic consequences, with particular reference to the Orange Free State goldfields. *The Civil Engineer in South Africa,* 5(5).

Jooste, J., unpublished. *Flexural strength of unreinforced alternative masonry walls,* s.l.: Stellenbosch University.

Joseph, B. & Mathew, G., 2012. Influence of aggregate content on the behavior of fly ash based geopolymer concrete. *Scientia Iranica,* 19(5), pp. 1188-1194.

JSD, 1995. *Code of Practice: Foundations and Superstructures for Single Storey Residential Buildings of Masonry Construction,* s.l.: Joint Structural Division.

Khubisa, M., 2017. Shoddy RDP houses leave homeowners fuming. *Phoenix Sun*, 15 September.

Kruger, A., Retief, J. & Goliger, A., 2017. Development of an updated fundamental basic wind speed map for SANS 10160-3. *Journal of the South African Insitution of Civil Engineering,* 59(4), pp. 12-25.

Kumar, N. & Barbato, M., 2019. New constitutive model for interface elements in finite-element modeling of masonry. *Journal of Engineering Mechanics,* 145(5).

KZNDHS, 2010. *An investigation into existing tools that could inform quality assurance in low income housing,* Durban: KwaZulu Natal Department of Human Settlements.

Laing, H., 2011. *The "CMA House" - Bringing detail and durability to affordable housing.* Cape Town, The South African Housing Foundations.

Laubscher, J., 2011. *An investigation of the National Building Regulations to promote uniformity and sustainability in the South African Environment,* Pretoria: University of Pretoria.

Laubscher, J., 2014. *Reviewing challenges between the need for government-subsidized housing in South Africa and the sustainability requirements of the National Building Regulations.* Barcelona, s.n.

Lofti, H. & Shing, P., 1994. Interface model applied to fracture of masonry structures. *Journal of Structural Engineering,* Volume 120, pp. 63-80.

Lourenço, P., 1996. *Computational Strategies for Masonry Structures,* Delft: Delft University Press.

Lourenço, P., 1998. Experimental and numerical issues in the modelling of the mechanical behaviour of masonry. In: P. Roca, J. Gonzalez, E. Onate & P. Lourenço, eds. *Structural analysis of historical constructions II.* Barcelona: CIMNE.

Lourenço, P., 1998. *Sensitivity analysis of masonry structures.* s.l., s.n., pp. 563-574.

Lourenço, P. & Rots, J., 1997. Multisurface interface model for analysis of masonry structures. *Journal of Engineering Mechanics,* Volume 123, pp. 660-669.

Macorini, L. & Izzuddin, B., 2011. A non-linear interface element for 3D mesoscale analysis of brick-masonry structures. *International Journal for Numerical Methods in Engineering,* Volume 85, pp. 1584-1608.

Mahachi, J., Bradley, R. & Goliger, A., 2018. *Wind storm damage to houses: Planning and design consideration.* Pretoria, CSIR, pp. 82-92.

Mahachi, J., Goliger, A. & Wagenaar, F., 2004. *Structural performance of residential housing in South Africa.* Cape Town, s.n.

Mahachi, J., Khanye, L. & Goliger, A., 2007. *Calibration of brick masonry partial safety factor for the South African code.* Cape Town, s.n.

Mahini, S., 2015. Smeared crack material modelling for the nonlinear analysis of CFRP-strenghtened brick vaults with adobe piers. *Construction and Building Materials,* Volume 74, pp. 201-218.

Maskell, D., Heath, A. & Walker, P., 2014. Inorganic stabilisation for extruded earth masonry units. *Construction and Building Materials,* Volume 71, pp. 602-609.

Massart, T., Peerlings, R., Geers, M. & Gottcheiner, S., 2005. Mesoscopic modeling of failure in brick masonry accounting for three-dimensional effects. *Engineering Fracture Mechanics,* Volume 72, pp. 1238-1253.

Maybery, V., 2017. *Susceptibility of low cost housing to seismic activity in South Africa,* s.l.: Stellenbosch University.

May, P., 2003. Performance-based regulation and regulatory regimes: The saga of leaky buildings.. *Law & Policy,* Volume 25, pp. 381-401.

May, P., 2010. Performance-based regulation. *Jerusalem Papers in Regulation & Governance, ISBN: 2079-5882.*

Meacham, B., 2010. *Performance-Based Building Regulatory Systems - Principles and Experiences. ISBN 978 0 7559 9238 6,* s.l.: Inter-jurisdictional Regulatory Collaboration Committee.

Mellegård, H. & Steinert, A., 2016. *Compressed stabilised earth blocks in Nepal: A study of the rehabilitation of buildings in rural villages after the Gorkha Earthquake,* Gothenburg, Sweden: s.n.

Miccoli, L., Garofano, A., Fontana, P. & Muller, U., 2015. Experimental testing and finite element modelling of earth block masonry. *Engineering Structures,* Volume 104, pp. 80-94.

Miccoli, L., Muller, U. & Fontana, P., 2014. Mechanical behaviour of earthen materials: A comparison between earth block masonry, rammed earth and cob. *Construction and Building Materials,* Volume 61, pp. 327-339.

Milani, G., 2008. 3D upper bound limit analysis of multi-leaf masonry walls. *International Journal of Mechanical Sciences,* Volume 50, pp. 817-836.

Milani, G., Lourenço, P. & Tralli, A., 2006. Homogenised limit analysis of masonry walls, Part 1: Failure surfaces. *Computers and Structures,* Volume 84, pp. 166-180.

Millogo, Y. & Morel, J., 2012. Microstructural characterization and mechanical properties of cement stabilised adobes. *Materials and Structures,* Volume 45, pp. 1311-1318.

Mkhonto, J., 2014. *An assessment of quality management practices in low cost housing projects delivery in Mpumalanga Province,* Pretoria: Tshwane University of Technology.

Mohamad, G., 2007. *Mechanism failure of concrete block masonry under compression,* Guimaraes: University of Minho.

Montoya, R., Aperador, W. & Bastidas, D., 2009. Influence of conductivity on cathodic protection of reinforced alkali-activated slag mortar using the finite element method. *Corrosion Science,* Volume 51, pp. 2857-2862.

Morton, J., 2012. *Designer's Guide to Eurocode 6: Design of Masonry Structures EN 1996-1-1.* London: ICE Publishing.

Muringathuparambil, R., Musango, J., Brent, A. & Currie, P., 2017. Developing building typologies to examine energy efficiency in representative low cost buildings in Cape Town townships. *Sustainable Cities and Society,* Volume 33, pp. 1-17.

NA to BS EN 1996-1-1, 2005. *UK National Annex to Eurocode 6. Design of masonry structures. General rules for reinforced and unreinforced masonry structures.* London: BSI.

Najafgholipour, M., Maheri, M. & Lourenço, P., 2013. Capacity interaction in brick masonry under simultaneous in-plane and out-of-plane loads. *Construction and Building Materials,* Volume 38, pp. 619-626.

Nazief, M., 2014. *Finite element characterization of the behaviour of masonry infill shear walls with and without openings,* Alberta: University of Alberta.

NBS, 1977. *Performance Criteria Resource Document for Innovative Construction,* Washington DC: Department of Housing and Urban Development.

Ndamashe, S., 2019. *Research and Development Specialist, Agrement South Africa* [Interview] (25 June 2019).

Nguyen, K., Ahn, N., Le, T. & Lee, K., 2016. Theoretical and experimental study on mechanical properties and flexural strength of fly ash-geopolymer concrete. *Construction and Building Materials,* Volume 106, pp. 65-77.

NHBRC, 1999. *Home Building Manual, Part 1 & 2.* s.l.:National Home Builders Registration Council.

NHBRC, 2015. *National Home Builders Registration Council - Home Building Manual and Guide.* Johannesburg: NHBRC, ISBN: 978-0-620-68292-3.

NHC, 2009. *National Housing Code.* s.l.:s.n.

NPC, 2011. *National Development Plan: Vision for 2030.* s.l.:National Planning Commission, ISBN 978-0-621-40475-3.

Oleszkiewicz, I., 1994. *The concept and practice of performance-based building regulations,* s.l.: National Research Council of Canada, Report IRC-IR-697.

Olivier, J., Janssens-Maenhout, G. & Peters, J., 2012. *Trends in Global CO2 Emissions.* [Online] Available at: http://edgar.jrc.ec.europa.eu/CO2REPORT2012.pdf

Page, A., 1978. Finite element model for masonry. *Journal of the Structural Division,* 104(8), pp. 1267-1285.

Page, A., 1981. *The biaxial compressive strength of brick masonry.* s.l., s.n., pp. 893-906.

Palacio, K., 2013. *Practical recommnedations for nonlinear structural analysis in DIANA,* Delft, Netherlands: TNO DIANA BV.

Pan, Z., Sanjayan, J. & Rangan, B., 2011. Fracture properties of geopolymer paste and concrete. *Magazine of Concrete Research,* 63(10), pp. 763-771.

Ramirez, E. et al., 2015. *Mechanical analysis of adobe archaeological masonry under uniaxial compressive loading: The case of Huaca de la Luna.* Seville, Spain, s.n.

Raut, S., Ralegaonkar, R. & Madavgane, S., 2011. Development of sustainable construction material using industrial and agricultural solid waste: A review of waste-create bricks. *Construction and Building Materials,* Volume 25, pp. 4037-4042.

Retief, J. & Dunaiski, P., 2009. *Background to SANS 10160: Basis of structural design and actions for buildings and industrial structures.* 1st ed. Stellenbosch: SUN MeDIA.

Reyes, E., Casati, M. & Galvez, 2008. Cohesive crack model for mixed mode fracture of brick masonry. *International Journal of Fracture,* Volume 151, pp. 29-55.

Reynolds, L., 2007. The South African Energy Efficiency Standards for Buildings. *Vector,* pp. 70-77.

Roca, P., Cervera, M., Gariup, G. & Pela', L., 2010. Structural analysis of masonry historical constructions. Classical and advanced approaches. *Archives of Computational Methods in Engineering,* Volume 17, pp. 299-325.

Rots, J., 1991. Numerical simulation of cracking in structural masonry. *Heron,* 36(2), pp. 49-63.

Rots, J., 1997. Numerical Models in Diana. In: J. Rots, ed. *Structural Masonry.* Rotterdam: A.A. Balkema, pp. 53-56.

SABS 0164-1, 1980. *Code of Practice - The Structural Use of Masonry, Part 1: Unreinforced Masonry Walling.* Pretoria: South African Bureau of Standards.

Salmanpour, A. H., 2017. *Displacement Capacity of Structural Masonry. PhD Thesis,* s.l.: ETH Zurich, Switzerland.

Sandoval, C., Roca, P., Bernat, E. & Gil, L., 2011. Testing and numerical modelling of buckling failure of masonry walls. *Construction and Building Materials,* Volume 25, pp. 4394-4402.

Sanjayan, J., Nazari, A. & Pouraliakbar, H., 2015. FEA modelling of fracture toughness of steel fibre-reinforced geopolymer composites. *Materials and Design,* Volume 76, pp. 215-222.

Sanjuán, M., Zaragoza, A. & Agüí, J., 2011. Standardization for an innovative world. *Cement and Concrete Research,* Volume 41, pp. 767-774.

SANS 10160-1, 2018. *Basis of structural design and actions for buildings and industrial structures, Part 1: Basis of structural design,* Pretoria: South African Bureau of Standards, ISBN: 978-0-626-26428-4.

SANS 10160, 2011. *Basis of Structural Design and Actions for Buildings and Industrial Structures.* 1.1 ed. Pretoria: South African Bureau of Standards, ISBN: 978-0-626-26608-4.

SANS 10160-2, 2011. *Basis of structural design and actions for buildings and industrial structures, Part 2: Self-weight and imposed loads,* Pretoria: South African Bureau of Standards, ISBN: 978-0-626-26429-1.

SANS 10160-3, 2018. *Basis of structural design and actions for buildings and industrial structures, Part 3: Wind,* Pretoria: South African Bureau of Standards, ISBN: 978-0-626-26430-7.

SANS 10160-4, 2017. *Basis of structural design and actions for buildings and industrial structures, Part 4: Seismic actions and general requirements for buildings.* Pretoria: South African Bureau of Standards, ISBN: 978-0-626-26431-4.

SANS 10164-1, 1989. *The structural use of masonry, Part 1: Unreinforced masonry walling.* Pretoria: South African Bureau of Standards, ISBN: 0-626-11256-7.

SANS 10400, 2010. *The Application of the National Building Regulations.* 3 ed. Pretoria: South African Bureau of Standards, ISBN: 978-0-626-25157-4.

SANS 10400-A, 2010. *The Application of the National Building Regulations, Part A: General Principles and Requirements.* 3 ed. Pretoria: South African Bureau of Standards, ISBN: 978-0-626-25157-4.

SANS 10400-B, 2012. *The Application of the National Building Regulations, Part B: Structural Design.* 3 ed. Pretoria: South African Bureau of Standards, ISBN: 978-0-626-27630-0.

SANS 10400-K, 2011. *The Application of the National Building Regulations, Part K: Walls.* 3 ed. Pretoria: South African Bureau of Standards, ISBN 978-0-626-25193-2.

SANS 10400-L, 2011. *The application of the National Building Regulations.* Pretoria: South African Bureau of Standards, ISBN: 978-0-626-2522-9.

SANS 10400-L, 2011. *The Application of the National Building Regulations, Part L: Roofs,* Pretoria: South African Bureau of Standards, ISBN: 978-0-626-25222-9.

SANS 10400-XA, 2011. *The application of the National Building Regulations, Part X: Environmental Sustainability, Part XA: Energy usage in buildings.* Pretoria: South African Bureau of Standards, ISBN: 978-0-626-25224-3.

SANS 1215, 2008. *Concrete Masonry Units.* 1.3 ed. Pretoria: South African Bureau of Standards, ISBN: 978-0-626-20624-6.

SANS 227, 2007. *Burnt Clay Masonry Units.* 4.4 ed. Pretoria: South African Bureau of Standards, ISBN: 978-0-626-19745-2.

SANS 285, 2010. *Calcium Silicate Masonry Units.* 3.3 ed. Pretoria: South African Bureau of Standards, ISBN: 978-0-626-23625-0.

SANS 50771-3, 2015. *Specification for masonry units, Part 3: Aggregate concrete masonry units (Dense and lightweight aggregates).* 1 ed. Pretoria: South African Bureau of Standards, ISBN: 978-0-626-32366-0.

SANS 50771-4, 2007. *Specification for masonry units, Part 4: Autoclaved aerated concrete masonry units.* 1 ed. Pretoria: South African Bureau of Standards, ISBN: 978-0-626-19728-5.

SANS 51196, 2018. *Eurocode 6: Design of masonry structures.* 1 ed. Pretoria: South African Bureau of Standards.

SANS 51996-1-1, 2018. *Eurocode 6: Design of masonry structures - Part 1-1: General rules for reinforced and unreinforced masonry structures.* 1 ed. Pretoria: South African Bureau of Standards.

SANS 51996-3, 2018. *Eurocode 6 - Design of masonry structures - Part 3: Simplfied calculation methods for unreinforced masonry structures.* 1 ed. Pretoria: South African Bureau of Standards.

Sarchi, L., Varum, H., Monteiro, R. & Silveira, D., 2018. Seismic behaviour of two Portuguese adobe buildings: part II - numerical modeling and fragility assessment. *International Journal of Architectural Heritage,* Volume 12, pp. 936-950.

Schubert, P., 1988. *Compressive and tensile strength of masonry.* London, Elsevier Applied Science, pp. 406-419.

Šejnoha, M. et al., 2013. Fracture properties of cement and alkali activated fly ash based concrete with application to segmental tunnel lining. *Advances in Engineering Software,* Volume 62-63, pp. 61-71.

Sexton, M. & Barrett, P., 2005. Performance-based building and innovation: balancing client and industry needs. *Building Research & Information,* Volume 33, pp. 142-148.

Shakir, A. & Mohammed, A., 2013. Manufacturing of bricks in the past, in the present and in the future: A state of the art review. *International Journal of Advances in Applied Sciences,* 2(3), pp. 145-156.

Shieh-Beygi, B. & Pietruszczak, S., 2008. Numerical analysis of structural masonry: mesoscale approach. *Computers and Structures,* Volume 86, pp. 1958-1973.

Shiso, E., 2019. *In-plane structural response of single-storey unreinforced walls constructed using alternative masonry units,* s.l.: Stellenbosch University.

Sibiya, Z., 2018. *Analyzing the persistent nature of quality issues in low-cost housing projects,* Johannesburg: University of the Witwatersrand.

Silva, R. et al., 2014. *Modelling the structural behaviour of rammed earth components.* Stirlingshire, s.n.

Silva, R. et al., 2012. On the development of unmodified mud grouts for repairing earth constructions: Rheology, strength and adhesion. *Materials and Structures,* Volume 45, pp. 1497-1512.

Sisulu, L., 2016. *Housing Backlog at 2.1 million, says Minister Sisulu,* s.l.: Engineering News.

Sitton, J., Zeinali, Y., Heidarian, W. & Story, B., 2018. Effect of mix design on compressed earth block strength. *Construction and Building Materials,* Volume 158, pp. 124-131.

Sousa, R., Guedes, J. & Sousa, H., 2015. Characterization of the uniaxial compression behaviour of unreinforced masonry - Sensitivity analysis based on a numerical and experimental approach. *Archives of Civil and Mechanical Engineering,* Volume 15, pp. 532-547.

Spada, A., Giambanco, G. & Rizzo, 2009. Damage and plasticity at the interfaces in composite materials and structures. *Computer Methods in Applied Mechanics and Engineering,* Volume 198, pp. 3884-3901.

Sparks, P., Liu, H. & Saffir, H., 1989. Wind damage to masonry buildings. *Journal of Aerospace Engineering,* 2(4), pp. 186-198.

Srisanthi, V., Keshav, L., Kumar, P. & Jayakumar, 2014. Finite element and experimental analysis of 3D masonry compressed stabilised earth block and brick building models against earthquake forces. *Periodica Polytechnica Civil Engineering,* 58(3), pp. 255-265.

Statistics South Africa, 2013. *General Household Survey 2013,* Pretoria: Statistics South Africa.

Statistics South Africa, 2018. *General Household Survey 2018,* Pretoria: Statistics South Africa.

Steyn, B., 2011. *Sub-standard housing: Department notches up R 58 billion bill,* s.l.: s.n.

Sýkora, M. & Holický, M., 2010. Probabilistic model for masonry strength or existing structures. *Engineering Mechanics,* 174(1), pp. 61-70.

Talocchino, G., 2005. *Design and construction criteria for domes in low-cost housing,* Johannesburg: Univeristy of the Witwatersrand.

Tarque, N. et al., 2010. *Numerical modelling of in-plane behaviour of adobe walls.* Aveiro, Portugal, s.n.

Tarque, N. et al., 2012. *Elastic and inelastic parameters for representing the seismic in-plane behaviour of adobe wall.* Lima, Peru, s.n.

Tarque, N. et al., 2014. Nonlinear dynamic analysis of a full-scale unreinforced adobe model. *Earthquake Spectra,* Volume 4, pp. 1643-1661.

Tennant, A., 2016. *Behaviour of cement-stabilized soil block masonry under flexure,* Chicago: s.n.

Tennant, A., Foster, C. & Venkatarama Reddy, B., 2013. Verification of masonry building code to flexural behaviour of cement-stabilized soil block. *Journal of Materials in Civil Engineering,* Volume 25, pp. 303-307.

Thudén, A. & Toivonen, A., 2018. *Analysis of earthquake resistant compressed stabilised earth block building in rural Nepal,* Gothenburg, Sweden: s.n.

Tomaževič, M., 2009. Shear resistance of masonry walls and Eurocode 6: Shear versus tensile strength. *Materials and Structures,* Volume 42, pp. 889-907.

UBC, 1997. *Uniform Building Code.* Whittier, California: International Conference of Building Officials.

Vaculik, J., 2012. *Unreinforced Masonry Walls Subjected to Out-of-Plane Seismic Actions,* Adelaide: PhD Thesis, University of Adelaide, School of Civil, Environmental and Mining Engineering.

Van Der Klashorst, E., 2015. *Evaluation of rational design procedures for alternative masonry units,* Stellenbosch: Stellenbosch University.

Van Der Kolf, T., 2014. *The seismic analysis of a typical South African unreinforced masonry structure,* s.l.: Stellenbosch University.

Van Der Pluijm, R., 1992. *Material properties of masonry and its components under tension and shear.* Saskatoon, University of Saskatchewan.

Van Der Pluijm, R., 1993. *Shear behaviour of bed joints.* Philadelphia, s.n., pp. 125-136.

Van Der Pluijm, R., 1999. *Out-of-plane bending of masonry: behaviour and strength,* Eindhoven: Eindhoven University of Technology.

Van Der Pluijm, R., Rutten, H. & Celeen, M., 2000. *Shear behaviour of bed joints.* Madrid, s.n., pp. 1849-1862.

Van Wyk, L., 2010. *The efficacy of innovative technologies in subsidised housing in South Africa: A case study.* Pretoria, CSIR.

Van Zijl, G., 2000. *Computational modelling of masonry creep and shrinkage,* Delft: Delft University of Technology.

Van Zijl, G., 2004. Modeling masonry shear-compression: Role of dilatancy highlighted. *Journal of Engineering Mechanics,* 130(11), pp. 1289-1296.

Venkatarama Reddy, B. & Jagadish, K., 2003. Embodied energy of common and alternative building materials and technologies. *Energy and Buildings,* Volume 35, pp. 129-137.

Venkatarama Reddy, B., Lal, R. & Nanjunda Rao, K., 2007. Optimum soil grading for the soil-cement blocks. *Journal of Materials in Civil Engineering,* 19(2), pp. 139-148.

Vermeltfoort, A., Martens, D. & Van Zijl, G., 2007. Brick-mortar interface effects on masonry under compression. *Canadian Journal of Civil Engineering,* Volume 34, pp. 1475-1485.

Walker, P., 1995. Strength, durability and shrinkage characteristics of cement stabilised soil blocks. *Cement and Concrete Composites,* Volume 17, pp. 301-310.

Watermeyer, R., 1996. Recent developments in providing houses of masonry construction in South Africa. *The Structural Engineer,* 74(19), pp. 325-331.

Watermeyer, R., 2004. *The impact of structural engineering on the sustainability of human settlements in developing countries.* Cape Town, s.n.

Watermeyer, R. & Milford, R., 2003. *The use of performance based building codes to attain sustainable housing objectives: the South African approach..* Washington DC, USA, s.n.

Watermeyer, R. & Tromp, B., 1992. A systematic approach to the design and construction of single-storey residential masonry structures on problem soils. *The Civil Engineer in South Africa,* Issue March, pp. 83-96.

WBCSD, 2009. *Cement Industry and CO2 Performance. Getting the Numbers Right.* [Online] Available at: http://www.wbcsdcement.org/pdf/CSI%20GNR%20Report%20final_updated%20Nov11_LR.pdf

Williams, E., Akers, S. & Reed, P., 2007. *Laboratory characterization of gray masonry concrete,* Vicksburg: US Army Engineer Research and Development Center.

Wium, J., 2010. Background to draft SANS 10160 (2009): Part 4 Seismic Loading. *Journal of the South African Institution of Civil Engineering,* 52(1), pp. 20-27.

WTO, 1997. *World Trade Organisation.* [Online] Available at: www.wto.org [Accessed July 2012].

Zhang, L., 2013. Production of bricks from waste materials - A review. *Construction and Building Materials,* Volume 47, pp. 643-655.

Zucchini, A. & Lourenço, P., 2002. A micro-mechanical model for the homogenisation of masonry. *International Journal of Solids and Structures,* Volume 39, pp. 3233-3255.

Zuguzane, N., Smallwood, J. & Emuze, F., 2012. Perceptions of the quality of low-income houses in South Africa: Defects and their causes. *Acta Structilia,* 19(1).

Appendix A: Wind Design Loads

Further details to the determination of the critical wind design loads are presented. The pertinent general wind action parameters, applicable to both wall configurations, presented and discussed in Section 7.3.2, are repeated here for clarity. Thereafter, the calculation processes are presented for each wall configuration separately.

Table A1: Wind load parameters to SANS 10160-3 (2018)

Parameter	Symbol	Value	Clause
Fundamental Value of Basic Wind Speed	v_b	44 m/s	7.2.2
Terrain Category	-	C	Table 2
Terrain Roughness Factor	$c_r(z)$	0.73	7.3.2, Table 3
Topography Factor	$c_0(z)$	1	7.3.3
Air Density	ρ	1.2 kg/m³	Table 4
Peak Wind Pressure	$q_p(z)$	1213 N/m²	7.4, Eq 6

A1. Wind Design Loads: W1

The critical design load pressures for W1, presented in Table 7.4, are repeated here for ease of reference. First, the determination of the pressure coefficients is presented, where after the calculation process of the wind design load pressures is provided for the SLS and ULS-W load case for W1.

Table A2: Critical SLS and ULS-W design load pressures for W1

	SLS	ULS-W	
Roof Selfweight	-10.05×10^{-3}	-9.00×10^{-3}	N/mm²
Roof Wind	43.92×10^{-3}	117.14×10^{-3}	N/mm²
OP Zone A	1.39×10^{-3}	3.71×10^{-3}	N/mm²
OP Zone B	1.05×10^{-3}	2.79×10^{-3}	N/mm²
IP	24.41×10^{-3}	65.09×10^{-3}	N/mm²

To arrive at critical pressure coefficients, wall W1 (6m long) is considered within the context of a 40m² Category 1 house. The accompanying gable wall (not under consideration) is thus 6.8m long. The same wall W1, indicated in red in the following tables, is under consideration for every load condition. Three wind directions are applied, rendering the wall under consideration the windward wall (Table A3), the leeward wall (Table A4) or the side wall (Table A5) respectively. Additionally, variation in openings is taken into account. The case of all windows and doors closed is designated by 'SLS & ULS-W'. 'ACC-W-D' designates the accidental case of doors and windows open in wall zone D, creating openings three times greater than in the remaining facades. 'ACC-W-E' is defined likewise for wall zone E.

With reference to SANS 10160-3 (2018), the wall external pressure coefficients are determined according to Figure 8 and Table 6, roof external pressure coefficients to Figure 11 and Tables 10 and 11, and the internal pressure coefficients to Clause 8.3.9.5.

Table A3: Pressure coefficients for W1 windward

External Pressure Coefficient – Wall

Zone	C_{pe}
A	1.20
B	0.80
C	0.50
D	0.80
E	0.50

External Pressure Coefficient – Roof

Zone	C_{pe}
F	0.90
G	0.80
H	0.30
I	0.40
J	1.00

Internal Pressure Coefficient

Load Case	C_{pi}
SLS & ULS-W	0.20
ACC-W-D	0.72
ACC-W-E	-0.45

132

Table A4: Pressure coefficients for W1 leeward

External Pressure Coefficient – Wall

Zone	C_{pe}
A	1.20
B	0.80
C	0.50
D	0.80
E	0.50

External Pressure Coefficient – Roof

Zone	C_{pe}
F	0.90
G	0.80
H	0.30
I	0.40
J	1.00

Internal Pressure Coefficient

Load Case	C_{pi}
SLS & ULS-W	0.20
ACC-W-D	0.45
ACC-W-E	-0.72

133

Table A5: Pressure coefficients for W1 sidewall

External Pressure Coefficient – Wall
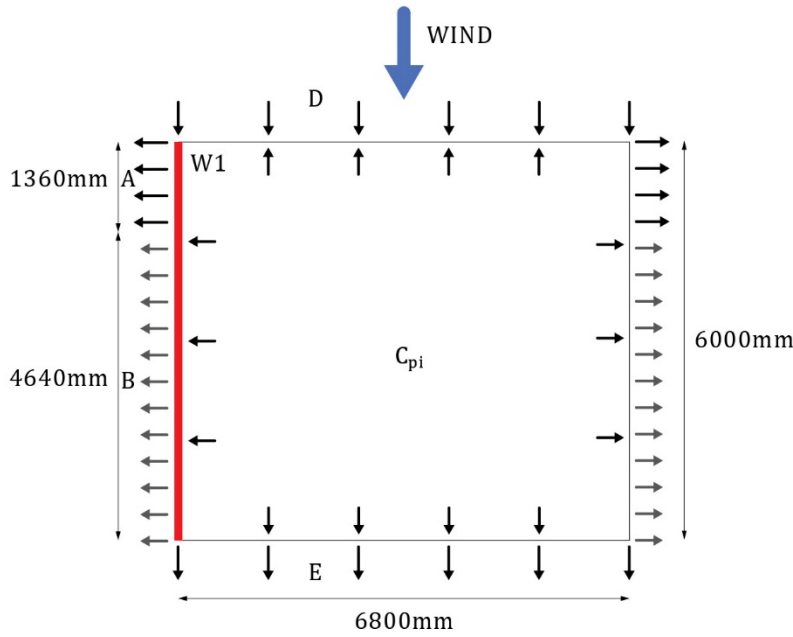
Zone	C_{pe}
A	**1.20**
B	**0.80**
D	**0.80**
E	**0.50**

External Pressure Coefficient – Roof
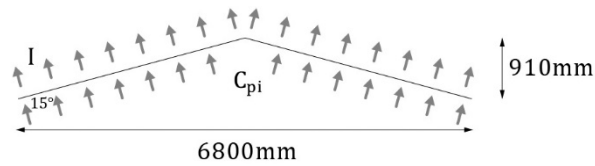
Zone	C_{pe}
I	**0.40**

Internal Pressure Coefficient

Load Case	C_{pi}
SLS & ULS-W	**0.20**
ACC-W-D or E	0.79

The combined effect of the pressure coefficients for the case of all windows and doors closed (SLS & ULS-W) is the critical load case for all load directions. Furthermore, W1 as the sidewall is the critical wind direction. The critical pressure coefficients are marked as bold in Table A5. From here on, calculations for the determination of the critical load pressures for W1 as sidewall for the SLS and ULS-W case are presented in Tables A6 to A12.

Table A6: Dimensions for W1 SLS & ULS-W sidewall

Category 1 House Dimensions			
b	crosswind dimension	6.80	m
d	sidewall dimension	6.00	m
h_{W1}	height of W1	2.70	m
h_{gable}	accompanying gable height	0.91	m
h	house height	3.61	m
t_{W1}	thickness of W1	0.14	m
N_T	number of trusses	5	-
A_{TB}	area of truss bearing (1 block)	0.04	m²

Table A7: Roof selfweight design load pressure for W1 SLS and ULS-W sidewall

Timber Truss Selfweight (per half roof)			
ρ_T	timber density	5000	N/m³
A_{BC}	bottom chord section: 152 × 38	5776	mm²
A_{TC} and A_W	top chord and web section: 114 × 38	4332	mm²
L_{BC}	bottom chord length	3.40	m
L_{TC}	top chord length	3.52	m
L_W	web length	3.64	m
V_T	timber volume / half roof: $N_T \times (A_{BC} \times L_{BC} + A_{TC} \times L_{TC} + A_W \times L_W) =$	0.25	m³
F_T	timber selfweight per half roof: $V_T \times \rho_T = 0.25 \times 5000 =$	1267	N
Metal Sheeting Selfweight (per half roof)			
w_S	0.5mm metal sheeting selfweight	39.50	N/m²
A_S	metal sheeting area per half of roof: $L_{TC} \times d = 3.52 \times 6.00 =$	21.12	m²
F_S	metal sheeting selfweight per half roof: $w_S \times A_S = 39.50 \times 21.12 =$	834	N
Roof Selfweight Design Load Pressure			
F_R	roof selfweigth per half roof: $F_T + F_S = 1267 + 834 =$	2101	N
w_R	roof selfweight per truss bearing: $F_R/(N_T \times A_{TB}) = 2010/(5 \times 0.04)$	10 005	N/m²
$w_{R,d}$ (SLS)	design roof selfweight per truss bearing: $\gamma_F \times w_{R,d} = 1.0 \times 10\,005 =$	10 005	N/m²
		10.05x10⁻³	**N/mm²**
$w_{R,d}$ (ULS-W)	design roof selfweight per truss bearing: $\gamma_F \times w_{R,d} = 0.9 \times 10\,005 =$	9 005	N/m²
		9.00x10⁻³	**N/mm²**

Table A8: Wind zone surface areas for W1 SLS and ULS-W sidewall

Wind Zone Lengths – SANS 10160-3 (SANS 10160-3, 2018) Figures 8 & 11

e	smaller of b or $2h$	6.80	m
A	$e/5$	1.36	m
B	$d - e/5$	4.64	m
D and E	crosswind dimension	6.80	m

Wind Zone Surface Areas

A	$e/5 \times h_{W1}$	3.67	m²
A'	wind zone A with openings	2.69	m²
B	$(d - e/5) \times h_{W1}$	12.53	m²
B'	wind zone B with openings	8.71	m²
D' and E'	gable wall contribution to IP load of W1, 45° load distribution	4.87	m²
I	$L_{TC} \times d = 3.52 \times 6.00 =$	21.12	m²

Table A9: Total pressure coefficients for W1 SLS and ULS-W sidewall

Total Pressure Coefficients (see Table A5)

$C_{p,A}$	$C_{pe} + C_{pi} = 1.2 + 0.2 =$	1.4	-
$C_{p,B}$	$C_{pe} + C_{pi} = 0.8 + 0.2 =$	1.0	-
$C_{p,D}$	$C_{pe} + C_{pi} = 0.8 - 0.2 =$	0.6	-
$C_{p,E}$	$C_{pe} + C_{pi} = 0.5 + 0.2 =$	0.7	-
$C_{p,I}$	$C_{pe} + C_{pi} = 0.4 + 0.2 =$	0.6	-

Table A10: Roof wind design load pressure for W1 SLS and ULS-W sidewall

Roof Wind Design Load Pressure

w_I	$C_{p,I} \times q_p(z) = 0.6 \times 1213 =$	728	N/m²
F_I	wind force: $w_I \times I = 728 \times 21.12 =$	15 374	N
w_I	roof wind load per truss bearing: $F_W/(N_T \times A_{TB}) = 15\ 374/(5 \times 0.04)$	73 195	N/m²
$w_{I,d}$ (SLS)	design roof wind load per truss bearing: $\gamma_F \times w_I = 0.6 \times 73\ 195 =$	43 917	N/m²
		43.92x10⁻³	**N/mm²**
$w_{I,d}$ (ULS-W)	design roof wind load per truss bearing: $\gamma_F \times w_I = 1.6 \times 73\ 195 =$	117 138	N/m²
		117.14x10⁻³	**N/mm²**

Table A11: OP design load pressure for W1 SLS and ULS-W sidewall

OP Design Load Pressure – Zone A

w_A	$C_{p,A} \times q_p(z) = 1.4 \times 1213 =$	1699	N/m²
A/A'	load distribution ratio to compensate openings (see Table A8)	1.37	-
$w_{A'}$	$w_A \times A/A' = 1699 \times 1.37 =$	2327	N/m²
$w_{A'd}$ (SLS)	design load pressure: $\gamma_F \times w_{A'} = 0.6 \times 2327 =$	1392	N/m²
		1.39x10⁻³	**N/mm²**
$w_{A'd}$ (ULS-W)	design load pressure: $\gamma_F \times w_{A'} = 1.6 \times 2327 =$	3712	N/m²
		3.71x10⁻³	**N/mm²**

OP Design Load Pressure – Zone B

w_B	$C_{p,B} \times q_p(z) = 1.0 \times 1213 =$	1213	N/m²
B/B'	load distribution ratio to compensate openings (see Table A8)	1.44	-
$w_{B'}$	$w_B \times B/B' = 1213 \times 1.44 =$	1746	N/m²
$w_{B'd}$ (SLS)	OP design load pressure: $\gamma_F \times w_{B'} = 0.6 \times 1746 =$	1048	N/m²
		1.05x10⁻³	**N/mm²**
$w_{B'd}$ (ULS-W)	OP design load pressure: $\gamma_F \times w_{B'} = 1.6 \times 1746 =$	2793	N/m²
		2.79x10⁻³	**N/mm²**

OP Total Design Force

$F_{A+B,d}$ (SLS)	OP design force on W1: $w_{A'd} \times A' + w_{B'd} \times B'$ (SLS)	**12 482**	**N**
$F_{A+B,d}$ (ULS-W)	OP design force on W1: $w_{A'd} \times A' + w_{B'd} \times B'$ (ULS-W)	**33 285**	**N**

Table A12: IP design load pressure for W1 SLS and ULS-W sidewall

IP Design Load Pressure (due to Zones D & E)

$F_{D'+E'}$	total IP force: $(C_{p,D} \times D' + C_{p,E} \times E') \times q_p(z)$		
	$= (0.6 \times 4.87 + 0.7 \times 4.87) \times 1213 =$	7689	N
$W_{D'+E'}$	linearly varying line load over height of wall:		
	$2 \times F_{D+E}/h_{W1} = 2 \times 7689/2.70 =$	5695	N/m
$w_{D'+E'}$	linearly varying load distributed over width of wall:		
	$W_{D+E}/t_{W1} = 5695/0.14 =$	40 682	N/m²
$w_{D'+E',d}$ (SLS)	design load pressure: $\gamma_F \times w_{D'+E'} = 0.6 \times 40\ 682 =$	24 409	N/m²
		24.41x10⁻³	**N/mm²**
$w_{D'+E',d}$ (ULS-W)	design load pressure: $\gamma_F \times w_{D'+E'} = 1.6 \times 40\ 682 =$	65 092	N/m²
		65.09x10⁻³	**N/mm²**

IP Total Design Force (due to Zones D & E)

$F_{D'+E',d}$ (SLS)	IP design force on W1: $\gamma_F \times F_{D'+E'} = 0.6 \times 7689 =$	**4613**	**N**
$F_{D'+E',d}$ (ULS-W)	IP design force on W1: $\gamma_F \times F_{D'+E'} = 1.6 \times 7689 =$	**12 302**	**N**

A2. Wind Design Loads: W2

The critical design load pressures for W2, presented in Table 7.5, are repeated here for ease of reference. First, the determination of the pressure coefficients is presented, where after the calculation process of the wind design load pressures is provided for the SLS and ULS-W load case for W2.

Table A13: Critical SLS and ULS-W design loads for W2

	SLS	ULS-W	
OP Zone A	2.26×10^{-3}	6.02×10^{-3}	N/mm²
OP Zone B	1.00×10^{-3}	2.66×10^{-3}	N/mm²
IP	17.58×10^{-3}	46.86×10^{-3}	N/mm²

To arrive at critical pressure coefficients, gable wall W2 (4.95m long) is considered within the context of a 40m² Category 1 house. The accompanying panel wall (not under consideration) is thus 8.0m long. The same wall W2, indicated in red in the following tables, is under consideration for every load condition. Three wind directions are applied, rendering the wall under consideration the windward wall (Table A14), the leeward wall (Table A15) or the side wall (Table A16) respectively. Additionally, variation in openings is taken into account. The case of all windows and doors closed is designated by 'SLS & ULS-W'. 'ACC-W-D' designates the accidental case of doors and windows open in wall zone D, creating openings three times greater than in the remaining facades. 'ACC-W-E' is defined likewise for wall zone E.

With reference to SANS 10160-3 (2018), the wall external pressure coefficients are determined according to Figure 8 and Table 6, roof external pressure coefficients to Figure 11 and Tables 10 and 11, and the internal pressure coefficients to Clause 8.3.9.5.

Table A14: Pressure coefficients for W2 windward

External Pressure Coefficient – Wall	**Zone**	**C_{pe}**
	A	1.20
	B	0.80
	C	0.50
	D	0.80
	E	0.50

Internal Pressure Coefficient	**Load Case**	**C_{pi}**
	SLS & ULS-W	0.30
	ACC-W-D	0.72
	ACC-W-E	-0.45

Table A15: Pressure coefficients for W2 leeward

External Pressure Coefficient – Wall

Zone	C_{pe}
A	1.20
B	0.80
C	0.50
D	0.80
E	0.50

Internal Pressure Coefficient

Load Case	C_{pi}
SLS & ULS-W	0.20
ACC-W-D	0.45
ACC-W-E	-0.72

Table A16: Pressure coefficients for W2 sidewall

External Pressure Coefficient – Wall

Zone	C_{pe}
A	**1.20**
B	**0.80**
D	**0.80**
E	**0.50**

Internal Pressure Coefficient

Load Case	C_{pi}
SLS & ULS-W	**0.20**
ACC-W-D	0.80
ACC-W-E	-

The combined effect of the pressure coefficients for the case of all windows and doors closed (SLS & ULS-W) is the critical load case for all load directions. Furthermore, W2 as the sidewall is the critical wind direction. The critical pressure coefficients are marked as bold in Table A16. From here on, calculations for the determination of the critical load pressures for W2 as sidewall for the SLS and ULS-W case are presented in Tables A17 to A21.

Table A17: Dimensions for W2 SLS and ULS-W sidewall

Category 1 House Dimensions			
b	crosswind dimension	8.00	m
d	sidewall dimension	4.95	m
h_{W2}	height of W2 (without gable)	2.60	m
h_{gable}	gable height	0.67	m
h	house height	3.27	m
t_{W2}	thickness of W2	0.14	m

Table A18: Wind zone surface areas for W2 SLS and ULS-W sidewall

Wind Zone Lengths – SANS 10160-3 (SANS 10160-3, 2018) Figures 8 & 11			
e	smaller of b or $2h$	6.54	m
A	$e/5$	1.31	m
B	$d - e/5$	3.69	m
D and E	crosswind dimension	8.00	m
Wind Zone Surface Areas			
A	$e/5 \times h_{W2} + gable\ portion$	3.63	m²
A'	wind zone A with openings	1.64	m²
B	$(d - e/5) \times h_{W2} + gable\ portion$	11.04	m²
B'	wind zone B with openings	8.06	m²
D' and E'	panel wall contribution to IP load of W1, 45° load distribution	3.38	m²

Table A19: Total pressure coefficients for W2 SLS and ULS-W sidewall

Total Pressure Coefficients (see Table A16)			
$C_{p,A}$	$C_{pe} + C_{pi} = 1.2 + 0.2 =$	1.4	-
$C_{p,B}$	$C_{pe} + C_{pi} = 0.8 + 0.2 =$	1.0	-
$C_{p,D}$	$C_{pe} + C_{pi} = 0.8 - 0.2 =$	0.6	-
$C_{p,E}$	$C_{pe} + C_{pi} = 0.5 + 0.2 =$	0.7	-

Table A20: OP design load pressure for W2 SLS and ULS-W sidewall

OP Design Load Pressure – Zone A

w_A	$C_{p,A} \times q_p(z) = 1.4 \times 1213 =$	1699	N/m²
A/A'	load distribution ratio to compensate for openings (see Table A18)	2.22	-
$w_{A'}$	$w_A \times A/A' = 1699 \times 2.22 =$	3763	N/m²
$w_{A'd}$ (SLS)	design load pressure: $\gamma_F \times w_{A'} = 0.6 \times 3772 =$	2258	N/m²
		2.26x10⁻³	**N/mm²**
$w_{A'd}$ (ULS-W)	design load pressure: $\gamma_F \times w_{A'} = 1.6 \times 3772 =$	6020	N/m²
		6.02x10⁻³	**N/mm²**

OP Design Load Pressure – Zone B

w_B	$C_{p,B} \times q_p(z) = 1.0 \times 1213 =$	1213	N/m²
B/B'	load distribution ratio to compensate openings (see Table A18)	1.37	-
$w_{B'}$	$w_B \times B/B' = 1213 \times 1.37 =$	1662	N/m²
$w_{B'd}$ (SLS)	design load pressure: $\gamma_F \times w_{B'} = 0.6 \times 1662 =$	997	N/m²
		1.00x10⁻³	**N/mm²**
$w_{B'd}$ (ULS-W)	design load pressure: $\gamma_F \times w_{B'} = 1.6 \times 1662 =$	2659	N/m²
		2.66x10⁻³	**N/mm²**

OP Total Design Force – Zones A & B

$F_{A+B,d}$ (SLS)	OP design force on W2: $w_{A'd} \times A' + w_{B'd} \times B'$	**11 530**	**N**
$F_{A+B,d}$ (ULS-W)	OP design force on W2: $w_{A'd} \times A' + w_{B'd} \times B'$	**30746**	**N**

Table A21: IP design load pressure for W2 SLS and ULS-W sidewall

IP Design Load Pressure - due to Zones D & E

$F_{D'+E'}$	total IP force: $\left(C_{p,D} \times D' + C_{p,E} \times E' \right) \times q_p(z)$		
	$= (0.6 \times 3.38 + 0.7 \times 3.38) \times 1213 =$	5331	N
$W_{D'+E'}$	linearly varying line load over height of wall:		
	$2 \times F_{D+E}/h_{W1} = 2 \times 5331/2.60 =$	4100	N/m
$w_{D'+E'}$	linearly varying load distributed over width of wall:		
	$W_{D+E}/t_{W1} = 4100/0.14 =$	29 295	N/m²
$w_{D'+E',d}$(SLS)	design load pressure: $\gamma_F \times w_{D'+E'} = 0.6 \times 29\ 285 =$	17 575	N/m²
		17.58x10⁻³	**N/mm²**
$w_{D'+E',d}$(ULS-W)	design load pressure: $\gamma_F \times w_{D'+E'} = 1.6 \times 29\ 285 =$	46 856	N/m²
		46.86x10⁻³	**N/mm²**

IP Total Design Force - due to Zones D & E

$F_{D'+E',d}$ (SLS)	IP design force on W2: $\gamma_F \times F_{D'+E'} = 0.6 \times 5331 =$	**3 199**	**N**
$F_{D'+E',d}$ (ULS-W)	IP design force on W2: $\gamma_F \times F_{D'+E'} = 1.6 \times 5331 =$	**8 530**	**N**

Appendix B: Seismic Design Loads

Further details to the determination of the seismic design loads are presented. The pertinent general seismic action parameters and assumptions, applicable to both wall configurations, presented and discussed in Section 7.3.3, are repeated here for clarity, together with the calculation process followed for both wall configurations.

The critical design load pressures for W1 and W2, presented in Table 7.4 and Table 7.5 respectively, are repeated here in Table B2 for ease of reference. First, the determination of the pressure coefficients is presented, where after the calculation process of the seismic design load pressures is provided for the ULS-S load case for W1 and W2 simultaneously.

Table B2: Critical ULS-S design load pressures for W1 and W2

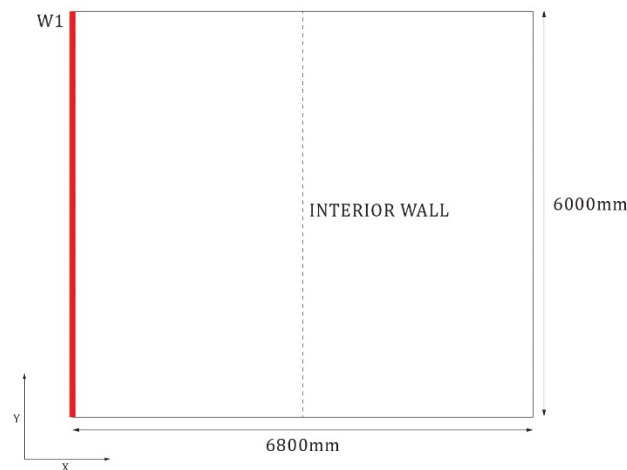|	W1	W2	
OP	0.79×10^{-3}	0.96×10^{-3}	N/mm²
IP	53.88×10^{-3}	56.43×10^{-3}	N/mm²

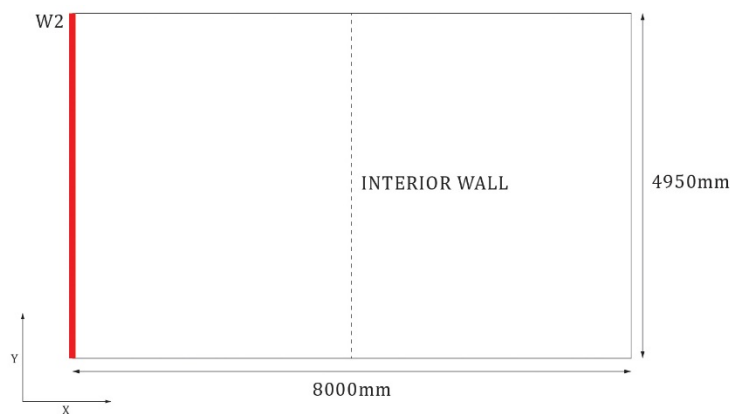Figure B1: Shear wall distribution for house with W1

Figure B2: Shear wall distribution for house with W2

Table B3: Seismic design loads for W1 and W2 to SANS 10160-4 (2017)

	Design Response Spectrum	W1	W2		SANS 10160-4
h_t	building height	3.61	3.27	m	-
C_T	fundamental period of vibration factor	0.05	0.05	-	8.5.2.1
T	SDOF vibration period	0.131	0.131	s	8.5.2.1, Eq. 11
a_g	horizontal peak ground acceleration	0.15	0.15	g	5.2, Figure 1
q	behaviour factor	1.5	1.5	-	8.2, Table 4
β	horizontal design spectrum lower bound	0.2	0.2	-	5.3
$S_d(T)$	normalized design response spectra	0.27	0.26		5.3
Design Base Shear					
ρ_W	wall density	2000	2000	kg/m³	-
V_W	total house walls volume	9.1	9.9	m³	-
F_W	total house walls weight: $\rho \times V_W$	179 023	194 884	N	-
F_R	total roof weight (see Table A7)	4 202	4 064	N	-
W_n	sustained vertical load: $F_W + F_R$	183 225	198 948	N	8.3
V_n	design base shear: $S_d(T) \times V_n$	49 033	51 349	N	8.5.1
Shear Force in Wall					
$n_{W,x}$	no of shear walls in x direction (see Fig B1 & B2)	2	2	-	-
$n_{W,y}$	no of shear walls in y direction (see Fig B1 & B2)	3	3	-	-
k_x	relative stiffness of wall in x direction: $1/n_{W,x}$	1/2	1/2	-	8.5.4.2
k_y	relative stiffness of wall in y direction: $1/n_{W,y}$	1/3	1/3	-	8.5.4.2
V_x	shear force in each wall in x direction: $k_x \times V_n$	24 517	25 674	N	-
V_y	shear force in each wall in x direction: $k_y \times V_n$	16 344	17 116	N	-
Seismic Design Load					
E_{100}	100% seismic IP load: $1.0 \times V_y$	16 344	17 116	N	8
E_{30}	30% seismic OP load: $0.3 \times V_x$	7 355	7 702	N	8
γ_1	building importance factor	1.0	1.0	-	Table 3
ρ	reliability or redundancy factor	1.2	1.2	-	Equation 6
$E_{IP,d}$	$\gamma_1 \times \rho \times E_{100}$	19 613	20 539	N	Equation 5
$E_{OP,d}$	$\gamma_1 \times \rho \times E_{30}$	8 826	9 243	N	Equation 5
IP Seismic Design Load Pressures					
w_{IP}	uniform IP load over wall height: $E_{IP,d}/(h_W \times t_W)$	53 883	56 427	N/m²	-
$w_{IP,d}$	IP design load pressure: $\gamma_F \times w_{IP} = 1.0 \times w_{IP}$	53 883	56 427	N/m²	
		53.88x10⁻³	**56.43x10⁻³**	**N/mm²**	
OP Seismic Design Load Pressures					
A_W	wall surface area with openings	11.15	9.68	m²	
w_{OP}	uniform OP load over wall: $E_{OP,d}/A_W$	792	955	N/m²	
$w_{OP',d}$	OP design load pressure: $\gamma_F \times w_{OP'} = 1.0 \times w_{OP'}$	792	955	N/m²	
		0.79x10⁻³	**0.96x10⁻³**	**N/mm²**	